Characterizing the Evolution of Fresh and Aged Water-Soluble Brown Carbon Chromophores in Wildfire Smoke

Lisa Azzarello

A DISSERTATION SUBMITTED TO THE FACULTY OF GRADUATE STUDIES IN PARTIAL FULFILLMENT OF THE REQUIREMENTS FOR THE DEGREE OF

DOCTOR OF PHILOSOPHY

GRADUATE PROGRAM IN CHEMISTRY

YORK UNIVERSITY

TORONTO, ONTARIO

March 2026

Abstract

Wildfires are an important source of carbonaceous aerosol that impact air quality and the Earth's radiative budget. Organic aerosol that is partially water soluble and absorbs in the ultraviolet to visible spectral range is referred to as "brown carbon" (BrC). There remains uncertainty regarding BrC's optical properties and atmospheric evolution. This dissertation investigates BrC across laboratory, airborne, and ground-based measurements.

Chapter two examines airborne measurements of western U.S. wildfire smoke aged 0-5 hrs during FIREX-AQ. Brown carbon absorption was measured online using a particle-into-liquid sampler (PILS) and aqueous samples were collected for offline SEC-UV analysis. Absorption was dominated by low molecular weight (MW) (< 500 Da) species and exhibited variable trends with plume age. Comparisons between the online PILS and offline SEC-UV absorption measurements revealed differences between absolute absorption and wavelength dependence. These results emphasized the importance of intercomparison between measurement techniques when investigating BrC absorption.

Chapter three focuses on controlled combustion experiments from the FIREX FireLab study. Western U.S. fuels were pyrolyzed and BrC absorption, total aerosol absorption, and aerosol composition was investigated online and offline at ambient and thermal denuded conditions. Offline filters were characterized using SEC-UV, a volatility basis set framework, and the octanol-water partitioning coefficient log(K_{ow}) was estimated. At ambient conditions, absorption was dominated by low volatility compounds of low MW. After thermal denuding, a fraction of BrC persisted, where the absorption contribution by high MW species increased. The log(K_{ow}) values indicated moderately hydrophobic (log(K_{ow}) >3) species which provided insight into their atmospheric persistence.

Chapter four investigates aged wildfire emissions during a smoke intrusion in Toronto. Size-resolved aerosols were collected for offline chromatographic analyses. Absorption was dominated by high MW species with moderate hydrophobicity, and elevated levels of alkylamines (NR_3H^+/NH_4^+ of 0.3-3.6) were observed. Alkylamines were not detected in fresh FIREX FireLab emissions, suggesting the ratios observed in Toronto reflect atmospheric aging and mixed urban-biomass burning influences rather than direct wildfire emissions.

This work demonstrates that BrC chemical and absorption properties evolve after emission, and highlights the importance of integrating chromatographic methods, laboratory experiments, and field measurements to constrain the evolution of BrC.

Acknowledgements

In the winter of 2018, I took an advanced analytical separation methods course with Dr. Cora Young. I initially took the class to learn more about analytical methods used in industry, but I did not realize it would change the trajectory of my path. I remember on the first day of class, Cora prompted the classic icebreaker where we went around the room, and each classmate had to share an interesting fact about themselves. I don't remember much of what was said, but I remember Cora telling us about her research, and in later classes, showing photos of sample collection in the Arctic. This was the first time I learned about the depths of environmental research and marked the beginning of my interest in atmospheric chemistry.

First and foremost, I would like to thank my supervisor, Dr. Cora Young. Without your belief in my capabilities, I would not have had the opportunity to be part of FIREX-AQ. You taught me it's okay to ask questions and how to approach challenges with intention and persistence. I am incredibly grateful for your support and mentorship throughout this time.

I would also like to thank Dr. Trevor VandenBoer for your guidance and perspective. You were the first to train me in chromatography, which became the foundation of much of this work. You encouraged me to think critically while always being willing to help.

I am also sincerely grateful to the FIREX-AQ team for teaching me the intricacies and logistics of field campaigns and for helping me develop scientific intuition. Your collective efforts made my research goals possible. In particular, I would like to thank Dr. Rebecca Washenfelder for your mentorship and encouragement. Thank you for showing me both the challenges and excitement of field work, for your willingness to help me improve, your scientific advice, and encouragement whenever I encountered setbacks.

I would also like to thank Dr. Robert McLaren for his thoughtful questions, encouragement, and support as a committee member from the beginning. Thank you to Dr. Neil Tandon and Dr. Ran Zhao for being a part of my defense committee.

To the past and present members of the CJY and VDB research groups, especially my IC colleagues and CB 324 office mates, thank you for the laughs, collaboration and countless conversations that made the challenges more manageable and the success more meaningful.

Finally, I would like to thank my family and friends for their support and for reminding me to take breaks when I needed it the most. To my friends' dogs, thank you for being a consistent source of comfort.

This work would not have been possible without all of you.

Table of Contents

List of Tables

List of Figures

List of Symbols, Nomenclature, and Abbreviations

°C	Degrees Celsius
Δ	Change (delta)
%	Percent
λ	Wavelength (lamda)
σ	Standard deviation (sigma)
μm	Micrometer
μL	Microlitre
μS	Micro-siemens
1D-VBS	One-dimensional volatility basis set
2D-VBS	Two-dimensional volatility basis set
ACN	Acetonitrile
AAE	Aerosol Angstrom Exponent
AMS	Aerosol Mass Spectrometer
BC	Black carbon
BrC	Brown carbon
C* or C_{sat}	Saturation concentration
Ca^{2+}	Calcium ion
Cl^-	Chloride ion
CO_2	Carbon dioxide
CO	Carbon monoxide
CWFIS	Canadian Wildland Fire Information System
Da	Daltons
DMA	Dimethylamine
DEA	Diethylamine
DIW	De-ionized water
EC	Elemental Carbon
ELVOC	Extremely low volatile organic compounds
FLAME	The Fire Lab at Missoula Experiments
FIRMS	Fire Information for Resource Management System US/Cananda
FIREX	Fire Influence on Regional to Global Environments Experiment

FIREX-AQ	Fire Influence on Regional to Global Environments and Air Quality
GPC	Gel-permeation chromatography
GFC	Gel-filtration chromatography
ha	Hectares
HPLC	High-performance liquid chromatography
HYSPLIT	Hybrid single-particle LaGrangian integrated trajectory model
H_2O	Water
iMPA	Iso-monopropylamine
IVOC	Intermediate volatile organic compounds
I/SVOC	Intermediate and semi-volatile organic compounds
IC	Ion chromatography
IC-CD	Ion chromatography with conductivity detection
K^+	Potassium ion
KBDI	Keetch-Byram Drought Index
Km	Kilometer
K_{ow}	Octanol-water partitioning coefficient
LOD	Limit of detection
LOQ	Limit of quantification
LVOC	Low-volatile organic compounds
LWCC	Liquid waveguide capillary cell
MAC	Mass absorption coefficient
m^3	Cubic meter
mAU	milli-absorption units
MBA	Monobutylamine
MEA	Monoethylamine
MEtA	Monoethanolamine
Mg^{2+}	Magnesium ion
MOUDI	Micro-orifice uniform deposit impactor
MSA	Methanesulfonic acid
MTBS	Monitoring Trends in Burn Severity
MPA	Monopropylamine

MW	Molecular weight
Na^+	Sodium ion
NAM	North American Mesoscale Forecast System
NaOH	Sodium hydroxide
NO_3^-	Nitrate ion
NR_3H^+	Alkylamine
NH_4NO_3	Ammonium nitrate
$(NH_4)_2SO_4$	Ammonium sulphate
NH_3	Ammonia
NIFC	National Interagency Fire Center
NOAA	National Oceanic and Atmospheric Administration
NO_x	Nitrogen oxides
NO_3	Nitrate radical
NVOCS	non-volatile organic compounds
OA	Organic aerosol
O:C	Oxygen to carbon ratio
OH	Hydroxyl radical
o.d.	Outer diameter
O_3	Ozone
PAH	Polycyclic aromatic hydrocarbons
PM	Particulate matter
$PM_{2.5}$	Particulate matter less than 2.5 μm
PM_{10}	Particulate matter less than 10 μm
PILS	Particle-into-liquid sampler
PO_4^{2-}	Phosphate ion
POA	Primary organic aerosol
pg	Picograms
NR_3H^+	Alkylamines
RF	Radiative forcing
RH	Relative humidities
RIE	Relative ionization efficiency

RPLC	Reversed-phase liquid chromatography
RT	Retention time
Slpm	Standard liter per minute
SO_4^{2-}	Sulphate ion
SOA	Secondary organic aerosol
SEC-UV	Size-exclusion chromatography with UV-vis detection
SRHA	Suwannee River humic acid
SVOC	semi-volatile organic compounds
Tg	Teragram
TEA	Triethylamine
TFIM	Trajectory-fire interception method
TMA	Trimethylamine
TOF	Time-of-flight
TOC	Total organic carbon
TSP	Total suspended particulate
U.S.	United States
UV-vis	Ultraviolet-visible region
VBS	Volatility basis set
WSOC	Water-soluble organic carbon
W/m^2	Watts per square meter

List of Appendices

Preface

This thesis is comprised of a series of manuscripts that are in preparation for or have been previously published in peer-reviewed journals. As a result, repetition of introductory and experimental details occurs throughout the chapters. All manuscripts were authored by Lisa Azzarello with critical comments provided by Dr. Cora J. Young. All research and manuscript preparation was conducted under the guidance of Dr. Cora J. Young. The specific contributions of co-authors are listed below.

Chapter 1: Introduction

Contributions – Prepared by Lisa Azzarello with editorial comments by Dr. Cora J. Young.

Chapter 2: Characterization of water-soluble brown carbon chromophores from wildfire plumes in the western US using size exclusion chromatography. *Atmospheric Chemistry and Physics* 2023, *23* (24), 15643–15654.

Lisa Azzarello[1], Rebecca A. Washenfelder[2], Michael A. Robinson[2,3], Alessandro Franchin[2,3,4], Caroline C. Womack[2,3], Christopher D. Holmes[5] Steven S. Brown[2,6], Ann Middlebrook[2], Tim Newberger [7], Colm Sweeney [7], Cora J. Young[1]

[1]Department of Chemistry, York University, Toronto, ON, M3J 1P3, Canada

[2]Chemical Sciences Laboratory, National Oceanic and Atmospheric Administration, 325 Broadway, Boulder, CO 80305, USA

[3]Cooperative Institute for Research in Environmental Sciences (CIRES), University of Colorado, Boulder, CO, 80309, USA

[4]Now at: National Center for Atmospheric Research, Boulder, CO, USA

[5]Earth, Ocean, and Atmospheric Science, Florida State University, Tallahassee, FL 32304, USA

[6]Department of Chemistry, University of Colorado Boulder, Boulder, Colorado, USA

[7]Global Monitoring Laboratory, National Oceanic and Atmospheric Administration, 325 Broadway, Boulder, CO 80305, USA

Contributions: Lisa Azzarello and Rebecca A. Washenfelder collected the online absorption measurements and samples for the offline analysis. Rebecca A. Washenfelder designed the BrC-PILS and processed the online measurements. Lisa Azzarello and Cora J. Young developed and completed the SEC-UV analysis. Michael A. Robinson, Alessandro Franchin, and Caroline C. Womack contributed to the collection of the water samples. Christoper D. Holmes contributed to the plume age analysis. Tim Newberger and Colm Sweeney contributed to the carbon monoxide

measurements. Steven S. Brown, Ann Middlebrook, Rebecca A. Washenfelder, Michael A. Robinson, and Alessandro Franchin contributed to the overall success of inflight sampling. The manuscript was written by Lisa Azzarello with input from all authors.

Chapter 3: Molecular Properties of Brown Carbon Aerosol from Biomass Burning of Wildland Fuels at the Fire Sciences Laboratory *ACS EST Air* 2025, *2* (5), 759–772

Lisa Azzarello[1], Rebecca A. Washenfelder[2,a] , Caroline C. Womack[2], Alessandro Franchin[2,3,b,] Ann M. Middlebrook[2], Cora J. Young[1,]*

[1]Department of Chemistry, York University, Toronto, ON, M3J 1P3, Canada

[2]Chemical Sciences Laboratory, National Oceanic and Atmospheric Administration, 325 Broadway, Boulder, CO 80305, USA

[3]Cooperative Institute for Research in Environmental Sciences (CIRES), University of Colorado, Boulder, CO, 80309, USA

[a]Now at: Cooperative Institute for Research in Environmental Sciences (CIRES), University of Colorado, Boulder, CO, 80309, USA

[b]Now at: National Center for Atmospheric Research, Boulder, CO, 80301, USA

Contributions: Rebecca A. Washenfelder designed the BrC-PILS and processed the online measurements. Ann Middlebrook and Alessandro Franchin operated the aerosol mass spectrometer and provided the data. Rebecca A. Washenfelder, Ann Middlebrook, Alessandro Franchin, and Caroline C. Womack contributed to the overall success of the online and offline sampling during the controlled burns at the Missoula Fire Laboratory. The manuscript was written by Lisa Azzarello with input from all authors.

Chapter 4: Investigating the role of aging on the organic and inorganic composition of size-resolved biomass burning aerosol.

Lisa Azzarello[1], Leyla Salehpoor[1], Gailmyra Fuentes[1], Teles C. Furlani[1a], Rebecca Washenfelder[2b], Caroline Womack[2] Trevor C. VandenBoer[1], Cora J. Young[1]

[1]Department of Chemistry, York University, Toronto, ON, M3J 1P3, Canada

[2]Chemical Sciences Laboratory, National Oceanic and Atmospheric Administration, 325 Broadway, Boulder, Colorado 80305, United States

[a]Now at: Ministry of the Environment, Conservation and Parks

[b]Now at: Research Affiliate Cooperative Institute for Research in Environmental Sciences (CIRES), University of Colorado, Boulder, CO, 80309, USA

Contributions: Rebecca A. Washenfelder and Caroline C. Womack filters collected during the FIREX FireLab 2016 campaign. Teles C. Furlani deployed the nanoMOUDI for sampling, Leyla Salehpoor supported the alkylamine analysis where this method was developed with Trevor C. VandenBoer. Lisa Azzarello and Gailmyra Fuentes prepped MOUDI samples for SEC-UV and IC-CD analysis. The manuscript was written by Lisa Azzarello with input from co-authors.

Chapter 5: Conclusions and Future Directions

Contributions: Prepared by Lisa Azzarello with editorial comments from Cora J. Young

Other publications during PhD

1. F. A. Rivera-Adorno, **L. Azzarello** et al. Aircraft Measurements from a U.S. Western Wildfire Demonstrating Day and Night Differences in the Chemical Composition and Optical Properties of Biomass Burning Aerosols and Their Atmospheric Evolution. American Chemical Society Earth and Space Chemistry. 2025.
2. F. A. Rivera-Adorno, J. M. Tomlin, N. Nahar Lata, **L. Azzarello** et al. Chemical Imaging of Atmospheric Biomass Burning Particles from North American Wildfires. American Chemical Society ES&T Air. 2025.
3. R. A. Washenfelder, **L. Azzarello**, et al. Complexity in the evolution of, composition, and spectroscopy of brown carbon in aircraft measurements of wildfire plumes. Geophysical Research Letters. 2022.

Chapter 1

Introduction

1.1 Wildfire background

Wildfires are a naturally occurring phenomenon in forested regions. Historically, fires played an important role in maintaining biodiversity within ecosystems and enabling evolutionary processes by creating open and closed landscapes to promote habitat heterogeneity. It has been suggested that broadly spaced resources due to wildfires influenced early hominid foraging behavior, potentially contributing to the evolution of bipedalism.[1] Fire-prone ecosystems are also abundant in flowering plants, pollinators, and herbivores, which is thought to have fostered chemical diversification in vegetation where many of these compounds enhanced flammability and today are widely used in industry for consumerism.[2] Historically, low-intensity surface fires prevented fuel accumulation and limited the occurrence of high-intensity wildfires. However, in the 20th century, the United States (U.S) implemented and overused fire suppression strategies that gradually accumulated understory fuels which contributed to the transition from surface fires to high-intensity crown fires.[3] Fire severity describes ecological impact and can be contextualized by damage to vegetation (high severity corresponds to > 80% overstory mortality, moderate severity describes 30-80% mortality, and low severity refers to < 30% of vegetation is killed).[4] Many western U.S. coniferous forests became susceptible to crown fires because of dense understory fuels which caused widespread vertical connectivity (ladder fuels connect ground layer to forest canopy).[5] As result, present-day wildfires are often more severe, widespread, and more ecologically disruptive.

In addition to fire suppression tactics, other drivers that contribute to wildfire occurrences include ignition sources, continuous fuels, drought conditions, and meteorological factors. Lightning is the primary natural ignition source and with shifts in climate there are changes to the spatial and temporal distribution of lightning strikes where its implications for wildfire activity is

an ongoing area of research.[6] Anthropogenic ignitions (e.g. those originating from campfires, powerlines, equipment sparks) have become increasingly important, particularly in wildland-urban interfaces. Anthropogenic influences have also modified fuels in ways that can both suppress and exacerbate wildfire spread. Urbanization has fragmented landscapes and reduced fuel continuity, which can decrease the spread of wildfire in certain regions. In contrast, overfire suppression has increased fuel loads which has enhanced susceptibility to ignition and fire spread, especially during drought conditions.[7] Elevated carbon dioxide (CO_2) levels further enhance wildfire spread by promoting plant growth which can increase fuel density and continuity across fire-prone landscapes.[8] In some regions invasive plant species further intensify wildfire risk. For example, during the 2020 Dome Fire, invasive grasses (red brome) in California's Mojave National Preserve grew and added continuous fuels between shrubs causing 43,473 acres to burn including 1.3 million Joshua Trees which are native to the land.[9]

Drought conditions are also an indicator of fire spread potential. Depending on the ecosystem, woody (e.g. boreal forests) or grassy (e.g. Great Plains, savannas), drought can increase or decrease the likelihood of fire spreading. In woody-dominated ecosystems, drought can increase the probability of fire because it creates continuous standing dead biomass. Contrastingly, in grassy regions, prolonged drought is associated with reduced fire activity because the density or continuity of fuel in these regions depends on rainfall. When drought limits biomass growth, less fuel is available to burn, which can result in fewer or smaller fires.[7] Meteorological conditions also govern fire behaviour; for example, high wind speeds enhance oxygen supply, increase evapotranspiration, and disperse embers while elevated temperatures and low humidity reduce energy required for ignition.[7]

Wildfire potential is commonly assessed using fire weather indices which utilize meteorological data. In North America, the Keetch-Byram Drought Index (KBDI)[10] and the Canadian Fire Weather Index (CFWI)[11] are used by the U.S Forest Service and the Canadian Forest Service for fire management practices.[12] The KBDI estimates flammability of organic matter using the daily maximum temperature and precipitation with values ranging from 0 (low fire potential) to 800 (extreme drought).[10] The CFWI also incorporates basic meteorological data to assess the moisture of organic soil layers and long-term moisture deficits, where typical CFWI values range from 0 to 20 while values that exceed 30 indicate extreme wildfire risk.[11] These indices are routinely applied to assess fire risk and resource allocation throughout North America.

1.1.1 Canadian wildfires

Canadian forests cover nearly 362 million hectares (ha), which comprise an estimated 8.5% of the global forested area.[13,14] Wildfires in Canadian forested land have always been present; however, in recent years wildfires in Canada have been record setting. Canada's climate is warming at twice the global rate where the mean annual temperature has increased 1.7°C since 1948[15] and the annual area burned in the country has steadily increased since the 1950s, where the length of wildfire season also increased in recent decades (Figure 1-1).[16] In central and western Canada, it is projected that fire-conducive weather will continually increase the frequency and intensity of wildfires.[17] A climate attribution study for eastern Canada during wildfire seasons between 1940 to 2023 indicated that anthropogenic influenced climate change has contributed to rising temperatures and decreasing relative humidities (RH).[18] In 2020, Wang et al. predicted that the annual area burned in Canada would increase to 11 Mha by the end of the 21st century.[17] However, in 2023, Canadian wildfires were so intense, a record breaking 15 million ha of land was burned, which was more than seven times the average annual burned area compared to the previous

four decades.[19] The year 2023 also coincided with the warmest and driest year since 1980[20] and the carbon emission total was estimated at 647 teragram (TgC), comparable in magnitude to India's annual fossil fuel emissions.[21]

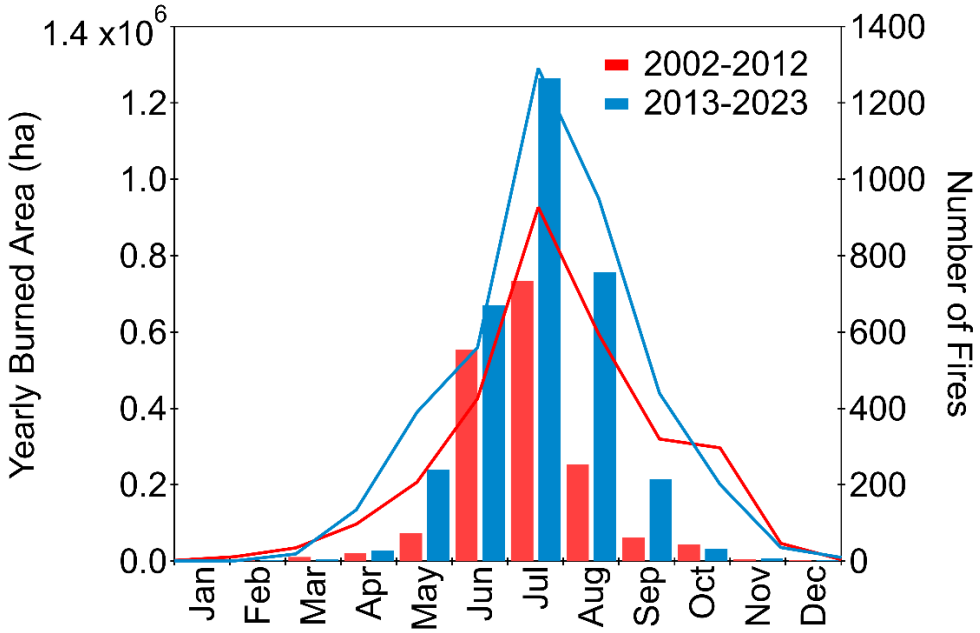

Figure 1-1. Average yearly burned area (bars) and number of wildfires (lines) in Canada by month from 2002-2021 and from 2013-2023.[22]

In Ontario, Canada, the forested landscape is dominated by boreal and taiga forests where some of the largest fires in Canada have burned.[23] These forests have a large percentage of coniferous trees which are susceptible to high intensity crown fires.[24] The wildfire season in 2021 was record setting for the province (Figure 1-2). Between April to October 2021 there were drought conditions that led to a total of 1198 forest fires which was above the ten-year average of 839 fires. A total of 793,325 ha burned in Ontario, which was over four times greater than the annual provincial average since 1990.[25] Figure 1-2 also shows that there is in overall increase in acres

burned since the early 2000s. This increase in wildfire activity has important implications on air quality and atmospheric chemistry in downwind urban regions.

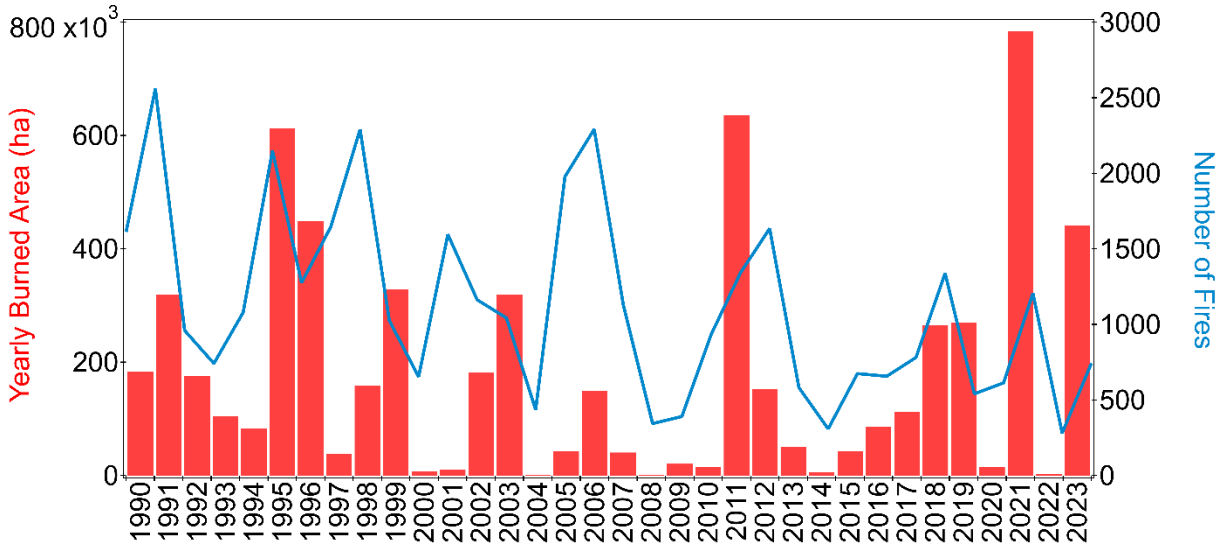

Figure 1-2. Average yearly burned area (right axis) and number of wildfires (left axis) in Ontario, Canada by year.[25]

1.1.2 Wildfires in the western United States

Historical wildfire activity in the western U.S. was mainly driven by climate, with biomass burning increasing during periods of elevated temperatures and extended drought conditions and decreasing when temperatures and drought declined.[26] Marlon et al. presented paleoenvironmental reconstructions and determined that fire activity across the western U.S. was in dynamic equilibrium with climate and human activities marked an impact on biomass burning after the late 1800s.[26] Anthropogenic impacts on forest fires in the western U.S. became pronounced following the Euro-American settlement in the late 19th century. Ignition patterns changed with land clearance, agricultural expansion, and the implementation of fire suppression. Additional land-use practices such as livestock grazing and the introduction of non-native species modified fuel

composition. As a result, since the late 1800s, wildfire activity in the western U.S diverged from trends predicted by climate alone.[26]

In recent decades, wildfire activity has intensified in terms of area of burned and fire severity. Historically, western U.S. forests mainly experienced frequent, low-severity fires that enhanced ecosystem resilience by limiting fuel accumulation and increasing resistance to drought.[27,28] Contrastingly, high-severity fires can result in long term forest loss with impacts on carbon storage and biodiversity. Annual area burned by high–severity fire increased eight-fold in western U.S. forests from 1985 to 2017.[29] More recent analyses from 1985-2022 indicated, during this period, total area burned increased by approximately an order of magnitude and area burned under "high severity" conditions increased 15-fold.[30] These increases have occurred in a range of forest types and linked to increasing fire season length and fuel aridity.[30] Parks et al. predicted continued intensification of these trends, with total area burned projected to increase by roughly 2.9 fold and area burned under high severity conditions by about 4-fold by the mid-21st century under current climate conditions.[30]

According to the Monitoring Trends in Burn Severity (MTBS), more than 90% of the wildfires in the western U.S. occur between May to September, coinciding with peak temperatures, low RH, and limited precipitation.[31] Records from the MTBS show that the mean annual area burned across the western U.S. during 2001 to 2019 was about 3.35 million acres, which was nearly double that of the previous period from 1984 to 2000 (1.69 million acres).[32] The significance of these trends was presented in the record breaking 2020 wildfire season; according to the National Interagency Fire Center (NIFC) report, the area burned by wildfires in 2020 wildfire season reached 8.8 million acres, more than five times the average during 1984 to 2000.[33,34] To illustrate these trends, Figure 1-3 shows wildfire statistical data for California.

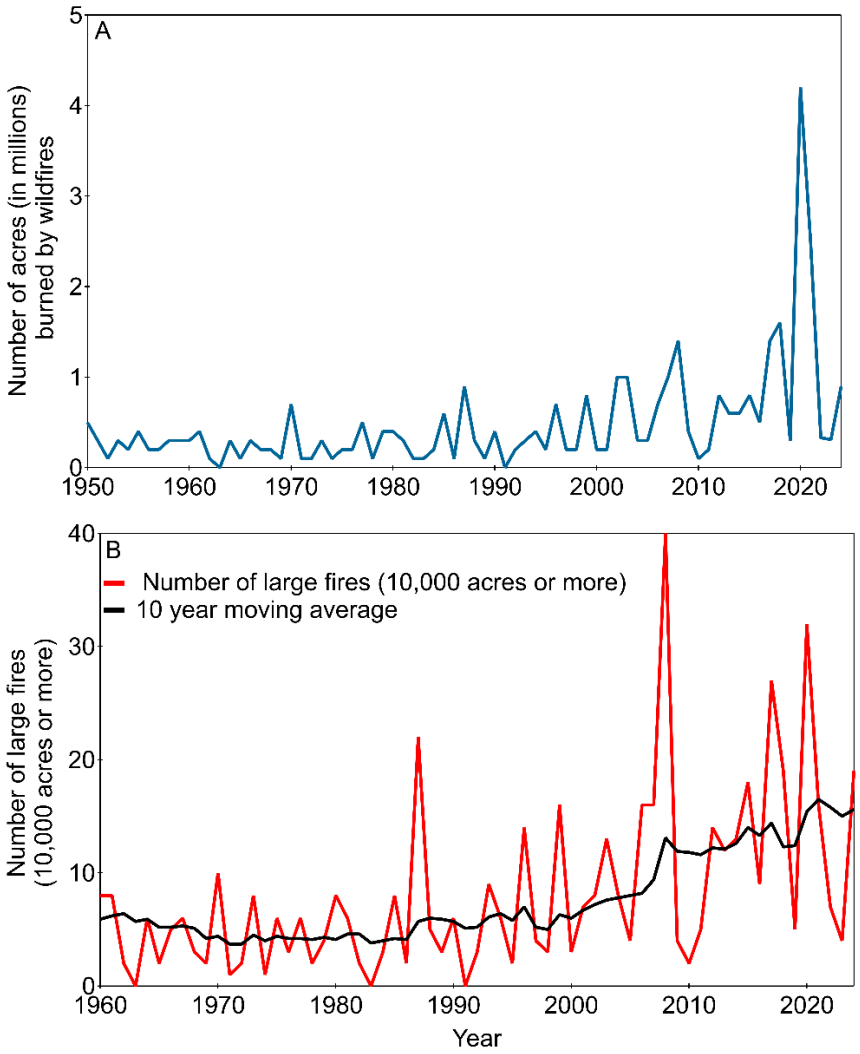

Figure 1-3. (A) Number of acres (in millions) burned by wildfires in California each year and (B) shows the number of large fires (10,000 acres or more) each year, with the red line indicating the 10-year moving average.[35]

The consequences of increasing high severity wildfires in the western U.S have atmospheric and societal impacts. Emissions are transported downwind, affecting air quality across the central U.S. Historically, wildfire season in the west generally did not overlap with severe weather seasons in the central U.S.; however, in recent years, the wildfire season is starting progressively earlier, which has resulted in wildfire seasons overlapping between the west and central U.S.[36,37] When wildfires occur simultaneously in these regions, this can result in severe

convective storms and weather hazards in the central U.S.[36] The consequences have also made an impact on long-term air quality trends. The U.S. experienced decades of declining particulate matter less than 2.5 μm ($PM_{2.5}$) emissions, largely attributed to the Clean Air Act;[38,39] however, this progress has stagnated or in some cases, even reversed in some regions of the U.S.[40] Recent analyses using ground- and satellite-based air pollution data from 2000 to 2022 quantified the contribution of wildfire smoke to $PM_{2.5}$ trends and deduced that since 2016, wildfires have influenced trends in average annual $PM_{2.5}$ concentrations in three-quarters of the U.S. On average, wildfire emissions have eroded about 25% of prior multi-decadal progress in reducing $PM_{2.5}$, where progress has been setback by 50% in the western U.S.[40] Wildfire $PM_{2.5}$ concentrations are unregulated under current air quality frameworks. In the absence of intervention, the impact wildfires have on national air quality trends is likely to continue.[40,41]

1.1.3 Societal impacts of wildfires

Wildfires are an increasingly important societal concern due to their growing environmental, economic, and public health impacts. Expansion of development near forested areas has increased the number of communities and infrastructure exposed to wildfire risk, resulting in substantial economic losses and displacement of communities.[42] In both Canada and the U.S., wildfires have caused significant economic disruption through damage to infrastructure. For example, in California, the estimated economic impact from lost infrastructure and homes, health costs, and business disruptions reached 148.5 billion in 2018 which translated to approximately 1.5% of the state's GDP.[43] In 2023, wildfires in U.S. were estimated to cost between $394 to $893 billion annually when accounting for factors such as diminished real estate value, health impacts from smoke, and watershed pollution.[44] In Canada, the cost of wildfire protection has increased by about $150 million per decade since the 1970s, exceeding $1 billion dollars in

six of the last ten years.[45] The 2016 wildfires in Fort McMurray, Alberta, illustrate the scale of these impacts as 85,000 people were displaced and over 2400 structures were destroyed which amounted to estimated $9 billion in total loses.[46]

Beyond their immediate destructive effects, wildfires significantly impact human health. Exposure to wildfire smoke has been associated with respiratory and cardiovascular illnesses,[47] increased hospital visits,[45,47,48] and premature mortality.[49] During June 2023 wildfire events in Ontario, Canada, $PM_{2.5}$ levels in Ottawa reached 79.3 $\mu g/m^3$ (13 times greater than the annual average), impacting nearly 9 million people across the province and corresponded to an estimated health cost of $1.28 billon.[50] Smoke from these Ontario wildfires in June 2023 was transported into New York City, where it was estimated that 9.2 mg of smoke particles were deposited into the lungs of exposed individuals, alongside a 40% increase in asthma related emergency department visits.[48] Amidst the more frequent and larger wildfires in recent years, these observations highlight that the state of wildfires, economic systems, and public health are interconnected. This underscores the importance of assessing the societal impacts to develop and inform mitigation strategies and public health responses to wildfire events.

1.2 Wildfire emissions: atmospheric particulate matter and size distribution

To assess the atmospheric chemistry of an air mass, natural and anthropogenic sources must be considered. Wildfires can be considered natural sources when ignited by lightning or anthropogenic when started by humans. Regardless of ignition type, wildfires are an important source of particulate matter (PM), volatile organic compounds (VOCs), nitrogen oxides, and carbon species such as elemental carbon (EC), brown carbon (BrC), methane (CH_4), CO_2, and carbon monoxide (CO) to the atmosphere (Figure 1-4). After emission, these species are transported and undergo a range of chemical and physical transformations in the atmosphere which

impact air quality. Particulate matter is an important metric when assessing air quality standards. Standards have evolved over time, shifting from mass of total suspended particulate (TSP) to mass of suspended particulate less than 10 μm in size (PM_{10}), and then further modified to consider $PM_{2.5}$. The rationale behind this progression reflects human health concerns; larger particles are filtered by the upper respiratory tract, while particles less than 2.5 μm are respirable.[51]

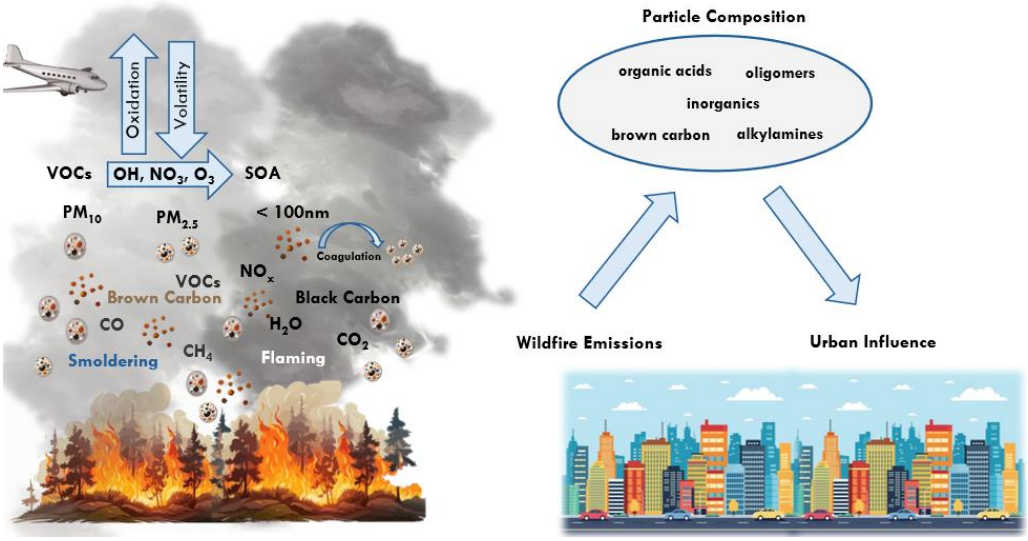

Figure 1-4. Wildfires are an important source of PM, VOCs, nitrogen oxides, and carbon species such as EC, BrC, CH_4, CO_2, and CO to the atmosphere. After emission, these species are transported and undergo a range of chemical and physical transformations, which can have implications on urban air quality.

1.2.1 Particulate matter: size distribution

Particulate matter can be solid or liquid with diameters between ~0.002 and ~100 μm and can be directly emitted (primary) or formed in the atmosphere (secondary source).[52] Particulate matter properties that are important to consider when assessing their role in atmospheric processes include: number concentration, particle size distribution, chemical composition, and optical properties. Particle size is important for both human health concerns and for determining aerosol chemistry and physics in the atmosphere; therefore, it is important to describe our understanding of particle size distribution and its evolution. Coarse mode particles (>2.5 μm) are typically emitted

via mechanical processes, such as wind-blown dust or sea-spray bubbles. Transport of coarse mode particles in the atmosphere can occur via convective processes; however, if large enough, they can be removed by gravitational settling.[52] Fine mode particles (<2.5 μm) include the accumulation range (0.08 to ~2μm) and the nuclei range (also known as Aitken; 0.01 to 0.08 μm). Particles in the accumulation range are typically formed by the coagulation of nuclei-range or with other accumulation range particles, as well as through the condensation of low volatility species. Particles in the nuclei range form in the atmosphere by gas-to-particle conversion or directly from combustion sources, where these particles act as nuclei for the condensation of low vapour pressure gaseous species allowing them to grow to accumulation size. The ultrafine mode consists of particles < 0.01μm and are typically produced by homogenous nucleation. Although, the nuclei range and ultrafine mode account for the majority of particle number, the accumulation range represents a large fraction of the total aerosol surface area.[52]

Due to differing sources and secondary processes in the atmosphere, chemical compositions can vary depending on the size range. Secondary PM can form through multiple pathways which can be summarized: (i) gas-phase reactions forming products with low vapour pressure (e.g. reactions between aromatics with hydroxyl radical (OH) to form oxygenated products) that subsequently nucleate to form new particles or condense onto pre-existing particles or coagulate, (ii) heterogeneous reactions between gases and existing particles to form condensed-phase products, and (iii) aqueous-phase chemistry within fog, cloud, or aerosol particles. Ultrafine mode and nuclei range particles tend to contain secondary species such as sulphate and oxidized organics. Particles in the accumulation range derived from combustion processes typically contain EC and BrC species. The composition of coarse particles can also reflect their sources; for example, containing sea salt (Na^+, Cl^-), dust minerals, or biological matter (e.g. pollen).[52]

1.2.2 Evolution of particulate matter size distribution

Wildfires are an important source of aerosol. The toxicity of PM to human[53,54] and its radiative effects[55] has been linked to particle size. Particle size distributions can vary depending on fuel characteristics and combustion conditions (flaming or smoldering) and evolve as smoke ages (condensation and coagulation).[56–58] Flaming and smoldering conditions can produce different size ranges which can reflect differences in temperature, oxidation efficiency, and particle number concentrations. Previous laboratory and field studies assessed the impact burn and measurement conditions have on size distribution. Hosseini et al. conducted controlled combustion experiments of western U.S. fuels and showed that particle size increased during flaming conditions (~0.5 μm) and during smoldering combustion, the size distribution was bimodal (around 0.01 and 0.05 μm).[56] This observation is consistent with high combustion temperatures producing supersaturated vapours which can cool and condense onto existing particles and due to the high particle concentration coagulation is enhanced. However, fuel moisture can complicate this interpretation; Chakrabarty et al. conducted controlled burns of fuels with varying moisture levels; the count mean diameter for dry fuels was 0.03 to 0.07 μm and this range increased to 0.12 to 0.14 μm for wet fuels.[59] This observation may appear contradictory to the findings presented by Hosseini et al. because when wet fuels burn smoldering conditions typically result. Flaming conditions can promote more particle growth compared to smoldering under the same fuel conditions; however, wet fuels contribute additional water vapor, where condensation and coagulation processes are enhanced so the average particle size can increase. These laboratory studies demonstrate the complexity in assessing the chemical and physical reactions that impact size distribution within a smoke plume.

In addition to measuring localized particle size distribution, to thoroughly assess the climate and health impacts of PM emitted from wildfires, we must assess the evolution of this distribution. Aerosol number size distribution describes the number of particles per unit volume of air as a function of particle size. As a smoke plume ages, the distribution can shift to larger sizes during aging due to condensation and coagulation.[60–63] Field studies have shown that smoke aged less than 1 hr was dominated by particles with median diameters between 0.1 μm to 0.15 μm, and as the smoke aged to several days, the median diameters increased to 0.2 to 0.3 μm.[61] Previous modelling studies suggested that coagulation had the most impact on particle diameter at high particle concentrations with slow dilution rates[57,58] and condensation of secondary organic aerosol (SOA) can further shift the size distribution.[64–66]

Biomass burning also emits volatile and semi-volatile primary organic aerosol (POA), which can evaporate during plume dilution and shift the size distribution by decreasing particle sizes. The net impact of organic aerosol (OA) condensation and evaporation on particle size distribution is variable because these two pathways can occur simultaneously in smoke plumes, with wildfire size, intensity, and dilution rate influencing the OA concentration in the center and perimeter of the smoke plume.[67] Airborne measurements by June et al. observed that high initial smoke concentration plumes (OA > 1000 ug/m^3) exhibited more evaporation after the first transect than in lower concentration plumes (OA < 100 ug/m^3). As a result, particle diameters in more dense plumes grew more rapidly, with diameter growth of over 100 nm in 8 hrs despite having a net decrease in OA enhancement ratios, demonstrating that coagulation was the primary cause of growth with the rate being influenced by dilution.[67] Changes in particle size during plume aging can also influence the persistence of distinct particle morphologies. For example, measurements during an urban smoke intrusion showed that submicron particles (0.15 μm to 0.45 μm), enriched

with carbon and near spherical in shape, consistent with tar balls, penetrated indoor spaces.[68] Although their formation pathway is uncertain, these can form during aging through condensation of gas-phase organics, dehydration reactions, and polymerization of organics.[69] These findings demonstrate that particle size distribution evolves during atmospheric transport and investigating the persistence of aerosol from biomass burning is important for human health concerns as residential filtration systems can be inefficient at trapping submicron particles.

1.3 Wildfires impact on radiative forcing

Radiative forcing (RF) describes changes in the Earth-atmosphere energy balance when the amount of incoming solar radiation differs from the amount of outgoing infrared radiation. The imbalance between the incoming shortwave radiation from the sun and outgoing longwave radiation emitted as heat alters the global radiative budget.[70] Radiative forcing is measured in watts per square meter (W/m^2) and refers to a species impact to change the radiative flux of the Earth-atmosphere relative to the year 1750 because prior to the industrial revolution, incoming and outgoing radiation was close to balanced.[71] Greenhouse gases (H_2O, CO_2, CH_4, N_2O) absorb infrared radiation which is radiated back to Earth's surface, and produces a net warming effect. Aerosols also have an impact on climate because they can intensify or mitigate the effects of greenhouse gases.[72] Aerosol can scatter or absorb solar radiation where species that scatter have a cooling effect (negative RF) and absorption has a warming effect (positive RF). The efficiency with which aerosols scatter or absorb radiation is dependent on the wavelength (λ) of the radiation, the distribution of particle sizes, their shapes, and on their refractive index which is influenced by their chemical composition and mixing state.[73] Absorbing aerosol contain carbonaceous species such BC and BrC whereas scattering is associated with particles composed of non-absorbing materials such as sulphates.[74] When particles are smaller than the wavelength of incident radiation,

this is described as Rayleigh scattering which preferentially scatters shorter wavelengths such as blue light. Wildfire smoke introduces larger particles that scatter light though Mie scattering and contain light-absorbing species like BrC which absorbs in the UV-vis region. This combined scattering and absorption of shorter wavelengths reduces the transmission of blue light, allowing longer wavelengths such as red and orange to pass, which can produce the characteristic orange or red discoloration of the sky during smoke events.[75]

On a global scale, atmospheric aerosol mass is estimated to be dominated by (listed in decreasing mass abundances): mineral dust, sea salt, natural and anthropogenic sulphates, carbonaceous aerosol including emissions from biomass burning.[76] Although biomass burning aerosol represents a fraction of total aerosol mass, they are of importance due to the increase in wildfire activity and their diverse optical properties. Globally, wildfire aerosol are estimated to have a net direct radiative effect of 0.17 W/m^2.[77] Assessing absorption properties of OA from wildfires is complex because of their evolution downwind driven by changes in particle size distribution and chemical composition.[64,78–80] Field observations have demonstrated the complexity between wildfire aerosol and its radiative effects. During the Biomass Burning Operational Project (BBOP), smoke sampled 2-3.5 hrs downwind of fires in the Pacific northwest exhibited increased scattering (normalized for dilution) with age; this study suggested that wildfire plumes may exert a net-cooling effect within a few hours of emission.[81] These findings highlight the importance of considering the evolution of aerosol optical properties when assessing the radiative impacts of wildfire emissions.

1.3.1 Brown carbon impact on radiative forcing

Black carbon (BC) is emitted from wildfire and is a well characterized absorber of solar radiation. Black carbon has a positive radiative forcing (estimated to be+0.61 W/m^2 to +1.1 W/m^2

[77,82]) that is globally second only to CO_2 (+1.56 W/m^2 [77]). Wildfires are also an important source of BrC which absorbs in the ultraviolet-visible region (UV-vis); uncertainty still remains of its impact on the global radiative budget.[83] Brown carbon emissions have been reported to be two orders of magnitude larger than BC, making atmospheric BrC absorption important to investigate.[78] Previous studies estimate the global direct radiative effect of BrC absorption range between +0.03 W/m^2 and +0.57 W/m^2.[84,85] This large range reflects uncertainties in BrC composition and optical properties as there is a vast chemical diversity of BrC chromophores. Brown carbon refers to a complex mixture of compounds spanning a range of molecular weights (MW) and sizes, functional groups, volatilities, and solubilities.[86–90] Field measurements demonstrate the complexity of representing BrC in chemical transport models because its magnitude in absorption has shown to either decrease or increase with atmospheric aging. Brown carbon can undergo photobleaching (also referred to as whitening) driven by photolysis and reactions with atmospheric oxidants (e.g. OH, O_3), which leads to the degradation of chromophores and therefore can decrease light absorption over the course of hours to days.[87–89,91] Wang et al. implemented a photobleaching scheme in a chemical transport model and observed the global BrC absorption direct radiative effect decreased from +0.1 W/m^2 to +0.048 W/m^2 when they included photobleaching.[92] The work by Brown et al. also supports the importance of considering atmospheric processing to assess the impact of BrC; this study found global BrC absorption direct radiative effect values of +0.13 W/m^2 and +0.06 W/m^2 with and without photobleaching, respectively.[93]

These modelling studies that incorporated photobleaching processes demonstrate a decrease in estimated RF which emphasizes the importance of representing aging processes for BrC. However, to further complicate the evolution of BrC absorption properties, there have been

studies that have observed absorption enhancement. High NO_x environments and nighttime chemistry involving the nitrate radical (NO_3) can slow down photobleaching due to formation of nitrogen containing chromophores.[86,94] For example, polycyclic aromatic hydrocarbons (PAHs) are commonly emitted from biomass burning and can undergo gas-phase and heterogeneous oxidation with NO_3 to produce nitro-PAHs that are less volatile and more light-absorbing than their precursors.[95] The scarcity of nighttime observations further contributes to the uncertainty in quantifying the impact of BrC on the global radiative budget.

The optical properties of carbonaceous aerosol are commonly characterized by assessing the wavelength dependence on absorption:

$$\text{Equation 1.1 } MAC(\lambda) = K\,\lambda^{-AAE}$$

where MAC is the mass absorption coefficient (or mass absorption efficiency) measured in units of cm^2/g, K is constant related to aerosol mass concentration, and AAE is the aerosol angstrom exponent.[96–98]

The AAE quantifies how strongly an optical property (absorption or extinction) depends on wavelength. The most common way to calculate AAE is:

$$\text{Equation 1.2 } AAE = \frac{-log\left(\frac{\sigma_{\lambda 1}}{\sigma_{\lambda 2}}\right)}{log\left(\frac{\lambda_1}{\lambda_2}\right)}$$

where σ represent optical property (absorption or scattering).[99,100] The AAE quantifies how strongly absorption depends on wavelength and is represented by the slope of a log σ versus log λ. When AAE is close to 1, this indicates that absorption is dominated by BC, and an AAE greater than 1 indicates absorption is dominated by BrC.[97] The AAE increases with decreasing particle size; it will typically have a value of 2 when scattering process is dominated by fine particles and close to zero when scattering is dominated by coarse particles.[99] Previous studies have distinguished BC from BrC; Kirchstetter et al. observed a wavelength dependence with an AAE

value of 2.2, which after solvent extraction of organic constituents the AAE decreased to 1.3.[101] However, because there are additional effects associated with external versus internal mixing of BC, organics, and BrC within aerosol, the threshold values that differentiate BC from BrC in field samples is uncertain.[102,103] For example, coatings on BC with non-absorbing components results in a lensing effect which focuses more light onto the absorbing BC core.[104,105] The extent of this effect is determined by the wavelength dependent refractive index of the non-absorbing organic material, particle morphology, and coating thickness.[102,106] In a modelling study by Lack and Cappa, they showed that AAE values, ranging from 1-1.6 can be observed for internally mixed OC/BC particles and suggested that when AAE exceeds 1.6, this should be considered BrC.[102]

Overall, the radiative impact of wildfire aerosol and BrC is governed by complex relationships between emissions, particle size distribution, chemical composition, and aging processes that alter chemical composition. To better understand the contribution of BrC to the radiative budget it is necessary to integrate controlled laboratory studies and field campaigns to better inform modelling approaches that account for evolving optical properties of organic aerosol.

1.4 Research campaigns: controlled burns and airborne measurements

To assess the evolution of species emitted from biomass burning, it is necessary to characterize the chemical composition of primary emissions. Controlled burns allow emissions to be measured under defined conditions, either in the absence of atmospheric aging or with controlled processing. By selecting specific fuel types and combustion conditions, controlled burns provide insight into the chemical, physical, and optical properties and enable comparisons across ecosystems and geographical regions. For example, Lyu et al. investigated emissions from boreal peat from northern Alberta, Canada,[107] Glenn et al. measured emissions from fuels found in ecoregions within southeastern U.S,[108] Schnitzler et al. burned red oak which is widely found in

eastern Canada,[109] and Fleming et al. summarized compounds emitted from fuels characteristic of the western U.S.[90] The culmination of controlled burn studies established the basis for understanding how fuel type and combustion conditions influence the composition of biomass burning emissions prior to atmospheric aging.

Among controlled burn experiments, laboratory-based fire research facilities have provided systematic analyses. Major research campaigns were conducted at the U.S. Forest Service Fire Science Laboratory in Missoula, Montana. The Fire Lab at Missoula Experiments (FLAME) and FireLab studies were a series of research campaigns that took place from 2006 to 2012 and aimed to investigate physical, chemical, and optical properties of primary emissions. Subsequent campaigns aimed to expand the scope by including fuels found in the southeastern, southwestern, and northern U.S. as well as fuels that commonly burn throughout Asia and Africa (FLAME-4 campaign). The series of FLAME and FireLab campaigns evolved into the FIREX (Fire Influence on Regional to Global Environments Experiment) FireLab 2016 study which focused on improving our understanding about emissions from fuels specifically characteristic to the western U.S.

Early FLAME campaigns (FLAME-1 and FLAME-2) provided general insight into the size distribution and chemical composition of biomass burning aerosol. Levin et al. reported that the mean particle diameter ranged from 0.20 to 0.57 μm across a range of fuels and offline filter-based analysis using ion chromatography with conductivity detection (IC-CD) showed that the dominant inorganic ions included potassium (K^+), sodium (Na^+), ammonium (NH_4^+) chloride (Cl^-), nitrate (NO_3^-), and sulphate (SO_4^{2-}), with relative abundances varying between fuel types.[110] While the early FLAME and FireLab campaigns established the chemical and physical characteristics of primary biomass burning emissions, the subsequent FIREX FireLab 2016

experiment increased emphasis on optical properties of OA, including investigating the properties of BrC. Fleming et al. reported BrC chromophores include high and low MW compounds with conjugated systems and diverse functional groups (e.g. vanillic acid, umbelliferone, sinapaldehyde, and kaempferol).[90] Jen et al. applied two-dimensional gas chromatography and observed intermediate and semi-volatile organic compounds (I/SVOCs) including PAHs, oxygenated aromatic heterocycles, benzoic acids, oxygenated aliphatic, and nitro-organics.[111]

Although laboratory-based measurements are important to characterize the properties of primary biomass burning emissions, the evolution of aerosol composition and optical properties, including that of BrC is influenced by atmospheric aging (e.g. dilution, photolysis, oxidation reactions). Airborne field campaigns and outdoor ground-based measurements address the limitations of controlled burns and can expand the scope of our understanding. By measuring smoke plumes downwind of active fires, aircraft and ground-based sampling studies capture the effects of atmospheric aging and allows us to characterize emissions over timescales ranging from hours to days. Various research campaigns that employed the use of aircrafts for airborne measurements to study the evolution of biomass burning emissions include the Studies of Emissions and Atmospheric Composition, Clouds and Climate Coupling by Regional Surveys (SEAC^{4}RS) (2013), Fire Influence on Regional to Global Environments and Air Quality (FIREX-AQ) (2019), and Western Wildfire Experiment for Cloud Chemistry, Aerosol Absorption, and Nitrogen (WE-CAN) (2018); where all these studies assessed the evolution of absorption properties of BrC downwind of wildfires. Zeng et al. highlights the complexity of BrC aging by summarizing BrC absorption as a function of plume age for over 15 fires sampled during FIREX-AQ and SEAC^{4}RS and found that absorption data is highly variable with no clear trend describing absorption evolution within the first 10 hrs of aging. In some sampling flights, absorption

increased, decreased, or remained consistent highlighting the competing roles of photobleaching and secondary BrC formation.[112] This variability emphasizes the continued importance of controlled laboratory studies, which can be designed to investigate specific processes such the effects of photooxidation and absorption enhancement.[87,113,114]

Together, laboratory experiments, airborne observations, and ground-based measurements provide a complementary framework for interpreting the evolution of BrC in the atmosphere. Controlled burns constrain primary emissions while real-world measurements capture the effects of multiple aging processes. The integration of controlled burns and airborne measurements is essential for improving our understanding of observed variability in BrC absorption and its impact of the global radiative budget.

1.5 Brown carbon: sources and composition

The brown colour of BrC results from a combination of chromophores that have varying abilities to absorb light.[115] The chemical diversity results in variability in optical properties, reactivity, and atmospheric lifetimes, contributing to uncertainty in its radiative effects. The two dominant sources of BrC to the atmosphere include primary emissions by combustion processes, where wildfires are an important source and secondary formation in which BrC species are produced or modified during atmospheric processes after emission.

The chemical composition of primary BrC is influenced by fuel type and combustion conditions. Primary BrC directly emitted from combustion reflects the chemical diversity produced by the pyrolysis of lignin and cellulose.[116] Smoldering conditions are characterized by lower temperatures and incomplete combustion which tends to favour the production of BrC whereas flaming combustion occurs at higher temperatures releasing complete combustion products. Primary BrC consists of a complex mixture of aromatic and oxygenated compounds

(Figure 1-5), including phenols, methoxyphenols, nitroaromatics, and PAHs. Nitroaromatic compounds are amongst the most well-established BrC chromophores and have been identified in the gas-phase and in aerosol PM.[117–119] When present in the particle phase, these compounds can contribute to BrC light absorption. Nitroaromatic compounds can form through secondary reactions with aromatic hydrocarbons such as benzene, toluene, and xylene under high NO_x and flaming conditions.[120–124] Although primary BrC can dominate near source absorption, the composition and optical properties evolve following emission.

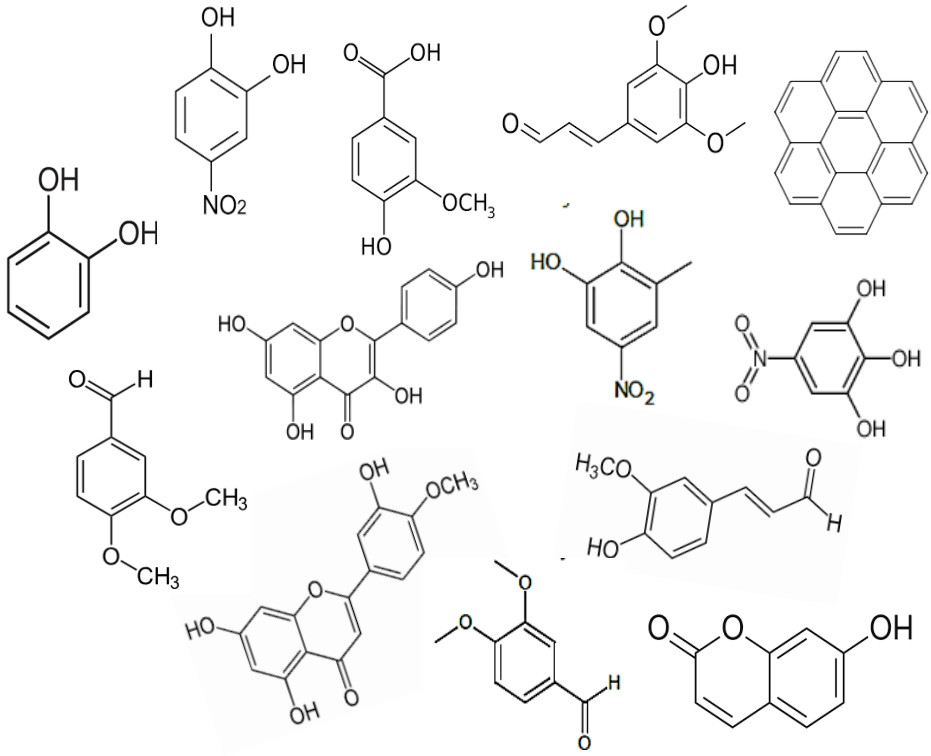

Figure 1-5. Examples of molecular structure representing BrC chromophores.

1.5.1 Secondary processes that lead to BrC formation

Secondary BrC formation is driven by a range of atmospheric processes including gas-phase oxidation, aqueous phase reactions, heterogeneous oxidation by oxidants such as O_3, OH, and NO_3, and photochemical reactions. These processes can enhance absorption through the

formation of more absorbing compounds or reduce absorption through the degradation of chromophores. The formation of light-absorbing molecules from gas-phase reactions that condense to from SOA have been observed to produce secondary BrC. The nitration of aromatic precursors in the presence of NO_x or NO_3 is an important pathway, where absorptivity of SOA generally increases with NO_x.[119,125,126] For example, the oxidation of toluene in high NO_x conditions formed over 15 absorbing molecules, with nitroaromatics accounting for 60% of the absorption measured between 300 to 400 nm.[127] Similarly, catechol, emitted from biomass burning reacts readily with OH or NO_3 radicals to form SOA, where the dominant product is 4-nitrocatechol.[125,128]

Atmospheric liquid water impacts the fate of aerosol and water-soluble gases and is a medium for BrC formation. Aerosol particles can take up water at elevated RH, enabling aqueous-phase reactions driven by sunlight through direct photolysis and indirectly by forming oxidants (e.g. OH). Laboratory studies by Wong et al. investigated the implications of exposing biomass burning derived aqueous extracts to UVB light and observed that high MW and low MW species underwent initial photoenhancement, followed by photobleaching.[129] Similarly, oxidation of nitrophenols by aqueous phase OH resulted in an initial enhancement of in absorption by formation of oxygenated compounds, followed by absorption loss due to fragmentation from cleavage of aromatic rings with continued OH oxidation.[130,131] Further, excited organic chromophores can act as photosensitizers in the aqueous phase; upon light absorption BrC species can form excited triplet state ($^3C^*$), which can participate in secondary chemistry or can produce singlet molecular oxygen ($^1O_2$).[132–136] An additional aqueous phase pathway includes photonitration of functionalized aromatics (e.g. phenol, guaiacol, methylcatechol, and vanillin) in the presence of UV light and dissolved nitrite to form nitroaromatic compounds.[137–139]

Secondary BrC can also form through condensed-phase reactions that produce oligomeric species. Oligomers derived from aromatic precursors have been observed in SOA, where they can form from reactions with aromatic monomers such as phenol, guaiacol, syringol, vanillin, and other phenolic carbonyls during photochemical processing and OH oxidation.[140] Oligomers potentially contribute to BrC absorption as high MW species which have been identified in field samples.[141,142] The mechanism of formation of oligomer compounds is through radical coupling reactions either through an oxygen atom from a hydroxyl function group or a carbon atom in the aromatic ring.[132] Aromatic oligomers can absorb light at longer wavelengths than individual monomers due to the extended π-conjugation.[143]

Heterogenous reactions also contribute to secondary BrC. For example, O_3 reacts readily with unsaturated compounds, and more slowly with aromatics, including PAHs.[144] Ozonolysis of particulate products such as methylglyoxal can result in smaller organic acids (e.g. formic, acetic, and pyruvic acids) through fragmentation, while formation of carbonyl groups can enhance absorption enough to offset bleaching from bond cleavage.[145] Alkylamines are also of interest in atmospheric aerosol chemistry because they contribute to secondary BrC formation. Alkylamines are emitted from biogenic sources (e.g. marine organisms,[146] and biomass burning[147]) and anthropogenic sources (e.g. vehicles exhaust[148] and treatment of sewage and waste[149]). Although alkylamine concentrations are typically 1–3 orders of magnitude lower than NH_3 in the atmosphere, they still can play an important role aerosol chemistry because they compete with NH_3 in acid-base reactions that drive gas-particle partitioning.[150]Alkylamines are generally more basic (pK_a = 9.25–10.98) than NH_3 (pK_a = 9.25), which can promote the formation of stable salts and particle growth. In addition to acid-base chemistry, alkylamines can also react with organic compounds to form light-absorbing species. Small water-soluble carbon compounds such as

hydroxyacetone, glycolaldehyde, glyoxal, and acetaldehyde could undergo browning reactions or aldol condensation reactions in presence of ammonium salts[151–154] or primary amines.[155–157] These reactions can produce nitrogen-containing chromophores such as imines and enamines where the formation depends on the structure of the precursor amine (e.g. primary or secondary) and the availability of carbonyl species.[158] Laboratory studies by De Haan et al. showed that condensed-phase reactions between monomethylamine (MMA) and glyoxal can produce oligomers, imidazole, and other light-absorbing compounds, where these studies highlight potential pathways in which alkylamines contribute to BrC chemistry.[157]

1.6 Biomass burning analysis

1.6.1 Volatility basis set and thermodenuder experiments

Biomass burning derived OA consist of species with varying volatilities. The speciation of intermediate and semi-volatile organic compounds is important to assess the competing effects of POA volatilization and SOA formation.[159] The distribution of gas and particle phases can shift with changes in emissions, dilution, temperature, and chemical transformation. Donahue et al. introduced a framework referenced as the one-dimensional volatility basis set (1D-VBS) where organic aerosol components are grouped into bins according to their saturation concentrations (C* or C_{sat}), which is estimated from vapour pressure and MWs of pure compounds. Each bin in the VBS is separated by one order of magnitude in saturation concentration.[160] Below are the equations that represent partition coefficient, ξ_i, and defines the saturation concentration, C_i^* (C_{sat}):

Equation 1.3 $$\xi_i = \left(1 + \frac{C_i^*}{C_{OA}}\right)^{-1};$$

Equation 1.4 $$C_{OA} = \Sigma C_i \xi_i$$

Equation 1.5 $$C_i^* = \frac{C_i^{vap} C_{OA}}{C_i^{aer}} = \frac{M_i 10^6 \zeta_i \, p_{L,i}^{\circ}}{760 \, RT}$$

C_{OA} is the mass concentration of condensed-phase organic molecules (ug/m^3), ξ_i is the partition coefficient, C_i^{aer} is the mass concentration of compound i (ug/m^3), C_i^{vap} is the concentration in the vapor phase (ug/m^3), M_i is MW (g/mol), ζ_i is the activity coefficient (assumed to be one), $p_{L,i}^{\circ}$ is the saturation vapor pressure of compound i (in torr), R is the gas constant and T is the temperature (in Kelvin).[160] The 1D-VBS evolved to include a second dimension; in addition to saturation concentration, this two-dimension volatility set (2D-VBS) considers the oxygen to carbon ratio (O:C) to further describe volatility and chemical evolution of OA. This framework asserts that organic compounds with: (i) C* < 0.01 ug/m^3 are in the condensed phase (non-volatile organic compounds, NVOCs), (ii) C* < 0. 1 ug/m^3 refers to the compounds mostly in the condensed phase (low-volatility organic compounds, LVOC), (iii) 1 < C* < 100 ug/m^3 fractions of these compounds will be found in both gas and particle phase (semi-volatile organic compounds, SVOC), (iv) C* > 1000 ug/m^3 refers to the compounds mostly in the gas phase (intermediate volatility organic compounds, IVOCs), and (v) C*>10^6 are volatile organic compounds (VOC), which are compounds represented in gas-phase chemistry.[161] The 2D-VBS characterizes the behaviour of OA mixtures with the following parameters: (i) carbon-carbon interaction (non-polar), (ii) oxygen-oxygen interactions (polar), and (iii) the non-ideal carbon-oxygen interaction.[162] In considering these three types of interactions that exist within organic aerosol mixtures, Donahue et al. showed that the log(C_{sat}) has a linear relationship with the number of carbon atoms – the greater number of carbon atoms the lower log(C*); therefore, the condensed phase is favoured. Further, upon oxidation, the addition of oxygen-containing functional groups also impacts log(C_{sat}). The addition of one hydroxyl group decreases C_{sat} by approximately two bins per added oxygen and the addition of a carbonyl group decrease C_{sat} by one bin per added oxygen. Therefore, more oxygenation corresponds to a lower C_{sat} which represents lower volatility

due to increased intermolecular interactions between condensed phase polar molecules capable of hydrogen bonding.[162]

To measure the volatility distribution of OA, thermal denuding experiments have been utilized.[163] Thermodenuder experiments with varying temperatures can be used to calculate mass fraction remaining or absorption fraction remaining as a function of temperature where the thermodenuder temperature is converted to C_{sat} using empirical measurements of known compounds.[163] In a thermodenuder, particles are flowing and heated to a fixed temperature and the evaporation rate of compounds from particles is determined by thermodynamic properties of the compounds (vapor pressure and enthalpy of vaporization), the mole fraction of the compound within the particles, and the strength of the of the interactions of particle components (i.e., carbon-carbon, carbon-oxygen, and oxygen-oxygen).[164] In addition to volatilization, aerosol mass measured after thermal denuding can also be affected by physical particle losses within the instrument, such as diffusion to the walls or thermophoretic migration towards cooler surfaces if there is a temperature gradient. These losses can be characterized by measuring the ratio between ambient and thermal denuded non-volatile, inorganic aerosol species (e.g. sulphate or chloride) and applying a correction factor.[165]

The extent of gas-particle partitioning of a smoke plume is dependent on biomass burning OA concentration and the air temperature; therefore, variability in the range of $\log(C_{sat})$ between studies is observed. For example, Pagonis et al. conducted airborne thermodenuder measurements during FIREX-AQ where the thermal denuder was heated to 40 to 45 °C to simulate evaporation if smoke was transported to lower altitudes.[165] In that study, the volatility of OA was evaluated using the enhancement ratio $\Delta PM/\Delta CO$, which represents the increase in PM relative to CO and is commonly used to account for dilution effects in smoke plumes. For smoke aged 0 to 30 hrs,

they reported log(C_{sat}) value ranging from -1 to 2, where log(C_{sat}) increased with increasing ΔPM/ΔCO.[165] May et al. measured thermally denuded smoke emissions from controlled burns and presented a set of partitioning parameters that represented all the thermal denuder experiments which included both plume and ambient like conditions. Their data spanned an organic aerosol concentration of 1 to 5000 μg m^{-3} and a temperature range of 30 to 120 °C, from which they suggested that log(C_{sat}) was between -2 to 4.[166] Variability in partitioning parameters derived from different forest fires and controlled burns could be attributed to differing temperatures, emission factors, combustion efficiencies, dilution rates, organic aerosol concentration, and MW of emitted species. Characterizing the volatility distribution biomass burning derived OA is useful to help us understand the evolution of BrC because the volatility of organic compounds influences their partitioning between the gas and particle phase and therefore impacts the persistence of chromophores during plume aging.

1.7 Aerosol sampling method

1.7.1 Online measurements

Online methods provide real time measurements of aerosol properties, while offline measurements generally refer to the collection of particulate matter (e.g. filters) which is subjected to storage and handling prior to laboratory-based analyses. Each approach offers distinct advantages and limitations, and both methods have been proven to characterize chemical and physical properties wildfire smoke including BrC. Online measurements have been employed during controlled combustion experiments and aircraft-based measurements. These measurements provide high time resolution observations which offer insight into aerosol composition, particle formation, diurnal variation, atmospheric lifetimes, and even source attribution. For BrC

specifically, online sampling is useful to study absorption evolution as function of plume age and investigate chromophore formation and degradation.[112]

An aerosol mass spectrometer (AMS) is an important online sampling instrument that can provide insight into chemical composition of submicron aerosol. Various AMS designs have been developed to measure particles ranging from 10 nm to 10 μm; however, this broad range can present challenges for measurements. For example, 10 μm particle is estimated to contain hundreds of picograms (pg) of material whereas a 10 nm particle roughly contains nine orders of magnitude less mass.[167] As a result, real-time analysis of ultrafine particles by an AMS relies on measuring an ensemble of particles. The AMS operation involves sampling aerosol through an inlet system optimized for a specific size range where a series of aerodynamic lenses focus particles into a narrow beam. Particles enter source region where they are vaporized and ionized. The ionization method (e.g. electron impact, multiphoton ionization, chemical ionization) employed depends on the class of targeted compounds. Mass analyzers used in AMS instruments can include time-of-flight (TOF), quadrupole mass filters, or ion traps.[167] There are two modes of operation which include mass spectrum mode and particle time of flight mode. In mass spectrum mode, the inlet chopper is open, and particles of all transmitted sizes will arrive at the vaporization and ionization chamber where a quadrupole mass analyzer operates in scan mode to determine an average signal of all particle sizes. In particle time of flight mode, the chopper controls the particle beam, by allowing particles in the range of 50-1000 nm to be aerodynamically sized based on their arrival time at the detector.[168] Despite their applicability to wildfire research, they also have some limitations relevant to BrC research. For example, some aerosol components such as salts or high MW oligomers may be inefficiently vaporized, and organic species can include semi-volatile

compounds that can vaporize in the inlet. Therefore, AMS measurements generally provide insight into bulk aerosol composition.[167]

To measure water-soluble BrC absorption online, a key instrument used is a particle-into-liquid sampler (PILS). The PILS is designed to sample the water-soluble fraction of OA. The PILS consists of three sections a saturator, mixing region, and a particle growth segment.[169] In the saturator area a steady flow of water is heated to create steam where this is injected into the PILS mixing chamber where the steam is introduced to the ambient aerosol. The mixing of the steam and the cooler aerosol creates a super saturated environment that facilitates particles to grow into droplets large enough to be collected by impaction to form a continuous aqueous flow which can be directed downstream to analytical instruments.[170] To study BrC, a PILS can be coupled with a liquid waveguide capillary cell (LWCC) for real-time UV-visible absorption measurements and the PILS has also been integrated with total organic carbon (TOC) analyzers[96,171] and ion chromatography to measure inorganic aerosol species.[172]

The particle growth process in a PILS is analogous to cloud condensation nuclei activation, and therefore particle collection efficiency can depend on particle size and hygroscopicity. Larger and more hygroscopic particles will grow to a collectable size more readily under supersaturated conditions compared to small or more hydrophobic particles.[170] The PILS collection efficiency can be investigated experimentally by introducing aerosolized particles (e.g. sucrose) and comparing the measured water-soluble organic carbon (WSOC) concentrations from the PILS to expected aerosol concentrations derived from particle size distributions measured with an optical particle counter.[171] Sucrose particles are hygroscopic and this approach does not fully address hydrophobic aerosol components present in biomass burning emissions. To account for this, corrections based on comparisons with methanol-soluble absorption measured from filter samples can be applied.[171]

1.7.2 Offline measurements

To expand on the findings from online measurements, offline analyses can be incorporated into studying biomass burning derived aerosol. A micro-orifice uniform deposit impactor (MOUDI) is a useful instrument to collect size-resolved aerosol and be integrated with offline methodologies such as liquid chromatography. Depending on the model, a MOUDI can collect across the ultrafine, fine, and coarse modes. The assembly is comprised of pump that draws in a stream of air through an inlet and through a series of stages that successively collect smaller aerosols. Each impactor stage contains the impaction plate for the stage above and the nozzles for the stage below.[173] The diameter of the nozzles of subsequent stages decreases as each lower stage collects smaller aerosol deposits than the stage above it. However, the number of nozzles increases from one stage to the next.[173,174] Low pressure drops between each stage are achieved due to the small dimensions of the nozzles as the aerosols are deposited at low jet velocities. Uniform collection of particles onto the filter occurs because of the relative rotation of the impaction plate and the nozzle plates.[174] Uniform distribution of aerosol onto the filter is a useful feature as it helps to prevent aerosol deposit overload. Following the collection of size-resolved aerosol, the filters are extracted (e.g. with ultrapure water) and liquid extracts can then be used for various chromatographic analyses to investigate chemical, absorption, or size-related properties.

1.7.3 Comparing online and offline analyses

Comparisons between online and offline measurements are useful to investigate BrC absorption. Previous studies have reported differences between online and offline absorption measurements.[141,175] For example, Di Lorenzo et al. compared size exclusion chromatography with UV-vis detection (SEC-UV) to absorption from filter extracts with online PILS-LWCC measurements and observed a moderate correlation ($R^2 = 0.53$); the differences between the online

and offline analyses were attributed to variations in solubilization methods.[141] The offline SEC-UV analysis relied on sonication whereas the in-situ method only selects the most water-soluble species and relies on immediate solubilization upon collision with the impaction plate.[172] Other studies have also demonstrated that solvent selection and extraction efficiency can influence the offline measured absorption compared to online measurements.[175] These findings demonstrate that integrating online and offline analyses can help constrain how methodological factors influence measured optical properties.

1.7.4 Chromatography analyses

1.7.4.1 Size-exclusion chromatography

There are two types of size exclusion chromatography: (i) gel-permeation chromatography (GPC) which is commonly applied to separate synthetic polymers using an organic mobile phase[176] and (ii) gel-filtration chromatography (GFC) which used an aqueous mobile phase to separate biological molecules such as proteins and humic substances.[177–179] Regardless of GPC or GFC, a size exclusion column is packed with a porous medium (stationary phase), which separates molecules based on their hydrodynamic diameter, not chemical interactions with the stationary phase. The column packing is equilibrated with a mobile phase which fills the pores and facilitates the movement of analyte species through the column. The mobile phase is optimized to reduce interactions between the stationary phase and analytes. Molecules can penetrate the pores to varying degrees depending on their size. As the mobile phase carries the sample through the porous stationary phase, molecules that exceed the size of the pores will flow directly through the column at the same speed of the mobile phase, passing the pores. This will result in an early elution time within the void volume. If the chemical species are small enough to penetrate the pores, they will

spend more time in the column and elute later. Molecules that are smaller than the smallest pores, will elute in the column exclusion volume.

Common mobile phases for GFC analyses include a mixture of an organic solvent such as acetonitrile (ACN) or methanol with a buffer solution (e.g. phosphate or ammonium acetate ($NH_4CH_3CO_2$). The composition of the mobile phase is optimized to reduce secondary processes and ensure separation of the analytes is based on size. The ratio of organic to aqueous is dependent on the solubility of analytes (e.g. diverse polarity of BrC compounds), reducing hydrophobic interactions between the stationary phase and analytes, and column combability (e.g. some GFC columns cannot exceed 70% organic by volume). The aqueous solution is commonly referred to as a buffer because it can help to maintain pH and to suppress ionic interactions. When $NH_4CH_3CO_2$ is dissolved in water, partial protonation of acetate (CH_3COO-) forms acetic acid (CH_3COOH) producing conditions that can stabilize pH at 4.75.[180] The alkalinization of $NH_4CH_3CO_2$ solution generates NH_3 via the deprotonation of NH_4^+, creating buffering capacity around the pK_a of ammonium (9.25). Therefore, ammonium acetate dissolved in water has an inherent buffering capacity in acidic (pH at 4.75 ± 1) and basic ranges (9.25 ± 1).[180] The addition of acetonitrile to ammonium acetate dissolved in water reduces the buffer capacity and shifts the buffering ranges of $NH_4CH_3CO_2$ dissolved in water to approximately pH 5.5 ± 1 and pH 9 ± 1.[181,182] Ammonium acetate also minimizes electrostatic interactions between the compounds and the stationary phase. This has proven effective in previous size exclusion chromatography with UV-vis detection (SEC-UV) analyses of biomass burning derived samples investigating MW properties of fresh and aged BrC.[88,107,141] If the electrostatic interactions are negligible, SEC separation is based on hydrodynamic volume, which is a function of MW and the density of the compounds.[183]

1.7.4.2 Size-exclusion chromatography coupled to ultraviolet-visible detection

Size-exclusion chromatography coupled with ultraviolet-visible detection allows us to investigate the absorption properties of chemical species separated into different size ranges. The mobile phase will enter the flow cell of the diode array detector, where higher MW species will enter first. A diode array detector contains two light sources, a deuterium lamp for ultraviolet (UV) detection and a tungsten lamp for visible (vis) detection, providing a wavelength detection range from 190 to 800 nm. The diode array detector contains an achromat which is a lens that receives light from both lamps and focuses it so the light beam can pass through the flow cell, where the measurement beam travels from the flow cell to a lens that focuses it through slit. The optical grating diffracts the light beam into its component wavelengths and directs the light onto the photodiode array, which is series of 1024 photosensitive elements which converts the light into an electrical signal.[184] As an example, Figure 1-6 displays an example of an absorption density plot of Suwannee River humic acid (SRHA). Humic acids are often used as proxies for BrC because they are highly oxygenated and conjugated systems that absorb in the UV-vis region and have broad MW distributions which resemble oxidized organic aerosol observed in aged biomass burning plumes. Investigating the MW of organic species is an established research topic because it allows us to infer chemical and physical characteristics; for example, adsorption, hydrophobic organic partitioning, electrostatic effects, and water treatment.[185–190]

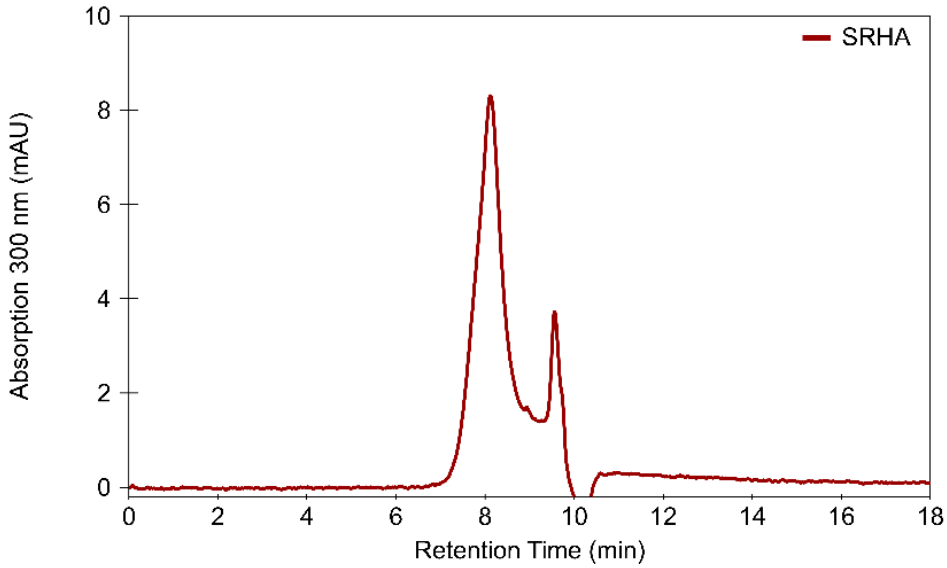

Figure 1-6. Absorption density plot of SRHA at 300 nm measured by SEC-UV.

Lower MW species tend to have smaller radii and are more hydrophilic whereas higher MW species tend to have greater aromaticity, which can permit hydrophobic interactions. The chemical species that comprise humic substances resemble BrC due to their chemical functionality, partial water-solubility, ability to absorb in the UV-vis range, and is comprised of species with varying MWs. An application of SEC-UV is to estimate the MW of humic substances and BrC by calibrating the SEC column to estimate the MW based on elution time. Size exclusion columns have a negative log-linear relationship between MW and retention time (RT) within the void and exclusion volumes.[141,191] There are two calibration methods that have been used to estimate the MW of biomass derived samples. The first method uses standards that span the MW range of the SEC column. Wong et al. (2017, 2019) used standards of known MWs, such as blue dextran, bovine serum, myoglobin, apotinin, and 2-nitrobenzaldehye where they plotted Log(MW) versus RT, where the linear fit represents the molecules that had weak interactions with the stationary phase and eluted between the column's void and exclusion volumes.[88,129] This method has limitations because not all of the standards have comparable chemical properties or densities as

BrC chromophores, and it has been cautioned to use chemical standards to calibrate an SEC column to estimate the MW of humic substances.[192] The second calibration method exploits the negative log-linear relationship between MW and elution volume to estimate MW of BrC species. Di Lorenzo et al. internally calibrated a SEC column by first running humic acid and biomass burning extracts on a SEC column with a MW range of 10 000 to 100 Da where peaks were observed at retention times that correspond to the void (~10 000 Da) and exclusion (~ 100 Da) volumes. The same samples were then run on a preferred SEC column which had a wider MW range (75 000 to 250 Da) using the same mobile phase and flow rate conditions. Since the two SEC columns have overlapping MW ranges, the peaks observed on the preferred column corresponded to ~10 000 Da and ~ 100 Da, where a log-linear fit between these points was applied to estimate MW of BrC species eluting between the void and exclusion volume of the wider range column.[141] This method proved to be effective to estimate MW ranges of BrC because it relies less on calibration solutions having the same chemical properties to BrC because it considers the elution times of the observed void and exclusion volumes.

1.7.4.3 Ion chromatography with conductivity detection

The main components of an ion chromatography (IC) system include a pump, eluent reservoirs, a high-pressure valve, a separation column, a suppressor, and a conductivity detector. The high-pressure valve consists of six ports and can rotate depending on if the sample is being retrieved by the autosampler (load position) or if the sample is being injected onto the column (inject position). The pump delivers mobile phase throughout the system; when the valve is in the inject position, the mobile phase combines with the sample volume which then flows through the separation column. Ion chromatography is typically used for the separation of inorganic anions and cations. The stationary phases of a column used to separate anions and cations is commonly

functionalized with quaternary ammonium and carboxylic acid groups, respectively. The separation of analytes is based on their affinity to the stationary phase, which can be driven by charge density. The mobile phase contains ions that displace analytes retained to the stationary phase, the time at which these species elute is referred to as the retention time.[193] A common mobile phase when separating inorganic anions contains hydroxide ions (OH^-) (e.g. NaOH) and a typical mobile phase when separating inorganic cations contains methanesulfonic acid (MSA). Prior to the analytes reaching the detector, the background conductivity from ions in the mobile phase is suppressed. A suppressor is a device that neutralizes and removes eluent ions, leaving the target ions in pure water for more sensitive detection.[194] Following suppression, the eluent containing ionic analytes in introduced to the conductivity detector where a voltage is applied across two electrodes to create an electric field. The flow of the ions establishes an electric current, which is converted to a conductivity signal where this signal is proportional to the concentration of ions.[193]

Ion chromatography with conductivity detection had been applied to quantify a wide range inorganic anions (e.g. F^-, Cl^-, NO_2^-, NO_3^-, SO_4^{2-}, PO_4^{3-}), organic acids (e.g. acetic acid, formic acid), inorganic cations (e.g. K^+, Na^+, Li^+, Ca^{2+}, Mg^{2+}), and alkylamines (e.g. dimethylamine (DMA), diethylamine (DEA), and trimethylamine (TMA)) to assess the chemical composition of environmental matrices such as rain water,[195,196] aerosol,[197] and humic substances.[198] By characterizing the chemical composition of such matrices provides insight into sources and fates of contaminants which strengthens our understanding of their impacts on human health and climate.

1.7.4.4 Reverse phase liquid chromatography analysis

Reversed-phase liquid chromatography (RPLC) is a prevalent method of high-performance liquid chromatography (HPLC). The main components of a reversed-phase LC system resemble

that of IC-CD setup (i.e. contains a pump that delivers eluent, high pressure valve to facilitate the injection of a sample volume into the column, and a detector). Reversed-phase LC utilizes a non-polar stationary phase and polar mobile phase to enable the separation of analytes. The stationary phase is comprised of silica particles that are derivatized with hydrocarbon chains. There are multiple different types of reversed-phase LC columns commercially available where the selection of a column depends on the analytes of interest and separation optimization. Alkyl-bonded columns include hydrocarbon chains that vary in carbon length such as C_8 and C_{18}, where analytes are retained due to hydrophobic interactions such as London dispersion forces. There are reversed-phase LC columns that contain chains of phenyl groups to facilitate retention through π-π interactions.

The C18 column is commonly used in environmental and atmospheric chemistry applications because it can separate analytes of diverse polarities, from polar species to moderately nonpolar organics, and is compatible with various organic modifiers. When a sample enters the column, analytes partition between the mobile and stationary phase. Polar compounds interact more favorably with the mobile phase and will elute earlier whereas less polar compounds preferentially partition into the hydrophobic stationary phase and are retained longer. For samples that contain diverse or unknown polarities commonly utilize gradient separation scheme where the percentage of the organic modifier increases over the course of the separation. The composition of the mobile phase is selected primarily based on solubility and the required elution strength. Acetonitrile and methanol are common organic solvents combined with water to comprise the mobile phases when separating analytes with environmental matrices. Acetonitrile mixed with water has greater elution strength than methanol mixed with water because it is less polar and aprotic (no hydrogen bonding); therefore, it solvates non-polar species better which prevents

hydrophobic interactions with the stationary phase. Mobile phase additives (e.g. acetic acid, formic acid, trifluoroacetic acid) in mobile phases have multiple purposes depending on the function of the additive.[199] For example, biomass burning derived samples may be functionalized with phenolics, amines, or carboxylic acids which are ionizable, and the addition of acetic acid (pK_a = 4.8) can keep weak acids protonated (in their neutral form) which enables some interaction with the stationary phase preventing early elution with limited separation.

The retention of an analyte onto a reversed-phase column is associated with its partitioning coefficient between water and octanol. For this work, octanol is a suitable organic phase because it is amphiphilic in structure, containing a hydrophobic alkyl chain and a polar hydroxyl group which resembles the moderately polar character of organic aerosol. The ratio of a compound's concentration in octanol to its concentration in water when the two phases are in equilibrium is denoted by K_{ow} (R1.6).[200]

$$\text{Equation 1.6} \quad K_{ow} = \frac{[A]_{octanol}}{[A]_{water}}$$

The greater the value of K_{ow}, the greater the tendency to partition into a medium with appreciable organic composition; the value K_{ow} provides context about the compounds hydrophobicity; therefore, can be used to infer the fate of organic compounds in the environment. Reversed-phase LC has been used to estimate K_{ow} values of compounds that correspond to resolved peaks.[201–204] Compounds with higher K_{ow} values have a greater affinity to the stationary phase of a reverse phase column and will elute later compared to compounds with lower K_{ow} values. This phenomenon is assessed by considering the parameters in R1.7.

$$\text{Equation 1.7} \quad k' = \frac{t_r - t_0}{t_0}$$

The retention factor is k' and is governed by t_r which is the retention time of compound, and t_o which is the retention time of a compound that was not retained on the column. The

relationship between log(K_{ow}) and log(k') is linear which allows the estimation of K_{ow} for unknown compounds. To predict log(K_{ow}) that correspond to peaks of species resolved using a gradient elution scheme, multiple isocratic separations need to be performed. This procedure includes isocratic separations of standard compounds with known log(K_{ow}) values with mobile phase compositions that reflect the composition of the gradient scheme at retention times of unknown compounds eluted off the column. The accuracy of this approach depends on the calibration procedure, particularly the availability of standards with established log(K_{ow}) values.[205] Various reversed-phase LC analyses have investigated the hydrophobicity of compounds in various environmental samples, such as halogenated organic compounds[206] and PAHs.[207] These studies acquired log(K_{ow}) values comparable to literature values and suggesting the usefulness of reversed-phase chromatography to inferring the fate of organic compounds in the environment.

The atmospheric fate of BrC species is governed by a combination of factors including molecular size, polarity, and volatility which influence whether a compound remains in the particle phase or partitions into the gas phase. Characterizing the polarity of BrC through log(K_{ow}) provides insight into the affinity of these compounds for organic aerosol and therefore their persistence during atmospheric aging. Characterizing the polarity of BrC species helps link molecular composition with optical properties which is important because compounds that persist in the organic aerosol phase can contribute to light absorption and therefore influence direct radiative effects of PM.

1.8 Research objectives

This work applies (i) airborne measurements of western U.S wildfires during FIREX-AQ, (ii) controlled combustion measurements of fuels found in the western U.S during FIREX FireLab, and (iii) ground-based measurements during a smoke intrusion in Toronto, Ontario to expand our

understanding of the chemical composition, optical properties, volatility, and atmospheric evolution of BrC.

In Chapter 2, the measurements made during FIREX-AQ provide insight into near source and downwind BrC and emphasize methodical considerations relevant to chromatographic analyses. During the field campaign, smoke aged approximately 0-5 hrs was sampled downwind of wildfire. Online measurements of water-soluble BrC total absorption were compared to offline absorption by SEC-UV to assess the contribution of high and low MW BrC species and to investigate how chromatographic separation conditions impact observed optical properties.

The controlled combustion experiments conducted during the FIREX FireLab research campaign at the Missoula Fire Sciences Laboratory during FIREX 2016 are presented in Chapter 3. The study focused on wildfire fuels typical of the western U.S. with measurements by online and offline instrumentation under thermodenuded and ambient conditions (undenuded). Online aerosol measurements included water-soluble BrC, total aerosol absorption, and aerosol chemical composition. Offline filter samples were analyzed using SEC-UV to characterize molecular size and reverse-phase high performance liquid chromatography (HPLC-UV) to characterize polarity. We use these online and offline measurements to examine: i) BrC volatility and the O:C ratio in the context of the two-dimensional volatility basis set; ii) BrC molecular weight contribution to absorption; and iii) BrC octanol-water partitioning properties.

To investigate the evolution of BrC during atmospheric transport, size-resolved aerosol was collected during a smoke intrusion event in Toronto. These results are presented in Chapter 4. A cascade impactor was deployed to sample aerosol aged approximately 30-40 hrs that originated from forest fires burning in northern Ontario. Multiple chromatographic methods were applied to characterize the chemical and optical properties of the aerosol; SEC-UV was used to determine

the absorption contribution of high and low MW BrC species, HPLC-UV was applied to estimate log(K_{ow}) values to assess hydrophobicity, and IC-CD to measure inorganic anions and cation, and alkylamines. The objective of this work is to compare these results with previous analyses of fresh and aged biomass burning aerosol to evaluate if BrC evolution during atmospheric transport is consistent across different plumes.

Collectively these measurements enable the comparison between fresh, laboratory generated, and atmospherically aged wildfire aerosol, providing the opportunity to evaluate the consistency of BrC chemical and optical properties transformation across these different sampling conditions.

1.9 References

(1) Lieberman, D. E. *The Story of the Human Body: Evolution, Health, and Disease*; Vintage, 2014.

(2) Pausas, J. G.; Alessio, G. A.; Moreira, B.; Segarra-Moragues, J. G. Secondary Compounds Enhance Flammability in a Mediterranean Plant. *Oecologia* 2016, *180* (1), 103–110. https://doi.org/10.1007/s00442-015-3454-8.

(3) Keeley, J. E.; Pausas, J. G. Distinguishing Disturbance from Perturbations in Fire-Prone Ecosystems. *International Journal of Wildland Fire* 2019, *28* (4), 282–287. https://doi.org/10.1071/WF18203.

(4) Northwest Fire Science Consortium. What Is? Fire Severity. https://www.nwfirescience.org/sites/default/files/publications/Fire%20Severity.pdf.

(5) Swetnam, T. W.; Farella, J.; Roos, C. I.; Liebmann, M. J.; Falk, D. A.; Allen, C. D. Multiscale Perspectives of Fire, Climate and Humans in Western North America and the Jemez Mountains, USA. *Philos Trans R Soc Lond B Biol Sci* 2016, *371* (1696). https://doi.org/10.1098/rstb.2015.0168.

(6) Romps, D. M.; Seeley, J. T.; Vollaro, D.; Molinari, J. Climate Change. Projected Increase in Lightning Strikes in the United States Due to Global Warming. *Science* 2014, *346* (6211), 851–854. https://doi.org/10.1126/science.1259100.

(7) Pausas, J. G.; Keeley, J. E. Wildfires and Global Change. *Frontiers in Ecology and the Environment* 2021, *19* (7), 387–395. https://doi.org/10.1002/fee.2359.

(8) Piao, S.; Wang, X.; Park, T.; Chen, C.; Lian, X.; He, Y.; Bjerke, J. W.; Chen, A.; Ciais, P.; Tømmervik, H.; Nemani, R. R.; Myneni, R. B. Characteristics, Drivers and Feedbacks of Global Greening. *Nature Reviews Earth & Environment* 2020, *1* (1), 14–27. https://doi.org/10.1038/s43017-019-0001-x.

(9) National Park Service, N. P. C. Dome Fire, 2023. https://www.nps.gov/moja/learn/nature/dome-fire.htm.

(10) Keetch, J. J.; Byram, G. M. A Drought Index for Forest Fire Control. *Res. Pap. SE-38. Asheville, NC: U.S. Department of Agriculture, Forest Service, Southeastern Forest Experiment Station. 35 p.* 1968.

(11) Government of Canada. Canada's Fire Weather Index System, 2025. https://natural-resources.canada.ca/forest-forestry/wildland-fires/canada-fire-weather-index-system.

(12) Brown, E. K.; Wang, J.; Feng, Y. US Wildfire Potential: A Historical View and Future Projection Using High-Resolution Climate Data. *Environmental Research Letters* 2021, *16* (3), 034060. https://doi.org/10.1088/1748-9326/aba868.

(13) Government of Canada. *The State of Canada's Forests Annual Report*; 2022. https://natural-resources.canada.ca/forest-forestry/state-canada-forests/state-canada-forests.

(14) Food and Agriculture Organization of the United Nations. *Global Forest Resources Assessment 2020*; 2020. https://doi.org/10.4060/ca9825en.

(15) Bush, E.; Lemmen, D. S. *Canada's Changing Climate Report; Government of Canada*; 2019. https://publications.gc.ca/collections/collection_2019/eccc/En4-368-2019-eng.pdf.

(16) Hanes, C. C.; Wang, X.; Jain, P.; Parisien, M.-A.; Little, J. M.; Flannigan, M. D. Fire-Regime Changes in Canada over the Last Half Century. *Can. J. For. Res.* 2019, *49* (3), 256–269. https://doi.org/10.1139/cjfr-2018-0293.

(17) Wang, X.; Studens, K.; Parisien, M.-A.; Taylor, S. W.; Candau, J.-N.; Boulanger, Y.; Flannigan, M. D. Projected Changes in Fire Size from Daily Spread Potential in Canada over the 21st Century. *Environmental Research Letters* 2020, *15* (10), 104048. https://doi.org/10.1088/1748-9326/aba101.

(18) Barnes, C. *Climate Change More than Doubled the Likelihood of Extreme Fire Weather Conditions in Eastern Canada. Scientific Reports*; 2023. https://doi.org/10.25561/105981.

(19) Jain, P.; Barber, Q. E.; Taylor, S. W.; Whitman, E.; Castellanos Acuna, D.; Boulanger, Y.; Chavardès, R. D.; Chen, J.; Englefield, P.; Flannigan, M.; Girardin, M. P.; Hanes, C. C.; Little, J.; Morrison, K.; Skakun, R. S.; Thompson, D. K.; Wang, X.; Parisien, M.-A. Drivers and Impacts of the Record-Breaking 2023 Wildfire Season in Canada. *Nature Communications* 2024, *15* (1), 6764. https://doi.org/10.1038/s41467-024-51154-7.

(20) GES DISC MERRA-2 Tavg1 2d Slv Nx: 2d,1-Hourly, Time-Averaged, Single-Level, Assimilation, Single-Level Diagnostics V5.12.4. https://doi.org/10.5067/VJAFPLI1CSIV.

(21) Byrne, B.; Liu, J.; Bowman, K. W.; Pascolini-Campbell, M.; Chatterjee, A.; Pandey, S.; Miyazaki, K.; van der Werf, G. R.; Wunch, D.; Wennberg, P. O.; Roehl, C. M.; Sinha, S. Carbon Emissions from the 2023 Canadian Wildfires. *Nature* 2024, *633* (8031), 835–839. https://doi.org/10.1038/s41586-024-07878-z.

(22) Group on Earth Observations and Copernicus Work Programs. Global Wildfire Information System Current Statistic Portal: Americas: Canada. https://gwis.jrc.ec.europa.eu/apps/country.profile/overview/ADM0/CAN.

(23) Stocks, B. J.; Mason, J. A.; Todd, J. B.; Bosch, E. M.; Wotton, B. M.; Amiro, B. D.; Flannigan, M. D.; Hirsch, K. G.; Logan, K. A.; Martell, D. L.; Skinner, W. R. Large Forest

Fires in Canada, 1959–1997. *Journal of Geophysical Research: Atmospheres* 2002, *107* (D1), FFR 5-1. https://doi.org/10.1029/2001JD000484.

(24) Braun, W. J.; Jones, B. L.; Lee, J. S. W.; Woolford, D. G.; Wotton, B. M. Forest Fire Risk Assessment: An Illustrative Example from Ontario, Canada. *Journal of Probability and Statistics* 2010, *2010* (1), 823018. https://doi.org/10.1155/2010/823018.

(25) National Forestry Database; Canadian Council of Forest Ministries. *Forest Area Burned and Number of Forest Fires*; 2025. http://nfdp.ccfm.org/en/data/fires.php#tab321.

(26) Marlon, J. R.; Bartlein, P. J.; Gavin, D. G.; Long, C. J.; Anderson, R. S.; Briles, C. E.; Brown, K. J.; Colombaroli, D.; Hallett, D. J.; Power, M. J.; Scharf, E. A.; Walsh, M. K. Long-Term Perspective on Wildfires in the Western USA. *Proceedings of the National Academy of Sciences* 2012, *109* (9), E535 LP-E543. https://doi.org/10.1073/pnas.1112839109.

(27) Norlen, C. A.; Hemes, K. S.; Wang, J. A.; Randerson, J. T.; Battles, J. J.; Tubbesing, C. L.; Goulden, M. L. Recent Fire History Enhances Semi-Arid Conifer Forest Drought Resistance. *Forest Ecology and Management* 2024, *573*, 122331. https://doi.org/10.1016/j.foreco.2024.122331.

(28) Coppoletta, M.; Merriam, K. E.; Collins, B. M. Post-Fire Vegetation and Fuel Development Influences Fire Severity Patterns in Reburns. *Ecological Applications* 2016, *26* (3), 686–699. https://doi.org/10.1890/15-0225.

(29) Parks, S. A.; Abatzoglou, J. T. Warmer and Drier Fire Seasons Contribute to Increases in Area Burned at High Severity in Western US Forests From 1985 to 2017. *Geophysical Research Letters* 2020, *47* (22), e2020GL089858. https://doi.org/10.1029/2020GL089858.

(30) Parks, S. A.; Coop, J. D.; Davis, K. T. Intensifying Fire Season Aridity Portends Ongoing Expansion of Severe Wildfire in Western US Forests. *Global Change Biology* 2025, *31* (8), e70429. https://doi.org/10.1111/gcb.70429.

(31) Picotte, J. J.; Bhattarai, K.; Howard, D.; Lecker, J.; Epting, J.; Quayle, B.; Benson, N.; Nelson, K. Changes to the Monitoring Trends in Burn Severity Program Mapping Production Procedures and Data Products. *Fire Ecology* 2020, *16* (1), 16. https://doi.org/10.1186/s42408-020-00076-y.

(32) Zhuang, Y.; Fu, R.; Santer, B. D.; Dickinson, R. E.; Hall, A. Quantifying Contributions of Natural Variability and Anthropogenic Forcings on Increased Fire Weather Risk over the Western United States. *Proc Natl Acad Sci U S A* 2021, *118* (45). https://doi.org/10.1073/pnas.2111875118.

(33) Fu, R.; Hoell, A.; Mankin, J.; Sheffield, A.; Simpson, I. *Tackling Challenges of a Drier, Hotter, More Fire-Prone Future*; Eos, 2021. https://eos.org/opinions/tackling-challenges-of-a-drier-hotter-more-fire-prone-future.

(34) National Interagency Fire Center. *2020 National Large Incident Year To-Date Report*. https://web.archive.org/web/20210101044138/https://gacc.nifc.gov/.

(35) State of California; California Office of Environmental Health Hazard Assessment. Wildfires, 2025. https://oehha.ca.gov/climate-change/epic-2022/impacts-vegetation-and-wildlife/wildfires.

(36) Zhang, Y.; Fan, J.; Shrivastava, M.; Homeyer, C. R.; Wang, Y.; Seinfeld, J. H. Notable Impact of Wildfires in the Western United States on Weather Hazards in the Central United States. *Proceedings of the National Academy of Sciences* 2022, *119* (44), e2207329119. https://doi.org/10.1073/pnas.2207329119.

(37) Jacobo, J.; Ginger, Z. *Climate Change May Be Causing an Early Start to Fire Season in the West, Experts Say*; 2021. https://abcnews.go.com/US/climate-change-causing-early-start-fire-season-west/story?id=77737065.

(38) Currie, J.; Walker, R. What Do Economists Have to Say about the Clean Air Act 50 Years after the Establishment of the Environmental Protection Agency? *Journal of Economic Perspectives* 2019, *33* (4), 3–26. https://doi.org/10.1257/jep.33.4.3.

(39) Aldy, J. E.; Auffhammer, M.; Cropper, M.; Fraas, A.; Morgenstern, R. Looking Back at 50 Years of the Clean Air Act. *Journal of Economic Literature* 2022, *60* (1), 179–232. https://doi.org/10.1257/jel.20201626.

(40) Burke, M.; Childs, M. L.; de la Cuesta, B.; Qiu, M.; Li, J.; Gould, C. F.; Heft-Neal, S.; Wara, M. The Contribution of Wildfire to PM(2.5) Trends in the USA. *Nature* 2023, *622* (7984), 761–766. https://doi.org/10.1038/s41586-023-06522-6.

(41) Burke, M.; Driscoll, A.; Heft-Neal, S.; Xue, J.; Burney, J.; Wara, M. The Changing Risk and Burden of Wildfire in the United States. *Proceedings of the National Academy of Sciences* 2021, *118* (2), e2011048118. https://doi.org/10.1073/pnas.2011048118.

(42) Gritzo, L. A. (Lou). Perspective Article: Mitigating Social and Economic Impact of Wildfires. *Applications in Energy and Combustion Science* 2024, *20*, 100285. https://doi.org/10.1016/j.jaecs.2024.100285.

(43) Wang, D.; Guan, D.; Zhu, S.; Kinnon, M. M.; Geng, G.; Zhang, Q.; Zheng, H.; Lei, T.; Shao, S.; Gong, P.; Davis, S. J. Economic Footprint of California Wildfires in 2018. *Nature Sustainability* 2021, *4* (3), 252–260. https://doi.org/10.1038/s41893-020-00646-7.

(44) U.S. Congress Joint Economic Committee. *Climate-Exacerbated Wildfires Cost the U.S. between $394 to $893 Billion Each Year in Economic Costs and Damages*; 2023. https://www.jec.senate.gov/public/_cache/files/9220abde-7b60-4d05-ba0a-8cc20df44c7d/jec-report-on-total-costs-of-wildfires.pdf.

(45) Canadian Climate Institute. Fact Sheet: Climate Change and Wildfires, 2025. https://climateinstitute.ca/wp-content/uploads/2024/07/Fact-sheet-wildfires-Canadian-Climate-Institute.pdf.

(46) Alam, R.; Islam, S.; Mosely, E.; Thomas, S.; Dowdell, V.; Doel, D. Rapid Impact Assessment of Fort McMurray Wildfire. https://climateinstitute.ca/wp-content/uploads/2024/07/Fact-sheet-wildfires-Canadian-Climate-Institute.pdf.

(47) Heaney, A.; Stowell, J. D.; Liu, J. C.; Basu, R.; Marlier, M.; Kinney, P. Impacts of Fine Particulate Matter From Wildfire Smoke on Respiratory and Cardiovascular Health in California. *GeoHealth* 2022, *6* (6), e2021GH000578. https://doi.org/10.1029/2021GH000578.

(48) Smith, A. *Canadian Wildfire Smoke Cooled New York by 3 Degrees and Trapped Air Toxicants*. https://www.rutgers.edu/news/canadian-wildfire-smoke-cooled-new-york-3-degrees-and-trapped-air-toxicants.

(49) Matz, C. J.; Egyed, M.; Wang, X.; Duhamel, A.; Xi, G.; Rittmaster, R.; Pentcheva, N.; Stieb, D. M. Health Impact Analysis of Wildfire Smoke-PM(2.5) in Canada (2019-2023). *Geohealth* 2026, *10* (2), e2025GH001565. https://doi.org/10.1029/2025GH001565.

(50) Sawyer, D.; Stiebert, S.; Welburn, C. Canadian Climate Institute. With the Forest Ablaze, the Health Costs Hit Home, 2026.

(51) Finlayson-Pitts, B. J.; Pitts, J. N. CHAPTER 2 - The Atmospheric System. In *Chemistry of the Upper and Lower Atmosphere*; Finlayson-Pitts, B. J., Pitts, J. N., Eds.; Academic Press: San Diego, 2000; pp 15–42. https://doi.org/10.1016/B978-012257060-5/50004-6.

(52) Finlayson-Pitts, B. J.; Pitts, J. N. CHAPTER 9 - Particles in the Troposphere. In *Chemistry of the Upper and Lower Atmosphere*; Finlayson-Pitts, B. J., Pitts, J. N., Eds.; Academic Press: San Diego, 2000; pp 349–435. https://doi.org/10.1016/B978-012257060-5/50011-3.

(53) Jalava, P. I.; Salonen, R. O.; Hälinen, A. I.; Penttinen, P.; Pennanen, A. S.; Sillanpää, M.; Sandell, E.; Hillamo, R.; Hirvonen, M.-R. In Vitro Inflammatory and Cytotoxic Effects of Size-Segregated Particulate Samples Collected during Long-Range Transport of Wildfire Smoke to Helsinki. *Toxicology and Applied Pharmacology* 2006, *215* (3), 341–353. https://doi.org/10.1016/j.taap.2006.03.007.

(54) Johnston, H. J.; Mueller, W.; Steinle, S.; Vardoulakis, S.; Tantrakarnapa, K.; Loh, M.; Cherrie, J. W. How Harmful Is Particulate Matter Emitted from Biomass Burning? A Thailand Perspective. *Current Pollution Reports* 2019, *5* (4), 353–377. https://doi.org/10.1007/s40726-019-00125-4.

(55) Ramnarine, E.; Kodros, J. K.; Hodshire, A. L.; Lonsdale, C. R.; Alvarado, M. J.; Pierce, J. R. Effects of Near-Source Coagulation of Biomass Burning Aerosols on Global Predictions of Aerosol Size Distributions and Implications for Aerosol Radiative Effects. *Atmospheric*

Chemistry and Physics 2019, *19* (9), 6561–6577. https://doi.org/10.5194/acp-19-6561-2019.

(56) Hosseini, S.; Li, Q.; Cocker, D.; Weise, D.; Miller, A.; Shrivastava, M.; Miller, J. W.; Mahalingam, S.; Princevac, M.; Jung, H. Particle Size Distributions from Laboratory-Scale Biomass Fires Using Fast Response Instruments" Published in Atmos. Chem. Phys., 10, 8065–8076, 2010. *Atmospheric Chemistry and Physics* 2010, *10* (17), 8511–8511. https://doi.org/10.5194/acp-10-8511-2010.

(57) Sakamoto, K. M.; Laing, J. R.; Stevens, R. G.; Jaffe, D. A.; Pierce, J. R. The Evolution of Biomass-Burning Aerosol Size Distributions Due to Coagulation: Dependence on Fire and Meteorological Details and Parameterization. *Atmospheric Chemistry and Physics* 2016, *16* (12), 7709–7724. https://doi.org/10.5194/acp-16-7709-2016.

(58) Hodshire, A. L.; Bian, Q.; Ramnarine, E.; Lonsdale, C. R.; Alvarado, M. J.; Kreidenweis, S. M.; Jathar, S. H.; Pierce, J. R. More Than Emissions and Chemistry: Fire Size, Dilution, and Background Aerosol Also Greatly Influence Near-Field Biomass Burning Aerosol Aging. *Journal of Geophysical Research: Atmospheres* 2019, *124* (10), 5589–5611. https://doi.org/10.1029/2018JD029674.

(59) Chakrabarty, R. K.; Moosmüller, H.; Garro, M. A.; Arnott, W. P.; Walker, J.; Susott, R. A.; Babbitt, R. E.; Wold, C. E.; Lincoln, E. N.; Hao, W. M. Emissions from the Laboratory Combustion of Wildland Fuels: Particle Morphology and Size. *Journal of Geophysical Research: Atmospheres* 2006, *111* (D7). https://doi.org/10.1029/2005JD006659.

(60) Capes, G.; Johnson, B.; McFiggans, G.; Williams, P. I.; Haywood, J.; Coe, H. Aging of Biomass Burning Aerosols over West Africa: Aircraft Measurements of Chemical Composition, Microphysical Properties, and Emission Ratios. *Journal of Geophysical Research: Atmospheres* 2008, *113* (D23). https://doi.org/10.1029/2008JD009845.

(61) Janhäll, S.; Andreae, M. O.; Pöschl, U. Biomass Burning Aerosol Emissions from Vegetation Fires: Particle Number and Mass Emission Factors and Size Distributions. *Atmospheric Chemistry and Physics* 2010, *10* (3), 1427–1439. https://doi.org/10.5194/acp-10-1427-2010.

(62) Carrico, C. M.; Prenni, A. J.; Kreidenweis, S. M.; Levin, E. J. T.; McCluskey, C. S.; DeMott, P. J.; McMeeking, G. R.; Nakao, S.; Stockwell, C.; Yokelson, R. J. Rapidly Evolving Ultrafine and Fine Mode Biomass Smoke Physical Properties: Comparing Laboratory and Field Results. *Journal of Geophysical Research: Atmospheres* 2016, *121* (10), 5750–5768. https://doi.org/10.1002/2015JD024389.

(63) Hodshire, A. L.; Ramnarine, E.; Akherati, A.; Alvarado, M. L.; Farmer, D. K.; Jathar, S. H.; Kreidenweis, S. M.; Lonsdale, C. R.; Onasch, T. B.; Springston, S. R.; Wang, J.; Wang, Y.; Kleinman, L. I.; Sedlacek III, A. J.; Pierce, J. R. Dilution Impacts on Smoke Aging: Evidence in Biomass Burning Observation Project (BBOP) Data. *Atmospheric Chemistry and Physics* 2021, *21* (9), 6839–6855. https://doi.org/10.5194/acp-21-6839-2021.

(64) Yokelson, R. J.; Crounse, J. D.; DeCarlo, P. F.; Karl, T.; Urbanski, S.; Atlas, E.; Campos, T.; Shinozuka, Y.; Kapustin, V.; Clarke, A. D.; Weinheimer, A.; Knapp, D. J.; Montzka, D. D.; Holloway, J.; Weibring, P.; Flocke, F.; Zheng, W.; Toohey, D.; Wennberg, P. O.; Wiedinmyer, C.; Mauldin, L.; Fried, A.; Richter, D.; Walega, J.; Jimenez, J. L.; Adachi, K.; Buseck, P. R.; Hall, S. R.; Shetter, R. Emissions from Biomass Burning in the Yucatan. *Atmospheric Chemistry and Physics* 2009, *9* (15), 5785–5812. https://doi.org/10.5194/acp-9-5785-2009.

(65) Cubison, M. J.; Ortega, A. M.; Hayes, P. L.; Farmer, D. K.; Day, D.; Lechner, M. J.; Brune, W. H.; Apel, E.; Diskin, G. S.; Fisher, J. A.; Fuelberg, H. E.; Hecobian, A.; Knapp, D. J.; Mikoviny, T.; Riemer, D.; Sachse, G. W.; Sessions, W.; Weber, R. J.; Weinheimer, A. J.; Wisthaler, A.; Jimenez, J. L. Effects of Aging on Organic Aerosol from Open Biomass Burning Smoke in Aircraft and Laboratory Studies. *Atmospheric Chemistry and Physics* 2011, *11* (23), 12049–12064. https://doi.org/10.5194/acp-11-12049-2011.

(66) Bian, Q.; Jathar, S. H.; Kodros, J. K.; Barsanti, K. C.; Hatch, L. E.; May, A. A.; Kreidenweis, S. M.; Pierce, J. R. Secondary Organic Aerosol Formation in Biomass-Burning Plumes: Theoretical Analysis of Lab Studies and Ambient Plumes. *Atmospheric Chemistry and Physics* 2017, *17* (8), 5459–5475. https://doi.org/10.5194/acp-17-5459-2017.

(67) June, N. A.; Hodshire, A. L.; Wiggins, E. B.; Winstead, E. L.; Robinson, C. E.; Thornhill, K. L.; Sanchez, K. J.; Moore, R. H.; Pagonis, D.; Guo, H.; Campuzano-Jost, P.; Jimenez, J. L.; Coggon, M. M.; Dean-Day, J. M.; Bui, T. P.; Peischl, J.; Yokelson, R. J.; Alvarado, M. J.; Kreidenweis, S. M.; Jathar, S. H.; Pierce, J. R. Aerosol Size Distribution Changes in FIREX-AQ Biomass Burning Plumes: The Impact of Plume Concentration on Coagulation and OA Condensation/Evaporation. *Atmospheric Chemistry and Physics* 2022, *22* (19), 12803–12825. https://doi.org/10.5194/acp-22-12803-2022.

(68) Sparks, T. L.; Wagner, J. Composition of Particulate Matter during a Wildfire Smoke Episode in an Urban Area. *Aerosol Science and Technology* 2021, *55* (6), 734–747. https://doi.org/10.1080/02786826.2021.1895429.

(69) Sedlacek III, A. J.; Buseck, P. R.; Adachi, K.; Onasch, T. B.; Springston, S. R.; Kleinman, L. Formation and Evolution of Tar Balls from Northwestern US Wildfires. *Atmospheric Chemistry and Physics* 2018, *18* (15), 11289–11301. https://doi.org/10.5194/acp-18-11289-2018.

(70) Anderson, T. L.; Charlson, R. J.; Schwartz, S. E.; Knutti, R.; Boucher, O.; Rodhe, H.; Heintzenberg, J. Atmospheric Science. Climate Forcing by Aerosol--a Hazy Picture. *Science* 2003, *300* (5622), 1103–1104. https://doi.org/10.1126/science.1084777.

(71) Bellouin, N.; Quaas, J.; Gryspeerdt, E.; Kinne, S.; Stier, P.; Watson-Parris, D.; Boucher, O.; Carslaw, K. S.; Christensen, M.; Daniau, A.-L.; Dufresne, J.-L.; Feingold, G.; Fiedler, S.; Forster, P.; Gettelman, A.; Haywood, J. M.; Lohmann, U.; Malavelle, F.; Mauritsen, T.; McCoy, D. T.; Myhre, G.; Mülmenstädt, J.; Neubauer, D.; Possner, A.; Rugenstein, M.; Sato, Y.; Schulz, M.; Schwartz, S. E.; Sourdeval, O.; Storelvmo, T.; Toll, V.; Winker, D.;

Stevens, B. Bounding Global Aerosol Radiative Forcing of Climate Change. *Reviews of Geophysics* 2020, *58* (1), e2019RG000660. https://doi.org/10.1029/2019RG000660.

(72) Buseck, P. R.; Pósfai, M. Airborne Minerals and Related Aerosol Particles: Effects on Climate and the Environment. *Proceedings of the National Academy of Sciences* 1999, *96* (7), 3372–3379. https://doi.org/10.1073/pnas.96.7.3372.

(73) Hansen, J. E.; Travis, L. D. Light Scattering in Planetary Atmospheres. *Space Science Reviews* 1974, *16* (4), 527–610. https://doi.org/10.1007/BF00168069.

(74) Li, J.; Carlson, B. E.; Yung, Y. L.; Lv, D.; Hansen, J.; Penner, J. E.; Liao, H.; Ramaswamy, V.; Kahn, R. A.; Zhang, P.; Dubovik, O.; Ding, A.; Lacis, A. A.; Zhang, L.; Dong, Y. Scattering and Absorbing Aerosols in the Climate System. *Nature Reviews Earth & Environment* 2022, *3* (6), 363–379. https://doi.org/10.1038/s43017-022-00296-7.

(75) Plait, P. Why Does Smoke Turn the Sky Orange? https://www.scientificamerican.com/article/why-does-smoke-turn-the-sky-orange/.

(76) Andreae, M. O. *Future Climates of the World: A ModelingPerspective, World Survey of Climatology,*; ed. Henderson-Sellers, A.(Elsevier, Amsterdam), 1995; Vol. 16.

(77) Bond, T. C.; Doherty, S. J.; Fahey, D. W.; Forster, P. M.; Berntsen, T.; DeAngelo, B. J.; Flanner, M. G.; Ghan, S.; Kärcher, B.; Koch, D.; Kinne, S.; Kondo, Y.; Quinn, P. K.; Sarofim, M. C.; Schultz, M. G.; Schulz, M.; Venkataraman, C.; Zhang, H.; Zhang, S.; Bellouin, N.; Guttikunda, S. K.; Hopke, P. K.; Jacobson, M. Z.; Kaiser, J. W.; Klimont, Z.; Lohmann, U.; Schwarz, J. P.; Shindell, D.; Storelvmo, T.; Warren, S. G.; Zender, C. S. Bounding the Role of Black Carbon in the Climate System: A Scientific Assessment. *Journal of Geophysical Research: Atmospheres* 2013, *118* (11), 5380–5552. https://doi.org/10.1002/jgrd.50171.

(78) Akagi, S. K.; Yokelson, R. J.; Wiedinmyer, C.; Alvarado, M. J.; Reid, J. S.; Karl, T.; Crounse, J. D.; Wennberg, P. O. Emission Factors for Open and Domestic Biomass Burning for Use in Atmospheric Models. *Atmospheric Chemistry and Physics* 2011, *11* (9), 4039–4072. https://doi.org/10.5194/acp-11-4039-2011.

(79) May, A. A.; Lee, T.; McMeeking, G. R.; Akagi, S.; Sullivan, A. P.; Urbanski, S.; Yokelson, R. J.; Kreidenweis, S. M. Observations and Analysis of Organic Aerosol Evolution in Some Prescribed Fire Smoke Plumes. *Atmospheric Chemistry and Physics* 2015, *15* (11), 6323–6335. https://doi.org/10.5194/acp-15-6323-2015.

(80) Selimovic, V.; Yokelson, R. J.; McMeeking, G. R.; Coefield, S. In Situ Measurements of Trace Gases, PM, and Aerosol Optical Properties during the 2017 NW US Wildfire Smoke Event. *Atmospheric Chemistry and Physics* 2019, *19* (6), 3905–3926. https://doi.org/10.5194/acp-19-3905-2019.

(81) Kleinman, L. I.; Sedlacek III, A. J.; Adachi, K.; Buseck, P. R.; Collier, S.; Dubey, M. K.; Hodshire, A. L.; Lewis, E.; Onasch, T. B.; Pierce, J. R.; Shilling, J.; Springston, S. R.; Wang, J.; Zhang, Q.; Zhou, S.; Yokelson, R. J. Rapid Evolution of Aerosol Particles and Their Optical Properties Downwind of Wildfires in the Western US. *Atmospheric Chemistry and Physics* 2020, *20* (21), 13319–13341. https://doi.org/10.5194/acp-20-13319-2020.

(82) Wang, R.; Balkanski, Y.; Boucher, O.; Ciais, P.; Schuster, G. L.; Chevallier, F.; Samset, B. H.; Liu, J.; Piao, S.; Valari, M.; Tao, S. Estimation of Global Black Carbon Direct Radiative Forcing and Its Uncertainty Constrained by Observations. *Journal of Geophysical Research: Atmospheres* 2016, *121* (10), 5948–5971. https://doi.org/10.1002/2015JD024326.

(83) Washenfelder, R.; Attwood, A.; Brock, C.; Guo, H.; Xu, L.; Weber, R.; Ng, N.; Allen, H.; Ayres, B.; Baumann, K.; Cohen, R.; Draper, D.; Duffey, K.; Edgerton, E.; Fry, J.; Hu, W.; Jimenez, J.; Palm, B.; Romer, P.; Brown, S. Biomass Burning Dominates Brown Carbon Absorption in the Rural Southeastern United States. *Geophysical Research Letters* 2015, *42* (2), 653–664. https://doi.org/10.1002/2014GL062444.

(84) Hammer, M. S.; Martin, R. V.; van Donkelaar, A.; Buchard, V.; Torres, O.; Ridley, D. A.; Spurr, R. J. D. Interpreting the Ultraviolet Aerosol Index Observed with the OMI Satellite Instrument to Understand Absorption by Organic Aerosols: Implications for Atmospheric Oxidation and Direct Radiative Effects. *Atmospheric Chemistry and Physics* 2016, *16* (4), 2507–2523. https://doi.org/10.5194/acp-16-2507-2016.

(85) Lin, G.; Penner, J. E.; Flanner, M. G.; Sillman, S.; Xu, L.; Zhou, C. Radiative Forcing of Organic Aerosol in the Atmosphere and on Snow: Effects of SOA and Brown Carbon. *Journal of Geophysical Research: Atmospheres* 2014, *119* (12), 7453–7476. https://doi.org/10.1002/2013JD021186.

(86) Zhong, M.; Jang, M. Dynamic Light Absorption of Biomass-Burning Organic Carbon Photochemically Aged under Natural Sunlight. *Atmospheric Chemistry and Physics* 2014, *14* (3), 1517–1525. https://doi.org/10.5194/acp-14-1517-2014.

(87) Sumlin, B. J.; Pandey, A.; Walker, M. J.; Pattison, R. S.; Williams, B. J.; Chakrabarty, R. K. Atmospheric Photooxidation Diminishes Light Absorption by Primary Brown Carbon Aerosol from Biomass Burning. *Environ. Sci. Technol. Lett.* 2017, *4* (12), 540–545. https://doi.org/10.1021/acs.estlett.7b00393.

(88) Wong, J. P. S.; Nenes, A.; Weber, R. J. Changes in Light Absorptivity of Molecular Weight Separated Brown Carbon Due to Photolytic Aging. *Environmental Science & Technology* 2017, *51* (15), 8414–8421. https://doi.org/10.1021/acs.est.7b01739.

(89) Chen, J.-H.; Puttu, U.; Huynh, H. N.; Ahern, A. T.; Ball, K.; Bates, K. H.; Brock, C. A.; Campos, T.; Coggon, M. M.; Crounse, J. D.; de Gouw, J.; DiGangi, J. P.; Diskin, G. S.; Gkatzelis, G. I.; Halliday, H. S.; Hu, L.; Koss, A. R.; Li, Y.; Lyu, M.; Michailoudi, G.; Murphy, S. M.; Nowak, J. B.; Palm, B. B.; Peischl, J.; Permar, W.; Perring, A. E.; Pokhrel,

R. P.; Schafer, N. B.; Schwarz, J. P.; Sekimoto, K.; Selimovic, V.; Stockwell, C. E.; Sullivan, A. P.; Thornton, J. A.; Wagner, N. L.; Wang, S.; Warneke, C.; Wennberg, P. O.; Zeng, L.; Yokelson, R. J.; Weber, R. J.; Xu, L. Atmospheric Evolution of Brown Carbon from Wildfires in North America. *Environ. Sci. Technol.* 2025, *59* (32), 17145–17159. https://doi.org/10.1021/acs.est.5c09020.

(90) Fleming, L. T.; Lin, P.; Roberts, J. M.; Selimovic, V.; Yokelson, R.; Laskin, J.; Laskin, A.; Nizkorodov, S. A. Molecular Composition and Photochemical Lifetimes of Brown Carbon Chromophores in Biomass Burning Organic Aerosol. *Atmospheric Chemistry and Physics* 2020, *20* (2), 1105–1129. https://doi.org/10.5194/acp-20-1105-2020.

(91) Forrister, H.; Liu, J.; Scheuer, E.; Dibb, J.; Ziemba, L.; Thornhill, K. L.; Anderson, B.; Diskin, G.; Perring, A. E.; Schwarz, J. P.; Campuzano-Jost, P.; Day, D. A.; Palm, B. B.; Jimenez, J. L.; Nenes, A.; Weber, R. J. Evolution of Brown Carbon in Wildfire Plumes. *Geophysical Research Letters* 2015, *42* (11), 4623–4630. https://doi.org/10.1002/2015GL063897.

(92) Wang, X.; Heald, C. L.; Liu, J.; Weber, R. J.; Campuzano-Jost, P.; Jimenez, J. L.; Schwarz, J. P.; Perring, A. E. Exploring the Observational Constraints on the Simulation of Brown Carbon. *Atmospheric Chemistry and Physics* 2018, *18* (2), 635–653. https://doi.org/10.5194/acp-18-635-2018.

(93) Brown, H.; Liu, X.; Feng, Y.; Jiang, Y.; Wu, M.; Lu, Z.; Wu, C.; Murphy, S.; Pokhrel, R. Radiative Effect and Climate Impacts of Brown Carbon with the Community Atmosphere Model (CAM5). *Atmospheric Chemistry and Physics* 2018, *18* (24), 17745–17768. https://doi.org/10.5194/acp-18-17745-2018.

(94) Li, C.; He, Q.; Schade, J.; Passig, J.; Zimmermann, R.; Meidan, D.; Laskin, A.; Rudich, Y. Dynamic Changes in Optical and Chemical Properties of Tar Ball Aerosols by Atmospheric Photochemical Aging. *Atmospheric Chemistry and Physics* 2019, *19* (1), 139–163. https://doi.org/10.5194/acp-19-139-2019.

(95) Keyte, I. J.; Harrison, R. M.; Lammel, G. Chemical Reactivity and Long-Range Transport Potential of Polycyclic Aromatic Hydrocarbons – a Review. *Chem. Soc. Rev.* 2013, *42* (24), 9333–9391. https://doi.org/10.1039/C3CS60147A.

(96) Hecobian, A.; Zhang, X.; Zheng, M.; Frank, N.; Edgerton, E. S.; Weber, R. J. Water-Soluble Organic Aerosol Material and the Light-Absorption Characteristics of Aqueous Extracts Measured over the Southeastern United States. *Atmospheric Chemistry and Physics* 2010, *10* (13), 5965–5977. https://doi.org/10.5194/acp-10-5965-2010.

(97) Laskin, A.; Laskin, J.; Nizkorodov, S. A. Chemistry of Atmospheric Brown Carbon. *Chemical Reviews* 2015, *115* (10), 4335–4382. https://doi.org/10.1021/cr5006167.

(98) Zezhen Cheng, A. T. L., Khairallah M. Atwi, Zhenhong Yu, Anita Avery, Edward C. Fortner, Leah Williams, Francesca Majluf, Jordan E. Krechmer. Evolution of the Light-Absorption Properties of Combustion Brown Carbon Aerosols Following Reaction with

Nitrate Radicals. *Aerosol Science and Technology* 2020, *54* (7), 849–863. https://doi.org/10.1080/02786826.2020.1726867.

(99) Titos, G.; Foyo-Moreno, I.; Lyamani, H.; Querol, X.; Alastuey, A.; Alados-Arboledas, L. Optical Properties and Chemical Composition of Aerosol Particles at an Urban Location: An Estimation of the Aerosol Mass Scattering and Absorption Efficiencies. *Journal of Geophysical Research: Atmospheres* 2012, *117* (D4). https://doi.org/10.1029/2011JD016671.

(100) Moosmüller, H.; Chakrabarty, R. K.; Ehlers, K. M.; Arnott, W. P. Absorption Ångström Coefficient, Brown Carbon, and Aerosols: Basic Concepts, Bulk Matter, and Spherical Particles. *Atmospheric Chemistry and Physics* 2011, *11* (3), 1217–1225. https://doi.org/10.5194/acp-11-1217-2011.

(101) Kirchstetter, T. W.; Novakov, T.; Hobbs, P. V. Evidence That the Spectral Dependence of Light Absorption by Aerosols Is Affected by Organic Carbon. *Journal of Geophysical Research: Atmospheres* 2004, *109* (D21). https://doi.org/10.1029/2004JD004999.

(102) Lack, D. A.; Cappa, C. D. Impact of Brown and Clear Carbon on Light Absorption Enhancement, Single Scatter Albedo and Absorption Wavelength Dependence of Black Carbon. *Atmospheric Chemistry and Physics* 2010, *10* (9), 4207–4220. https://doi.org/10.5194/acp-10-4207-2010.

(103) Lack, D. A.; Langridge, J. M. On the Attribution of Black and Brown Carbon Light Absorption Using the Ångström Exponent. *Atmospheric Chemistry and Physics* 2013, *13* (20), 10535–10543. https://doi.org/10.5194/acp-13-10535-2013.

(104) Fuller, K. A.; Malm, W. C.; Kreidenweis, S. M. Effects of Mixing on Extinction by Carbonaceous Particles. *Journal of Geophysical Research: Atmospheres* 1999, *104* (D13), 15941–15954. https://doi.org/10.1029/1998JD100069.

(105) Shiraiwa, M.; Pfrang, C.; Pöschl, U. Kinetic Multi-Layer Model of Aerosol Surface and Bulk Chemistry (KM-SUB): The Influence of Interfacial Transport and Bulk Diffusion on the Oxidation of Oleic Acid by Ozone. *Atmospheric Chemistry and Physics* 2010, *10* (8), 3673–3691. https://doi.org/10.5194/acp-10-3673-2010.

(106) Adler, G.; Flores, J. M.; Abo Riziq, A.; Borrmann, S.; Rudich, Y. Chemical, Physical, and Optical Evolution of Biomass Burning Aerosols: A Case Study. *Atmospheric Chemistry and Physics* 2011, *11* (4), 1491–1503. https://doi.org/10.5194/acp-11-1491-2011.

(107) Lyu, M.; Thompson, D. K.; Zhang, N.; Cuss, C. W.; Young, C. J.; Styler, S. A. Unraveling the Complexity of Atmospheric Brown Carbon Produced by Smoldering Boreal Peat Using Size-Exclusion Chromatography with Selective Mobile Phases. *Environ. Sci.: Atmos.* 2021, *1* (5), 241–252. https://doi.org/10.1039/D1EA00011J.

(108) Glenn, C. K.; El Hajj, O.; McQueen, Z.; Poland, R. P.; Penland, R.; Roberts, E. T.; Choi, J. H.; Bai, B.; Shin, N.; Anosike, A.; Kumar, K. V.; Abdurrahman, M. I.; Liu, P.; Amster, I.

J.; Smith, G. D.; Flanagan, S.; Callaham, M. A.; Loudermilk, E. L.; O'Brien, J. J.; Saleh, R. Brown Carbon Emissions from Biomass Burning under Simulated Wildfire and Prescribed-Fire Conditions. *ACS EST Air* 2024, *1* (9), 1124–1136. https://doi.org/10.1021/acsestair.4c00089.

(109) Schnitzler, E. G.; Liu, T.; Hems, R. F.; Abbatt, J. P. D. Emerging Investigator Series: Heterogeneous OH Oxidation of Primary Brown Carbon Aerosol: Effects of Relative Humidity and Volatility. *Environ Sci Process Impacts* 2020, *22* (11), 2162–2171. https://doi.org/10.1039/d0em00311e.

(110) Levin, E. J. T.; McMeeking, G. R.; Carrico, C. M.; Mack, L. E.; Kreidenweis, S. M.; Wold, C. E.; Moosmüller, H.; Arnott, W. P.; Hao, W. M.; Collett Jr., J. L.; Malm, W. C. Biomass Burning Smoke Aerosol Properties Measured during Fire Laboratory at Missoula Experiments (FLAME). *Journal of Geophysical Research: Atmospheres* 2010, *115* (D18). https://doi.org/10.1029/2009JD013601.

(111) Jen, C. N.; Hatch, L. E.; Selimovic, V.; Yokelson, R. J.; Weber, R.; Fernandez, A. E.; Kreisberg, N. M.; Barsanti, K. C.; Goldstein, A. H. Speciated and Total Emission Factors of Particulate Organics from Burning Western US Wildland Fuels and Their Dependence on Combustion Efficiency. *Atmospheric Chemistry and Physics* 2019, *19* (2), 1013–1026. https://doi.org/10.5194/acp-19-1013-2019.

(112) Zeng, L.; Dibb, J.; Scheuer, E.; Katich, J. M.; Schwarz, J. P.; Bourgeois, I.; Peischl, J.; Ryerson, T.; Warneke, C.; Perring, A. E.; Diskin, G. S.; DiGangi, J. P.; Nowak, J. B.; Moore, R. H.; Wiggins, E. B.; Pagonis, D.; Guo, H.; Campuzano-Jost, P.; Jimenez, J. L.; Xu, L.; Weber, R. J. Characteristics and Evolution of Brown Carbon in Western United States Wildfires. *Atmospheric Chemistry and Physics* 2022, *22* (12), 8009–8036. https://doi.org/10.5194/acp-22-8009-2022.

(113) Browne, E. C.; Zhang, X.; Franklin, J. P.; Ridley, K. J.; Kirchstetter, T. W.; Wilson, K. R.; Cappa, C. D.; Kroll, J. H. Effect of Heterogeneous Oxidative Aging on Light Absorption by Biomass Burning Organic Aerosol. *Aerosol Science and Technology* 2019, *53* (6), 663–674. https://doi.org/10.1080/02786826.2019.1599321.

(114) Hettiyadura, A. P. S.; Garcia, V.; Li, C.; West, C. P.; Tomlin, J.; He, Q.; Rudich, Y.; Laskin, A. Chemical Composition and Molecular-Specific Optical Properties of Atmospheric Brown Carbon Associated with Biomass Burning. *Environ Sci Technol* 2021, *55* (4), 2511–2521. https://doi.org/10.1021/acs.est.0c05883.

(115) Hems, R. F.; Schnitzler, E. G.; Liu-Kang, C.; Cappa, C. D.; Abbatt, J. P. D. Aging of Atmospheric Brown Carbon Aerosol. *ACS Earth and Space Chemistry* 2021, *5* (4), 722–748. https://doi.org/10.1021/acsearthspacechem.0c00346.

(116) Simoneit, B. R. T. Biomass Burning — a Review of Organic Tracers for Smoke from Incomplete Combustion. *Applied Geochemistry* 2002, *17* (3), 129–162. https://doi.org/10.1016/S0883-2927(01)00061-0.

(117) Mohr, C.; Lopez-Hilfiker, F. D.; Zotter, P.; Prévôt, A. S. H.; Xu, L.; Ng, N. L.; Herndon, S. C.; Williams, L. R.; Franklin, J. P.; Zahniser, M. S.; Worsnop, D. R.; Knighton, W. B.; Aiken, A. C.; Gorkowski, K. J.; Dubey, M. K.; Allan, J. D.; Thornton, J. A. Contribution of Nitrated Phenols to Wood Burning Brown Carbon Light Absorption in Detling, United Kingdom during Winter Time. *Environ. Sci. Technol.* 2013, *47* (12), 6316–6324. https://doi.org/10.1021/es400683v.

(118) Bianco, A.; Riva, M.; Baray, J.-L.; Ribeiro, M.; Chaumerliac, N.; George, C.; Bridoux, M.; Deguillaume, L. Chemical Characterization of Cloudwater Collected at Puy de Dôme by FT-ICR MS Reveals the Presence of SOA Components. *ACS Earth Space Chem.* 2019, *3* (10), 2076–2087. https://doi.org/10.1021/acsearthspacechem.9b00153.

(119) Harrison, M. A. J.; Barra, S.; Borghesi, D.; Vione, D.; Arsene, C.; Iulian Olariu, R. Nitrated Phenols in the Atmosphere: A Review. *Atmospheric Environment* 2005, *39*, 231–248. https://doi.org/10.1016/j.atmosenv.2004.09.044.

(120) Grosjean, D. Atmospheric Fate of Toxic Aromatic Compounds. *Science of The Total Environment* 1991, *100*, 367–414. https://doi.org/10.1016/0048-9697(91)90386-S.

(121) Nakayama, T.; Sato, K.; Matsumi, Y.; Imamura, T.; Yamazaki, A.; Uchiyama, A. Wavelength and NO_x Dependent Complex Refractive Index of SOAs Generated from the Photooxidation of Toluene. *Atmospheric Chemistry and Physics* 2013, *13* (2), 531–545. https://doi.org/10.5194/acp-13-531-2013.

(122) Lin, P.; Liu, J.; Shilling, J. E.; Kathmann, S. M.; Laskin, J.; Laskin, A. Molecular Characterization of Brown Carbon (BrC) Chromophores in Secondary Organic Aerosol Generated from Photo-Oxidation of Toluene. *Phys. Chem. Chem. Phys.* 2015, *17* (36), 23312–23325. https://doi.org/10.1039/C5CP02563J.

(123) Liu, P. F.; Abdelmalki, N.; Hung, H.-M.; Wang, Y.; Brune, W. H.; Martin, S. T. Ultraviolet and Visible Complex Refractive Indices of Secondary Organic Material Produced by Photooxidation of the Aromatic Compounds Toluene and M-Xylene. *Atmospheric Chemistry and Physics* 2015, *15* (3), 1435–1446. https://doi.org/10.5194/acp-15-1435-2015.

(124) Wang, Y.; Hu, M.; Wang, Y.; Zheng, J.; Shang, D.; Yang, Y.; Liu, Y.; Li, X.; Tang, R.; Zhu, W.; Du, Z.; Wu, Y.; Guo, S.; Wu, Z.; Lou, S.; Hallquist, M.; Yu, J. Z. The Formation of Nitro-Aromatic Compounds under High NOx and Anthropogenic VOC Conditions in Urban Beijing, China. *Atmospheric Chemistry and Physics* 2019, *19* (11), 7649–7665. https://doi.org/10.5194/acp-19-7649-2019.

(125) Finewax, Z.; de Gouw, J. A.; Ziemann, P. J. Identification and Quantification of 4-Nitrocatechol Formed from OH and NO3 Radical-Initiated Reactions of Catechol in Air in the Presence of NOx: Implications for Secondary Organic Aerosol Formation from Biomass Burning. *Environ. Sci. Technol.* 2018, *52* (4), 1981–1989. https://doi.org/10.1021/acs.est.7b05864.

(126) Xie, M.; Chen, X.; Hays, M. D.; Lewandowski, M.; Offenberg, J.; Kleindienst, T. E.; Holder, A. L. Light Absorption of Secondary Organic Aerosol: Composition and Contribution of Nitroaromatic Compounds. *Environ Sci Technol* 2017, *51* (20), 11607–11616. https://doi.org/10.1021/acs.est.7b03263.

(127) Liu, J.; Lin, P.; Laskin, A.; Laskin, J.; Kathmann, S. M.; Wise, M.; Caylor, R.; Imholt, F.; Selimovic, V.; Shilling, J. E. Optical Properties and Aging of Light-Absorbing Secondary Organic Aerosol. *Atmospheric Chemistry and Physics* 2016, *16* (19), 12815–12827. https://doi.org/10.5194/acp-16-12815-2016.

(128) Decker, Z. C. J.; Zarzana, K. J.; Coggon, M.; Min, K.-E.; Pollack, I.; Ryerson, T. B.; Peischl, J.; Edwards, P.; Dubé, W. P.; Markovic, M. Z.; Roberts, J. M.; Veres, P. R.; Graus, M.; Warneke, C.; de Gouw, J.; Hatch, L. E.; Barsanti, K. C.; Brown, S. S. Nighttime Chemical Transformation in Biomass Burning Plumes: A Box Model Analysis Initialized with Aircraft Observations. *Environ. Sci. Technol.* 2019, *53* (5), 2529–2538. https://doi.org/10.1021/acs.est.8b05359.

(129) Wong, J. P. S.; Tsagkaraki, M.; Tsiodra, I.; Mihalopoulos, N.; Violaki, K.; Kanakidou, M.; Sciare, J.; Nenes, A.; Weber, R. J. Atmospheric Evolution of Molecular-Weight-Separated Brown Carbon from Biomass Burning. *Atmospheric Chemistry and Physics* 2019, *19* (11), 7319–7334. https://doi.org/10.5194/acp-19-7319-2019.

(130) Zhao, R.; Kenseth, C. M.; Huang, Y.; Dalleska, N. F.; Kuang, X. M.; Chen, J.; Paulson, S. E.; Seinfeld, J. H. Rapid Aqueous-Phase Hydrolysis of Ester Hydroperoxides Arising from Criegee Intermediates and Organic Acids. *J Phys Chem A* 2018, *122* (23), 5190–5201. https://doi.org/10.1021/acs.jpca.8b02195.

(131) Hems, R. F.; Abbatt, J. P. D. Aqueous Phase Photo-Oxidation of Brown Carbon Nitrophenols: Reaction Kinetics, Mechanism, and Evolution of Light Absorption. *ACS Earth Space Chem.* 2018, *2* (3), 225–234. https://doi.org/10.1021/acsearthspacechem.7b00123.

(132) Smith, J. D.; Sio, V.; Yu, L.; Zhang, Q.; Anastasio, C. Secondary Organic Aerosol Production from Aqueous Reactions of Atmospheric Phenols with an Organic Triplet Excited State. *Environmental Science & Technology* 2014, *48* (2), 1049–1057. https://doi.org/10.1021/es4045715.

(133) Yu, L.; Smith, J.; Laskin, A.; Anastasio, C.; Laskin, J.; Zhang, Q. Chemical Characterization of SOA Formed from Aqueous-Phase Reactions of Phenols with the Triplet Excited State of Carbonyl and Hydroxyl Radical. *Atmospheric Chemistry and Physics* 2014, *14* (24), 13801–13816. https://doi.org/10.5194/acp-14-13801-2014.

(134) Corral Arroyo, P.; Bartels-Rausch, T.; Alpert, P. A.; Dumas, S.; Perrier, S.; George, C.; Ammann, M. Particle-Phase Photosensitized Radical Production and Aerosol Aging. *Environ. Sci. Technol.* 2018, *52* (14), 7680–7688. https://doi.org/10.1021/acs.est.8b00329.

(135) Rossignol, S.; Aregahegn, K. Z.; Tinel, L.; Fine, L.; Nozière, B.; George, C. Glyoxal Induced Atmospheric Photosensitized Chemistry Leading to Organic Aerosol Growth. *Environ. Sci. Technol.* 2014, *48* (6), 3218–3227. https://doi.org/10.1021/es405581g.

(136) Kaur, R.; Anastasio, C. First Measurements of Organic Triplet Excited States in Atmospheric Waters. *Environ. Sci. Technol.* 2018, *52* (9), 5218–5226. https://doi.org/10.1021/acs.est.7b06699.

(137) Kitanovski, Z.; Čusak, A.; Grgić, I.; Claeys, M. Chemical Characterization of the Main Products Formed through Aqueous-Phase Photonitration of Guaiacol. *Atmospheric Measurement Techniques* 2014, *7* (8), 2457–2470. https://doi.org/10.5194/amt-7-2457-2014.

(138) Pang, H.; Zhang, Q.; Lu, X.; Li, K.; Chen, H.; Chen, J.; Yang, X.; Ma, Y.; Ma, J.; Huang, C. Nitrite-Mediated Photooxidation of Vanillin in the Atmospheric Aqueous Phase. *Environ Sci Technol* 2019, *53* (24), 14253–14263. https://doi.org/10.1021/acs.est.9b03649.

(139) Vidović, K.; Kroflič, A.; Šala, M.; Grgić, I. Aqueous-Phase Brown Carbon Formation from Aromatic Precursors under Sunlight Conditions. *Atmosphere* 2020, *11* (2). https://doi.org/10.3390/atmos11020131.

(140) Smith, J. D.; Kinney, H.; Anastasio, C. Phenolic Carbonyls Undergo Rapid Aqueous Photodegradation to Form Low-Volatility, Light-Absorbing Products. *Atmospheric Environment* 2016, *126*, 36–44. https://doi.org/10.1016/j.atmosenv.2015.11.035.

(141) Di Lorenzo, R. A.; Washenfelder, R. A.; Attwood, A. R.; Guo, H.; Xu, L.; Ng, N. L.; Weber, R. J.; Baumann, K.; Edgerton, E.; Young, C. J. Molecular-Size-Separated Brown Carbon Absorption for Biomass-Burning Aerosol at Multiple Field Sites. *Environmental Science and Technology* 2017, *51* (6), 3128–3137. https://doi.org/10.1021/acs.est.6b06160.

(142) Azzarello, L.; Washenfelder, R. A.; Robinson, M. A.; Franchin, A.; Womack, C. C.; Holmes, C. D.; Brown, S. S.; Middlebrook, A.; Newberger, T.; Sweeney, C.; Young, C. J. Characterization of Water-Soluble Brown Carbon Chromophores from Wildfire Plumes in the Western USA Using Size-Exclusion Chromatography. *Atmospheric Chemistry and Physics* 2023, *23* (24), 15643–15654. https://doi.org/10.5194/acp-23-15643-2023.

(143) Magalhães, A. C. O.; Esteves da Silva, J. C. G.; Pinto da Silva, L. Density Functional Theory Calculation of the Absorption Properties of Brown Carbon Chromophores Generated by Catechol Heterogeneous Ozonolysis. *ACS Earth Space Chem.* 2017, *1* (6), 353–360. https://doi.org/10.1021/acsearthspacechem.7b00061.

(144) Abbatt, J. P. D.; Lee, A. K. Y.; Thornton, J. A. Quantifying Trace Gas Uptake to Tropospheric Aerosol: Recent Advances and Remaining Challenges. *Chem. Soc. Rev.* 2012, *41* (19), 6555–6581. https://doi.org/10.1039/C2CS35052A.

(145) Sareen, N.; Moussa, S. G.; McNeill, V. F. Photochemical Aging of Light-Absorbing Secondary Organic Aerosol Material. *J. Phys. Chem. A* 2013, *117* (14), 2987–2996. https://doi.org/10.1021/jp309413j.

(146) Wang, X.-C.; Lee, C. Sources and Distribution of Aliphatic Amines in Salt Marsh Sediment. *Organic Geochemistry* 1994, *22* (6), 1005–1021. https://doi.org/10.1016/0146-6380(94)90034-5.

(147) Lobert, J. M.; Scharffe, D. H.; Hao, W. M.; Crutzen, P. J. Importance of Biomass Burning in the Atmospheric Budgets of Nitrogen-Containing Gases. *Nature* 1990, *346* (6284), 552–554. https://doi.org/10.1038/346552a0.

(148) Pierson, W. R.; Brachaczek, W. W. Emissions of Ammonia and Amines from Vehicles on the Road. *Environ. Sci. Technol.* 1983, *17* (12), 757–760. https://doi.org/10.1021/es00118a013.

(149) Calderón, S. M.; Poor, N. D.; Campbell, S. W. Estimation of the Particle and Gas Scavenging Contributions to Wet Deposition of Organic Nitrogen. *Atmospheric Environment* 2007, *41* (20), 4281–4290. https://doi.org/10.1016/j.atmosenv.2006.06.067.

(150) Bergman, T.; Laaksonen, A.; Korhonen, H.; Malila, J.; Dunne, E. M.; Mielonen, T.; Lehtinen, K. E. J.; Kühn, T.; Arola, A.; Kokkola, H. Geographical and Diurnal Features of Amine-Enhanced Boundary Layer Nucleation. *Journal of Geophysical Research: Atmospheres* 2015, *120* (18), 9606–9624. https://doi.org/10.1002/2015JD023181.

(151) Shapiro, E. L.; Szprengiel, J.; Sareen, N.; Jen, C. N.; Giordano, M. R.; McNeill, V. F. Light-Absorbing Secondary Organic Material Formed by Glyoxal in Aqueous Aerosol Mimics. *Atmospheric Chemistry and Physics* 2009, *9* (7), 2289–2300. https://doi.org/10.5194/acp-9-2289-2009.

(152) Nguyen, T. B.; Lee, P. B.; Updyke, K. M.; Bones, D. L.; Laskin, J.; Laskin, A.; Nizkorodov, S. A. Formation of Nitrogen- and Sulfur-Containing Light-Absorbing Compounds Accelerated by Evaporation of Water from Secondary Organic Aerosols. *Journal of Geophysical Research: Atmospheres* 2012, *117* (D1). https://doi.org/10.1029/2011JD016944.

(153) Nozière, B.; Dziedzic, P.; Córdova, A. Formation of Secondary Light-Absorbing "Fulvic-like" Oligomers: A Common Process in Aqueous and Ionic Atmospheric Particles? *Geophysical Research Letters* 2007, *34* (21). https://doi.org/10.1029/2007GL031300.

(154) Woo, J. L.; Kim, D. D.; Schwier, A. N.; Li, R.; McNeill, V. F. Aqueous Aerosol SOA Formation: Impact on Aerosol Physical Properties. *Faraday Discuss.* 2013, *165* (0), 357–367. https://doi.org/10.1039/C3FD00032J.

(155) De Haan, D. O.; Hawkins, L. N.; Kononenko, J. A.; Turley, J. J.; Corrigan, A. L.; Tolbert, M. A.; Jimenez, J. L. Formation of Nitrogen-Containing Oligomers by Methylglyoxal and

Amines in Simulated Evaporating Cloud Droplets. *Environ. Sci. Technol.* 2011, *45* (3), 984–991. https://doi.org/10.1021/es102933x.

(156) Sedehi, N.; Takano, H.; Blasic, V. A.; Sullivan, K. A.; De Haan, D. O. Temperature- and pH-Dependent Aqueous-Phase Kinetics of the Reactions of Glyoxal and Methylglyoxal with Atmospheric Amines and Ammonium Sulfate. *Atmospheric Environment* 2013, *77*, 656–663. https://doi.org/10.1016/j.atmosenv.2013.05.070.

(157) De Haan, D. O.; Tolbert, M. A.; Jimenez, J. L. Atmospheric Condensed-Phase Reactions of Glyoxal with Methylamine. *Geophysical Research Letters* 2009, *36* (11). https://doi.org/10.1029/2009GL037441.

(158) Qiu, C.; Zhang, R. Multiphase Chemistry of Atmospheric Amines. *Phys. Chem. Chem. Phys.* 2013, *15* (16), 5738–5752. https://doi.org/10.1039/C3CP43446J.

(159) Hatch, L. E.; Rivas-Ubach, A.; Jen, C. N.; Lipton, M.; Goldstein, A. H.; Barsanti, K. C. Measurements of I/SVOCs in Biomass-Burning Smoke Using Solid-Phase Extraction Disks and Two-Dimensional Gas Chromatography. *Atmospheric Chemistry and Physics* 2018, *18* (24), 17801–17817. https://doi.org/10.5194/acp-18-17801-2018.

(160) Donahue, N. M.; Robinson, A. L.; Stanier, C. O.; Pandis, S. N. Coupled Partitioning, Dilution, and Chemical Aging of Semivolatile Organics. *Environ. Sci. Technol.* 2006, *40* (8), 2635–2643. https://doi.org/10.1021/es052297c.

(161) Donahue, N. M.; Robinson, A. L.; Pandis, S. N. Atmospheric Organic Particulate Matter: From Smoke to Secondary Organic Aerosol. *Atmospheric Environment* 2009, *43* (1), 94–106. https://doi.org/10.1016/j.atmosenv.2008.09.055.

(162) Donahue, N. M.; Epstein, S. A.; Pandis, S. N.; Robinson, A. L. A Two-Dimensional Volatility Basis Set: 1. Organic-Aerosol Mixing Thermodynamics. *Atmospheric Chemistry and Physics* 2011, *11* (7), 3303–3318. https://doi.org/10.5194/acp-11-3303-2011.

(163) Faulhaber, A. E.; Thomas, B. M.; Jimenez, J. L.; Jayne, J. T.; Worsnop, D. R.; Ziemann, P. J. Characterization of a Thermodenuder-Particle Beam Mass Spectrometer System for the Study of Organic Aerosol Volatility and Composition. *Atmospheric Measurement Techniques* 2009, *2* (1), 15–31. https://doi.org/10.5194/amt-2-15-2009.

(164) Cappa, C. D. A Model of Aerosol Evaporation Kinetics in a Thermodenuder. *Atmospheric Measurement Techniques* 2010, *3* (3), 579–592. https://doi.org/10.5194/amt-3-579-2010.

(165) Pagonis, D.; Selimovic, V.; Campuzano-Jost, P.; Guo, H.; Day, D. A.; Schueneman, M. K.; Nault, B. A.; Coggon, M. M.; DiGangi, J. P.; Diskin, G. S.; Fortner, E. C.; Gargulinski, E. M.; Gkatzelis, G. I.; Hair, J. W.; Herndon, S. C.; Holmes, C. D.; Katich, J. M.; Nowak, J. B.; Perring, A. E.; Saide, P.; Shingler, T. J.; Soja, A. J.; Thapa, L. H.; Warneke, C.; Wiggins, E. B.; Wisthaler, A.; Yacovitch, T. I.; Yokelson, R. J.; Jimenez, J. L. Impact of Biomass Burning Organic Aerosol Volatility on Smoke Concentrations Downwind of Fires. *Environ. Sci. Technol.* 2023, *57* (44), 17011–17021. https://doi.org/10.1021/acs.est.3c05017.

(166) May, A. A.; Levin, E. J. T.; Hennigan, C. J.; Riipinen, I.; Lee, T.; Collett Jr., J. L.; Jimenez, J. L.; Kreidenweis, S. M.; Robinson, A. L. Gas-Particle Partitioning of Primary Organic Aerosol Emissions: 3. Biomass Burning. *Journal of Geophysical Research: Atmospheres* 2013, *118* (19), 11,327-11,338. https://doi.org/10.1002/jgrd.50828.

(167) Nash, D. G.; Baer, T.; Johnston, M. V. Aerosol Mass Spectrometry: An Introductory Review. *International Journal of Mass Spectrometry* 2006, *258* (1), 2–12. https://doi.org/10.1016/j.ijms.2006.09.017.

(168) Jimenez, J. L.; Jayne, J. T.; Shi, Q.; Kolb, C. E.; Worsnop, D. R.; Yourshaw, I.; Seinfeld, J. H.; Flagan, R. C.; Zhang, X.; Smith, K. A.; Morris, J. W.; Davidovits, P. Ambient Aerosol Sampling Using the Aerodyne Aerosol Mass Spectrometer. *Journal of Geophysical Research: Atmospheres* 2003, *108* (D7). https://doi.org/10.1029/2001JD001213.

(169) Weber, R. J.; Orsini, D.; Daun, Y.; Lee, Y.-N.; Klotz, P. J.; Brechtel, F. A Particle-into-Liquid Collector for Rapid Measurement of Aerosol Bulk Chemical Composition. *Aerosol Science and Technology* 2001, *35* (3), 718–727. https://doi.org/10.1080/02786820152546761.

(170) Orsini, D. A.; Ma, Y.; Sullivan, A.; Sierau, B.; Baumann, K.; Weber, R. J. Refinements to the Particle-into-Liquid Sampler (PILS) for Ground and Airborne Measurements of Water Soluble Aerosol Composition. *Atmospheric Environment* 2003, *37* (9), 1243–1259. https://doi.org/10.1016/S1352-2310(02)01015-4.

(171) Washenfelder, R. A.; Azzarello, L.; Ball, K.; Brown, S. S.; Decker, Z. C. J.; Franchin, A.; Fredrickson, C. D.; Hayden, K.; Holmes, C. D.; Middlebrook, A. M.; Palm, B. B.; Pierce, R. B.; Price, D. J.; Roberts, J. M.; Robinson, M. A.; Thornton, J. A.; Womack, C. C.; Young, C. J. Complexity in the Evolution, Composition, and Spectroscopy of Brown Carbon in Aircraft Measurements of Wildfire Plumes. *Geophysical Research Letters* 2022, *49* (9), e2022GL098951. https://doi.org/10.1029/2022GL098951.

(172) Sullivan, A. P.; Weber, R. J.; Clements, A. L.; Turner, J. R.; Bae, M. S.; Schauer, J. J. A Method for On-Line Measurement of Water-Soluble Organic Carbon in Ambient Aerosol Particles: Results from an Urban Site. *Geophysical Research Letters* 2004, *31* (13). https://doi.org/10.1029/2004GL019681.

(173) Marple, V.; Olson, B.; Romay, F.; Hudak, G.; Geerts, S. M.; Lundgren, D. Second Generation Micro-Orifice Uniform Deposit Impactor, 120 MOUDI-II: Design, Evaluation, and Application to Long-Term Ambient Sampling. *Aerosol Science and Technology* 2014, *48* (4), 427–433. https://doi.org/10.1080/02786826.2014.884274.

(174) Marple, V. A.; Rubow, K. L.; Behm, S. M. A Microorifice Uniform Deposit Impactor (MOUDI): Description, Calibration, and Use. *Aerosol Science and Technology* 1991, *14* (4), 434–446. https://doi.org/10.1080/02786829108959504.

(175) Cheng, Z.; Atwi, K.; Hajj, O. E.; Ijeli, I.; Fischer, D. A.; Smith, G.; Saleh, R. Discrepancies between Brown Carbon Light-Absorption Properties Retrieved from Online and Offline Measurements. *Aerosol Science and Technology* 2021, *55* (1), 92–103. https://doi.org/10.1080/02786826.2020.1820940.

(176) Meunier, D. M.; Wade, J. H.; Janco, M.; Cong, R.; Gao, W.; Li, Y.; Mekap, D.; Wang, G. Recent Advances in Separation-Based Techniques for Synthetic Polymer Characterization. *Anal. Chem.* 2021, *93* (1), 273–294. https://doi.org/10.1021/acs.analchem.0c04352.

(177) Lin, C.-F.; Huang, Y.-J.; Hao, O. J. Ultrafiltration Processes for Removing Humic Substances: Effect of Molecular Weight Fractions and PAC Treatment. *Water Research* 1999, *33* (5), 1252–1264. https://doi.org/10.1016/S0043-1354(98)00322-4.

(178) Jokubauskaite, I.; Amaleviciute, K.; Lepane, V.; Slepetiene, A.; Slepetys, J.; Liaudanskiene, I.; Karcauskiene, D.; Booth, C. A. High-Performance Liquid Chromatography (HPLC)-Size Exclusion Chromatography (SEC) for Qualitative Detection of Humic Substances and Dissolved Organic Matter in Mineral Soils and Peats in Lithuania. *International Journal of Environmental Analytical Chemistry* 2015, *95* (6), 508–519. https://doi.org/10.1080/03067319.2015.1048435.

(179) Kummari, R.; Bose, K. Gel Filtration Chromatography. In *Textbook on Cloning, Expression and Purification of Recombinant Proteins*; Bose, K., Ed.; Springer Nature Singapore: Singapore, 2022; pp 199–219. https://doi.org/10.1007/978-981-16-4987-5_8.

(180) Konermann, L. Addressing a Common Misconception: Ammonium Acetate as Neutral pH "Buffer" for Native Electrospray Mass Spectrometry. *J. Am. Soc. Mass Spectrom.* 2017, *28* (9), 1827–1835. https://doi.org/10.1007/s13361-017-1739-3.

(181) Subirats, X.; Bosch, E.; Rosés, M. Buffer Considerations for LC and LC-MS. *Lc Gc North America* 2009, *27*, 1000–1004.

(182) Element Lab Solutions. *Ammonium Acetate Buffers*. https://www.elementlabsolutions.com/uk/chromatography-blog/post/ammonium-acetate-buffers.

(183) Pelekani, C.; Newcombe, G.; Snoeyink, V. L.; Hepplewhite, C.; Assemi, S.; Beckett, R. Characterization of Natural Organic Matter Using High Performance Size Exclusion Chromatography. *Environ. Sci. Technol.* 1999, *33* (16), 2807–2813. https://doi.org/10.1021/es9901314.

(184) Thermo Fisher Scientific Inc. Thermo Scientific Dionex UltiMate 3000 Series. https://tools.thermofisher.com/content/sfs/manuals/MAN-LC-DAD-MWD-Operation-Sep13-DOC4820-8250-1-4.pdf.

(185) Aiken, G. R.; Malcolm, R. L. Molecular Weight of Aquatic Fulvic Acids by Vapor Pressure Osmometry. *Geochimica et Cosmochimica Acta* 1987, *51* (8), 2177–2184. https://doi.org/10.1016/0016-7037(87)90267-5.

(186) de Wit, J. C. M.; van Riemsdijk, W. H.; Koopal, L. K. Proton Binding to Humic Substances. 1. Electrostatic Effects. *Environ. Sci. Technol.* 1993, *27* (10), 2005–2014. https://doi.org/10.1021/es00047a004.

(187) Tanaka, T.; Nagao, S.; Sakamoto, Y.; Ohnuki, T.; Ni, S.; Senoo, M. Distribution Coefficient in the Sorption of Radionuclides onto Ando Soil in the Presence of Humic Acid: Influence of the Molecular Size of Humic Acid. *Journal of nuclear science and technology* 1997, *34* (8), 829–834.

(188) Vermeer, A. W. P.; Koopal, L. K. Adsorption of Humic Acids to Mineral Particles. 2. Polydispersity Effects with Polyelectrolyte Adsorption. *Langmuir* 1998, *14* (15), 4210–4216.

(189) Zhou, Q.; Cabaniss, S. E.; Maurice, P. A. Considerations in the Use of High-Pressure Size Exclusion Chromatography (HPSEC) for Determining Molecular Weights of Aquatic Humic Substances. *Water Research* 2000, *34* (14), 3505–3514. https://doi.org/10.1016/S0043-1354(00)00115-9.

(190) Cabaniss, S. E.; Zhou, Q.; Maurice, P. A.; Chin, Y.-P.; Aiken, G. R. A Log-Normal Distribution Model for the Molecular Weight of Aquatic Fulvic Acids. *Environmental Science & Technology* 2000, *34* (6), 1103–1109.

(191) Di Lorenzo, R. A.; Young, C. J. Size Separation Method for Absorption Characterization in Brown Carbon: Application to an Aged Biomass Burning Sample. *Geophysical Research Letters* 2016, *43* (1), 458–465. https://doi.org/10.1002/2015GL066954.

(192) Yaw, W. W.; Kirkland, J. J.; Bly, D. D. *Modern Size Exclusion Chromatography*; John Wiley & Sons, Inc., New York, 1979.

(193) Weiss, J. *Handbook of Ion Chromatography*, 4th ed.; Wiley, 2016; Vol. 1,2,3.

(194) Thermo Fisher Scientific. Dionex DRS 600 / ERS 500e / ERS 500 Carbonate Suppressors User Guide, 2024. https://documents.thermofisher.com/TFS-Assets/CMD/manuals/man-031956-dionex-suppressors-man031956-en.pdf.

(195) Oikawa, K.; Saito, H. Ion Chromatographic Determination of Anions in Rainwater. *Chemosphere* 1982, *11* (9), 933–941. https://doi.org/10.1016/0045-6535(82)90141-2.

(196) Mai, Y.; Debruille, K.; Mikhail, I.; Gupta, V.; Murray, E.; Frantsuzov, R.; Paull, B. Measuring Nitrite and Nitrate in Rain and River Water Samples Using a Portable Ion Chromatograph in Step-Gradient Mode and High Sensitivity Detection Flow Cell. *J Sep Sci* 2025, *48* (4), e70134. https://doi.org/10.1002/jssc.70134.

(197) Xu, J.; Song, S.; Harrison, R. M.; Song, C.; Wei, L.; Zhang, Q.; Sun, Y.; Lei, L.; Zhang, C.; Yao, X.; Chen, D.; Li, W.; Wu, M.; Tian, H.; Luo, L.; Tong, S.; Li, W.; Wang, J.; Shi, G.; Huangfu, Y.; Tian, Y.; Ge, B.; Su, S.; Peng, C.; Chen, Y.; Yang, F.; Mihajlidi-Zelić, A.;

Đorđević, D.; Swift, S. J.; Andrews, I.; Hamilton, J. F.; Sun, Y.; Kramawijaya, A.; Han, J.; Saksakulkrai, S.; Baldo, C.; Hou, S.; Zheng, F.; Daellenbach, K. R.; Yan, C.; Liu, Y.; Kulmala, M.; Fu, P.; Shi, Z. An Interlaboratory Comparison of Aerosol Inorganic Ion Measurements by Ion Chromatography: Implications for Aerosol pH Estimate. *Atmospheric Measurement Techniques* 2020, *13* (11), 6325–6341. https://doi.org/10.5194/amt-13-6325-2020.

(198) Marko-Varga, Gyoergy.; Csiky, Istvan.; Joensson, J. Aake. Ion-Chromatographic Determination of Nitrate and Sulfate in Natural Waters Containing Humic Substances. *Anal. Chem.* 1984, *56* (12), 2066–2069. https://doi.org/10.1021/ac00276a020.

(199) Boyes, B.; Dong, M. Modern Trends and Best Practices in Mobile-Phase Selection in Reversed-Phase Chromatography. *LCGC North America* 2018, *36* (10).

(200) Hayward, S. J.; Lei, Y. D.; Wania, F. Comparative Evaluation of Three High-Performance Liquid Chromatography–Based Kow Estimation Methods for Highly Hydrophobic Organic Compounds: Polybrominated Diphenyl Ethers and Hexabromocyclododecane. *Environmental Toxicology and Chemistry* 2006, *25* (8), 2018–2027. https://doi.org/10.1897/05-675R.1.

(201) Finizio, A.; Vighi, M.; Sandroni, D. Determination of N-Octanol/Water Partition Coefficient (Kow) of Pesticide Critical Review and Comparison of Methods. *Chemosphere* 1997, *34* (1), 131–161. https://doi.org/10.1016/S0045-6535(96)00355-4.

(202) Dias, N. C.; Nawas, M. I.; Poole, C. F. Evaluation of a Reversed-Phase Column (Supelcosil LC-ABZ) under Isocratic and Gradient Elution Conditions for Estimating Octanol–Water Partition Coefficients. *Analyst* 2003, *128* (5), 427–433. https://doi.org/10.1039/B300574G.

(203) Kaune, A.; Knorrenschild, M.; Kettrup, A. Predicting 1-Octanol-Water Partition Coefficient by High-Performance Liquid Chromatography Gradient Elution. *Fresenius' Journal of Analytical Chemistry* 1995, *352* (3), 303–312. https://doi.org/10.1007/BF00322226.

(204) Lei, Y. D.; Wania, F.; Shiu, W. Y.; Boocock, D. G. B. HPLC-Based Method for Estimating the Temperature Dependence of n-Octanol−Water Partition Coefficients. *J. Chem. Eng. Data* 2000, *45* (5), 738–742. https://doi.org/10.1021/je9902488.

(205) Poole, S. K.; Poole, C. F. Separation Methods for Estimating Octanol-Water Partition Coefficients. *J Chromatogr B Analyt Technol Biomed Life Sci* 2003, *797* (1–2), 3–19. https://doi.org/10.1016/j.jchromb.2003.08.032.

(206) Han, S.; Liang, C.; Qiao, J.; Lian, H.; Ge, X.; Chen, H. A Novel Evaluation Method for Extrapolated Retention Factor in Determination of N-Octanol/Water Partition Coefficient of Halogenated Organic Pollutants by Reversed-Phase High Performance Liquid Chromatography. *Analytica Chimica Acta* 2012, *713*, 130–135. https://doi.org/10.1016/j.aca.2011.11.020.

(207) Sahu, S. K.; Pandit, G. G. Estimation of Octanol-Water Partition Coefficients for Polycylic Aromatic Hydrocarbons Using Reverse-Phase HPLC. *Journal of Liquid Chromatography & Related Technologies* 2003, *26* (1), 135–146. https://doi.org/10.1081/JLC-120017158.

Chapter 2

Characterization of water-soluble brown carbon chromophores from wildfire plumes in the western U.S. using size exclusion chromatography

2.1 Abstract

Wildfires are an important source of carbonaceous aerosol in the atmosphere. Organic aerosol that absorbs light in the ultraviolet to visible spectral range is referred to as "brown carbon" (BrC), and its impact on Earth's radiative budget has not been well characterized. We collected water-soluble brown carbon using a particle into liquid sampler (PILS) onboard a Twin Otter aircraft during the Fire Influence on Regional to Global Environments and Air Quality (FIREX-AQ) campaign. Samples were collected downwind of wildfires in the western United States from August to September 2019. We applied size exclusion chromatography (SEC) with ultraviolet-visible spectroscopy to characterize the molecular size distribution of BrC chromophores. The wildfire plumes had transport ages of 0 to 5 h and the absorption was dominated by chromophores with molecular weights <500 Da. With BrC normalized to a conserved biomass burning tracer, carbon monoxide, a consistent decrease in BrC absorption with plume age was not observed during FIREX-AQ. These findings are consistent with the variable trends in BrC absorption with plume age reported in recent studies. While BrC absorption trends were broadly consistent between the offline SEC analysis and the online PILS measurements, the absolute values of absorption and their spectral dependence differed. We investigate plausible explanations for the discrepancies observed between the online and offline analyses. This included solvent effects, pH, and sample storage. We suspect that sample storage impacted the absorption intensity of the offline measurements without impacting the molecular weight distribution of BrC chromophores.

2.2 Introduction

The wildfire season across the western United States has greatly intensified over the past century. The U.S. Forest Service reports that the amount of western U.S. land burned by "high severity" wildfires (i.e., fires that destroy more than 95% of vegetation) has increased eightfold since 1985.[1]A variety of factors influence the number and intensity of wildfires, including fuel availability, temperature, drought conditions, location of lightning strikes, and direct human influence. During the 20th century, fire suppression tactics were applied throughout the western U.S. and these efforts caused fuel to accumulate.[2] The combination of dry conditions, warmer temperatures, and fuel availability contributes to the intensity of present-day wildfires in the western U.S. Consequently, the impact that these climatic conditions have on wildfire activity has been established. However, feedback effects that wildfires have on climate is an ongoing area of research.

Wildfires emit carbonaceous particulate matter into the atmosphere.[3,4] Based on volatility and optical properties, carbonaceous aerosol particles emitted from biomass burning are categorized as elemental carbon (EC) and organic carbon (OC).[5] Elemental carbon, referred to as black carbon (BC), is refractory and is characterized by broad absorbance across the ultraviolet (UV) to infrared wavelengths.[6–8] The light-absorbing components of organic aerosols are referred to as brown carbon (BrC).[8] The direct absorption and scattering of solar radiation by these aerosol particles impacts the global radiative budget,[9,10] but there is uncertainty about the magnitude of this effect. Currently, more information is known about BC and its impact on climate than BrC, as BrC is more chemically complex and more reactive.[11,12] The direct radiative forcing of BC has been estimated to be the second largest anthropogenic climate forcing species[13] and studies have

suggested that BrC can contribute between 20 to 40 % to positive radiative forcing from total carbonaceous absorbing aerosol.[14–16]

Wildfire emissions are a dominant primary source of BrC.[17] The brown colour results from a combination of species with varying abilities to absorb light in the UV-visible region (from highly to weakly absorbing).[18] The pyrolysis of lignin and cellulose contributes to the major chemical constituents in wildfire plumes, such as phenolic compounds and organic acids.[19–21] Lignin pyrolysis products with aromatic functionalities absorb visible light and may contribute to the absorption properties of BrC.[18] Secondary processes also contribute to BrC formation. The generation of secondary organic aerosol (SOA) stemming from gas phase reaction products includes nitration of aromatic compounds in the presence of NO_x or NO_3.[22–24] For example, catechol can react with either the NO_3 or OH radical to form 4-nitrocatechol[23] and oxidation of toluene under elevated NO_x conditions has been observed to form over 15 absorbing compounds with nitroaromatics contributing up to 60% of absorption in the visible region.[25] Although there are hypotheses about the identity of BrC chromophores, up to 40% of BrC constituents remain unidentified.[26,27]

To characterize the absorbing constituents that contribute to BrC absorption, reverse phase high performance liquid chromatography (HPLC) coupled to high resolution mass spectrometry has been applied.[28] However, fresh and aged BrC consist of extremely low volatile organic compounds (ELVOCs) that may be irreversibly retained on a traditional C_{18} reverse phase HPLC column.[29] Size exclusion chromatography coupled to ultraviolet-visible absorption spectroscopy (SEC-UV) has been demonstrated as an alternative that successfully measures the absorption properties of high and low molecular weight (MW) ELVOCs in fresh and aged biomass burning-derived samples.[12,29,30] Analysis by SEC-UV has been previously applied to samples collected

during ground-based field measurement campaigns, where the method has established the quantification of BrC absorbance as a function of MW and provided insight into the composition of BrC. High MW (>400 Da) compounds with unknown structural identities have been determined to contribute to BrC absorption and the relative contribution to BrC absorption by high MW species increases with smoke age.[12,30,31] These findings suggested that lower MW species are less persistent in biomass burning smoke relative to higher MW species, likely due to volatilization, oxidation, polymerization, or other processes.[12,18]

The Fire Influence on Regional to Global Environments and Air Quality (FIREX-AQ) field campaign examined the impact of wildfires on atmospheric chemistry and air quality in the western United States. In this work, we present the SEC-UV analysis of water-soluble BrC that was collected on board the National Oceanic and Atmospheric Administration (NOAA) Twin Otter aircraft during plume transects downwind from western U.S forest fires. These represent the first aircraft samples analyzed by SEC-UV to characterize BrC. We compare the total absorption measured in online and offline samples and assign the BrC absorption to different MW classes. Finally, we examine how the composition of the mobile phase used in the SEC-UV analysis impacts elution time and spectral features. This provides cautionary information about interpreting absorption results in studies that apply chromatographic separation in an aqueous-organic matrix.

2.3 Experimental Approach

2.3.1 Overview of the FIREX-AQ field campaign

FIREX-AQ was a multi-platform field campaign that investigated wildfire emissions in the western United States (U.S) from Jul to Sep 2019. Instrumented aircraft and mobile laboratories were used to intercept and sample smoke plumes throughout multiple western U.S. states. These included a DC-8, ER-2, and two Twin Otter aircraft. This study focuses on smoke sampled by the

"Chemistry" Twin Otter aircraft, which was based in Boise, Idaho, from 29 Jul to 5 Sep 2019, and briefly in Cedar City, Utah, from 19 Aug to 23 Aug 2019. The Twin Otter payload included gas and aerosol instruments to measure smoke composition, transport, and transformation. This included CO measurements by near infrared cavity ring-down spectroscopy (G2401-m; Picarro Inc., Santa Clara, CA, USA).[32,33] A complete description of the payload installed on the Twin Otter can be found in Warneke et al.[34] The payload weight limited the duration of in-flight sampling to 2.5 – 3 hours, with a typical schedule of two or three flights per day during the afternoon, evening, or night. A total of 40 flights were completed in Arizona, Idaho, Nevada, Oregon, and Utah. Airmass back trajectory analyses were used to estimate the plume age of each transect, as described in Liao et al. and Washenfelder et al.[35,36] Briefly, the smoke age was calculated by summing the horizontal advection and vertical plume rise ages between the time of emission and the aircraft interception of the smoke plume. For the Twin Otter flights, many plume intercepts by the aircraft were approximately Lagrangian.[36]

2.3.2 Online measurement of water-soluble absorption and offline sample collection

The Brown Carbon-Particle into Liquid Sampler (BrC-PILS) collected online absorption data and offline aqueous samples for the SEC-UV analysis. A complete description of the BrC-PILS instrument and sampling can be found in Zeng et al. and Washenfelder et al.[36,37] Briefly, the BrC-PILS sampled smoke through a shared aerosol inlet on the Twin Otter. A parallel-plate carbon filter denuder removed volatile organic compounds prior to the aerosol entering the PILS. The PILS consisted of a steam generator and droplet impactor to collect aerosols into aqueous solution. The liquid flow then entered a liquid waveguide capillary cell (LWCC) to measure absorption. The instrument precision (3σ) for absorption at 365 nm was ±0.02 Mm^{-1} for 10 s in-flight data, with an uncertainty of ±11 %.[37] The flow exiting the LWCC was split between a total organic carbon

(TOC) analyzer and an automated 14-port valve. The valve directed aqueous sample flow to one of 12 polypropylene sample tubes for offline SEC-UV analysis (Figure A-1). Prior to deployment, each polypropylene tube was rinsed with 18.2 MΩ·cm deionized water (DIW) (Thermo Scientific Barnstead Smart2Pure) eight to ten times. The sample flow rate was monitored by a liquid mass flow meter prior to the flow diverting between the automated valve and the TOC analyzer. The sample flow was 1.53 mL min^{-1} during inflight sampling, and the excess 0.43 mL min^{-1} was collected into an individual polypropylene tube for 12 s to 10 min. During in-flight sampling, the flight scientist actively controlled the sample collection into each polypropylene tube to target transects of the smoke plume (example shown in Figure A-2). Six to twelve aqueous samples were collected for each flight, with 201 total samples from 39 science flights. Field blanks of the DIW used to operate the BrC-PILS were stored similarly in clean polypropylene sample tubes at the beginning, halfway point, and end of campaign. Once collected in the field, the samples and blanks were stored on ice for several hours prior to refrigeration until analysis.

2.3.3 Offline analysis by SEC-UV

Measurement by SEC-UV provides information about size-dependent light absorption properties of BrC chromophores. The offline aerosol samples were separated using an aqueous gel-filtration column with a MW range of 250 Da to 75 kDa (Polysep GFC P-3000, Phenomenex, Torrence, CA). Size-resolved components were detected using a diode array detector from 190 to 800 nm (UltiMate 3000, Thermo Scientific, Sunnyvale, CA) coupled to an ion chromatograph (ICS 6000; Thermo Scientific) pump with an AS autosampler (Thermo Scientific). The isocratic method was run using a mobile phase that contained a 1:1 mixture of acetonitrile and 25 mM ammonium acetate in solution at a flow rate of 1 mL min^{-1} and a sample injection volume of 100 µL. A solution of Suwannee River Humic Acid (SRHA II, International Humic Substances

Society, Saint Paul, MN, USA) was run prior to the FIREX-AQ samples to ensure proper operation of the SEC-UV set-up.

The aqueous samples collected by the BrC-PILS did not require post-sampling processing and were injected onto the SEC column under mobile phase flow to the diode array detector. The uncertainty for the offline total absorption measurements considers the uncertainty of the liquid flow and PILS collection efficiency, for a total uncertainty of ±10.5 %. Discussion of the SEC-UV method development and details of the conversion of SEC-UV signal to ambient absorption in units of Mm^{-1} can be found in the SI. We calculated BrC absorption as a function of MW by applying the calibration method described by Di Lorenzo and Young et al. (Figure A-3).[29] Sample measurements were blank subtracted. The detection limit of the total integrated absorption (equivalent to 3σ of n=6 field blanks) was 2.5±0.2 mAU×min and 0.70±0.02 mAU×min at 250 nm and 300 nm, respectively. This corresponds to a 3σ detection limit of approximately 525 Mm^{-1} at 250 nm and 150 Mm^{-1} at 300 nm.

2.3.4 Absorption in different mobile phases

To assess the impact of pH and mobile-phase composition on wavelength-dependent absorption, the ammonium acetate solution was adjusted to pH 5 and pH 9 with acetic acid and ammonium hydroxide, respectively, prior to combining with acetonitrile. A 15 µg/mL in DIW solution of Suwannee River Fulvic Acid (SRFA II; International Humic Substances Society, Saint Paul, MN, USA) and a FIREX-AQ aqueous sample were injected onto the diode array detector without the SEC column in line with the following mobile phases: DIW only; 25 mM ammonium acetate solution; the default mobile phase (described in Sect. 2.2.3); 25 mM ammonium acetate solution adjusted to pH 5; and 25 mM ammonium acetate solution adjusted to pH 9. Solutions of 4-nitrocatechol, 4-hydroxy-3-methoxy cinnamaldehyde, vanillin, and 7-hydroxycoumarin in DIW

with concentrations of 3.9×10^{-8}, 3.4×10^{-8}, 3.9×10^{-8}, 3.7×10^{-8} mol/mL, respectively, were prepared and injected onto the diode array detector to observe differences in their absorption profiles. To confirm the diode array detector results, measurements of the SRFA solution were also made with UV-visible spectroscopy (8453; Agilent Technologies, Santa Clara, CA, USA) where the solution was mixed (1:1 ratio) with the various mobile phases prior to transferring to a cuvette for absorption measurements (Figure A-7).

2.4 Results and discussion

2.4.1 Trends in absorption with plume age

We present molecular size-resolved absorption for flights that met the following criteria: (1) maximum CO concentrations greater than 0.2 ppmv; (2) three or more downwind plume transects; (3) three or more aqueous samples collected; and (4) consistent wind direction. Of the 201 aqueous samples collected, 47 samples from six flights met the criteria and are summarized in Table A1. Each aqueous sample had a measurable absorption signal in the deep UV region (250 to 300 nm), while the absorption signal above 300 nm was nearly indistinguishable from the blanks, because the samples were relatively dilute. The average (±standard deviation) integrated absorption of the 47 samples that met the criteria was 10.4±4.9 mAU×min (8134±3857 Mm^{-1}) and 0.36±0.28 mAU×min (316±214 Mm^{-1}) for 250 and 300 nm, respectively.

To account for plume dilution, we follow the convention of normalizing BrC absorption to a conserved tracer, to calculate $\Delta Abs_{\lambda,BrC}/\Delta CO$,[12,36–39] where ΔCO is the average CO mixing ratio measured during each aqueous sample collection subtracted by the average CO background outside the plume. Background BrC absorption at 365 nm (a common wavelength to report BrC absorption) was less than 0.2 Mm^{-1} and no background correction was made to determine $\Delta Abs_{\lambda,BrC}$.[36] The average CO and variation of CO measured for each flight are shown in Figure A-

9. Figure 2-1 shows $\Delta Abs_{300nm,BrC}$ /ΔCO as a function of plume age for the six selected flights, with a linear fit to each flight. The fitted slopes for $\Delta Abs_{300nm, BrC}$/ΔCO vs plume age vary from -0.21 to 0.88 Mm^{-1} $ppbv^{-1}$ $hour^{-1}$, and show different trends between flights. This indicates that BrC absorption increased downwind in some plumes and decreased downwind in others.

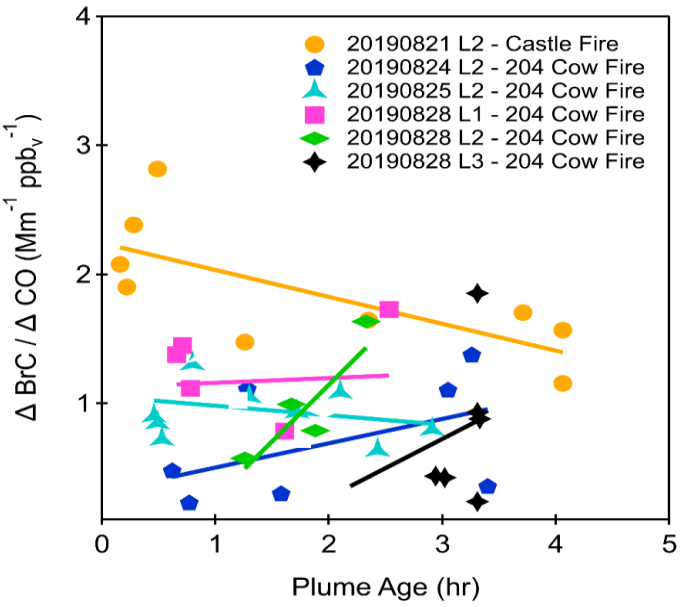

Figure 2-1. Ratio of absorption measured by SEC-UV at 300 nm to CO enhancement as a function of plume age for aqueous samples collected for six flights during FIREX-AQ 2019.

Previous studies of normalized BrC absorption with plume age have reported conflicting results. In the earliest aircraft study, Forrister et al. collected filter samples from two fires in the western U.S. and measured the BrC absorption from water and methanol extracts. They observed that BrC absorption at 365 nm decayed exponentially over a plume age range spanning 0 to 50 hours (Figure A-10).[38] Di Lorenzo et al. reported total absorption of size-resolved BrC chromophores using SEC-UV from three locations that were influenced to varying degrees by biomass burning smoke, and observed minimal $\Delta Abs_{\lambda,BrC}$/ΔCO change as a function of transport times from 10 to >72 hours (Figure A-10).[12] In contrast to these measurements of relatively aged biomass burning aerosol, two studies from other FIREX-AQ instruments showed different trends

for relatively fresh plumes. Using BrC-PILS measurements from the Twin Otter, Washenfelder et al. showed variable trends in $\Delta Abs_{365nm,BrC}/\Delta CO$ slope values ranging from -0.02 to 0.02 Mm^{-1} $ppbv^{-1}$ $hour^{-1}$ over 0 to 5 hours.[36] Using filter samples from the DC-8 aircraft, Zeng et al. showed showed that BrC increased, decreased, or was unchanged as a function of plume age over 0 to 8 hrs.[40] In another study of fresh plumes, aircraft based measurements during the Western Wildfire Experiment for Cloud Chemistry, Aerosol Absorption and Nitrogen (WE-CAN); Sullivan et al. investigated the evolution of water-soluble BrC at 405 nm normalized to CO and observed BrC depletion with a smoke age of <2 hours, and PILS water-soluble BrC absorption that broadly remained stable for a smoke age up to 9 hours.[39]

Our results are broadly consistent with measurements from FIREX-AQ and WE-CAN that sampled fresh plumes and differ from the studies that sampled more aged smoke. The relatively limited plume age range of the FIREX-AQ sampling makes it challenging to deduce long-term trends associated with changes in total absorption as a function of transport time. In addition, the disparity in $\Delta Abs_{\lambda,BrC}/\Delta CO$ time dependence between FIREX-AQ observations and those reported by Forrister et al. may be attributed to i) FIREX-AQ having sampled a greater number of western U.S forest fires; and ii) the younger age of the FIREX-AQ plumes. More in-flight sampling would be required to observe BrC absorption of plume ages 5 h to 50 h to determine if the results observed by Forrister et al. would also show variability with a greater number of fires, or if the BrC lifetime would converge to a similar value.

2.4.2 Chemical evolution of brown carbon with plume age

Chromophores <500 Da were responsible for most of the absorption at 250-300 nm measured in the aqueous samples (Figure 2-2, Figure A-11). For the 47 samples, molecular species >500 Da contributed an average of 3.0±1.9 % to total measured absorption at 250 nm, while

molecular species <500 Da contributed an average of 72±4.5 %. Absorption past the exclusion volume represents an unidentified MW, as elution past this retention time (Figure A-3) indicates non-SEC analyte-column interactions were occurring. The average contribution to total measured absorption by undefined MW species was 25.1±5.7 %. Previous SEC-UV analyses have observed elution beyond the exclusion volume and non-size exclusion effects.[31,41] Elution at later retention times has also been observed for fresh BrC separated in a mobile phase containing 50% acetonitrile.[41] This result was attributed to non-size exclusion effects, such as hydrophobic interactions of BrC with the SEC stationary phase, which may also have contributed to elution past the exclusion volume in our samples. The absorption density plots of the aqueous samples from the flights listed in Table S1 had similar size-resolved features with varying magnitude in absorption (Figure A-5).

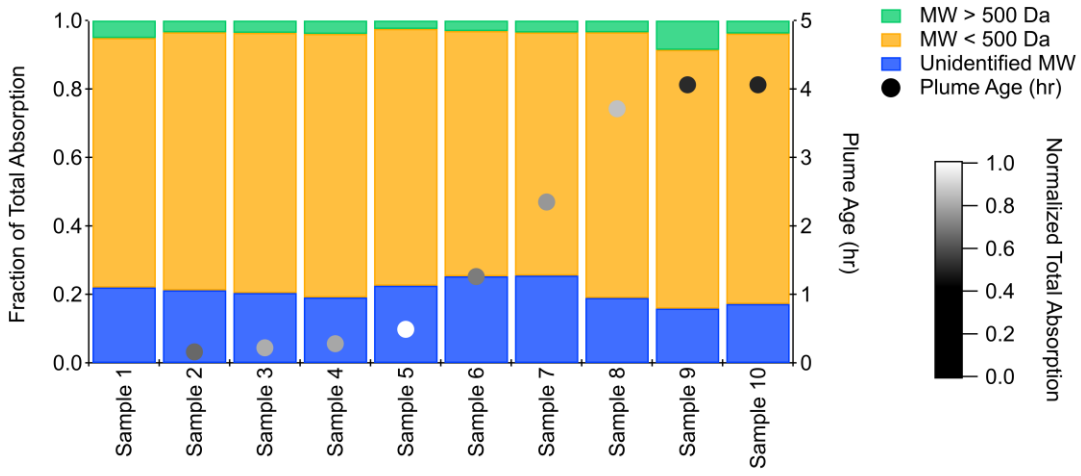

Figure 2-2. Absorption contribution at 300 nm of high (>500 Da), low (<500 Da), and unidentified molecular weight species for aqueous samples collected during the second flight leg on 21 Aug 2019.

These results are the first reported SEC-UV measurements of very fresh (0-5 hours) field samples of biomass burning smoke, and they confirm some of the observations from field studies that measured more aged smoke, as well as laboratory studies that generated fresh or aged smoke.

Previous studies that examined biomass burning BrC using SEC-UV have similarly concluded that fresh, less aged smoke contains a large fraction of lower MW absorbing species.[12,31,41] In the examination of field samples, Di Lorenzo et al. collected ambient biomass burning aerosols that had been aged 10 to >72 hours; they observed that low MW (<500 Da) chromophores contributed more to total absorption than higher MW (>500 Da) compounds in the least aged (10 to 15 hrs) biomass burning-derived filter extracts.[12] These findings resemble the absorption features of our FIREX-AQ samples, which span a plume age range from 0 to 5 hours. Wong et al. used SEC-UV to analyze filter extracts collected during fire seasons in Greece with atmospheric ages of 1 to ~70 hrs and observed that high MW species dominated total BrC absorption of the fresh and aged smoke.[30] Differences between the FIREX-AQ aqueous samples and the results presented by Wong et al. can be driven by varying types of fuel emissions, photochemical conditions, meteorology, and differences in back trajectory analyses.

Two studies have applied SEC-UV analysis to lab-generated or lab-aged smoke samples. Wong et al. pyrolyzed dry hardwood and aged the samples from 0 to 10 hours with UV light; they found that low MW chromophores dominated total absorption compared to high MW species, which is generally consistent with our observations.[31] Lyu et al. generated biomass burning aerosol from laboratory combustion of boreal peat and also analyzed the aerosol by SEC-UV. Under the same SEC-UV separation conditions, the FIREX-AQ water aqueous samples parallel the findings of Lyu et al., with low MW BrC chromophores dominating total absorption for unaged fresh smoke and smoke aged between 0 to 5 hrs in the atmosphere.[41]

2.4.3 Comparison of SEC-UV and BrC-PILS absorption

Online and offline absorption sampling are complimentary. The online sampling by the BrC-PILS provides continuous data with much higher time resolution (reported at 10 s), but it is

limited to two measurements: water-soluble absorption as a function of wavelength and water-soluble organic carbon concentration. In contrast, offline samples can be examined using SEC-UV, C_{18} chromatography, and other analytical techniques that are not feasible onboard an aircraft. During FIREX-AQ, the BrC-PILS measured online water-soluble absorption in the same aqueous flow that was collected for offline sampling. These are the only BrC samples whose absorption was measured online and then subsequently offline during FIREX-AQ. We observe differences between the online and offline samples. First, absorption by the offline SEC-UV at wavelengths greater than 300 nm did not exceed its detection limit. To facilitate comparison of absorption magnitudes, a power law fit was applied to the BrC-PILS absorption between 315–395 nm to extrapolate absorption to 300 nm (Figure 2-3). The total absorption by the SEC-UV measurements is approximately an order of magnitude greater than the BrC-PILS measurements at 300 nm (Figure 2-3). To determine if the differences could be attributed to differences in the diode array detector from the SEC-UV analysis and the BrC-PILS spectrometer, a standard solution of 4-nitrocatechol was run on both systems in pure water (without the SEC column in line and bypassing the PILS). At 350 nm, the agreement between the online, offline, and literature measurements of 4-nitrocatechol absorption was ±2.1% (Figure A-13). [42]

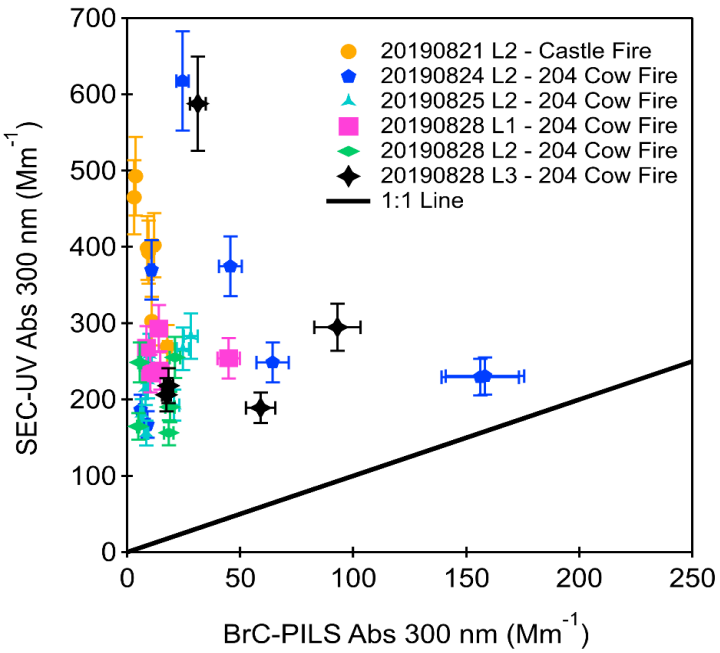

Figure 2-3. Total absorption measured offline by the SEC-UV (at 300 nm) compared to the total absorption measured online by the BrC-PILS (extrapolated to 300 nm using a power-law fit). Each colour represents a different flight leg and each marker represents the integrated absorption at 300 nm for each aqueous sample measured by SEC-UV. The online BrC-PILS absorption measurement was averaged over the collection time of each aqueous sample. The error bars represent the total uncertainty in the online and offline measurements.

The comparison between the online and offline work presented here can be compared to previous non-co-located online-offline intercomparison studies. Di Lorenzo et al. compared offline absorption measurements of filter extracts by SEC-UV to PILS-LWCC online measurements during the Southern Oxidant and Aerosol Study (SOAS).[12] Although the SEC-UV offline samples and online measurements during SOAS were not co-located, a median ratio (SEC-UV offline at 300 nm to PILS-LWCC online at 365 nm) of 0.9 and r^2 of 0.53 (Figure A-12). Zeng et al. also present an online-offline absorption comparison of water-soluble BrC collected on board the NASA DC-8 aircraft during FIREX-AQ where online absorption measurements by a LWCC and aqueous filter extracts injected onto a LWCC offline showed good agreement at 365 nm (r^2 = 0.84).[37] The correlation suggested that the filter measurement of BrC is not significantly influenced

by possible sampling artifacts associated with absorption of gases or evaporative loss of BrC components associated with filter collection.[37]

Differences observed in the FIREX-AQ aqueous samples indicate the necessity to investigate a potential explanation for these inconsistencies. Since the online BrC-PILS and offline SEC-UV samples represent the same samples, solubilization differences between aerosol collection methods cannot explain the variability observed between our measurements. Although reasonable agreement between online measurements and offline filter analyses has been demonstrated,[12,37] Resch et al. indicated that filter extracts that are not refrigerated immediately or extracts that remain refrigerated for an extended storage time are susceptible to compositional changes.[43] For logistical reasons, our aqueous samples were collected into polypropylene tubes in the field and were not immediately subjected to controlled refrigeration or to the SEC-UV analysis. The greater absorption observed by the SEC-UV analysis (Figure 2-3) could reflect the possible hydrolysis of oligomeric compounds stored in aqueous solution resulting in an increase in the intensity of precursor monomers as decomposition products.[43] We consider this, as well as other potential causes for the differences in the next section.

2.4.4 Investigating the impact of solvent effects, pH, and storage effects on absorption spectra

The analysis of fresh biomass burning samples by SEC-UV may be affected by mobile phase solvation effects, pH, and sample storage conditions. We analyze and discuss these variables below and make recommendations for SEC-UV analysis. Plausible chemical structures of chromophores responsible for BrC absorption have been identified and consist of conjugated systems functionalized with hydroxyls, amines, nitro, carbonyls, and carboxylic acid groups.[8,18,26,28,44–47] The molecular complexities of BrC species may be susceptible to changes in the absorption spectra depending on the analysis conditions.

First, we assess solvation effects due to changes in the mobile phase composition. The PILS solubilizes BrC in pure water for the online measurements to facilitate absorption measurements.[48] In contrast, the mobile phase used for the offline SEC-UV analysis was a mixture of acetonitrile and DIW with 25 mM ammonium acetate. Chromatographic packing materials are often incompatible with pure water and require a mixture with an organic solvent to elute compounds from the stationary phase or, in SEC separations, to prevent sorption to the stationary phase. For this reason, chromatographic partitioning-based separations occur in aqueous-organic mixtures, where the composition can be deliberately modified to optimize interactions of the target molecules between the stationary phase and mobile phase. In SEC, non-size exclusion interactions between the analyte and stationary phase are dominated by electrostatic and hydrophobic interactions.[49] If the analyte and stationary phase are identically charged, ion exclusion effects can occur, resulting in an earlier elution time as the analyte is prevented from entering the pores. If the analyte and stationary phase are oppositely charged, adsorption can result, leading to a later elution time. Hydrophobic effects can occur if the analyte interacts with hydrophobic sites of the column matrix.[49] The purpose of adding ammonium acetate to the mobile phase is to increase the ionic strength of the mobile phase and facilitate ion-pairing, which suppresses electrostatic interactions between the stationary phase and the polar and charged functional groups. The organic solvent used in our mobile phase was acetonitrile, which has been shown to be unreactive towards typical BrC components and has been recommended as an inert solvent for BrC extraction and analysis.[50–52] Therefore, we do not expect the mobile phase to chemically alter BrC compounds while effective at mitigating column stationary phase-analyte interactions.

While chemical changes caused by our mobile phase are unlikely, it is possible that other solvent effects on absorption could be occurring. Effects of solvent on molecular absorption are

well established in the photochemistry literature.[41,52–56]The polarity of the solvent affects the absorption wavelength by changing stabilization of the ground and/or excited states. With a decrease in solvent polarity, (acetonitrile-water is less polar relative to pure water), this can lead to a decrease in stabilization of the ground state of BrC compounds (such as 4-nitrocatchol), but this effect is molecule-dependent. The impact of solvation on red and blue spectral shifting will likely be several nanometers, which could contribute to the observed differences in the offline and online absorption measurements. Previous work has shown that acetonitrile could disrupt π- π interactions between BrC molecules, which could cause the liberation of adsorbed low MW BrC chromophores from larger chromophores or disrupt BrC aggregates.[41] Smaller, less conjugated systems typically absorb in the ultraviolet-blue wavelength region, and their $\pi \rightarrow \pi^*$ transition red shifts when more conjugated systems are fused together.[57] Thus, we would expect absorption measurements in the presence of acetonitrile to be blue-shifted relative to those in pure water. This represents a possible explanation for greater absorption intensity at lower wavelengths measured in the offline SEC-UV analysis compared to the online analysis.

Second, we assess the pH of the sample matrix, which is known to affect the absorption profile of BrC compounds. Multiple studies have investigated the impact of pH on wavelength-dependent absorption. For example, Phillips et al. directly adjusted the pH of SRFA and biomass-burning derived aqueous extracts (with sodium hydroxide or hydrochloric acid) and observed no measurable shift in the spectra to shorter or longer wavelengths; however they did observe that as the pH increased, there was an increase in the magnitude of absorption, which was more pronounced at higher wavelengths.[58] The pH of the default mobile phase solution was 7.2, while the pH of the deionized water solutions in the PILS was approximately 5 (due to carbon dioxide dissolution). To investigate the impact pH has on BrC absorption, we measured several compounds

that have been shown to contribute to BrC absorption (4-nitrocatechol, vanillin, 7-hydroxycoumarin, 4-hydroxy-3-methoxy cinnamaldehyde, and mixture of the four compounds) under different solvent and pH conditions: DIW, DIW with 25 mM ammonium acetate, as well as the mobile phase at pH 5, 7.2, and 9. When the matrix conditions have a pH greater than the pK_a of the compound in question, the species will deprotonate, resulting in a shift to longer wavelengths.[42] For compounds with a pK_a between 5 and 9 (i.e., 4-nitrocatechol, 7-hydroxycoumarin, vanillin), we observed this phenomenon (Figure A-6). To assess the impact of pH and mobile phase on a complex mixture, we also measured the absorption of a SRFA aqueous solution and a FIREX-AQ aqueous sample with the abovementioned mobile phases (Figure 2-4 and Figure A-8). In contrast to the individual BrC compounds, no major changes in the spectral shape were observed under different mobile phase conditions. To confirm these results, we measured the absorption of SRFA in each solvent using a separate spectrophotometer (Figure A-7). This suggests that the pK_a of the majority of functional groups in the absorbing compounds present were less than 5 or above 9. Nitroaromatic compounds typically have pK_a values between 5 and 8; suggesting low levels of this class of compounds present in the aqueous samples. This observation is comparable to the online BrC-PILS analysis; for aqueous absorption, Washenfelder et al. observed the average absorption contribution at 365 nm of 4-nitrocatchol was less than 1.1 % and the summed contribution to absorption by 2-nitrophenol, 4-nitrophenol, 4-nitrocatechol, 4-nitroguaiacol, and 2,4-dinitrophenolate was less than 3.6 %.[36] Since the absorption profile of SRFA and the FIREX-AQ sample appear similar in all mobile phase conditions, we have no evidence that pH of the mobile phase in the SEC separation conditions impacts the wavelength dependent absorption of the FIREX-AQ aqueous samples.

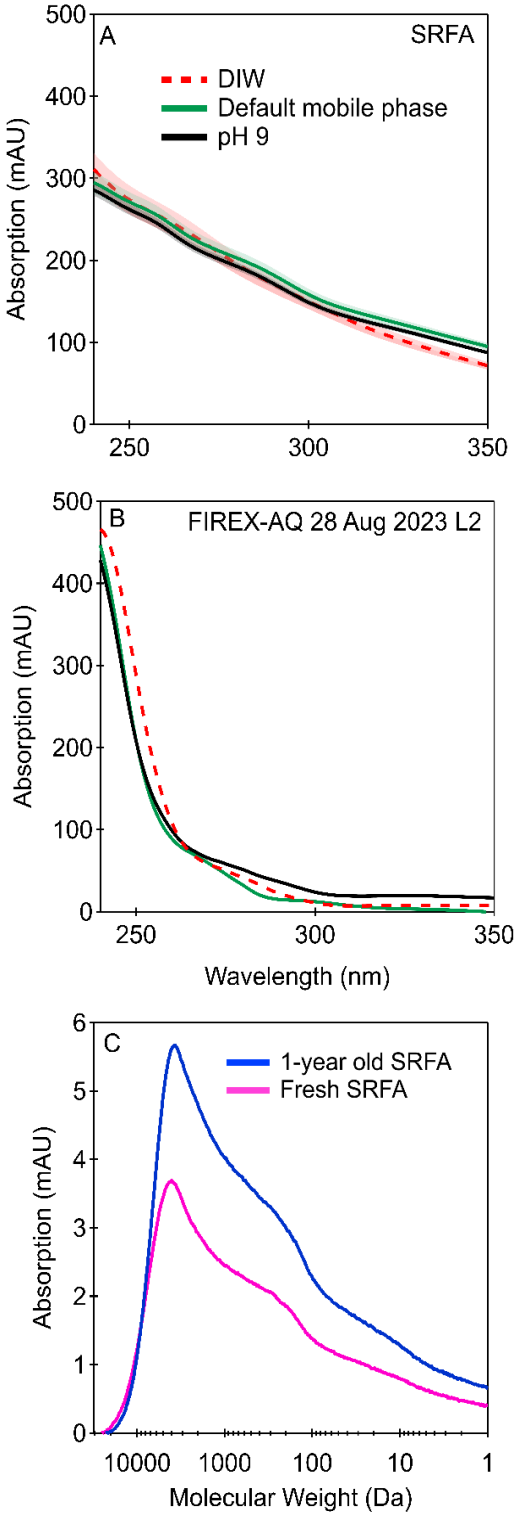

Figure 2-4. Absorption as a function of wavelength of (a) SRFA and (b) a FIREX-AQ aqueous sample collected on 28 Aug 2019 L3 with varying mobile phases. (c) Molecular weight profile of a freshly-made 15 µg/mL SRFA solution and the same solution one year later. The shaded region represents the coefficient of variation for absorption at each wavelength using n = 3 DIW.

Third, we assess the potential effect of storage on the aqueous samples measured by SEC-UV. A recent study by Resch et al. observed that biomass burning-derived filter extracts stored at temperatures above freezing may undergo compositional changes that can increase in signal for various compounds.[43] Hydrolysis reactions include converting alkenes to alcohols and esters to carboxylic acids, and the breakdown of oligomers. The hydrolysis of oligomers such as dimer esters stored in an aqueous solution can result in an increase in precursor monomers as decomposition products leading to an increase in signal.[43,59] Further, ammonium and alkylamines have been observed in high levels in biomass burning aerosols;[60] aqueous reactions between dicarbonyls (e.g., glyoxal, methylglyoxal) with ammonium and amines may also contribute to an increase in absorption intensity at pH 4 to 7.[61,62] The FIREX-AQ aqueous samples had a pH of 5 and were stored at 4 °C for two years prior to analysis. Assuming they contained dicarbonyl compounds and reduced nitrogenous species, it is possible reactions leading to products that can contribute to greater absorption during storage occurred. To further investigate the impacts of storage on a complex aqueous mixture, we measured the absorption spectra of two SRFA solutions: one freshly made and one stored for one year at 4 °C. We observed an increase in absorption in the aged SRFA solution, in which integrated absorption was 39 % higher than the freshly-made solution. This same effect was also observed with SRHA solutions (Figure A-14). Thus, it is possible that processes during storage could have led to increased absorption measured in the offline SEC samples.

Among the three processes discussed here, we conclude that the storage of aqueous extracts is the most plausible explanation for the higher absorption observed in the offline samples from FIREX-AQ. If hydrolysis reactions are occurring, we might expect this to impact the MW profile (i.e., SEC elution times). We examined the MW profile of freshly-made and one year-aged SRFA

solutions (Figure 2-4c). The increase in absorption with storage does not measurably affect the molecular size-resolved absorption of the mixtures. The same effect was observed for SRHA (Figure A-14). This demonstrates that any storage-induced changes in these complex mixtures of organic molecules have a minimal impact on the molecular weight relative to the wide MW range of the SEC column. The MW of the BrC species would have to change by ~ 100 Da to be noticeable on the MW scale of our separation (250 Da to 75 kDa). Such a drastic change in MW is unlikely the case in most hydrolysis reactions. Thus, our results above in which we broadly categorize MW species to be less than or greater than 500 Da are likely robust. The SEC separation of the aqueous samples signify that low MW (<500 Da) chromophores contribute more to total absorption than higher MW (>500 Da), this finding is supported by previous SEC-UV analyses of BrC aged less than 10 hrs.[12,41] The consistent MW profiles between the freshly-made and stored solutions of SRFA and SRHA reasonably suggest that storage did not have a major impact on the MW of BrC.

2.5 Conclusions and implications

During FIREX-AQ, instruments onboard the NOAA Twin Otter aircraft sampled smoke plumes from wildfires in the western United States with plume ages of 0 to 5 hours. The BrC-PILS measured water-soluble BrC absorption online and collected aerosol in aqueous solution for offline SEC-UV analysis. The aqueous samples were collected during downwind plume transects and the online data was collected continuously during inflight sampling. SEC-UV analysis shows that BrC absorption was dominated by chromophores <500 Da. This finding is consistent with reports of laboratory-generated fresh smoke samples. Integrated absorption at 300 nm from the SEC-UV analysis was used to calculate trends in normalized BrC absorption as a function of plume age. These trends were variable and did not show an exponential decay, which is consistent with recently published results from the FIREX-AQ field campaign that examined normalized BrC

absorption trends for plumes over 0 to 10 hours. Comparison of the online and offline analyses of the same aqueous extracts reveals discrepancies, specifically higher absorption intensity and absorption at lower wavelengths. These discrepancies between online and offline samples demonstrate the importance of considering the conditions in which the absorption measurements are made. The inconsistencies between the offline SEC-UV analysis and the online measurements are not explained by pH or solvent effects, but may be due to reactions occurring during storage. Although increases in absorption may occur during storage of aqueous solutions, it is less likely to impact the MW of the FIREX-AQ BrC species. This highlights that BrC species are more stable collected on filters rather than in aqueous solution and the importance of inter-comparison absorption measurements by multiple methods.

2.6 References

(1) Parks, S. A.; Abatzoglou, J. T. Warmer and Drier Fire Seasons Contribute to Increases in Area Burned at High Severity in Western US Forests From 1985 to 2017. *Geophysical Research Letters* **2020**, *47* (22), e2020GL089858. https://doi.org/10.1029/2020GL089858.

(2) Marlon, J. R.; Bartlein, P. J.; Gavin, D. G.; Long, C. J.; Anderson, R. S.; Briles, C. E.; Brown, K. J.; Colombaroli, D.; Hallett, D. J.; Power, M. J.; Scharf, E. A.; Walsh, M. K. Long-Term Perspective on Wildfires in the Western USA. *Proceedings of the National Academy of Sciences* **2012**, *109* (9), E535 LP-E543. https://doi.org/10.1073/pnas.1112839109.

(3) Bond, T. C.; Streets, D. G.; Yarber, K. F.; Nelson, S. M.; Woo, J.-H.; Klimont, Z. A Technology-Based Global Inventory of Black and Organic Carbon Emissions from Combustion. *Journal of Geophysical Research: Atmospheres* **2004**, *109* (D14). https://doi.org/10.1029/2003JD003697.

(4) van der Werf, G. R.; Randerson, J. T.; Giglio, L.; Collatz, G. J.; Mu, M.; Kasibhatla, P. S.; Morton, D. C.; DeFries, R. S.; Jin, Y.; van Leeuwen, T. T. Global Fire Emissions and the Contribution of Deforestation, Savanna, Forest, Agricultural, and Peat Fires (1997–2009). *Atmospheric Chemistry and Physics* **2010**, *10* (23), 11707–11735. https://doi.org/10.5194/acp-10-11707-2010.

(5) Turpin, B. J.; Cary, R. A.; Huntzicker, J. J. An In Situ, Time-Resolved Analyzer for Aerosol Organic and Elemental Carbon. *Aerosol Science and Technology* **1990**, *12* (1), 161–171. https://doi.org/10.1080/02786829008959336.

(6) Seinfeld, J. H.; Pankow, J. F. Organic Atmospheric Particulate Material. *Annual Review of Physical Chemistry* **2003**, *54* (1), 121–140. https://doi.org/10.1146/annurev.physchem.54.011002.103756.

(7) Andreae, M. O.; Gelencsér, A. Black Carbon or Brown Carbon? The Nature of Light-Absorbing Carbonaceous Aerosols. *Atmospheric Chemistry & Physics* **2006**, *6*, 3131–3148. https://doi.org/10.5194/acp-6-3131-2006.

(8) Laskin, A.; Laskin, J.; Nizkorodov, S. A. Chemistry of Atmospheric Brown Carbon. *Chemical Reviews* **2015**, *115* (10), 4335–4382. https://doi.org/10.1021/cr5006167.

(9) Boucher, O.; Randall, D.; Artaxo, P.; Bretherton, C.; Feingold, G. ; Forster, P.; Kerminen, V. M.; Kondo, Y.; Liao, H.; Lohmann, U. ;; Rasch, P.; Satheesh, S. K.; Sherwood, S.; Stevens, B.; Zhang, X. Y. Clouds and Aerosols. In: Climate Change 2013: The Physical Science Basis. Contribution of Working Group I to the Fifth Assessment Report of the Intergovernmental Panel on Climate Change. In *Climate Change 2013: The Physical Science Basis. Contribution of Working Group I to the Fifth Assessment Report of the Intergovernmental Panel on Climate Change*; Cambridge University Press: New York, NY, 2013.

(10) Forster, P.; Ramaswamy, V.; Artaxo, P.; Berntsen, T.; Betts, R. ; Fahey, D. W.; Haywood, J.; Lean, J.; Lowe, D. C.; Myhre, G. ; N.; J.; Prinn, R.; Raga, G.; Schulz, M.; Van Dorland, R. *In Climate Change 2007: The Physical Science Basis. Contribution of Working Group I to the Fourth Assessment Report of the Intergovernmental Panel on Climate Change*; Cambridge University Press: Cambridge, United Kingdom and New York, NY, 2007; pp 129−243, 2007. https://globalchange.mit.edu/publication/13723.

(11) Alan Buis. *The Climate Connections of a Record Fire Year in the U.S. West – Climate Change_ Vital Signs of the Planet*. Ask NASA Climate. https://climate.nasa.gov/blog/3066/the-climate-connections-of-a-record-fire-year-in-the-us-west/.

(12) Di Lorenzo, R. A.; Washenfelder, R. A.; Attwood, A. R.; Guo, H.; Xu, L.; Ng, N. L.; Weber, R. J.; Baumann, K.; Edgerton, E.; Young, C. J. Molecular-Size-Separated Brown Carbon Absorption for Biomass-Burning Aerosol at Multiple Field Sites. *Environmental Science and Technology* **2017**, *51* (6), 3128–3137. https://doi.org/10.1021/acs.est.6b06160.

(13) Ramanathan, V.; Carmichael, G. Global and Regional Climate Changes Due to Black Carbon. *Nat Geosci* **2008**, *1*. https://doi.org/10.1038/ngeo156.

(14) Feng, Y.; Ramanathan, V.; Kotamarthi, V. R. Brown Carbon: A Significant Atmospheric Absorber of Solar Radiation? *Atmospheric Chemistry and Physics* **2013**, *13* (17), 8607–8621. https://doi.org/10.5194/acp-13-8607-2013.

(15) Zhang, Y.; Forrister, H.; Liu, J.; Dibb, J.; Anderson, B.; Schwarz, J. P.; Perring, A. E.; Jimenez, J. L.; Campuzano-Jost, P.; Wang, Y.; Nenes, A.; Weber, R. J. Top-of-Atmosphere Radiative Forcing Affected by Brown Carbon in the Upper Troposphere. *Nature Geoscience* **2017**, *10* (7), 486–489. https://doi.org/10.1038/ngeo2960.

(16) Zeng, L.; Zhang, A.; Wang, Y.; Wagner, N. L.; Katich, J. M.; Schwarz, J. P.; Schill, G. P.; Brock, C.; Froyd, K. D.; Murphy, D. M.; Williamson, C. J.; Kupc, A.; Scheuer, E.; Dibb, J.; Weber, R. J. Global Measurements of Brown Carbon and Estimated Direct Radiative Effects. *Geophys Res Lett* **2020**, *47* (13), e2020GL088747. https://doi.org/10.1029/2020GL088747.

(17) Washenfelder, R.; Attwood, A.; Brock, C.; Guo, H.; Xu, L.; Weber, R.; Ng, N.; Allen, H.; Ayres, B.; Baumann, K.; Cohen, R.; Draper, D.; Duffey, K.; Edgerton, E.; Fry, J.; Hu, W.; Jimenez, J.; Palm, B.; Romer, P.; Brown, S. Biomass Burning Dominates Brown Carbon Absorption in the Rural Southeastern United States. *Geophysical Research Letters* **2015**, *42* (2), 653–664. https://doi.org/10.1002/2014GL062444.

(18) Hems, R. F.; Schnitzler, E. G.; Liu-Kang, C.; Cappa, C. D.; Abbatt, J. P. D. Aging of Atmospheric Brown Carbon Aerosol. *ACS Earth and Space Chemistry* **2021**, *5* (4), 722–748. https://doi.org/10.1021/acsearthspacechem.0c00346.

(19) Simoneit, B. R. T. Biomass Burning — a Review of Organic Tracers for Smoke from Incomplete Combustion. *Applied Geochemistry* **2002**, *17* (3), 129–162. https://doi.org/10.1016/S0883-2927(01)00061-0.

(20) Xie, M.; Chen, X.; Hays, M. D.; Holder, A. L. Composition and Light Absorption of N-Containing Aromatic Compounds in Organic Aerosols from Laboratory Biomass Burning. *Atmospheric chemistry and physics* **2019**, *19* (5), 2899–2915. https://doi.org/10.5194/acp-19-2899-2019.

(21) Smith, J. D.; Sio, V.; Yu, L.; Zhang, Q.; Anastasio, C. Secondary Organic Aerosol Production from Aqueous Reactions of Atmospheric Phenols with an Organic Triplet Excited State. *Environmental Science & Technology* **2014**, *48* (2), 1049–1057. https://doi.org/10.1021/es4045715.

(22) Harrison, M. A. J.; Barra, S.; Borghesi, D.; Vione, D.; Arsene, C.; Iulian Olariu, R. Nitrated Phenols in the Atmosphere: A Review. *Atmospheric Environment* **2005**, *39*, 231–248. https://doi.org/10.1016/j.atmosenv.2004.09.044.

(23) Finewax, Z.; de Gouw, J. A.; Ziemann, P. J. Identification and Quantification of 4-Nitrocatechol Formed from OH and NO3 Radical-Initiated Reactions of Catechol in Air in the Presence of NOx: Implications for Secondary Organic Aerosol Formation from Biomass Burning. *Environ. Sci. Technol.* **2018**, *52* (4), 1981–1989. https://doi.org/10.1021/acs.est.7b05864.

(24) Xie, M.; Chen, X.; Hays, M. D.; Lewandowski, M.; Offenberg, J.; Kleindienst, T. E.; Holder, A. L. Light Absorption of Secondary Organic Aerosol: Composition and Contribution of Nitroaromatic Compounds. *Environ Sci Technol* **2017**, *51* (20), 11607–11616. https://doi.org/10.1021/acs.est.7b03263.

(25) Liu, J.; Lin, P.; Laskin, A.; Laskin, J.; Kathmann, S. M.; Wise, M.; Caylor, R.; Imholt, F.; Selimovic, V.; Shilling, J. E. Optical Properties and Aging of Light-Absorbing Secondary Organic Aerosol. *Atmospheric Chemistry and Physics* **2016**, *16* (19), 12815–12827. https://doi.org/10.5194/acp-16-12815-2016.

(26) Lin, P.; Bluvshtein, N.; Rudich, Y.; Nizkorodov, S. A.; Laskin, J.; Laskin, A. Molecular Chemistry of Atmospheric Brown Carbon Inferred from a Nationwide Biomass Burning Event. *Environmental Science & Technology* **2017**, *51* (20), 11561–11570. https://doi.org/10.1021/acs.est.7b02276.

(27) Bluvshtein, N.; Lin, P.; Flores, M.; Segev, L.; Mazar, Y.; Tas, E.; Snider, G.; Weagle, C.; Brown, S.; Laskin, A.; Rudich, Y. Broadband Optical Properties of Biomass Burning Aerosol and Identification of Brown Carbon Chromophores. *Journal of Geophysical Research: Atmospheres* **2017**, *122* (10), 5441–5456. https://doi.org/10.1002/2016JD026230.

(28) Fleming, L. T.; Lin, P.; Roberts, J. M.; Selimovic, V.; Yokelson, R.; Laskin, J.; Laskin, A.; Nizkorodov, S. A. Molecular Composition and Photochemical Lifetimes of Brown Carbon

Chromophores in Biomass Burning Organic Aerosol. *Atmospheric Chemistry and Physics* **2020**, *20* (2), 1105–1129. https://doi.org/10.5194/acp-20-1105-2020.

(29) Di Lorenzo, R. A.; Young, C. J. Size Separation Method for Absorption Characterization in Brown Carbon: Application to an Aged Biomass Burning Sample. *Geophysical Research Letters* **2016**, *43* (1), 458–465. https://doi.org/10.1002/2015GL066954.

(30) Wong, J. P. S.; Tsagkaraki, M.; Tsiodra, I.; Mihalopoulos, N.; Violaki, K.; Kanakidou, M.; Sciare, J.; Nenes, A.; Weber, R. J. Atmospheric Evolution of Molecular-Weight-Separated Brown Carbon from Biomass Burning. *Atmospheric Chemistry and Physics* **2019**, *19* (11), 7319–7334. https://doi.org/10.5194/acp-19-7319-2019.

(31) Wong, J. P. S.; Nenes, A.; Weber, R. J. Changes in Light Absorptivity of Molecular Weight Separated Brown Carbon Due to Photolytic Aging. *Environmental Science & Technology* **2017**, *51* (15), 8414–8421. https://doi.org/10.1021/acs.est.7b01739.

(32) Crosson, E. R. A Cavity Ring-down Analyzer for Measuring Atmospheric Levels of Methane, Carbon Dioxide, and Water Vapor. *Applied Physics B* **2008**, *92* (3), 403–408. https://doi.org/10.1007/s00340-008-3135-y.

(33) Karion, A.; Sweeney, C.; Wolter, S.; Newberger, T.; Chen, H.; Andrews, A.; Kofler, J.; Neff, D.; Tans, P. Long-Term Greenhouse Gas Measurements from Aircraft. *Atmospheric Measurement Techniques* **2013**, *6* (3), 511–526. https://doi.org/10.5194/amt-6-511-2013.

(34) Warneke, C.; Schwarz, J. P.; Dibb, J.; Kalashnikova, O.; Frost, G.; Al-Saad, J.; Brown, S. S.; Brewer, Wm. A.; Soja, A.; Seidel, F. C.; Washenfelder, R. A.; Wiggins, E. B.; Moore, R. H.; Anderson, B. E.; Jordan, C.; Yacovitch, T. I.; Herndon, S. C.; Liu, S.; Kuwayama, T.; Jaffe, D.; Johnston, N.; Selimovic, V.; Yokelson, R.; Giles, D. M.; Holben, B. N.; Goloub, P.; Popovici, I.; Trainer, M.; Kumar, A.; Pierce, R. B.; Fahey, D.; Roberts, J.; Gargulinski, E. M.; Peterson, D. A.; Ye, X.; Thapa, L. H.; Saide, P. E.; Fite, C. H.; Holmes, C. D.; Wang, S.; Coggon, M. M.; Decker, Z. C. J.; Stockwell, C. E.; Xu, L.; Gkatzelis, G.; Aikin, K.; Lefer, B.; Kaspari, J.; Griffin, D.; Zeng, L.; Weber, R.; Hastings, M.; Chai, J.; Wolfe, G. M.; Hanisco, T. F.; Liao, J.; Campuzano Jost, P.; Guo, H.; Jimenez, J. L.; Crawford, J.; The FIREX-AQ Science Team. Fire Influence on Regional to Global Environments and Air Quality (FIREX-AQ). *Journal of Geophysical Research: Atmospheres* **2023**, *128* (2), e2022JD037758. https://doi.org/10.1029/2022JD037758.

(35) Liao, J.; Wolfe, G. M.; Hannun, R. A.; St. Clair, J. M.; Hanisco, T. F.; Gilman, J. B.; Lamplugh, A.; Selimovic, V.; Diskin, G. S.; Nowak, J. B.; Halliday, H. S.; DiGangi, J. P.; Hall, S. R.; Ullmann, K.; Holmes, C. D.; Fite, C. H.; Agastra, A.; Ryerson, T. B.; Peischl, J.; Bourgeois, I.; Warneke, C.; Coggon, M. M.; Gkatzelis, G. I.; Sekimoto, K.; Fried, A.; Richter, D.; Weibring, P.; Apel, E. C.; Hornbrook, R. S.; Brown, S. S.; Womack, C. C.; Robinson, M. A.; Washenfelder, R. A.; Veres, P. R.; Neuman, J. A. Formaldehyde Evolution in US Wildfire Plumes during the Fire Influence on Regional to Global Environments and Air Quality Experiment (FIREX-AQ). *Atmospheric Chemistry and Physics* **2021**, *21* (24), 18319–18331. https://doi.org/10.5194/acp-21-18319-2021.

(36) Washenfelder, R. A.; Azzarello, L.; Ball, K.; Brown, S. S.; Decker, Z. C. J.; Franchin, A.; Fredrickson, C. D.; Hayden, K.; Holmes, C. D.; Middlebrook, A. M.; Palm, B. B.; Pierce, R. B.; Price, D. J.; Roberts, J. M.; Robinson, M. A.; Thornton, J. A.; Womack, C. C.; Young, C. J. Complexity in the Evolution, Composition, and Spectroscopy of Brown Carbon in Aircraft Measurements of Wildfire Plumes. *Geophysical Research Letters* **2022**, *49* (9), e2022GL098951. https://doi.org/10.1029/2022GL098951.

(37) Zeng, L.; Sullivan, A. P.; Washenfelder, R. A.; Dibb, J.; Scheuer, E.; Campos, T. L.; Katich, J. M.; Levin, E.; Robinson, M. A.; Weber, R. J. Assessment of Online Water-Soluble Brown Carbon Measuring Systems for Aircraft Sampling. *Atmospheric Measurement Techniques* **2021**, *14* (10), 6357–6378. https://doi.org/10.5194/amt-14-6357-2021.

(38) Forrister, H.; Liu, J.; Scheuer, E.; Dibb, J.; Ziemba, L.; Thornhill, K. L.; Anderson, B.; Diskin, G.; Perring, A. E.; Schwarz, J. P.; Campuzano-Jost, P.; Day, D. A.; Palm, B. B.; Jimenez, J. L.; Nenes, A.; Weber, R. J. Evolution of Brown Carbon in Wildfire Plumes. *Geophysical Research Letters* **2015**, *42* (11), 4623–4630. https://doi.org/10.1002/2015GL063897.

(39) Sullivan, A. P.; Pokhrel, R. P.; Shen, Y.; Murphy, S. M.; Toohey, D. W.; Campos, T.; Lindaas, J.; Fischer, E. V.; Collett Jr., J. L. Examination of Brown Carbon Absorption from Wildfires in the Western US during the WE-CAN Study. *Atmospheric Chemistry and Physics* **2022**, *22* (20), 13389–13406. https://doi.org/10.5194/acp-22-13389-2022.

(40) Zeng, L.; Dibb, J.; Scheuer, E.; Katich, J. M.; Schwarz, J. P.; Bourgeois, I.; Peischl, J.; Ryerson, T.; Warneke, C.; Perring, A. E.; Diskin, G. S.; DiGangi, J. P.; Nowak, J. B.; Moore, R. H.; Wiggins, E. B.; Pagonis, D.; Guo, H.; Campuzano-Jost, P.; Jimenez, J. L.; Xu, L.; Weber, R. J. Characteristics and Evolution of Brown Carbon in Western United States Wildfires. *Atmospheric Chemistry and Physics* **2022**, *22* (12), 8009–8036. https://doi.org/10.5194/acp-22-8009-2022.

(41) Lyu, M.; Thompson, D. K.; Zhang, N.; Cuss, C. W.; Young, C. J.; Styler, S. A. Unraveling the Complexity of Atmospheric Brown Carbon Produced by Smoldering Boreal Peat Using Size-Exclusion Chromatography with Selective Mobile Phases. *Environ. Sci.: Atmos.* **2021**, *1* (5), 241–252. https://doi.org/10.1039/D1EA00011J.

(42) Hinrichs, R. Z.; Buczek, P.; Trivedi, J. J. Solar Absorption by Aerosol-Bound Nitrophenols Compared to Aqueous and Gaseous Nitrophenols. *Environ Sci Technol* **2016**, *50* (11), 5661–5667. https://doi.org/10.1021/acs.est.6b00302.

(43) Resch, J.; Wolfer, K.; Barth, A.; Kalberer, M. Effects of Storage Conditions on the Molecular-Level Composition of Organic Aerosol Particles. *Atmospheric Chemistry and Physics* **2023**, *23* (16), 9161–9171. https://doi.org/10.5194/acp-23-9161-2023.

(44) Hettiyadura, A. P. S.; Garcia, V.; Li, C.; West, C. P.; Tomlin, J.; He, Q.; Rudich, Y.; Laskin, A. Chemical Composition and Molecular-Specific Optical Properties of Atmospheric Brown

Carbon Associated with Biomass Burning. *Environ Sci Technol* **2021**, *55* (4), 2511–2521. https://doi.org/10.1021/acs.est.0c05883.

(45) Marrero-Ortiz, W.; Hu, M.; Du, Z.; Ji, Y.; Wang, Y.; Guo, S.; Lin, Y.; Gomez-Hermandez, M.; Peng, J.; Li, Y.; Secrest, J.; Zamora, M. L.; Wang, Y.; An, T.; Zhang, R. Formation and Optical Properties of Brown Carbon from Small α-Dicarbonyls and Amines. *Environ. Sci. Technol.* **2019**, *53* (1), 117–126. https://doi.org/10.1021/acs.est.8b03995.

(46) De Haan, D. O.; Tapavicza, E.; Riva, M.; Cui, T.; Surratt, J. D.; Smith, A. C.; Jordan, M.-C.; Nilakantan, S.; Almodovar, M.; Stewart, T. N.; de Loera, A.; De Haan, A. C.; Cazaunau, M.; Gratien, A.; Pangui, E.; Doussin, J.-F. Nitrogen-Containing, Light-Absorbing Oligomers Produced in Aerosol Particles Exposed to Methylglyoxal, Photolysis, and Cloud Cycling. *Environ. Sci. Technol.* **2018**, *52* (7), 4061–4071. https://doi.org/10.1021/acs.est.7b06105.

(47) Ji, Y.; Shi, Q.; Ma, X.; Gao, L.; Wang, J.; Li, Y.; Gao, Y.; Li, G.; Zhang, R.; An, T. Elucidating the Critical Oligomeric Steps in Secondary Organic Aerosol and Brown Carbon Formation. *Atmospheric Chemistry and Physics* **2022**, *22* (11), 7259–7271. https://doi.org/10.5194/acp-22-7259-2022.

(48) Weber, R. J.; Orsini, D.; Daun, Y.; Lee, Y.-N.; Klotz, P. J.; Brechtel, F. A Particle-into-Liquid Collector for Rapid Measurement of Aerosol Bulk Chemical Composition. *Aerosol Science and Technology* **2001**, *35* (3), 718–727. https://doi.org/10.1080/02786820152546761.

(49) Hong, P.; Koza, S.; Bouvier, E. S. P. A REVIEW SIZE-EXCLUSION CHROMATOGRAPHY FOR THE ANALYSIS OF PROTEIN BIOTHERAPEUTICS AND THEIR AGGREGATES. *Journal of Liquid Chromatography & Related Technologies* **2012**, *35* (20), 2923–2950. https://doi.org/10.1080/10826076.2012.743724.

(50) Walser, M. L.; Desyaterik, Y.; Laskin, J.; Laskin, A.; Nizkorodov, S. A. High-Resolution Mass Spectrometric Analysis of Secondary Organic Aerosol Produced by Ozonation of Limonene. *Phys. Chem. Chem. Phys.* **2008**, *10* (7), 1009–1022. https://doi.org/10.1039/B712620D.

(51) Bateman, A. P.; Walser, M. L.; Desyaterik, Y.; Laskin, J.; Laskin, A.; Nizkorodov, S. A. The Effect of Solvent on the Analysis of Secondary Organic Aerosol Using Electrospray Ionization Mass Spectrometry. *Environ Sci Technol* **2008**, *42* (19), 7341–7346. https://doi.org/10.1021/es801226w.

(52) Chen, K.; Raeofy, N.; Lum, M.; Mayorga, R.; Woods, M.; Bahreini, R.; Zhang, H.; Lin, Y.-H. Solvent Effects on Chemical Composition and Optical Properties of Extracted Secondary Brown Carbon Constituents. *Aerosol Science and Technology* **2022**, *56* (10), 917–930. https://doi.org/10.1080/02786826.2022.2100734.

(53) Lignell, H.; Hinks, M. L.; Nizkorodov, S. A. Exploring Matrix Effects on Photochemistry of Organic Aerosols. *Proceedings of the National Academy of Sciences* **2014**, *111* (38), 13780–13785. https://doi.org/10.1073/pnas.1322106111.

(54) Mo, Y.; Li, J.; Liu, J.; Zhong, G.; Cheng, Z.; Tian, C.; Chen, Y.; Zhang, G. The Influence of Solvent and pH on Determination of the Light Absorption Properties of Water-Soluble Brown Carbon. *Atmospheric Environment* **2017**, *161*, 90–98. https://doi.org/10.1016/j.atmosenv.2017.04.037.

(55) Zheng, D.; Yuan, X.-A.; Ma, H.; Li, X.; Wang, X.; Liu, Z.; Ma, J. Unexpected Solvent Effects on the UV/Vis Absorption Spectra of o-Cresol in Toluene and Benzene: In Contrast with Non-Aromatic Solvents. *Royal Society Open Science* **2018**, *5* (3), 171928. https://doi.org/10.1098/rsos.171928.

(56) Dalton, A. B.; Le, S. M.; Karimova, N. V.; Gerber, R. B.; Nizkorodov, S. A. Influence of Solvent on the Electronic Structure and the Photochemistry of Nitrophenols. *Environ. Sci.: Atmos.* **2023**, *3* (2), 257–267. https://doi.org/10.1039/D2EA00144F.

(57) Gorkowski, K.; Benedict, K. B.; Carrico, C. M.; Dubey, M. K. Complexities in Modeling Organic Aerosol Light Absorption. *J Phys Chem A* **2022**, *126* (29), 4827–4833. https://doi.org/10.1021/acs.jpca.2c02236.

(58) Phillips, S. M.; Bellcross, A. D.; Smith, G. D. Light Absorption by Brown Carbon in the Southeastern United States Is pH-Dependent. *Environ. Sci. Technol.* **2017**, *51* (12), 6782–6790. https://doi.org/10.1021/acs.est.7b01116.

(59) Zhao, R.; Kenseth, C. M.; Huang, Y.; Dalleska, N. F.; Kuang, X. M.; Chen, J.; Paulson, S. E.; Seinfeld, J. H. Rapid Aqueous-Phase Hydrolysis of Ester Hydroperoxides Arising from Criegee Intermediates and Organic Acids. *J Phys Chem A* **2018**, *122* (23), 5190–5201. https://doi.org/10.1021/acs.jpca.8b02195.

(60) Di Lorenzo, R. A.; Place, B. K.; VandenBoer, T. C.; Young, C. J. Composition of Size-Resolved Aged Boreal Fire Aerosols: Brown Carbon, Biomass Burning Tracers, and Reduced Nitrogen. *ACS Earth and Space Chemistry* **2018**, *2* (3), 278–285. https://doi.org/10.1021/acsearthspacechem.7b00137.

(61) Powelson, M. H.; Espelien, B. M.; Hawkins, L. N.; Galloway, M. M.; De Haan, D. O. Brown Carbon Formation by Aqueous-Phase Carbonyl Compound Reactions with Amines and Ammonium Sulfate. *Environ. Sci. Technol.* **2014**, *48* (2), 985–993. https://doi.org/10.1021/es4038325.

(62) Yang, L.; Huang, R.-J.; Shen, J.; Wang, T.; Gong, Y.; Yuan, W.; Liu, Y.; Huang, H.; You, Q.; Huang, D. D.; Huang, C. New Insights into the Brown Carbon Chromophores and Formation Pathways for Aqueous Reactions of α-Dicarbonyls with Amines and Ammonium. *Environ. Sci. Technol.* **2023**, *57* (33), 12351–12361. https://doi.org/10.1021/acs.est.3c04133.

Appendix A: Supporting Information for Chapter 2

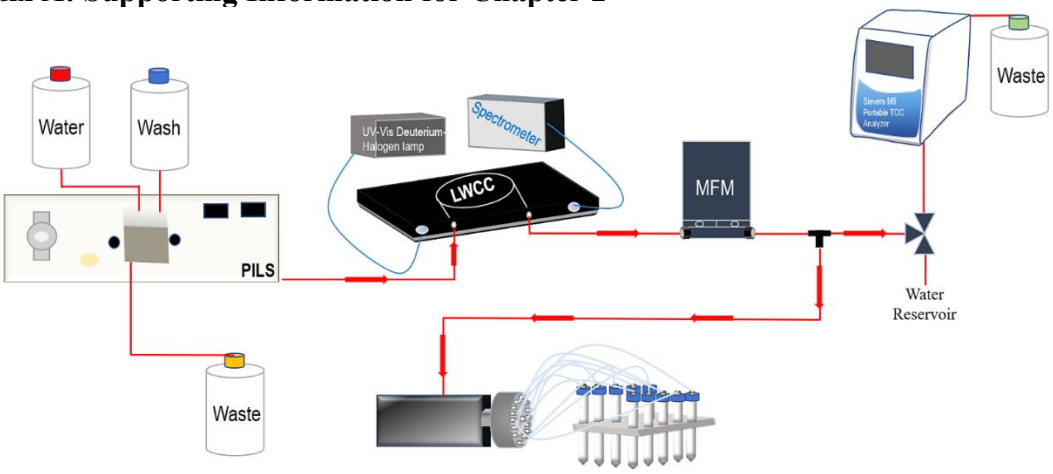

Figure A-1. A schematic showing the liquid flow within the BrC-PILS. MFM is liquid mass flow meter and LWCC is liquid waveguide capillary cell.

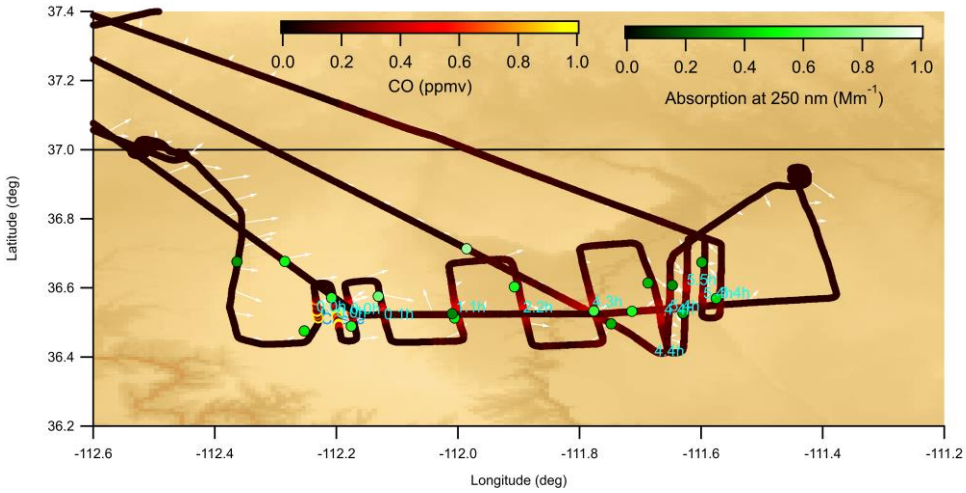

Figure A-2. Selected map of second flight on 21 Aug 2019 of the Castle fire. The circular markers are coloured by absorption at 250 nm measured by SEC-UV and represent the average location where liquid flow was diverted into a single polypropylene sample tube.

A.1 Mobile phase impact on SEC-UV elution profile

Analysis by SEC-UV allows us to examine the molecular size of BrC chromophores as a function of plume age. As the mobile phase carries the sample through the porous stationary phase of a SEC column, high MW molecules that exceed the size of the pores will flow directly through the column, passing the pores. This will result in an early elution time within the void volume. If absorbing species are small enough to penetrate the pores, they will spend more time in the column

and elute later. All molecules that are smaller than the limit to fully penetrate the pores of the stationary phase will elute in the exclusion volume. Figure A-3 displays single-wave size-exclusion chromatogram at 250 nm for aqueous samples collected on 21 Aug 2019. The absorption density of the aqueous samples listed in Table A1 had consistent size-resolved features with varying magnitude in absorption. The first peak between 8.5 to 9 minutes is characteristic of relatively higher MW compounds than the second peak between 9.5 to 11.

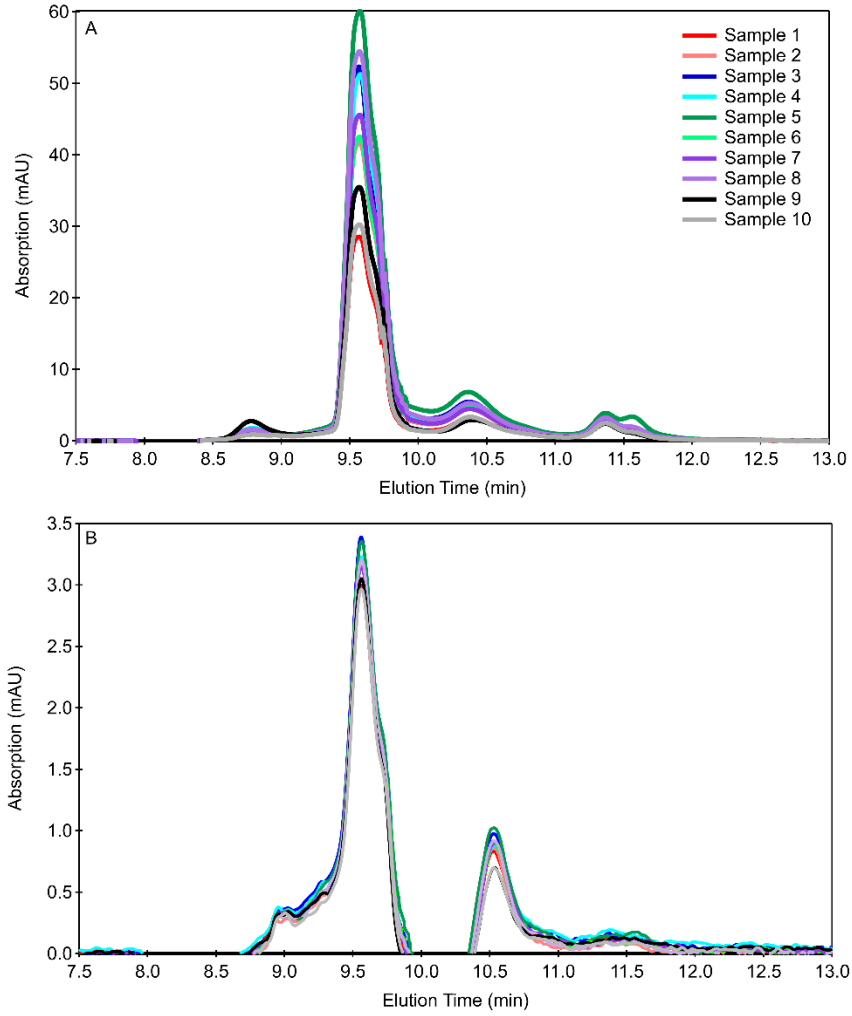

Figure A-3. Example of absorption density plot at (A) 250 nm and (B) 300 nm of FIREX-AQ aqueous samples collected during the second flight 21 Aug 2019, of the Castle fire. The mobile phase is equal parts acetonitrile and 25 mM ammonium acetate solution at a flow rate of 1 mL min^{-1}.

Figure A-4 displays single-wavelength size-exclusion chromatograms of an aqueous separation on the SEC-UV with varying mobile phase compositions. With equal parts methanol and 25 mM ammonium acetate solution solution, the low MW fractions eluted after exclusion volume of the SEC column (<250 Da). With the addition of acetonitrile, it appears that the apparent higher MW fraction then co-eluted with the low MW fraction (represented by a single peak in the orange trace; Figure A-4). Similar to the findings of Lyu et al. (2021) using equal parts acetonitrile and 25 mM ammonium acetate solution appears to be effective in suppressing interactions between the stationary phase of the SEC column and chromophores, as a narrow elution profile of a low MW fraction was observed.[1]

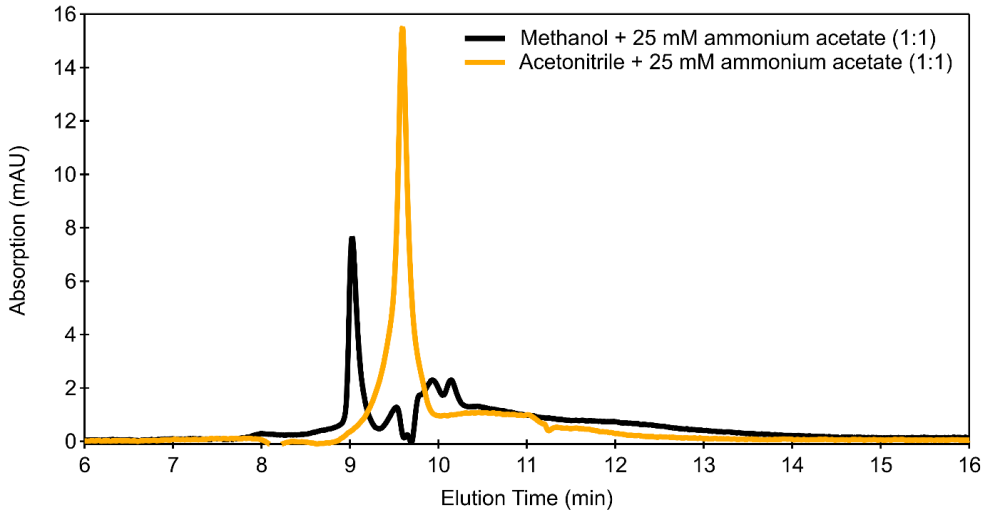

Figure A-4. Single-wavelength chromatogram at 250 nm of an aqueous sample run with equal parts 25 mM ammonium acetate solution and methanol (black) and equal parts 25 mM ammonium acetate solution and acetonitrile (orange).

The default mobile phase used was equal parts acetonitrile and DIW with 25 mM ammonium acetate. When ammonium acetate is dissolved in water, sub-stoichiometric acidification converts acetate to acetic acid producing conditions that can stabilize pH at 4.75.[2] The alkalinization of ammonium acetate solution generates NH_3 via the depronotation of NH_4^+, creating buffering capacity around the pka of ammonium (9.25). Therefore, ammonium acetate

dissolved in water has an inherent buffering capacity in acidic (pH at 4.75±1) and basic ranges (9.25±1).[2] The addition of acetonitrile to ammonium acetate dissolved in water reduces the buffer capacity and shifts the buffering ranges of ammonium acetate dissolved in water to approximately pH 5.5±1 and pH 9 ±1.[3] The purpose of the addition of the ammonium acetate to the mobile phase was to minimize electrostatic interactions between the compounds and the stationary phase of the column. This has proven effective in previous SEC-UV analyses of biomass burning derived samples investigating MW properties of fresh and aged BrC.[1,4-5] If the electrostatic interactions are negligible, SEC separation is based on hydrodynamic volume, which is a function of MW and the density of the compounds.[6] In Figure A-6, there is a red shift when mobile phase conditions have a pH greater than the pKa of the single compound. However, Figure A-7 shows that wavelength dependent absorption of the SRFA looks similar under all mobile phase conditions. This indicates that we do not anticipate pH impacting wavelength dependent absorption in the SEC-UV analysis.

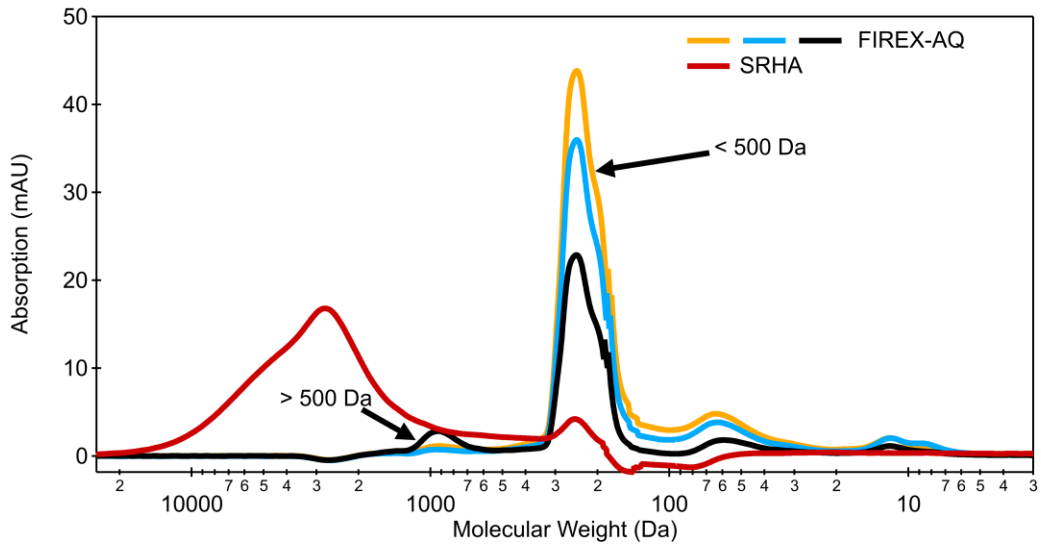

Figure A-5. Absorption density as a function of molecular weight of aqueous samples collected during FIREX-AQ water samples and Suwannee River humic acid. The mobile phase is equal parts acetonitrile and 25 mM ammonium acetate solution at a flow rate of 1 mL min^{-1}.

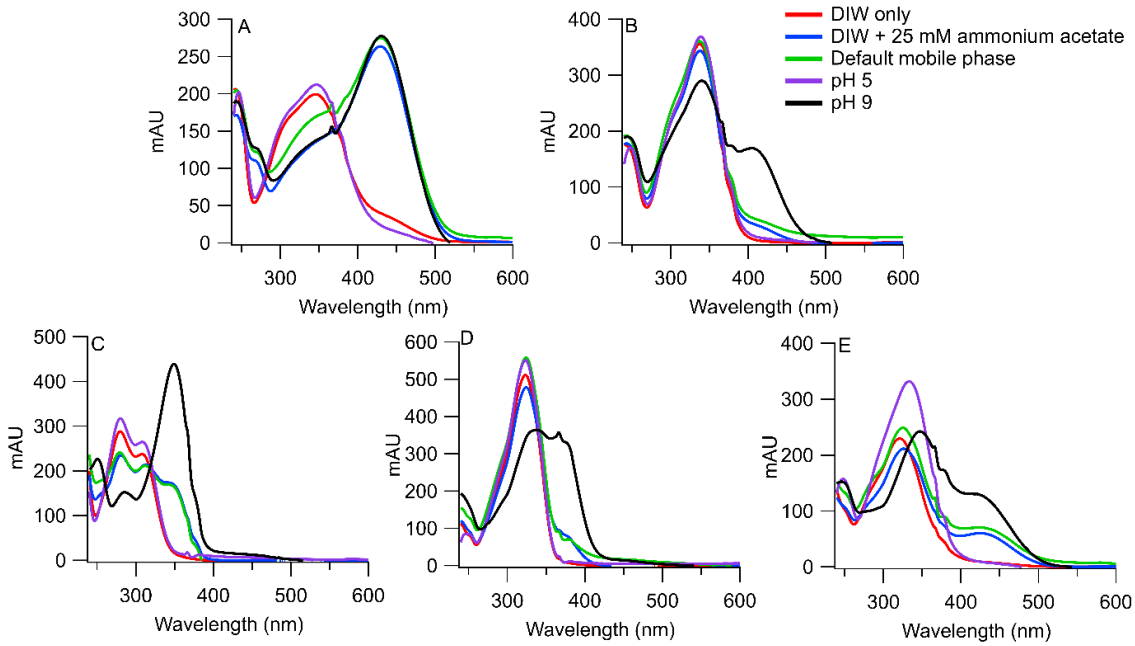

Figure A-6. Absorption as a function of wavelength measured in various mobile phases of (A) 4-nitrocatechol (B) 4-hydroxy-3-methoxy cinnamaldehyde (C) vanillin (D) 7-hydroxycoumarin and (E) a mixture of the four compounds by a diode array detector. The default mobile phase consists of 1:1 mixture of acetonitrile and DIW with 25 mM ammonium acetate. The purple and black traces represent pH controlled mobile phases, where the pH of the ammonium acetate solution was adjusted to pH 5 and pH 9 prior to the addition of the acetonitrile.

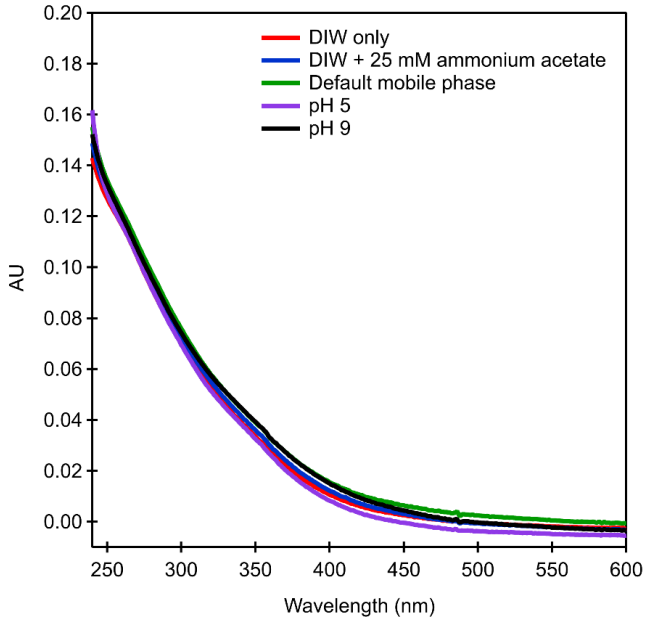

Figure A-7. Absorption as a function of wavelength of SRFA measured using a Agilent 8453 UV-visible Spectroscopy System. A solution of 15 µg/mL SRFA was diluted by 50 % by the mobile phase and then transferred to the cuvette prior to measurement. The default mobile phase consists of 1:1 mixture of acetonitrile and 25 mM ammonium acetate solution. The purple and orange traces represent pH controlled mobile phases, where the pH of the ammonium acetate solution was adjusted to pH 5 and pH 9 prior to the addition of the acetonitrile.

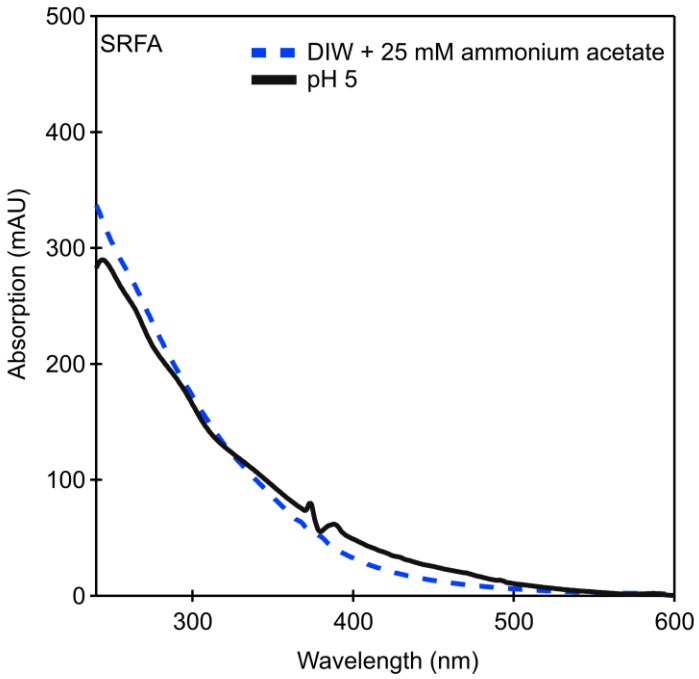

Figure A-8. Absorption as a function of wavelength of SRFA measured in a 25 mM ammonium acetate solution and in a mobile phase controlled to pH 5.

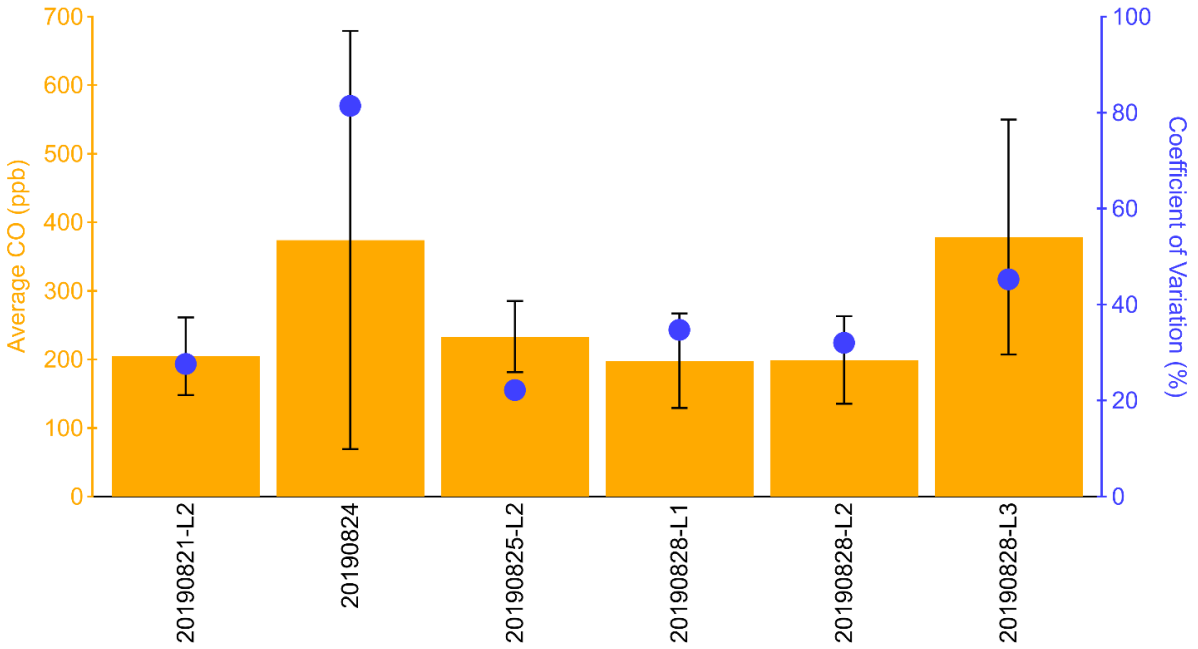

Figure A-9. Average and standard deviation of CO measured during each flight. Blue markers denote the coefficient of variation, which represents the standard deviation as a percent of the mean.

A.2: Conversion of SEC-UV signal to ambient absorption units of Mm^{-1}

To compare absorption of the water soluble BrC measured online by the BrC-PILS, the absorption data measured by SEC-UV was converted to inverse megameters, Mm^{-1}. The absorption of different MW fractions at a selected wavelength is determined by integrating the peak area. To apply the Beer-Lambert Law to the absorption profiles by the SEC-UV method, the dilution of the sample during this analysis must be considered. The absorbance of the sample, A_λ, is a function of injection volume, V_i, and the absorbance across a peak, $A_{\lambda p}$, is dependent on the volume across a peak, V_p. The value of V_p can be determined by multiplying the flow rate by the peak width. The peak area, a_p, is the product of the absorbance intensity (mAU) multiplied by the peak width (minutes), w_p.

Absorbance across a peak	Absorbance of sample collected
$A_{\lambda p} = \varepsilon\, l\, c_p$	$A_\lambda = \varepsilon\, l\, c$
$A_{\lambda p} = \varepsilon\, l\, n / V_p$	$A_\lambda = \varepsilon\, l\, n / V_i$
$\varepsilon = A_{\lambda p} \cdot V_p / l\, n$	$\varepsilon = A_\lambda \cdot V_i / l\, n$
$A_{\lambda p} = A_\lambda \cdot V_i / V_p$ Eq (1)	
Volume across peak $a_p = A_{\lambda p} \cdot w_p$	

$$w_p = V_p / F$$

$$\mathbf{A_{\lambda p} = a_p \cdot F / V_p \quad Eq\ (2)}$$

Combine Eq 1 & 2

$$a_p \cdot F / V_p = A_\lambda \cdot V_i / V_p$$

$$a_p \cdot F = A_\lambda \cdot V_i$$

$$\mathbf{A_\lambda = a_p \cdot F / V_i \quad Eq\ (3)}$$

For this analysis, the conversion of the absorbance (mAU) of a water sample (A_λ) to Mm^{-1} considers the volume collected by the PILS and the volume of air sampled by the inlet system as described in Washenfelder et al. (2022), and the PILS collection efficiency:[7]

$$\text{Absorption}(\text{Mm}^{-1}) = \frac{\text{peak area} \times \text{SEC Flow rate}}{\text{Injection Volume}} \times \frac{\text{PILS Flow}}{\text{Gas flow} \times \text{Optical path}} \times \ln(10) \times \text{PILSCollectionEff}$$

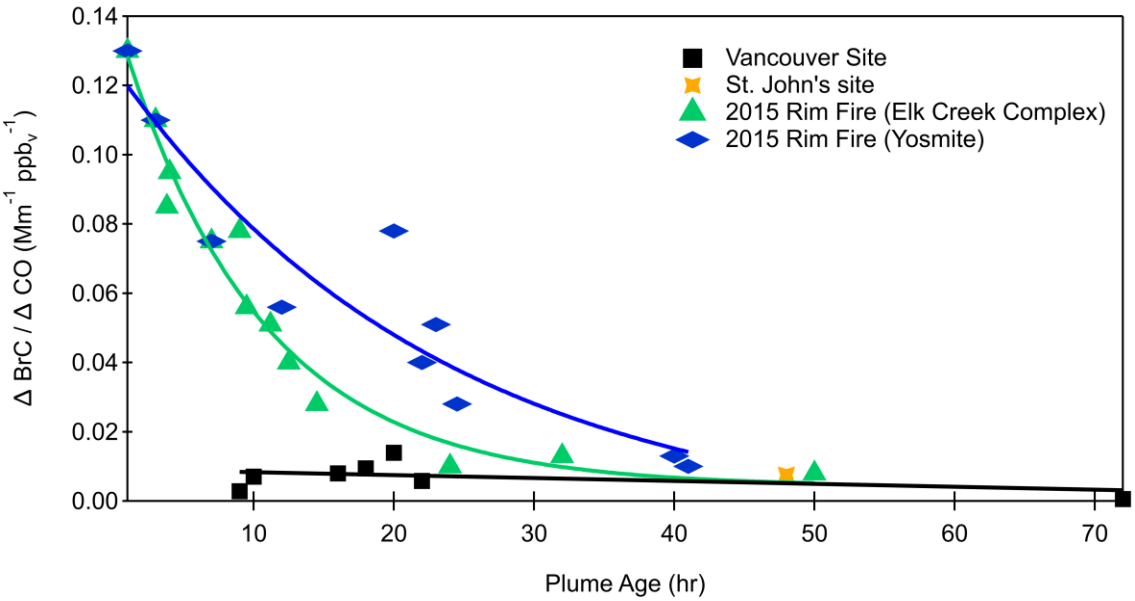

Figure A-10. Absorption at 365 nm to CO as a function of plume age of water extracts for smoke sampled of glass microfiber filters in Vancouver (Di Lorenzo et al., 2017).[4] The green and blue squares represent absorption at 365 nm to CO of water extracts sampled on Teflon filters aboard the NASA DC-8 aircraft during SEAC4RS (Forrister et al. 2015).[8]

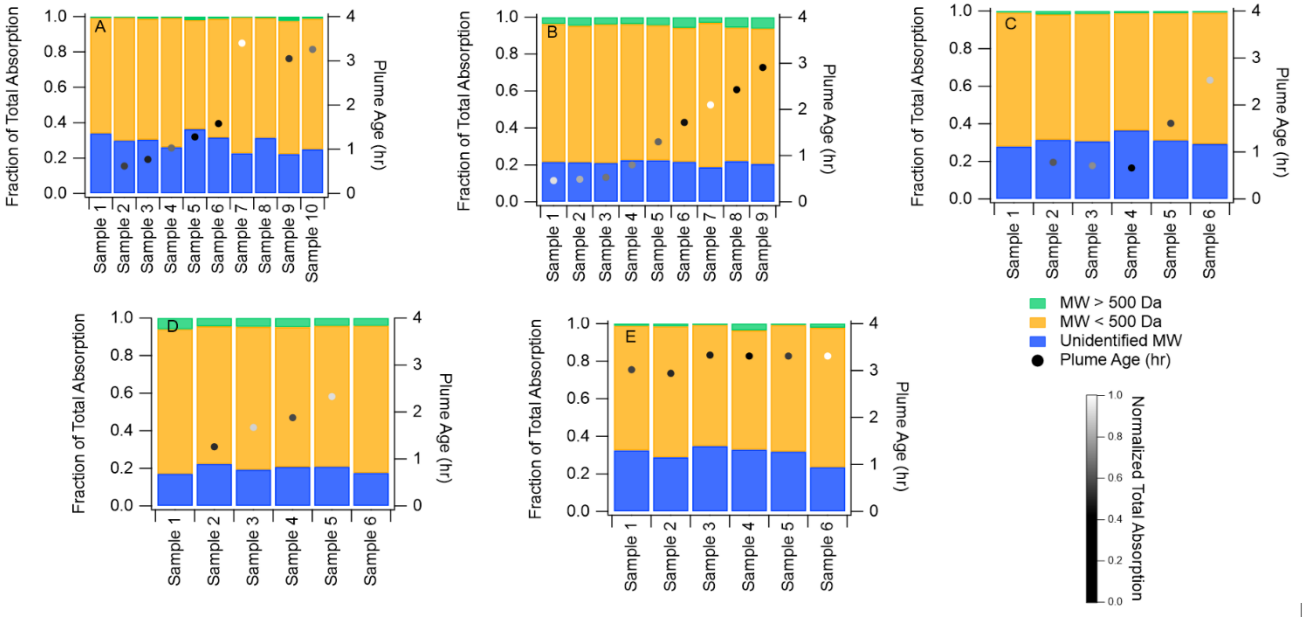

Figure A-11. Absorption contribution of high (>500 Da), low (<500 Da), and unidentified molecular weight species of aqueous samples collected during (A) 24 Aug 2019, (B) 25 Aug 2019 L2, (C) 28 Aug 2019 L1, (D)) 28 Aug 2019 L2, and (D)) 28 Aug 2019 L3.

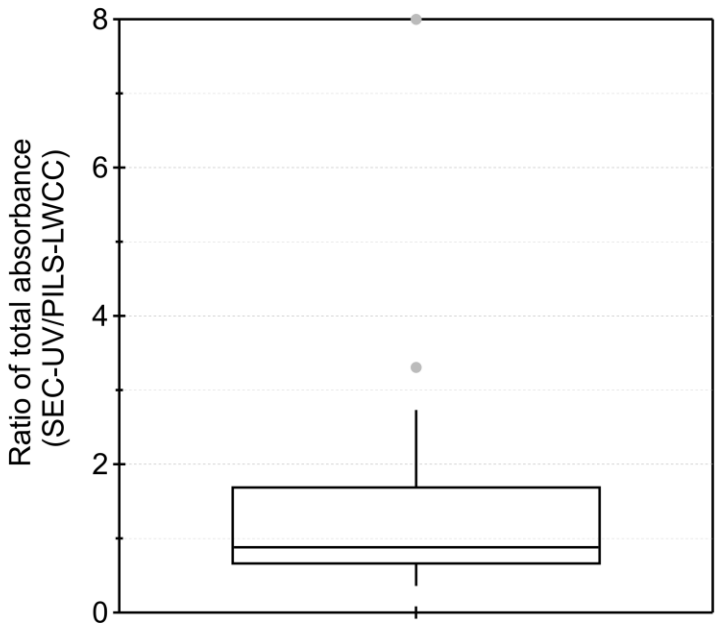

Figure A-12. Relationship between BrC absorption as measured by SEC−UV offline and by PILS−LWCC online during the Southern Oxidant and Aerosol Study (SOAS) in the Talladega National Forest in Alabama, USA. Offline samples were collected on a filter assembly of a broadband cavity enhanced spectrophotometer and online particle absorption was measured using a PILS-LWCC (Di Lorenzo et al., 2017).

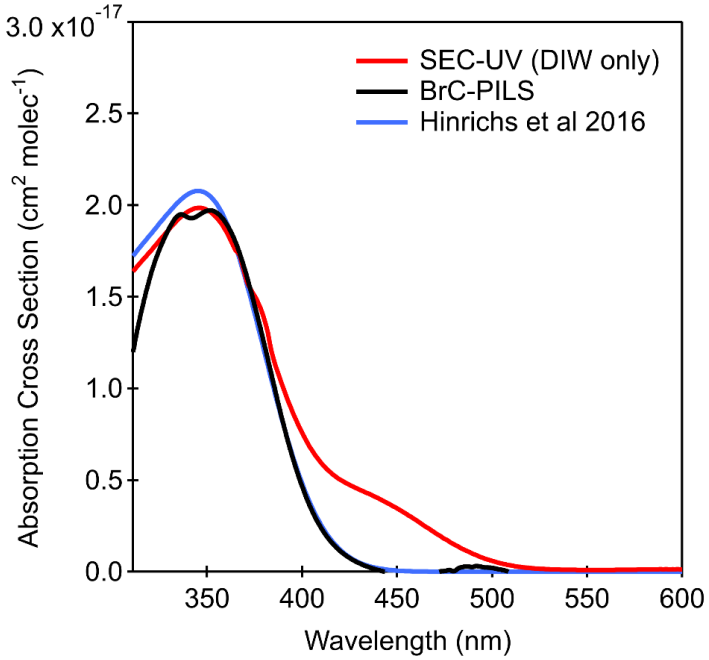

Figure A-13. Absorption cross section of 4-nitrocatechol measured by injection onto the LWCC of the BrC-PILS and onto the diode array detector of the SEC-UV set-up compared to Hinrichs et al. 2016.

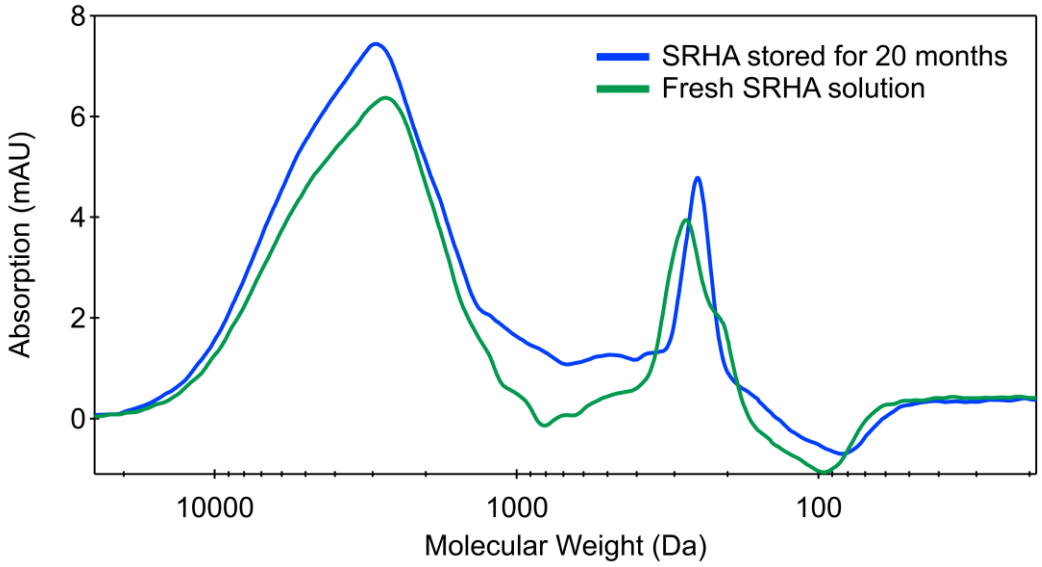

Figure A-14. Size separation of a fresh SRHA solution which was re-run 20 months later.

Table A1. Summary of flights completed by the NOAA "Chemistry" Twin Otter aircraft during FIREX-AQ 2019.

US State	Fire Name	Fuel	Date and Flight leg	Number of water samples collected	Number of Transects	Plume age range (hr)
Arizona	Castle	Grassland, timber, mixed conifer	20190821-L2	10	8	0.2 – 4.1
Oregon	204 Cow	Sub-alpine fir, timber, grass	20190824-L2	10	8	0.5 – 2.4
			20190825-L2	9	10	0.5 – 2.9
			20190828-L1	6	6	0.7 – 1.8
			20190828-L2	6	4	1.3 – 2.9
			20190828-L3	6	4	2.2 – 4.2

A.2 References

(1) Lyu, M., Thompson, D. K., Zhang, N., Cuss, C. W., Young, C. J., and Styler, S. A.: Unraveling the complexity of atmospheric brown carbon produced by smoldering boreal peat using size-exclusion chromatography with selective mobile phases, Environ. Sci.: Atmos., 1, 241–252, https://doi.org/10.1039/D1EA00011J, 2021.

(2) Konermann, L.: Addressing a Common Misconception: Ammonium Acetate as Neutral pH "Buffer" for Native Electrospray Mass Spectrometry, J. Am. Soc. Mass Spectrom., 28, 1827–1835, https://doi.org/10.1007/s13361-017-1739-3, 2017.

(3) Subirats, X., Bosch, E., and Rosés, M.: Buffer considerations for LC and LC-MS, Lc Gc North America, 27, 1000–1004, 2009.

(4) Di Lorenzo, R. A., Washenfelder, R. A., Attwood, A. R., Guo, H., Xu, L., Ng, N. L., Weber, R. J., Baumann, K., Edgerton, E., and Young, C. J.: Molecular-Size-Separated Brown Carbon Absorption for Biomass-Burning Aerosol at Multiple Field Sites, Environmental Science and Technology, 51, 3128–3137, https://doi.org/10.1021/acs.est.6b06160, 2017.

(5) Wong, J. P. S., Nenes, A., and Weber, R. J.: Changes in Light Absorptivity of Molecular Weight Separated Brown Carbon Due to Photolytic Aging, Environmental Science & Technology, 51, 8414–8421, https://doi.org/10.1021/acs.est.7b01739, 2017.

(6) Pelekani, C., Newcombe, G., Snoeyink, V. L., Hepplewhite, C., Assemi, S., and Beckett, R.: Characterization of Natural Organic Matter Using High Performance Size Exclusion Chromatography, Environ. Sci. Technol., 33, 2807–2813, https://doi.org/10.1021/es9901314, 1999.

(7) Washenfelder, R. A.; Azzarello, L.; Ball, K.; Brown, S. S.; Decker, Z. C. J.; Franchin, A.; Fredrickson, C. D.; Hayden, K.; Holmes, C. D.; Middlebrook, A. M.; Palm, B. B.; Pierce, R. B.; Price, D. J.; Roberts, J. M.; Robinson, M. A.; Thornton, J. A.; Womack, C. C.; Young, C. J. Complexity in the Evolution, Composition, and Spectroscopy of Brown Carbon in Aircraft Measurements of Wildfire Plumes. Geophysical Research Letters 2022, 49 (9), e2022GL098951. https://doi.org/10.1029/2022GL098951.

(8) Forrister, H.; Liu, J.; Scheuer, E.; Dibb, J.; Ziemba, L.; Thornhill, K. L.; Anderson, B.; Diskin, G.; Perring, A. E.; Schwarz, J. P.; Campuzano-Jost, P.; Day, D. A.; Palm, B. B.; Jimenez, J. L.; Nenes, A.; Weber, R. J. Evolution of Brown Carbon in Wildfire Plumes. Geophysical Research Letters 2015, 42 (11), 4623–4630. https://doi.org/10.1002/2015GL063897.

Chapter 3

Molecular Properties of Brown Carbon Aerosol from Biomass Burning of Wildland Fuels at the Fire Sciences Laboratory

3.1 Abstract

Wildfires are a large and increasing source of absorbing organic aerosol (brown carbon) in North America, with a direct impact on the global radiative budget. Brown carbon from wildfires is a complex and poorly characterized mixture of compounds with varying composition, volatility, and reactivity. We conducted controlled burns of western United States fuels at the Missoula Fire Sciences Laboratory during the FIREX FireLab 2016 study. We measured water-soluble brown carbon absorption, total aerosol absorption, and aerosol composition with a shared thermally denuded inlet at temperatures between ambient and 250 °C. We simultaneously collected filter samples at ambient temperature and 250 °C for detailed analysis of molecular size, hydrophobicity, and octanol-water partitioning coefficient log(K_{OW}) using chromatographic separation techniques with wavelength-resolved absorption detection. For the controlled burns, ~92% of the water-soluble brown carbon at 365 nm consisted of low-volatility organic compounds with log(C_{sat}) values between (-5.1 ± 2) to (0.4 ± 2) and oxygen-to-carbon ratios between 0.0–1.1. Species with molecular mass <500 Da contributed 82 ± 13% of the absorption at 365 nm, while species >500 Da contributed only 6.2 ± 3.7%. Thermodenuder temperatures of 250 °C were equivalent to log(C_{sat}) < -9 with observed oxygen-to-carbon ratios of 1.2 ± 0.3. We found that while only ~6% of water-soluble brown carbon at 365 nm persisted at these temperatures, approximately 50% of the total absorption in the offline samples remained, with an increased contribution by molecules >500 Da of 15 ± 12%. HPLC analysis showed that the compounds removed at 250 °C had log(K_{OW}) values between 2.9 ± 0.7 and 3.5 ± 0.7, and contained aliphatic, aromatic, hydroxyl, and carbonyl functional groups.

3.2 Introduction

Wildfire activity across the western United States has increased over recent decades due to natural climate variability and anthropogenic influences. Extensive increases in fire activity, including area burned[1], number of large fires[2], and fire season length[3], have been documented across the western U.S. Wildfire emission components include carbon dioxide, carbon monoxide, nitric oxide, methane, volatile organic compounds (VOCs), and carbonaceous aerosol and other particulate matter. Biomass burning emits about 31–36 Tg yr^{-1} of primary organic aerosol.[4,5] The composition, size, and mixing state of biomass burning aerosols determine the optical properties of smoke plumes in the atmosphere.[6] The fraction of organic aerosol that absorbs light in the ultraviolet (UV) to visible (vis) wavelength region is referred to as brown carbon (BrC).[7] Brown carbon remains a source of uncertainty in the estimate of the global radiative forcing of aerosol[8–10], but studies have suggested that BrC contributes to positive radiative forcing with up to 20% of total aerosol absorption.[11–13]

The radiative impact BrC has on Earth's climate is partly dictated by its atmospheric lifetime.[6,8] In the atmosphere, BrC is susceptible to a range of aging processes which include dilution and evaporation of more volatile components[14], photolysis, and heterogeneous oxidation with OH, O_3, and NO_3.[15–17] Atmospheric processing alters the absorption properties of BrC chromophores where photoenhancement or photobleaching can occur.[18] Washenfelder et al. and Zeng et al. sampled wildfire emissions in the western U.S. and observed that BrC absorption increased, decreased, or was unchanged as a function of plume age from 0 to 5 and 0 to 8 hrs, respectively.[19,20] Uncertainty remains about how aging processes alter the composition, volatility, and absorption properties.

The diversity in molecular size and structure of BrC is manifested as variability in volatility, solubility, and optical properties.[8] The combination of chromophores, whose ability to absorb in the UV-vis region varies, contributes to the observable brown colour.[21] A significant portion of BrC chromophores remain unidentified and there are gaps in our knowledge about secondary formation mechanisms. Several analytical approaches have been used to characterize the absorbing constituents that contribute to BrC absorption. Reverse-phase high performance liquid chromatography (HPLC) coupled to high resolution mass spectrometry[22] separates compounds based on polarity and size exclusion chromatography coupled to ultraviolet-visible absorption spectroscopy (SEC-UV) has successfully measured the absorption properties of high and low molecular weight (MW) BrC species in fresh and aged biomass burning-derived samples.[23–25] These findings suggested that lower MW species are less persistent in biomass burning smoke relative to higher MW species, likely due to volatilization, oxidation, polymerization, or other processes.[24]

Biomass burning derived organic aerosol consist of species with varying volatilities. Two-dimensional gas chromatography offers chemical characterization by separating compounds by volatility in the first dimension and by polarity in the second dimension.[26–28] The speciation of intermediate and semi-volatile organic compounds is important to assess the competing effects of primary organic aerosol volatilization and secondary organic aerosol formation.[27] From controlled burns of fuels specific to the western U.S., Jen et al. observed intermediate and semi-volatile organic compounds (I/SVOCs) which included polycyclic aromatic hydrocarbons, oxy aromatic heterocycles, benzoic acids, oxy aliphatic, and nitro-organics.[28] Donahue et al. introduced the one-dimensional volatility basis set, where organic aerosol components are grouped into bins according to their saturation concentrations ($\log(C_{sat})$).[29] Each bin is separated by one order of magnitude,

where gas-particle partitioning depends on dilution, temperature, and chemical transformation measured. The one-dimensional volatility basis set evolved to include a second dimension: the oxygen to carbon ratio (O:C).[30] To measure the volatility distribution of organic aerosol, thermal denuding experiments are commonly used.[31] In a thermodenuder, particles are flowing and heated to a fixed temperature and the evaporation rate of compounds from particles is determined by thermodynamic properties of the compounds, (vapor pressure and enthalpy of vaporization), the mole fraction of the compound within the particles, and the strength of the interactions of particle components (i.e., carbon-carbon, carbon-oxygen, and oxygen-oxygen).[32]

Numerous established methods have greatly improved our understanding about the chemical nature of BrC species; however, to our knowledge the application of the octanol-water partitioning coefficient (K_{ow}) has not been investigated. This parameter has an established relationship to molecular structure in liquid-phase environmental chemistry and provides insight into the hydrophobicity or polarity of organic compounds.[33,34] Measuring the K_{ow} of BrC species will further validate our interpretation and instill confidence in our measurements by reinforcing the relationships between BrC structure and gas-particle partitioning.

In this work, we analyze the volatility and chemical properties of BrC from controlled burns at the Missoula Fire Sciences Laboratory during FIREX FireLab 2016. The study focused on wildfire fuels typical of the western U.S. with measurements by online and offline instrumentation under thermodenuded and ambient (undenuded) conditions. Online aerosol measurements included water-soluble BrC, total aerosol absorption, and aerosol chemical composition for the average oxygen-to-carbon (O:C) ratio. Offline filter samples were analyzed using SEC-UV to characterize molecular size and reverse-phase high performance liquid chromatography (HPLC-UV) to characterize polarity. We use these online and offline

measurements to examine: i) BrC volatility and O:C ratio in the context of the two-dimensional volatility basis set; ii) BrC molecular weight; and iii) BrC octanol-water partitioning properties.

3.3 Experimental

3.3.1 Overview of the Fire Sciences Laboratory Experiment

The Fire Influence on Regional to Global Environments (FIREX) FireLab 2016 campaign was based at the U.S. Forest Service's Fire Sciences Laboratory in Missoula, Montana during October–November 2016. The Fire Sciences Laboratory has been described previously.[35,36] The main combustion chamber has internal dimensions of 12.5 m × 12.5 m × 22 m with a total volume of ~3000 m^3 as shown in Figure B-1a. Approximately 0.2 to 4.4 kg of fuel was placed on a fuel bed and ignited using a heating plate. During the burn experiments, the combustion room was sealed, and smoke was well-mixed for sampling over 2.5–3 hrs.[37,38] The instruments in this study were located in an adjacent room with inlets to the main burn chamber.[37]

Table B-1 lists the fuel type and conditions for the controlled burns in this study. The fuels were characteristic of the western U.S. and were primarily collected from the Clearwater Wildlife Management Area and the Lubrecht Experimental Forest.[36] The fuels included chaparral (manzanita and chamise), ponderosa pine, lodgepole pine, longleaf pine, Douglas fir, subalpine fir, Engelmann spruce, ceanothus, and juniper.

Two inlets with identical thermodenuders supplied flow to aerosol instruments for online measurements and filter samples for offline analysis. Some details of aerosol sampling strategy and results have been described previously.[37–39] Here, we present results from the chamber burns sampled with aerosol optical property instruments to examine the physical, chemical and optical properties of BrC. These inlets and instruments are described in detail below.

3.3.2 Online sampling of fresh biomass burning smoke

3.3.2.1 Aerosol inlet

The inlet for online aerosol measurements is described in Womack et al. and briefly summarized here and in Figure B-1b.[37] The inlet was connected to the burn chamber with ~30 m of 0.64 cm o.d. copper tubing.[37] The sample flow was treated with an inertial impactor with 50% cut point at an aerodynamic diameter of 1.0 µm (TE296; Tisch Environmental, Cleves, OH), a silica gel dryer, an activated carbon denuder to remove VOCs, nitrogen oxides (NO_y) and ozone (O_3), and a thermodenuder that allowed the sample flow to be heated to user-selected temperatures. A 2.0 volumetric L min^{-1} (vlpm) flow from the burn room was evenly split between a thermodenuder and a bypass channel. An automated two-position valve (Hanbay Inc, Pointe-Claire, Québec, Canada) directed 1.0 vlpm of thermodenuded or 1.0 vlpm of fresh smoke to a mixing volume with dilution for measurement by a set of aerosol instruments.

3.3.2.2 Thermodenuder

Thermodenuders followed the general design of Huffman et al., with the addition of charcoal fabric to absorb the volatilized species in the heated section.[40] Each thermodenuder consisted of a screen tube (80 cm long, 1.3 cm i.d.). The first 40 cm was heated, and the remaining 40 cm served as a cool-down region. With a flow rate of 1.0 vlpm, the residence time was 3.2 s, and the Reynolds number was 114. The thermodenuder temperature was varied between 25–300 °C, while the bypass channel remained at room temperature (approximately 25 °C) for undenuded sampling. The throughput efficiency of the thermodenuder was less than unity (86 ± 4 % at 250 °C for particles with diameter 100–300 nm) due to thermophoretic wall losses. The thermophoretic wall losses were characterized using non-volatile, inorganic aerosol and corrected in the data.

3.3.2.3 Determination of C_{sat} from thermodenuder temperature

The volatility of organic aerosol can be represented by its saturation vapour pressure, C_{sat}, which is defined as the vapour pressure concentration of a compound at a given reference temperature expressed in units of μg m^{-3}. Thermodenuder experiments with varying temperature can be used to calculate mass fraction remaining or absorption fraction remaining as a function of temperature. It is possible to interpret these measurements within the volatility basis set by converting thermodenuder temperature to C_{sat} using empirical measurements of known compounds[31] or a full kinetic model.[32] However, uncertainty in the values of C_{sat} exist for organic aerosol mixtures of unknown composition because the enthalpy of vaporization and mass accommodation coefficient are difficult to estimate[41] and may differ from experimental and modeled values. For this work, we have adopted the empirical description by Faulhaber et al. which was well-described by a full kinetic model[32] to convert thermodenuder temperature to C_{sat}.[31] The differences between the thermodenuders used in this work and those described previously are the addition of adsorbent material in the heated section to prevent re-condensation, smaller tube diameter (1.3 cm vs 2.2 cm), and reduced residence time (3.2 s vs 15 s). Considering both the differences in the thermodenuder operation, and the uncertainty in the enthalpy of vaporization and mass accommodation coefficient for a complex mixture of fresh biomass burning aerosol, we estimate that the uncertainty in the calculated log(C_{sat}) values is ± 2.

3.3.3 Online Aerosol Instruments

3.3.3.1 UV/Visible spectroscopy of water-soluble organic carbon

Water-soluble organic aerosol absorption and water-soluble organic carbon (WSOC) were measured using a BrC-PILS instrument. This instrument has been described previously[19,20] and further details are included in Appendix B. Spectra were acquired at 300–600 nm with an

integration time of 1 s, and soluble aerosol absorption in units of Mm^{-1} was calculated using Beer's Law.[20] The accuracy of the absorption and WSOC measurements were ± 16% and ± 18%, based on the uncertainties in the gas flow, liquid flow, collection efficiency of the PILS, and calibration of the TOC analyzer.

3.3.3.2 Photoacoustic spectroscopy

Total aerosol absorption was measured using a photoacoustic aerosol absorption spectrometer,[42,43] referred to as the cavity ringdown photoacoustic spectrometer (CRD-PAS). The CRD-PAS measured aerosol absorption at 401, 532, and 661 nm using an amplitude-modulated laser, resonant cavity, and sensitive microphone for each channel. The uncertainty in the aerosol absorption coefficients at 401 nm was ± 30% .[44]

3.3.3.3 Aerosol mass spectrometer (AMS)

Total organic aerosol mass was measured using a compact time-of-flight Aerosol Mass Spectrometer (c-TOF AMS; Aerodyne Research Inc., Billerica, MA) with unit mass resolution.[45] A light-scattering module allowed direct measurements of the AMS collection efficiency (CE_{LS}) due to particle bounce.[46] CE_{LS} was determined for particles larger than 300 nm in vacuum aerodynamic diameter and was considered statistically significant if more than 15 particles were detected by light scattering for each experimental condition. It typically decreased as a function of thermodenuder temperature (Figure B-2) and was included in the calculated organic aerosol mass to minimize bias with changing volatility. The O:C ratios were determined from the fraction of organic signal measured at mass-to-charge ratio (m/z) 44, following the parameterization in Canagaratna et al.[47] A default value of 1.4 for the relative ionization efficiency (RIE) of organic mass was used for all experiments and thermodenuder conditions. Because the O:C ratio for these experiments varied from 0 to 1.5, the value of RIE could have been as high as 7 for the organic

mass sampled with the lowest O:C ratios.[48] Thus, measurements of the organic mass for some of the ambient (undenuded) experiments could be biased high by as much as a factor of 5. While the standard uncertainty of the organic aerosol mass is typically ~ 38% for ambient measurements,[45] it is higher for these experiments due to the variability in composition as well as aerosol volatility.[37]

3.3.3.4 Optical Particle Counter

Total aerosol mass was determined using an optical particle counter (LAS 3340, TSI Inc., Shoreview, MN), which detects light scattered by individual particles intercepting a 633 nm laser beam. The LAS directly measures optical scattering and converts the signal to a size histogram assuming a purely scattering aerosol with a given refractive index. We converted the volume to mass using an assumed density of 1.8 g/cm^3.[49] Corrections are required to determine the size distribution of aerosols with a different refractive index or absorbing aerosol and there are large uncertainties for strongly absorbing aerosol such as black carbon particles, as described in Womack et al.[37]

3.4.4 Offline sampling of fresh biomass burning smoke

3.2.4.1 Collection and extraction of filter samples

The aerosol inlet for offline filter samples consisted of ~ 30 m of 0.64 cm o.d. copper tubing connected to an identical thermodenuder at 250 °C (Figure B-1c). A sampling flow rate of 2.0 slpm was controlled by a mass flow controller (Alicat Scientific, Tucson, AZ). A cyclone (URG-2000-30ED; URG Corp, Chapel Hill, NC) with nominal 2.5 μm cutpoint at 2.4 slpm removed large particles. Aerosol was collected on pre-muffled (500 °C, 4 h) 47 mm quartz fiber filters (Tissuquartz 2500QAT-UP; Pall Life Sciences, Washington, NY). The filters were placed in perfluoroalkoxy filter holders (Savillex Corp., Eden Prairie, MN) for sampling. During each burn,

we collected filters containing undenuded aerosol and 250 °C denuded aerosol, with typical collection times of 1–2 hrs. A total of 51 filter samples were collected from 19 fires.

After collection, the filters were wrapped in pre-muffled (500 °C, 4 h) aluminum foil, and stored in the dark at -20 °C until analysis. Each aerosol filter was subsampled using a 10 mm arch punch, placed in a pre-cleaned polypropylene sample tube, and sonicated with 1 mL of ultra-pure Milli-Q water (DIW; resistivity of 18.2 MΩ cm) for 1 hr.

3.3.4.2 Determination of molecular weight from SEC-UV analysis

The SEC-UV analysis was completed using an aqueous gel-filtration column with a MW range of 250 Da to 75 kDa (Polysep GFC P-3000; Phenomenex, Torrence, CA). Size-resolved components were detected using a diode array detector at wavelengths from 190 to 800 nm (UltiMate 3000; Thermo Scientific, Sunnyvale, CA) coupled to an ion chromatograph pump (ICS 6000; Thermo Scientific, Sunnyvale, CA) and autosampler (Thermo Scientific, Sunnyvale, CA). The isocratic mobile phase was a 1:1 mixture of acetonitrile and 25 mM aqueous ammonium acetate, flowing at 1 mL min^{-1} to separate 100 µL of injected sample. To estimate the MW distribution, we applied previously described methods.[23,50] The MW is grouped into three categories. High MW refers to species with MW greater than 500 Da and low MW encompasses species less than 500 Da. Unidentified MW describes peaks that eluted past the exclusion volume of the SEC column, preventing a definitive identification of MW.

3.3.4.3 Determination of octanol-water partition coefficient using HPLC-UV analysis

The HPLC offline analysis was completed using the same pump and detector as described above. Samples were separated using a C18 column (2.1 mm × 100 mm × 5 µm, Kinetex Phenomenex; Torrance, CA). The mobile phase was comprised of (A) 0.1% acetic acid in DIW and (B) acetonitrile combined as follows: 95% A held for 5 mins and linearly decreased over the

next 20 mins until a 5% A was reached. This was held for 15 min, and the conditions returned to 95% A in the following 1 min to re-equilibrate.

To describe the hydrophobicity of the compounds separated by HPLC-UV analysis, we use the octanol-water partition coefficient, K_{ow}. This assignment is based on the relationship between a capacity factor (k') and the elution by compounds with known $\log(K_{ow})$.[51] The HPLC-UV analysis of the filter extracts employed a gradient elution scheme; therefore, we determined the $\log(K_{ow})$ that corresponded to retention times of the resolved peaks using multiple isocratic separations.[33,52] Solutions of 4-nitrocatechol (>96%, Sigma Aldrich;), 4-hydroxy-3-methoxycinnamaldehyde (98%, Sigma Aldrich), 7-hydroxycoumarin (99%, Sigma Aldrich), biphenyl (99%, Sigma Aldrich), nitrobenzene (99%, Sigma Aldrich;), and toluene (99.5%, Sigma Aldrich;) with concentrations of 39, 34, 37, 3.9, 35, 35 nmol mL^{-1}, respectively, were prepared and run under the following isocratic conditions: (i) 65% A and 35% B, (ii) 50% A and 50% B, (iii) 35% A and 65% B, and (iv) 20% A and 80% B. To determine k', a solution of thiourea (99%, Sigma Aldrich) was used to identify the void volume. The $\log(K_{ow})$ of these standard compounds ranged from 1.66 to 4.01. Calibration plots and the determination of k' and $\log(K_{ow})$ are included in the SI.

3.4 Results and discussion

3.4.1 Mass and absorption fraction remaining versus thermodenuder temperature

Thermal denuding experiments can identify the volatility and associated absorption properties of biomass burning organic aerosol. In this study, we explore absorption changes for thermally denuded and undenuded aerosol to characterize volatility and other physical properties. Figure 3-1 shows a time series of water-soluble organic aerosol mass, total organic aerosol mass, total aerosol mass, water-soluble organic aerosol absorption, and total aerosol absorption measured during one thermal denuding experiment. The thermodenuder temperature varied between

25–260 °C. We observed that water-soluble organic aerosol mass and organic aerosol mass were progressively removed with greater thermodenuder temperatures. Similarly, thermal denuding reduced water-soluble organic aerosol absorption at the measured wavelengths. However, thermal denuding had a lesser effect on total mass and total absorption because those measurements included the presence of black carbon, which has extremely low volatility and is not removed at 250 °C. Thermal denuding was effective at volatilizing total organic aerosol and water-soluble organic carbon species from the controlled burns in this study.

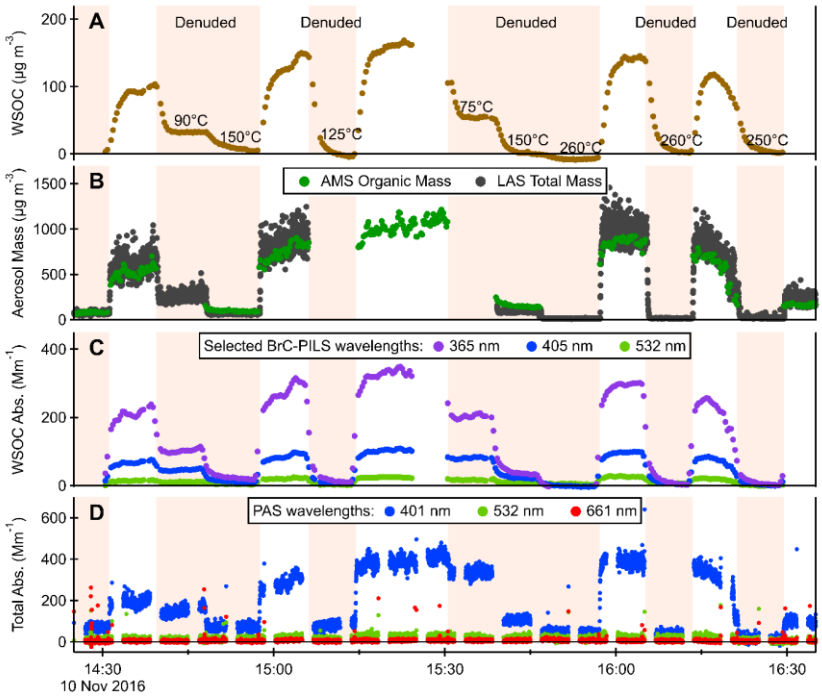

Figure 3-1. Example time series of thermodenuder experiments for a 2 hr period on 10 Nov 2016 showing: (A) water-soluble organic carbon aerosol mass measured by the BrC-PILS; (B) organic aerosol mass measured by the AMS and total aerosol mass measured by the LAS; (C) absorption by water-soluble organic aerosol at three wavelengths measured by the BrC-PILS; and (D) total aerosol absorption at three wavelengths measured by the PAS. Thermodenuder temperatures are labeled in panel (A).

Figures 3-2a and 3-2b show the mass fraction remaining and absorption fraction remaining as a function of thermal denuder temperature for five controlled burns consisting of subalpine fir, Engelmann spruce, ponderosa pine, and dung. The mass fraction for water-soluble organic aerosol

and total organic aerosol remaining show a similar shape, with 50% removal at 73 °C and 105 °C, respectively. The absorption fraction remaining measured by the BrC-PILS approaches 50% removal at 102 °C and 113 °C at 365 and 405 nm, respectively. As expected, the fraction of total absorption remaining does not approach zero at 250 °C due to the refractory black carbon. Figure 3-2c shows the dependence of O:C ratio on thermodenuder temperature. For undenuded organic aerosol, the O:C ratios are 0.25 ± 0.30, and increase to 1.2 ± 0.30 at 250 °C. This indicates that the lower volatility fraction of the organic aerosol is more oxidized.

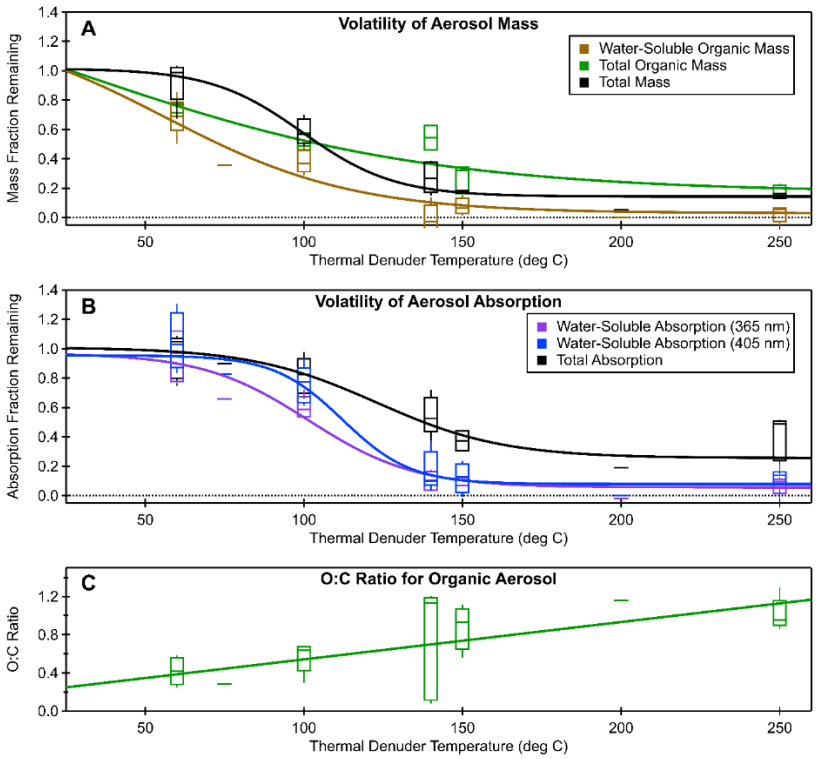

Figure 3-2. Summary of five sampled fires, showing (A) Mass fraction remaining as a function of thermodenuder temperature for water-soluble organic carbon measured by the BrC-PILS, total organic aerosol measured by the AMS, and total aerosol mass measured by the LAS together with sigmoidal fits. The 50% loss for water-soluble organic carbon and total organic aerosol is observed at 73 °C and 105 °C, respectively. (B) Absorption fraction remaining as a function of thermodenuder temperature for water-soluble absorption measured by the BrC-PILS at 365 and 405 nm and total absorption measured by the PAS at 401 nm with sigmoidal fits. The 50% loss for BrC-PILS absorption at 365 and 405 nm are observed at 102 and 113 °C. (C) O:C ratios for the organic aerosol mass measured by the AMS. All boxes represent 25th−75th percentiles with the line indicating the median.

3.4.2 Brown carbon in the two-dimensional volatility basis set

Figure 3-3a shows the water-soluble absorption fraction remaining at 365 nm and 405 nm in the two-dimensional volatility basis set for the five controlled burns compiled in Figure 3-2. The thermodenuder temperature was converted to log(C_{sat}) using empirical measurements of known compounds.[31] The uncertainty in the conversion is ± 2 units of log(C_{sat}), and is shown as purple (365 nm) and blue (405 nm) shading. The derivatives of the fitted absorptions are shown in Figure 3-3b. The O:C ratios determined from the AMS data are shown on the y-axis of Figure 3-3c. Each bin in the volatility basis set is separated by one order of magnitude in saturation concentration, where the distribution of gas and particle phases can shift with changes in emissions, dilution, temperature, and chemical transformation. The volatility basis set suggests that organic compounds with log(C_{sat}) < -3.5 exist in the condensed phase as extremely-low-volatility organic compounds (ELVOCs); compounds with -3.5 < log(C_{sat}) < -0.5 exist predominantly in the condensed phase as low-volatility organic compounds (LVOCs); and compounds with -0.5 < log(C_{sat}) < 2.5 exist in both gas and particle phases as SVOCs.[53] We find that most of the water-soluble absorption at 365 nm is due to LVOCs with a minor contribution from ELVOCs, with log(C_{sat}) = -5.1 to 0.4 and O:C ratios of 0.0–1.1. However, even at a thermodenuder temperature of 250 °C, not all the absorption was completely removed. Approximately 6% of the water-soluble organic aerosol absorption has log(C_{sat}) < -9 with O:C ratios greater than 1.2±0.3. Figure 3-3 also shows linear carbon chains with MW 250 and 500 g mol^{-1} and varying hydroxyl-group substitutions, following the theoretical parameterizations in Donahue et al., as an example that would be consistent with our volatility, O:C, and MW measurements.[30]

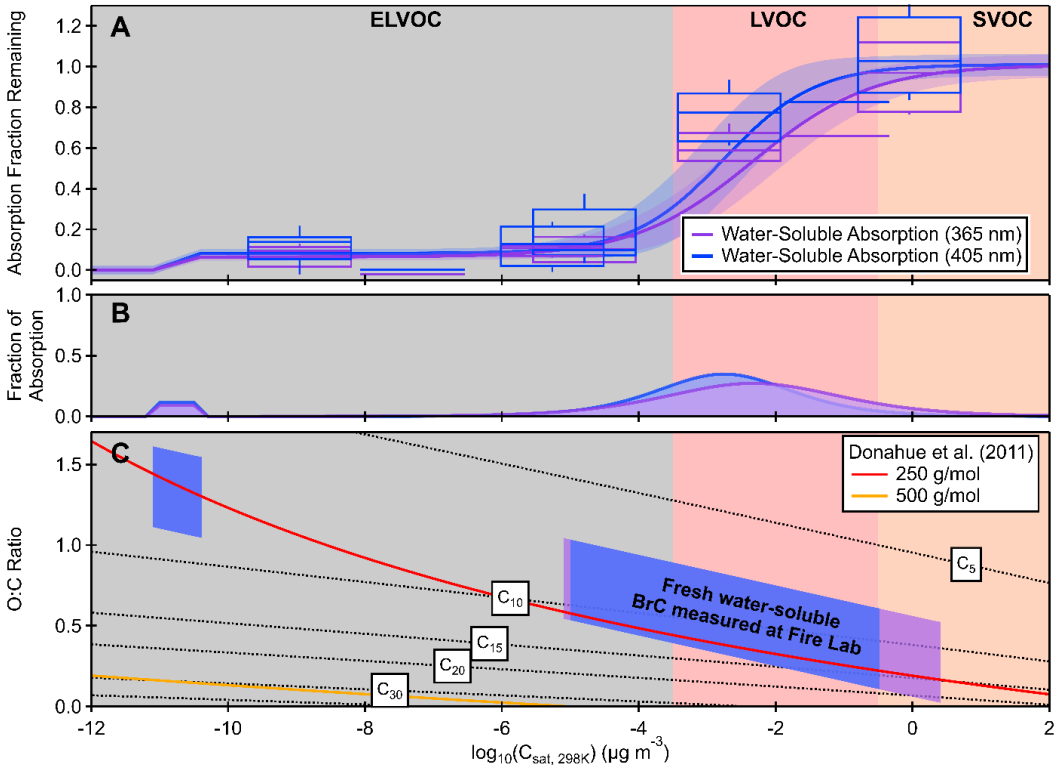

Figure 3-3. (A) Water-soluble absorption fraction remaining at 365 and 405 nm as a function of log($C_{sat,298K}$). ELVOC, LVOC, and SVOC regimes are shown as shaded areas. (B) Derivative of water-soluble absorption fraction at 365 and 405 nm, showing the distribution of compounds as a function of log($C_{sat,298K}$). Some water-soluble absorption was not removed at 250 °C, and therefore has an unknown log($C_{sat,298K}$) value less than –9.0. (C) Two-dimensional volatility basis set as described in Donahue et al.[53] The shaded areas show water-soluble BrC compounds that absorb at 365 and 405 nm with O:C values measured by the AMS. The orange and red lines represent the volatility and O:C ratios for linear organic molecules with hydroxyl-group substitutions, calculated following the parameterization in Donahue et al.[30]

3.4.3 Brown carbon molecular weight analysis

The SEC-UV analysis provides information on the molecular properties of BrC chromophores by measuring absorption as a function of MW. The contribution of high (> 500 Da), low (< 500 Da), and unidentified MW chromophores varies with wavelength. Figure 3-4 displays absorption chromatograms of undenuded and denunded aqueous extracts corresponding to the combustion of manzanita, excelsior, and ponderosa pine at three wavelengths: 250 nm, 300 nm,

and 365 nm. Figure 3-4 highlights the variability in absorption density within the UV range. Chromophores < 500 Da were responsible for the majority of the absorption in the denuded and undenuded aqueous extracts.

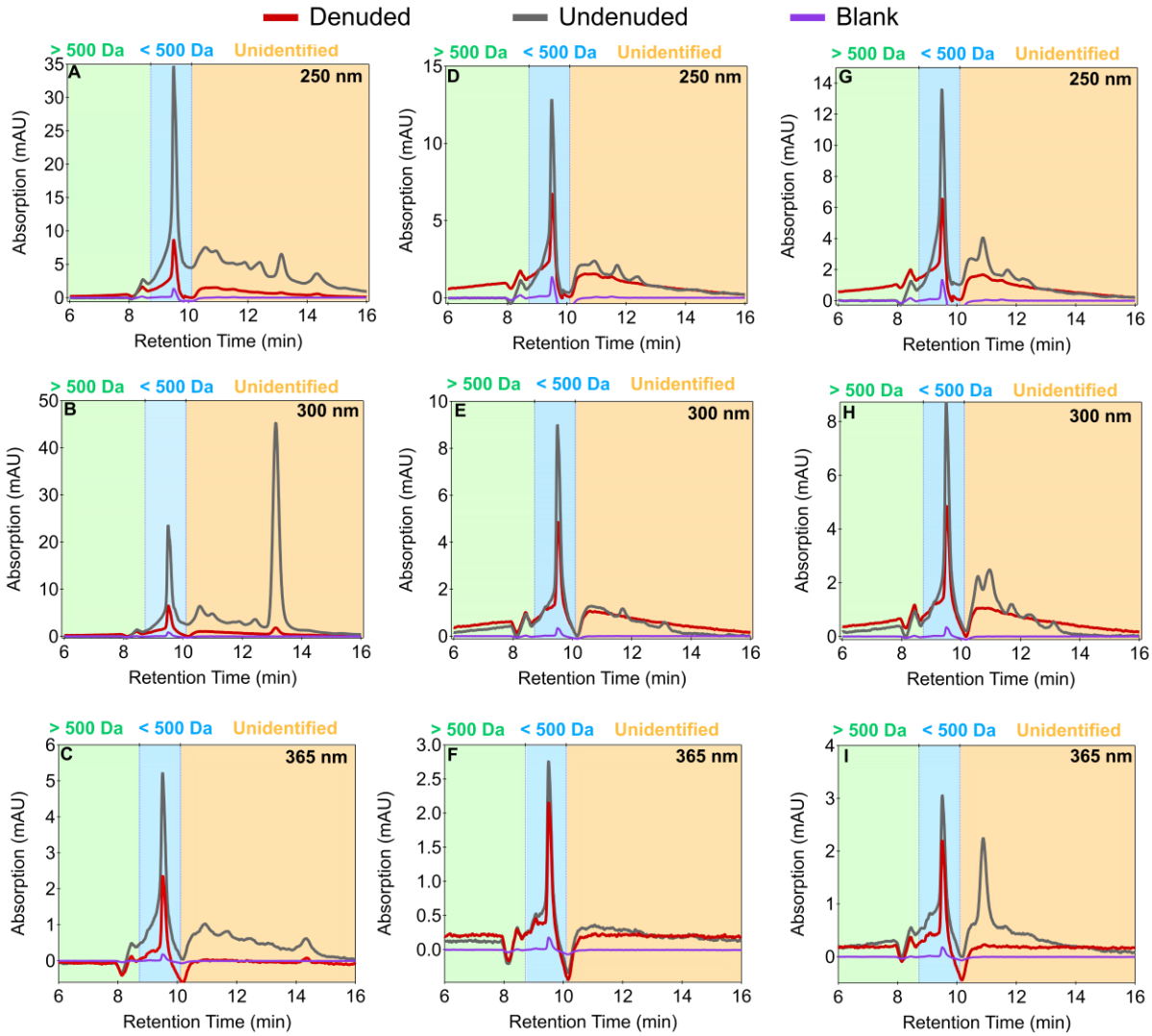

Figure 3-4. Absorption density plots measured by SEC-UV at 250 nm, 300 nm, and 365 nm from aqueous extracts of filters collected during denuded (250 °C) and undenuded (25 °C) sampling. The fuel types are: (a,b,c) manzanita (d,e,f) excelsior and (g,h,i) ponderosa pine.

Although the online and offline absorption measurements are both broadband, for simplicity we present comparisons at the commonly reported wavelength of 365 nm. The SEC-UV contribution to total absorption by the three MW classes at 365 nm is displayed in Figure 3-5.

For undenuded samples, the average contribution to total absorption by MW species > 500 Da was 6.2 ± 3.7 % and species < 500 Da contributed an average of 82 ± 13 %. In the denuded samples, MW species >500 Da contributed to 15 ± 12 % to total absorption and the average contribution of < 500 Da was 84 ± 16 %. Absorption past the exclusion volume represents an unidentified MW.[54–56,50] The average contribution to total measured absorption by the unidentified MW species was 12 ± 14 % and 1 ± 5 % for the undenuded and denuded samples, respectively. Our analysis shows that BrC in fresh biomass burning aerosol includes high MW ELVOCs (~ 6 %), which has been observed previously for both fresh and aged biomass burning aerosol generated in controlled burns.[24,57] Figure 3-5a displays the absorption ratio of denuded to undenuded absorption measured by SEC-UV. For the majority of the controlled burns, thermal denuding decreased the absorption signal by approximately 50%, similar to what is shown in Figure 3-2 for the total absorption. The low MW species are more volatile, and the removal of these species can be attributed to the decrease in absorption signal. In both the undenuded and denuded samples, the low MW species contributed the most to the total absorption signal. When comparing the contribution of high and low MW species between the denuded and undenuded sample pairs, the fraction of absorption by low MW species decreased and the contribution of high MW species increased as a result of thermal denuding due to their lower volatility. Differences exist between the undenuded and denuded MW absorption profiles. These observations demonstrate that fresh emissions from FIREX FireLab 2016 controlled burns are mainly composed of low MW species volatilized from thermal denuding at 250 °C.

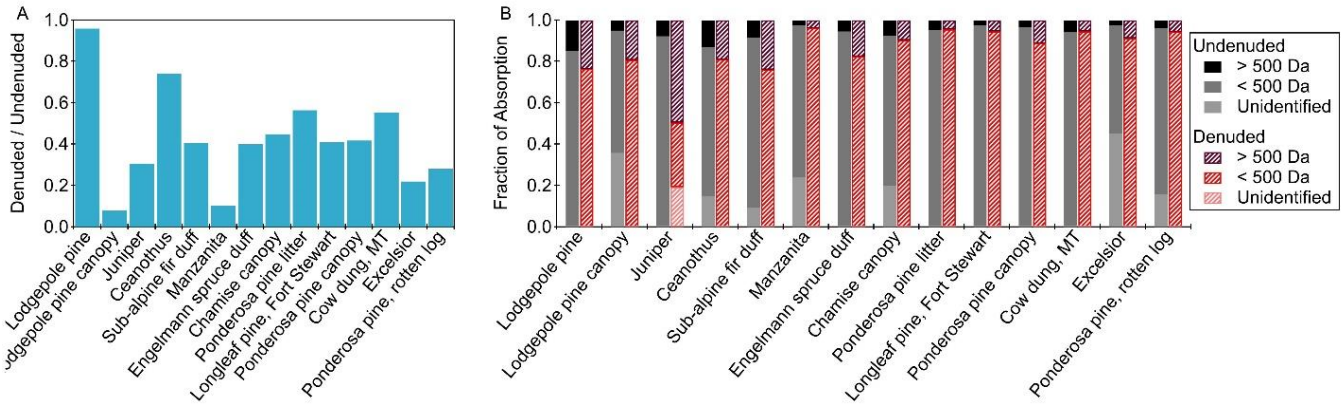

Figure 3-5. Absorption at 365 nm of aqueous extracts by SEC-UV analysis of the (A) denuded to undenuded ratio (B) absorption contribution of high (> 500 Da), low (< 500 Da), and unidentified MW species of each controlled burn of a specific fuel type.

3.4.4 Brown carbon octanol-water partitioning coefficient from HPLC-UV analysis

Reverse phase HPLC can be used to separate BrC species based on molecular polarity and further characterize the chemical properties and structures. It has been successful in identifying a variety of possible BrC chromophore structures.[22,58] Figure 3-6 shows reverse-phase HPLC-UV separation of BrC species for denuded and undenuded samples in which more polar compounds elute prior to relatively less polar compounds. Elution began at approximately 12 mins where the mobile phase composition was 40% organic phase and 60% aqueous phase and the last peak eluted at 22 mins, where the mobile phase composition was 95% organic phase and 5% aqueous phase. The integrated absorption by the undenuded samples was approximately 83% greater than the denuded samples, which was similar to the results from the SEC-UV analysis. A comparison of the integrated absorption signal from the HPLC-UV and SEC-UV is linear, with slope 0.99 ± 0.05 and $r^2 = 0.97$ (Figure B5). The agreement indicates that the two separation methods sampled the entire absorbing aerosol population. Reverse phase chromatography can be used to determine an octanol-water partitioning coefficient, $K_{ow,}$[51,52,33,59,60] which is often used to infer the fate of organic compounds in the environment. To our knowledge, K_{ow} of BrC mixtures has not previously been

measured. The greater the value of K_{ow}, the greater the tendency to partition into a medium with appreciable organic composition. Compounds with higher K_{ow} values have a greater affinity to the stationary phase of a reverse phase column and will elute later compared to compounds with lower K_{ow} values. We applied a series of isocratic analyses of standard solutions with known log(K_{ow}) values between 1.16–4.1, with the analysis shown in Figures B-3 and B-4. The peaks in Figure 3-6 eluted between 12 and 22 mins, which corresponds to log(K_{ow}) values between 2.9 ± 0.7 to 3.5 ± 0.7. Figure 3-6 also illustrates that thermal denuding was generally effective at removing compounds across this K_{ow} range, reflected by the absence or reduced signal of resolved peaks in the denuded compared to the undenuded samples. We can infer compounds with comparable experimental log(K_{ow}) values have chemical similarities. For instance, oxygenated species like alcohols, ketones, and ethers such as phenetole, benzophenone, 4-propyl phenol, and 4- butyl phenol have log(K_{ow}) values of 2.51, 3.18, 3.2, and 3.65, respectively.[61] This suggests that the peaks observed in Figure 3-6 correspond to compounds that are functionalized with aliphatic, aromatic, hydroxyl, and carbonyl groups.

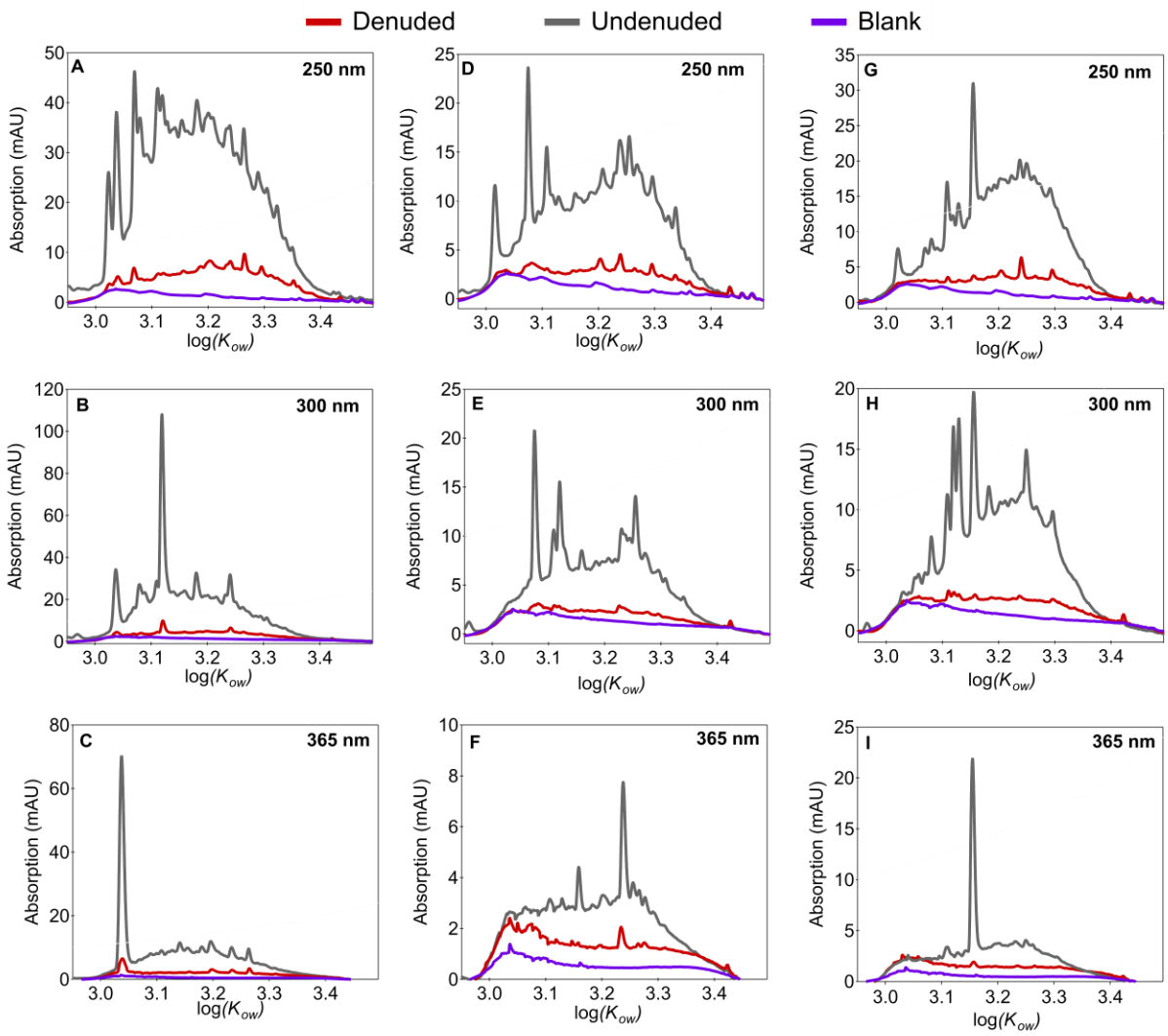

Figure 3-6. HPLC-UV separation at 250, 300, and 365 nm of aqueous extracts from filters collected during denuded and undenuded sampling. The fuel types are: (a,b,c) manzanita (d,e,f) excelsior, and (g,h,i) ponderosa pine.

3.4.5 Summary of brown carbon properties measured in fresh biomass burning smoke

Table 3-1 summarizes the physical and chemical properties that we measured for fresh biomass burning BrC. Overall, we observe that the majority of the water-soluble BrC at 365 nm (~ 92%) has log(C_{sat}) values between –5.1 to 0.4 and can be represented as LVOCs. A small fraction of BrC (approximately 6% at 365 nm) is not removed by heating to 250 °C, and the properties for this fraction are presented separately in Table 3-1. The log(C_{sat}) values for this

fraction are < -9, consistent with ELVOCs. The SEC-UV analysis shows that fresh emissions mainly consist of low MW chromophores, that contribute 82 ± 13% to the total absorption. The absorption at the different wavelengths in Figure 3-4 and Figure 3-6 supports the main findings of the SEC-UV analysis. The relatively greater absorption signal at 250 nm compared to 365 nm corroborates that the SEC-UV analysis measured low MW species because smaller, less conjugated systems typically absorb in the blue wavelength region. These low MW species were volatilized by thermal denuding at 250 °C and the contribution of high MW increased from 6.2 ± 3.7 % to 15 ± 12 % between the undenuded and thermally denuded samples. The HPLC-UV analysis suggests that the resolved peaks correspond to oxygenated and highly conjugated compounds with log(K_{ow}) values ranging from 2.9 ± 0.7 to 3.5 ± 0.7 and below an oxygen to carbon ratio of 0.5.

Table 3-1. Summary of chemical and physical properties for fresh biomass burning smoke during FIREX 2016. All absorption properties are for brown carbon at 365 nm.

	Higher volatility organic aerosol (Bulk undenuded)	**Lower volatility organic aerosol (Persists at >250 °C)**
Fraction of organic aerosol mass	50% removed at 105 °C	20% persists at >250 °C
Fraction of brown carbon (365 nm)	50% removed at 102 °C 92% removed between 30-190 °C	6% persists at > 250 °C
log(C_{sat})	-5.1 – +0.4	< -9
O:C Ratio	0 – 1.1	> 1.2 ± 0.3
Molecular weight < 500 g mol^{-1}	82 ± 13%	84 ± 16%
Molecular weight > 500 g mol^{-1}	6.2 ± 3.7%	15 ± 12%
Molecular weight uncharacterized	12 ± 14%	1 ± 5%
log(k_{OW})	(2.9 ± 0.7) – (3.5 ± 0.7)	(2.9 ± 0.7) – (3.5 ± 0.7)
HPLC-UV chromatograms	Unstructured absorption with resolved peaks	Unstructured absorption

3.4.6 Evaluation of volatility, brown carbon chromophores and structures

For organic aerosol, we measured O:C ratios of 0.1–0.6, 0.5–1.1, and 0.9–1.5 at log(C_{sat}) = 0, -5, and –9, respectively, which represents the relationship between volatility and chemical composition for the fresh smoke emissions. Oxygenated species can be directly emitted or formed upon oxidation in the atmosphere. Primary emissions from biomass burning typically have low oxygen to carbon (O:C) ratios.[62] We expect fresh emissions from the controlled burns to have low O:C ratios compared to smoke that has been aged in the atmosphere. Prior measurements of controlled combustion have reported O:C ratios of 0.1 to 0.5 for unaged smoke,[58,63] while atmospheric measurements have reported O:C ratios of 0.3–0.7 for smoke aged 0–8 hrs[64] and 0.3–0.9 for smoke aged 6–45 hrs.[65] It is important to note that none of these values are specific to BrC but instead represent bulk organic aerosol.

Our work expands upon the findings by Hatch et al. where they focused on the volatility distribution of benzenediols (log(C_{sat}) > 6) and the volatility distribution of compounds emitted during the combustion of the rotten log (log(C_{sat}) > 0) during FIREX FireLab 2016.[27] In this study, we examined water-soluble BrC and found that although the majority of the BrC could be classified as LVOCs with log(C_{sat}) values between –5.1 to 0.4 within the volatility basis set; some ELVOCs BrC persisted after denuding at 250 °C with log(C_{sat}) < -9. Previous studies have investigated the volatility of biomass burning organic aerosol from ground-based and airborne measurements. The ground-based measurements presented in Di Lorenzo et al. suggested low MW fractions oligomerize in the particle during transport forming larger MW species or high MW fractions can persist after 72 hrs of atmospheric transport.[24] These high MW species would contain between 20 to 30 carbons, are highly oxidized, have a log(C_{sat}) less than -8, and classified as ELVOCs.[24] The comparison of the log(C_{sat}) values between the ambient measurements of Di

Lorenzo et al. and our values presented in Figure 3-3 are reasonable, because we expect the primary emissions from the controlled burns in our study to be less oxidized than the ground-based measurements of aged smoke. As a result, we observe greater log(C_{sat})values, indicating the species we measured are more volatile.

Variability in the range of log(C_{sat}) between studies is observed. The extent of gas-particle partitioning of a smoke plume is dependent on biomass burning organic aerosol concentration and the air temperature. A study by Pagonis et al. conducted airborne thermal denuder measurements during FIREX-AQ where the thermal denuder was heated to 40 to 45 °C to simulate evaporation if smoke was transported to lower altitudes.[66] This study observed: log(C_{sat}) = -2 to 5 for smoke aged 0 to 30 hrs where log(C_{sat}) increased with increasing ΔPM/ΔCO.[66] May et al. measured thermally denuded smoke emissions from controlled burns and presented a set of partitioning parameters that represented all the thermal denuder experiments which included both plume and ambient like conditions.[67] Their data spanned an organic aerosol concentration of 1 to 5000 μg m^{-3} and a temperature range of 30 to 120 °C, from which they suggested that log(C_{sat}) = -2 to 4.[67] This range overlaps with our observations of fresh water-soluble BrC (Figure 3-3) with organic aerosol concentration of 1 to 1420 μg m^{-3} . The comparison of our volatility distribution with previous studies highlights the utility and intricacies of applying the two-dimensional volatility basis set. The log(C_{sat}) is an intrinsic property of species emitted from combustion processes; however, variability in the volatility distribution (log(C_{sat}) range) between different studies emphasizes that partitioning parameters derived from different forest fires and controlled burns could be attributed to differing temperatures, emission factors, combustion efficiencies, dilution rates, organic aerosol concentration, and MW of emitted species. For example, as organic aerosol concentration increases, more SVOCs can condense which will shift to lower log(C_{sat}) values

whereas higher temperatures increase evaporation which will shift toward greater log(C_{sat}) values**.** Furthermore, we have found that the AMS collection efficiency for freshly emitted smoke in the laboratory decreases with increasing thermodenuder temperature and after it is oxidized (Figure B-2). These factors impact the propensity for gas-phase species to partition into the particle phase and may explain the differences between the log(C_{sat}) ranges observed between studies.

The SEC-UV results presented here can be compared to earlier studies that applied SEC-UV to laboratory generated smoke and to wildfire measurements. Previous SEC-UV analyses studied the absorption density profiles of unaged BrC from controlled combustion of boreal peat and photolytic aged BrC from controlled wood pyrolysis.[25,56,68] Previous controlled combustion investigations that applied SEC-UV also observed absorption features past the exclusion volume of a SEC column.[50,56] Brown carbon is a complex mixture of hundreds to thousands of compounds[7]; elution past the exclusion volume has been attributed to hydrophobic interactions between the SEC stationary phase and BrC compounds.[50,54–56] To minimize these interactions, the mobile phase consists of ammonium acetate solution and acetonitrile, which is responsible for suppressing electrostatic interactions.[56] Wong et al. pyrolyzed dry hardwood and observed that low MW chromophores dominated total absorption,[68] which is consistent with our FIREX FireLab 2016 observations. Di Lorenzo et al. applied SEC-UV to ambient BrC collected from plumes aged up to 72 hrs and Azzarello et al. applied SEC-UV for aqueous samples that corresponded to 0 to 5 hours.[24,50] Di Lorenzo et al. observed that low MW chromophores contributed more to total absorption than higher MW compounds in the least aged (10 to 15 hrs) biomass-burning derived filter extracts.[24] Similarly, Azzarello et al. also observed total absorption dominated by low MW species of samples collected inflight over western U.S. wildfires.[50] These findings resemble the MW-resolved absorption profile of our FIREX 2016 aqueous extracts, in which unaged emissions

are dominated by low-MW chromophores. Further, various high MW organic compounds in biomass burning organic aerosol have been observed based on different mass spectrometry analyses.[22,69,70] Lee et al. examined aged biomass burning plumes and observed that high MW biomass burning derived organic aerosol can contribute to low volatility BrC species.[71] Our results align with these findings; emissions from FIREX FireLab 2016 are fresh and are therefore comprised of low MW species that can be effectively removed by thermal denuding.

The volatility basis set can serve as a framework to assess the relationship between volatility and chemical properties. Liang et al. reported $\log(C_{sat})$ = -2.5 - 4.5 for smoke sampled from three western U.S wildfires during FIREX-AQ where each saturation bin separated into a mass distribution of speciated compounds.[72] The saturation bins of $\log(C_{sat})$ = < 0.5 was dominated by terpenoids and monoacids.[72] Jen et al. applied two-dimensional gas chromatography and observed IVOCs and SVOCs emitted from the controlled combustions during FIREX FireLab 2016.[28] The classes of compounds included non-cyclic oxygenated aliphatic compounds.[28] This class of compounds have low O:C ratios, are low MW species, and align with $\log(K_{ow})$ values greater than 3 which is consistent with our observations.

Several other studies identified compounds emitted from controlled burns that contribute to BrC absorption using different analytical approaches. Hettiyadura et al. also employed a reverse phase HPLC gradient (highly aqueous to highly organic) to separate BrC compounds derived from the controlled combustion of hardwood.[58] They observed common BrC chromophores such as furan derivatives and methoxyphenols which are common decomposition products of cellulose[73,74] and lignin pyrolysis products[75] respectively.[58] These compounds have 7 to 10 carbon atoms, which is consistent with low MW (<500 Da) species and is consistent with our observations. Fleming et al. also employed a reverse phase HPLC gradient scheme comparable to Hettiyadura et al. to

separate BrC chromophores from controlled pyrolysis of fuels characteristic of the western U.S and observed the elution of compounds up to 10 carbons under similar separation conditions, which included vanillic acid, nitropyrogallol, salicylic acid, veratraldehyde, umbelliferone, nitrocatchol, and hydroxynitroguaiacol.[22,58] Jen et al. identified 149 compounds from various chemical classes containing 3 to 35 carbons and MWs ranging from 92 to 492 g/mol, where only three compounds identified had MW > 500 Da.[28] The observed species measured from previous reverse phase HPLC, and gas chromatography analyses identified that the majority of compounds that comprise fresh smoke have MW < 500 Da, which is consistent with our observations.

Fleming et al. applied HPLC-UV coupled to a high-resolution mass spectrometer to elucidate chemical structures of compounds emitted from controlled burns during FIREX FireLab 2016. They presented compounds that are < 300 Da, conjugated, and have O:C ratios ranging from 0.2 to 0.8.[22] To further discern if the compounds listed in Fleming et al. align with the chemical properties denoted in our study, we applied a structure-activity relationship to estimate the log(K_{ow}) of several compounds (Table B-5); the log(K_{ow}) values ranged from 0.98 to 2.79.[22,34] This is within the lower range of log(K_{ow}) values we determined through HPLC-UV analysis. The compounds kaempferol and diosmetin were listed by Fleming et al., which both have an O:C ratio of 0.4 and estimated log(K_{ow}) values of 2.79 and 2.12, respectively; our analysis suggests that the less hydrophobic chromophores we detected using SEC-UV and HLPC-UV are most closely related to compounds as such. We suspect that the remaining compounds we observed were larger or had less polar functional groups to potentially explain the greater log(K_{ow}) values we determined.

3.5 Implications

Understanding the transformation that BrC species can undergo in the atmosphere requires an understanding of the chemical properties of directly emitted compounds. The log(K_{ow})

compliments the SEC-UV and two-dimensional volatility basis set by offering additional insight into partitioning and atmospheric fate of BrC species measured during the controlled combustions. From the SEC-UV analysis, we learned that low MW chromophores dominated total absorption, and the volatility distribution indicated that the majority of BrC is classified as LVOCs. These findings may appear counter-intuitive because low-volatility species are typically associated with high MW, yet our results identified low MW and LVOCs. However, these findings are not contradictory, rather the SEC-UV and two-dimensional volatility basis set capture different aspects of BrC composition. For instance, LVOCs can include both low and high MW species – some oxygenated species that can be classified as both LVOC and low MW include nitroaromatics and dicarboxylic acids which are small in size but have low volatility due to their functionalization. We know that various other parameters also influence the volatility distribution (e.g. organic aerosol concentration and temperature); therefore, we applied log(K_{ow}) analysis to further support the atmospheric fate suggested by the two-dimensional volatility basis set. Our results indicate a log(K_{ow}) range of 2.9 to 3.5 which suggests that BrC species are moderately hydrophobic and will therefore have the ability to partition into the organic phase of aerosol. Compounds within this log(K_{ow}) range have the potential to persist in the atmosphere, where they can undergo oxidation processes making them more water-soluble over time. Therefore, the log(K_{ow}) analysis corroborates with the findings of the two-dimensional volatility basis set. Overall, our findings demonstrate that the log(K_{ow}) is a useful parameter in addition to the volatility basis set to contextualize the chemical properties of the compounds within volatility regimes.

3. 6 References

(1) Williams, A. P.; Abatzoglou, J. T. Recent Advances and Remaining Uncertainties in Resolving Past and Future Climate Effects on Global Fire Activity. *Current Climate Change Reports* **2016**, *2* (1), 1–14. https://doi.org/10.1007/s40641-016-0031-0.

(2) Dennison, P. E.; Brewer, S. C.; Arnold, J. D.; Moritz, M. A. Large Wildfire Trends in the Western United States, 1984–2011. *Geophysical Research Letters* **2014**, *41* (8), 2928–2933. https://doi.org/10.1002/2014GL059576.

(3) Westerling, A. L. Increasing Western US Forest Wildfire Activity: Sensitivity to Changes in the Timing of Spring. *Philosophical Transactions of the Royal Society B: Biological Sciences* **2016**, *371* (1696), 20150178. https://doi.org/10.1098/rstb.2015.0178.

(4) Andreae, M. O. Emission of Trace Gases and Aerosols from Biomass Burning – an Updated Assessment. *Atmospheric Chemistry and Physics* **2019**, *19* (13), 8523–8546. https://doi.org/10.5194/acp-19-8523-2019.

(5) Bond, T. C.; Doherty, S. J.; Fahey, D. W.; Forster, P. M.; Berntsen, T.; DeAngelo, B. J.; Flanner, M. G.; Ghan, S.; Kärcher, B.; Koch, D.; Kinne, S.; Kondo, Y.; Quinn, P. K.; Sarofim, M. C.; Schultz, M. G.; Schulz, M.; Venkataraman, C.; Zhang, H.; Zhang, S.; Bellouin, N.; Guttikunda, S. K.; Hopke, P. K.; Jacobson, M. Z.; Kaiser, J. W.; Klimont, Z.; Lohmann, U.; Schwarz, J. P.; Shindell, D.; Storelvmo, T.; Warren, S. G.; Zender, C. S. Bounding the Role of Black Carbon in the Climate System: A Scientific Assessment. *Journal of Geophysical Research: Atmospheres* **2013**, *118* (11), 5380–5552. https://doi.org/10.1002/jgrd.50171.

(6) Brown, H.; Liu, X.; Pokhrel, R.; Murphy, S.; Lu, Z.; Saleh, R.; Mielonen, T.; Kokkola, H.; Bergman, T.; Myhre, G.; Skeie, R. B.; Watson-Paris, D.; Stier, P.; Johnson, B.; Bellouin, N.; Schulz, M.; Vakkari, V.; Beukes, J. P.; van Zyl, P. G.; Liu, S.; Chand, D. Biomass Burning Aerosols in Most Climate Models Are Too Absorbing. *Nature Communications* **2021**, *12* (1), 277. https://doi.org/10.1038/s41467-020-20482-9.

(7) Laskin, A.; Laskin, J.; Nizkorodov, S. A. Chemistry of Atmospheric Brown Carbon. *Chemical Reviews* **2015**, *115* (10), 4335–4382. https://doi.org/10.1021/cr5006167.

(8) Saleh, R. From Measurements to Models: Toward Accurate Representation of Brown Carbon in Climate Calculations. *Current Pollution Reports* **2020**, *6* (2), 90–104. https://doi.org/10.1007/s40726-020-00139-3.

(9) Wang, X.; Heald, C. L.; Liu, J.; Weber, R. J.; Campuzano-Jost, P.; Jimenez, J. L.; Schwarz, J. P.; Perring, A. E. Exploring the Observational Constraints on the Simulation of Brown Carbon. *Atmospheric Chemistry and Physics* **2018**, *18* (2), 635–653. https://doi.org/10.5194/acp-18-635-2018.

(10) Zhang, A.; Wang, Y.; Zhang, Y.; Weber, R. J.; Song, Y.; Ke, Z.; Zou, Y. Modeling the Global Radiative Effect of Brown Carbon: A Potentially Larger Heating Source in the Tropical Free

Troposphere than Black Carbon. *Atmospheric Chemistry and Physics* **2020**, *20* (4), 1901–1920. https://doi.org/10.5194/acp-20-1901-2020.

(11) Feng, Y.; Ramanathan, V.; Kotamarthi, V. R. Brown Carbon: A Significant Atmospheric Absorber of Solar Radiation? *Atmospheric Chemistry and Physics* **2013**, *13* (17), 8607–8621. https://doi.org/10.5194/acp-13-8607-2013.

(12) Zeng, L.; Zhang, A.; Wang, Y.; Wagner, N. L.; Katich, J. M.; Schwarz, J. P.; Schill, G. P.; Brock, C.; Froyd, K. D.; Murphy, D. M.; Williamson, C. J.; Kupc, A.; Scheuer, E.; Dibb, J.; Weber, R. J. Global Measurements of Brown Carbon and Estimated Direct Radiative Effects. *Geophys Res Lett* **2020**, *47* (13), e2020GL088747. https://doi.org/10.1029/2020GL088747.

(13) Zhang, Y.; Forrister, H.; Liu, J.; Dibb, J.; Anderson, B.; Schwarz, J. P.; Perring, A. E.; Jimenez, J. L.; Campuzano-Jost, P.; Wang, Y.; Nenes, A.; Weber, R. J. Top-of-Atmosphere Radiative Forcing Affected by Brown Carbon in the Upper Troposphere. *Nature Geoscience* **2017**, *10* (7), 486–489. https://doi.org/10.1038/ngeo2960.

(14) Hodshire, A. L.; Ramnarine, E.; Akherati, A.; Alvarado, M. L.; Farmer, D. K.; Jathar, S. H.; Kreidenweis, S. M.; Lonsdale, C. R.; Onasch, T. B.; Springston, S. R.; Wang, J.; Wang, Y.; Kleinman, L. I.; Sedlacek III, A. J.; Pierce, J. R. Dilution Impacts on Smoke Aging: Evidence in Biomass Burning Observation Project (BBOP) Data. *Atmospheric Chemistry and Physics* **2021**, *21* (9), 6839–6855. https://doi.org/10.5194/acp-21-6839-2021.

(15) Browne, E. C.; Zhang, X.; Franklin, J. P.; Ridley, K. J.; Kirchstetter, T. W.; Wilson, K. R.; Cappa, C. D.; Kroll, J. H. Effect of Heterogeneous Oxidative Aging on Light Absorption by Biomass Burning Organic Aerosol. *Aerosol Science and Technology* **2019**, *53* (6), 663–674. https://doi.org/10.1080/02786826.2019.1599321.

(16) Li, C.; He, Q.; Hettiyadura, A. P. S.; Käfer, U.; Shmul, G.; Meidan, D.; Zimmermann, R.; Brown, S. S.; George, C.; Laskin, A.; Rudich, Y. Formation of Secondary Brown Carbon in Biomass Burning Aerosol Proxies through NO(3) Radical Reactions. *Environ Sci Technol* **2020**, *54* (3), 1395–1405. https://doi.org/10.1021/acs.est.9b05641.

(17) Schnitzler, E. G.; Liu, T.; Hems, R. F.; Abbatt, J. P. D. Emerging Investigator Series: Heterogeneous OH Oxidation of Primary Brown Carbon Aerosol: Effects of Relative Humidity and Volatility. *Environ Sci Process Impacts* **2020**, *22* (11), 2162–2171. https://doi.org/10.1039/d0em00311e.

(18) Schnitzler, E. G.; Gerrebos, N. G. A.; Carter, T. S.; Huang, Y.; Heald, C. L.; Bertram, A. K.; Abbatt, J. P. D. Rate of Atmospheric Brown Carbon Whitening Governed by Environmental Conditions. *Proc Natl Acad Sci U S A* **2022**, *119* (38), e2205610119. https://doi.org/10.1073/pnas.2205610119.

(19) Washenfelder, R. A.; Azzarello, L.; Ball, K.; Brown, S. S.; Decker, Z. C. J.; Franchin, A.; Fredrickson, C. D.; Hayden, K.; Holmes, C. D.; Middlebrook, A. M.; Palm, B. B.; Pierce, R. B.; Price, D. J.; Roberts, J. M.; Robinson, M. A.; Thornton, J. A.; Womack, C. C.; Young, C.

J. Complexity in the Evolution, Composition, and Spectroscopy of Brown Carbon in Aircraft Measurements of Wildfire Plumes. *Geophysical Research Letters* **2022**, *49* (9), e2022GL098951. https://doi.org/10.1029/2022GL098951.

(20) Zeng, L.; Sullivan, A. P.; Washenfelder, R. A.; Dibb, J.; Scheuer, E.; Campos, T. L.; Katich, J. M.; Levin, E.; Robinson, M. A.; Weber, R. J. Assessment of Online Water-Soluble Brown Carbon Measuring Systems for Aircraft Sampling. *Atmospheric Measurement Techniques* **2021**, *14* (10), 6357–6378. https://doi.org/10.5194/amt-14-6357-2021.

(21) Hems, R. F.; Schnitzler, E. G.; Liu-Kang, C.; Cappa, C. D.; Abbatt, J. P. D. Aging of Atmospheric Brown Carbon Aerosol. *ACS Earth and Space Chemistry* **2021**, *5* (4), 722–748. https://doi.org/10.1021/acsearthspacechem.0c00346.

(22) Fleming, L. T.; Lin, P.; Roberts, J. M.; Selimovic, V.; Yokelson, R.; Laskin, J.; Laskin, A.; Nizkorodov, S. A. Molecular Composition and Photochemical Lifetimes of Brown Carbon Chromophores in Biomass Burning Organic Aerosol. *Atmospheric Chemistry and Physics* **2020**, *20* (2), 1105–1129. https://doi.org/10.5194/acp-20-1105-2020.

(23) Di Lorenzo, R. A.; Young, C. J. Size Separation Method for Absorption Characterization in Brown Carbon: Application to an Aged Biomass Burning Sample. *Geophysical Research Letters* **2016**, *43* (1), 458–465. https://doi.org/10.1002/2015GL066954.

(24) Di Lorenzo, R. A.; Washenfelder, R. A.; Attwood, A. R.; Guo, H.; Xu, L.; Ng, N. L.; Weber, R. J.; Baumann, K.; Edgerton, E.; Young, C. J. Molecular-Size-Separated Brown Carbon Absorption for Biomass-Burning Aerosol at Multiple Field Sites. *Environmental Science and Technology* **2017**, *51* (6), 3128–3137. https://doi.org/10.1021/acs.est.6b06160.

(25) Wong, J. P. S.; Tsagkaraki, M.; Tsiodra, I.; Mihalopoulos, N.; Violaki, K.; Kanakidou, M.; Sciare, J.; Nenes, A.; Weber, R. J. Atmospheric Evolution of Molecular-Weight-Separated Brown Carbon from Biomass Burning. *Atmospheric Chemistry and Physics* **2019**, *19* (11), 7319–7334. https://doi.org/10.5194/acp-19-7319-2019.

(26) Hatch, L. E.; Luo, W.; Pankow, J. F.; Yokelson, R. J.; Stockwell, C. E.; Barsanti, K. C. Identification and Quantification of Gaseous Organic Compounds Emitted from Biomass Burning Using Two-Dimensional Gas Chromatography–Time-of-Flight Mass Spectrometry. *Atmospheric Chemistry and Physics* **2015**, *15* (4), 1865–1899. https://doi.org/10.5194/acp-15-1865-2015.

(27) Hatch, L. E.; Rivas-Ubach, A.; Jen, C. N.; Lipton, M.; Goldstein, A. H.; Barsanti, K. C. Measurements of I/SVOCs in Biomass-Burning Smoke Using Solid-Phase Extraction Disks and Two-Dimensional Gas Chromatography. *Atmospheric Chemistry and Physics* **2018**, *18* (24), 17801–17817. https://doi.org/10.5194/acp-18-17801-2018.

(28) Jen, C. N.; Hatch, L. E.; Selimovic, V.; Yokelson, R. J.; Weber, R.; Fernandez, A. E.; Kreisberg, N. M.; Barsanti, K. C.; Goldstein, A. H. Speciated and Total Emission Factors of Particulate Organics from Burning Western US Wildland Fuels and Their Dependence on

Combustion Efficiency. *Atmospheric Chemistry and Physics* **2019**, *19* (2), 1013–1026. https://doi.org/10.5194/acp-19-1013-2019.

(29) Donahue, N. M.; Robinson, A. L.; Stanier, C. O.; Pandis, S. N. Coupled Partitioning, Dilution, and Chemical Aging of Semivolatile Organics. *Environ. Sci. Technol.* **2006**, *40* (8), 2635–2643. https://doi.org/10.1021/es052297c.

(30) Donahue, N. M.; Epstein, S. A.; Pandis, S. N.; Robinson, A. L. A Two-Dimensional Volatility Basis Set: 1. Organic-Aerosol Mixing Thermodynamics. *Atmospheric Chemistry and Physics* **2011**, *11* (7), 3303–3318. https://doi.org/10.5194/acp-11-3303-2011.

(31) Faulhaber, A. E.; Thomas, B. M.; Jimenez, J. L.; Jayne, J. T.; Worsnop, D. R.; Ziemann, P. J. Characterization of a Thermodenuder-Particle Beam Mass Spectrometer System for the Study of Organic Aerosol Volatility and Composition. *Atmospheric Measurement Techniques* **2009**, *2* (1), 15–31. https://doi.org/10.5194/amt-2-15-2009.

(32) Cappa, C. D. A Model of Aerosol Evaporation Kinetics in a Thermodenuder. *Atmospheric Measurement Techniques* **2010**, *3* (3), 579–592. https://doi.org/10.5194/amt-3-579-2010.

(33) Hayward, S. J.; Lei, Y. D.; Wania, F. Comparative Evaluation of Three High-Performance Liquid Chromatography–Based Kow Estimation Methods for Highly Hydrophobic Organic Compounds: Polybrominated Diphenyl Ethers and Hexabromocyclododecane. *Environmental Toxicology and Chemistry* **2006**, *25* (8), 2018–2027. https://doi.org/10.1897/05-675R.1.

(34) Hansch, C.; Leo, A. Substituent Constants for Correlation Analysis in Chemistry and Biology; Wiley: New York, 1979; p 1–339.

(35) McMeeking, G. R.; Kreidenweis, S. M.; Baker, S.; Carrico, C. M.; Chow, J. C.; Collett Jr., J. L.; Hao, W. M.; Holden, A. S.; Kirchstetter, T. W.; Malm, W. C.; Moosmüller, H.; Sullivan, A. P.; Wold, C. E. Emissions of Trace Gases and Aerosols during the Open Combustion of Biomass in the Laboratory. *Journal of Geophysical Research: Atmospheres* **2009**, *114* (D19), 1–20. https://doi.org/10.1029/2009JD011836.

(36) Selimovic, V.; Yokelson, R. J.; Warneke, C.; Roberts, J. M.; de Gouw, J.; Reardon, J.; Griffith, D. W. T. Aerosol Optical Properties and Trace Gas Emissions by PAX and OP-FTIR for Laboratory-Simulated Western US Wildfires during FIREX. *Atmospheric Chemistry and Physics* **2018**, *18* (4), 2929–2948. https://doi.org/10.5194/acp-18-2929-2018.

(37) Womack, C. C.; Manfred, K. M.; Wagner, N. L.; Adler, G.; Franchin, A.; Lamb, K. D.; Middlebrook, A. M.; Schwarz, J. P.; Brock, C. A.; Brown, S. S.; Washenfelder, R. A. Complex Refractive Indices in the Ultraviolet and Visible Spectral Region for Highly Absorbing Non-Spherical Biomass Burning Aerosol. *Atmospheric Chemistry and Physics* **2021**, *21* (9), 7235–7252. https://doi.org/10.5194/acp-21-7235-2021.

(38) Manfred, K. M.; Washenfelder, R. A.; Wagner, N. L.; Adler, G.; Erdesz, F.; Womack, C. C.; Lamb, K. D.; Schwarz, J. P.; Franchin, A.; Selimovic, V.; Yokelson, R. J.; Murphy, D. M. Investigating Biomass Burning Aerosol Morphology Using a Laser Imaging Nephelometer. *Atmospheric Chemistry and Physics* **2018**, *18* (3), 1879–1894. https://doi.org/10.5194/acp-18-1879-2018.

(39) Gabriela Adler, R. J. Y., Nicholas L. Wagner, Kara D. Lamb, Katherine M. Manfred, Joshua P. Schwarz, Alessandro Franchin, Ann M. Middlebrook, Rebecca A. Washenfelder, Caroline C. Womack; Murphy, D. M. Evidence in Biomass Burning Smoke for a Light-Absorbing Aerosol with Properties Intermediate between Brown and Black Carbon. *Aerosol Science and Technology* **2019**, *53* (9), 976–989. https://doi.org/10.1080/02786826.2019.1617832.

(40) Huffman, J. A.; Ziemann, P. J.; Jayne, J. T.; Worsnop, D. R.; Jimenez, J. L. Development and Characterization of a Fast-Stepping/Scanning Thermodenuder for Chemically-Resolved Aerosol Volatility Measurements. *Aerosol Science and Technology* **2008**, *42* (5), 395–407. https://doi.org/10.1080/02786820802104981.

(41) Karnezi, E.; Riipinen, I.; Pandis, S. N. Measuring the Atmospheric Organic Aerosol Volatility Distribution: A Theoretical Analysis. *Atmospheric Measurement Techniques* **2014**, *7* (9), 2953–2965. https://doi.org/10.5194/amt-7-2953-2014.

(42) Langridge, J. M.; Richardson, M. S.; Lack, D.; Law, D.; Murphy, D. M. Aircraft Instrument for Comprehensive Characterization of Aerosol Optical Properties, Part I: Wavelength-Dependent Optical Extinction and Its Relative Humidity Dependence Measured Using Cavity Ringdown Spectroscopy. *Aerosol Science and Technology* **2011**, *45* (11), 1305–1318. https://doi.org/10.1080/02786826.2011.592745.

(43) Lack, D. A.; Richardson, M. S.; Law, D.; Langridge, J. M.; Cappa, C. D.; McLaughlin, R. J.; Murphy, D. M. Aircraft Instrument for Comprehensive Characterization of Aerosol Optical Properties, Part 2: Black and Brown Carbon Absorption and Absorption Enhancement Measured with Photo Acoustic Spectroscopy. *Aerosol Science and Technology* **2012**, *46* (5), 555–568. https://doi.org/10.1080/02786826.2011.645955.

(44) Mason, B.; Wagner, N. L.; Adler, G.; Andrews, E.; Brock, C. A.; Gordon, T. D.; Lack, D. A.; Perring, A. E.; Richardson, M. S.; Schwarz, J. P.; Shook, M. A.; Thornhill, K. L.; Ziemba, L. D.; Murphy, D. M. An Intercomparison of Aerosol Absorption Measurements Conducted during the SEAC4RS Campaign. *Aerosol Science and Technology* **2018**, *52* (9), 1012–1027. https://doi.org/10.1080/02786826.2018.1500012.

(45) Bahreini, R.; Ervens, B.; Middlebrook, A. M.; Warneke, C.; de Gouw, J. A.; DeCarlo, P. F.; Jimenez, J. L.; Brock, C. A.; Neuman, J. A.; Ryerson, T. B.; Stark, H.; Atlas, E.; Brioude, J.; Fried, A.; Holloway, J. S.; Peischl, J.; Richter, D.; Walega, J.; Weibring, P.; Wollny, A. G.; Fehsenfeld, F. C. Organic Aerosol Formation in Urban and Industrial Plumes near Houston and Dallas, Texas. *Journal of Geophysical Research: Atmospheres* **2009**, *114* (D7), 1–17. https://doi.org/10.1029/2008JD011493.

(46) Liao, J.; Brock, C. A.; Murphy, D. M.; Sueper, D. T.; Welti, A.; Middlebrook, A. M. Single-Particle Measurements of Bouncing Particles and in Situ Collection Efficiency from an Airborne Aerosol Mass Spectrometer (AMS) with Light-Scattering Detection. *Atmospheric Measurement Techniques* **2017**, *10* (10), 3801–3820. https://doi.org/10.5194/amt-10-3801-2017.

(47) Canagaratna, M. R.; Jimenez, J. L.; Kroll, J. H.; Chen, Q.; Kessler, S. H.; Massoli, P.; Hildebrandt Ruiz, L.; Fortner, E.; Williams, L. R.; Wilson, K. R.; Surratt, J. D.; Donahue, N. M.; Jayne, J. T.; Worsnop, D. R. Elemental Ratio Measurements of Organic Compounds Using Aerosol Mass Spectrometry: Characterization, Improved Calibration, and Implications. *Atmospheric Chemistry and Physics* **2015**, *15* (1), 253–272. https://doi.org/10.5194/acp-15-253-2015.

(48) Xu, W.; Lambe, A.; Silva, P.; Hu, W.; Onasch, T.; Williams, L.; Croteau, P.; Zhang, X.; Renbaum-Wolff, L.; Fortner, E.; Jimenez, J. L.; Jayne, J.; Worsnop, D.; Canagaratna, M. Laboratory Evaluation of Species-Dependent Relative Ionization Efficiencies in the Aerodyne Aerosol Mass Spectrometer. *Aerosol Science and Technology* **2018**, *52* (6), 626–641. https://doi.org/10.1080/02786826.2018.1439570.

(49) Bond, T. C.; Bergstrom, R. W. Light Absorption by Carbonaceous Particles: An Investigative Review. *Aerosol Science and Technology* **2006**, *40* (1), 27–67. https://doi.org/10.1080/02786820500421521.

(50) Azzarello, L.; Washenfelder, R. A.; Robinson, M. A.; Franchin, A.; Womack, C. C.; Holmes, C. D.; Brown, S. S.; Middlebrook, A.; Newberger, T.; Sweeney, C.; Young, C. J. Characterization of Water-Soluble Brown Carbon Chromophores from Wildfire Plumes in the Western USA Using Size-Exclusion Chromatography. *Atmospheric Chemistry and Physics* **2023**, *23* (24), 15643–15654. https://doi.org/10.5194/acp-23-15643-2023.

(51) Kaune, A.; Knorrenschild, M.; Kettrup, A. Predicting 1-Octanol-Water Partition Coefficient by High-Performance Liquid Chromatography Gradient Elution. *Fresenius' Journal of Analytical Chemistry* **1995**, *352* (3), 303–312. https://doi.org/10.1007/BF00322226.

(52) Han, S.; Liang, C.; Qiao, J.; Lian, H.; Ge, X.; Chen, H. A Novel Evaluation Method for Extrapolated Retention Factor in Determination of N-Octanol/Water Partition Coefficient of Halogenated Organic Pollutants by Reversed-Phase High Performance Liquid Chromatography. *Analytica Chimica Acta* **2012**, *713*, 130–135. https://doi.org/10.1016/j.aca.2011.11.020.

(53) Donahue, N. M.; Kroll, J. H.; Pandis, S. N.; Robinson, A. L. A Two-Dimensional Volatility Basis Set – Part 2: Diagnostics of Organic-Aerosol Evolution. *Atmospheric Chemistry and Physics* **2012**, *12* (2), 615–634. https://doi.org/10.5194/acp-12-615-2012.

(54) Specht, C. H.; Frimmel, F. H. Specific Interactions of Organic Substances in Size-Exclusion Chromatography. *Environ. Sci. Technol.* **2000**, *34* (11), 2361–2366. https://doi.org/10.1021/es991034d.

(55) Hong, P.; Koza, S.; Bouvier, E. S. P. A Review Size-exclusion Chromatography for the Analysis of Protein Biotherapeutics and their Aggregates. *Journal of Liquid Chromatography & Related Technologies* **2012**, *35* (20), 2923–2950. https://doi.org/10.1080/10826076.2012.743724.

(56) Lyu, M.; Thompson, D. K.; Zhang, N.; Cuss, C. W.; Young, C. J.; Styler, S. A. Unraveling the Complexity of Atmospheric Brown Carbon Produced by Smoldering Boreal Peat Using Size-Exclusion Chromatography with Selective Mobile Phases. *Environ. Sci.: Atmos.* **2021**, *1* (5), 241–252. https://doi.org/10.1039/D1EA00011J.

(57) Saleh, R.; Robinson, E. S.; Tkacik, D. S.; Ahern, A. T.; Liu, S.; Aiken, A. C.; Sullivan, R. C.; Presto, A. A.; Dubey, M. K.; Yokelson, R. J.; Donahue, N. M.; Robinson, A. L. Brownness of Organics in Aerosols from Biomass Burning Linked to Their Black Carbon Content. *Nature Geoscience* **2014**, *7* (9), 647–650. https://doi.org/10.1038/ngeo2220.

(58) Hettiyadura, A. P. S.; Garcia, V.; Li, C.; West, C. P.; Tomlin, J.; He, Q.; Rudich, Y.; Laskin, A. Chemical Composition and Molecular-Specific Optical Properties of Atmospheric Brown Carbon Associated with Biomass Burning. *Environ Sci Technol* **2021**, *55* (4), 2511–2521. https://doi.org/10.1021/acs.est.0c05883.

(59) Sahu, S. K.; Pandit, G. G. Estimation of Octanol-Water Partition Coefficients for Polycylic Aromatic Hydrocarbons Using Reverse-Phase HPLC. *Journal of Liquid Chromatography & Related Technologies* **2003**, *26* (1), 135–146. https://doi.org/10.1081/JLC-120017158.

(60) Liang, C.; Qiao, J.; Lian, H. Determination of Reversed-Phase High Performance Liquid Chromatography Based Octanol-Water Partition Coefficients for Neutral and Ionizable Compounds: Methodology Evaluation. *Journal of Chromatography A* **2017**, *1528*, 25–34. https://doi.org/10.1016/j.chroma.2017.10.064.

(61) Mackay, D.; Shiu, W.-Y.; Lee, S. C. *Handbook of Physical-Chemical Properties and Environmental Fate for Organic Chemicals*; CRC Press, 2006; Second Edition p 2348 - 2999.

(62) Palm, B. B.; Peng, Q.; Fredrickson, C. D.; Lee, B. H.; Garofalo, L. A.; Pothier, M. A.; Kreidenweis, S. M.; Farmer, D. K.; Pokhrel, R. P.; Shen, Y.; Murphy, S. M.; Permar, W.; Hu, L.; Campos, T. L.; Hall, S. R.; Ullmann, K.; Zhang, X.; Flocke, F.; Fischer, E. V.; Thornton, J. A. Quantification of Organic Aerosol and Brown Carbon Evolution in Fresh Wildfire Plumes. *Proceedings of the National Academy of Sciences* **2020**, *117* (47), 29469–29477. https://doi.org/10.1073/pnas.2012218117.

(63) Cheng, Z.; Atwi, K. M.; Yu, Z.; Avery, A.; Fortner, E. C.; Williams, L.; Majluf, F.; Krechmer, J. E.; Lambe, A. T.; Saleh, R. Evolution of the Light-Absorption Properties of Combustion Brown Carbon Aerosols Following Reaction with Nitrate Radicals. *Aerosol Science and Technology* **2020**, *54* (7), 849–863. https://doi.org/10.1080/02786826.2020.1726867.

(64) June, N. A.; Hodshire, A. L.; Wiggins, E. B.; Winstead, E. L.; Robinson, C. E.; Thornhill, K. L.; Sanchez, K. J.; Moore, R. H.; Pagonis, D.; Guo, H.; Campuzano-Jost, P.; Jimenez, J. L.;

Coggon, M. M.; Dean-Day, J. M.; Bui, T. P.; Peischl, J.; Yokelson, R. J.; Alvarado, M. J.; Kreidenweis, S. M.; Jathar, S. H.; Pierce, J. R. Aerosol Size Distribution Changes in FIREX-AQ Biomass Burning Plumes: The Impact of Plume Concentration on Coagulation and OA Condensation/Evaporation. *Atmospheric Chemistry and Physics* **2022**, *22* (19), 12803–12825. https://doi.org/10.5194/acp-22-12803-2022.

(65) Collier, S.; Zhou, S.; Onasch, T. B.; Jaffe, D. A.; Kleinman, L.; Sedlacek, A. J. I.; Briggs, N. L.; Hee, J.; Fortner, E.; Shilling, J. E.; Worsnop, D.; Yokelson, R. J.; Parworth, C.; Ge, X.; Xu, J.; Butterfield, Z.; Chand, D.; Dubey, M. K.; Pekour, M. S.; Springston, S.; Zhang, Q. Regional Influence of Aerosol Emissions from Wildfires Driven by Combustion Efficiency: Insights from the BBOP Campaign. *Environmental Science & Technology* **2016**, *50* (16), 8613–8622. https://doi.org/10.1021/acs.est.6b01617.

(66) Pagonis, D.; Selimovic, V.; Campuzano-Jost, P.; Guo, H.; Day, D. A.; Schueneman, M. K.; Nault, B. A.; Coggon, M. M.; DiGangi, J. P.; Diskin, G. S.; Fortner, E. C.; Gargulinski, E. M.; Gkatzelis, G. I.; Hair, J. W.; Herndon, S. C.; Holmes, C. D.; Katich, J. M.; Nowak, J. B.; Perring, A. E.; Saide, P.; Shingler, T. J.; Soja, A. J.; Thapa, L. H.; Warneke, C.; Wiggins, E. B.; Wisthaler, A.; Yacovitch, T. I.; Yokelson, R. J.; Jimenez, J. L. Impact of Biomass Burning Organic Aerosol Volatility on Smoke Concentrations Downwind of Fires. *Environ. Sci. Technol.* **2023**, *57* (44), 17011–17021. https://doi.org/10.1021/acs.est.3c05017.

(67) May, A. A.; Levin, E. J. T.; Hennigan, C. J.; Riipinen, I.; Lee, T.; Collett Jr., J. L.; Jimenez, J. L.; Kreidenweis, S. M.; Robinson, A. L. Gas-Particle Partitioning of Primary Organic Aerosol Emissions: 3. Biomass Burning. *Journal of Geophysical Research: Atmospheres* **2013**, *118* (19), 11,327-11,338. https://doi.org/10.1002/jgrd.50828.

(68) Wong, J. P. S.; Nenes, A.; Weber, R. J. Changes in Light Absorptivity of Molecular Weight Separated Brown Carbon Due to Photolytic Aging. *Environmental Science & Technology* **2017**, *51* (15), 8414–8421. https://doi.org/10.1021/acs.est.7b01739.

(69) Elias, V. O.; Simoneit, B. R. T.; Pereira, A. S.; Cabral, J. A.; Cardoso, J. N. Detection of High Molecular Weight Organic Tracers in Vegetation Smoke Samples by High-Temperature Gas Chromatography−Mass Spectrometry. *Environ. Sci. Technol.* **1999**, *33* (14), 2369–2376. https://doi.org/10.1021/es980706h.

(70) Smith, J. S.; Laskin, A.; Laskin, J. Molecular Characterization of Biomass Burning Aerosols Using High-Resolution Mass Spectrometry. *Anal. Chem.* **2009**, *81* (4), 1512–1521. https://doi.org/10.1021/ac8020664.

(71) Lee, A. K. Y.; Willis, M. D.; Healy, R. M.; Wang, J. M.; Jeong, C.-H.; Wenger, J. C.; Evans, G. J.; Abbatt, J. P. D. Single-Particle Characterization of Biomass Burning Organic Aerosol (BBOA): Evidence for Non-Uniform Mixing of High Molecular Weight Organics and Potassium. *Atmospheric Chemistry and Physics* **2016**, *16* (9), 5561–5572. https://doi.org/10.5194/acp-16-5561-2016.

(72) Liang, Y.; Stamatis, C.; Fortner, E. C.; Wernis, R. A.; Van Rooy, P.; Majluf, F.; Yacovitch, T. I.; Daube, C.; Herndon, S. C.; Kreisberg, N. M.; Barsanti, K. C.; Goldstein, A. H. Emissions of Organic Compounds from Western US Wildfires and Their Near-Fire Transformations. *Atmospheric Chemistry and Physics* **2022**, *22* (15), 9877–9893. https://doi.org/10.5194/acp-22-9877-2022.

(73) Emsley, A. M.; Stevens, G. C. Kinetics and Mechanisms of the Low-Temperature Degradation of Cellulose. *Cellulose* **1994**, *1* (1), 26–56. https://doi.org/10.1007/BF00818797.

(74) Wang, Z.; Bi, X.; Sheng, G.; Fu, J. Characterization of Organic Compounds and Molecular Tracers from Biomass Burning Smoke in South China I: Broad-Leaf Trees and Shrubs. *Atmospheric Environment* **2009**, *43* (19), 3096–3102. https://doi.org/10.1016/j.atmosenv.2009.03.012.

(75) Kumagai, S.; Matsuno, R.; Grause, G.; Kameda, T.; Yoshioka, T. Enhancement of Bio-Oil Production via Pyrolysis of Wood Biomass by Pretreatment with H2SO4. *Bioresource Technology* **2015**, *178*, 76–82. https://doi.org/10.1016/j.biortech.2014.09.146.

Appendix B: Supporting Information for Chapter 3

B.1 UV/Visible spectroscopy of water-soluble brown carbon

The BrC-PILS instrument has been presented previously and is described in detail by Zeng et al. and Washenfelder et al.[1,21,2] The differences in the spectrometer and sampling parameters during the FIREX 2016 study are described below. A gas sample flow of 12.0 slpm was drawn into a Particle-Into-Liquid Sampler (PILS 4001; Brechtel Manufacturing Inc., Hayward, CA, USA) which collected water-soluble aerosol into solution. The average liquid output flow was 1.5 mL min^{-1}, and insoluble aerosol components were removed using a filter (Puradisc 25 TF; GE Healthcare Life Sciences, Pittsburgh, PA, USA). The liquid flow continued through a 2.5 m liquid waveguide capillary cell (LWCC; World Precision Instrument, Sarasota, FL) and Total Organic Carbon analyzer (M9 Portable TOC Analyzer; GE 3 Analytical Instruments Inc., Boulder, CO, USA).

The liquid waveguide capillary cell was coupled to a deuterium/halogen light source (DH-mini; Ocean Optics Inc., Dunedin, FL, USA) and grating spectrometer (InSpectrum 150; Princeton Instruments, Acton, MA, USA) to measure absorption spectra. The spectrometer contained a 300 g/mm grating with 300 nm blaze rotated to give a spectral range of 300–600 nm and a 16-bit back-illuminated 250×1024 pixel CCD array detector cooled to −20 °C. Spectra were acquired with an integration time of 1.0 s and no additional averaging. Dark spectra were acquired with the spectrometer shutter closed. Soluble aerosol absorption in units of Mm^{-1} was calculated from Beer's Law as described in Zeng et al.[1]

During the Fire Lab experiments, BrC-PILS zeros were acquired by filtering the air sample for 4:20 min at 45−60 min intervals. The PILS collection efficiency was quantified by comparison to an optical particle counter and CRD-PAS with sucrose, Suwannee River Fulvic Acid, and

nigrosin aerosol. The Total Organic Carbon analyzer was calibrated using aqueous solutions of potassium hydrogen phthalate.

The accuracy of the BrC-PILS absorption and WSOC measurements were ±16% and ±18% during the FIREX 2016 study. These are determined from the uncertainties in the gas flow, liquid flow, collection efficiency of the PILS, and the calibration of the TOC analyzer. Each of these uncertainties may represent systematic rather than random errors, so they have been summed instead of adding in quadrature. The errors are comparable to those presented in Zeng et al.[1] During the Fire Lab 2016 study, the BrC-PILS instrument included an older spectrometer with slower readout time, which did not achieve the high precision of 0.03 Mm^{-1} (3σ) at 1 sec that was later reported in Zeng et al.[1] The analysis in this work includes averaging of measurements over time periods of 2–5 min and was not affected by the lower precision.

Table B-1. Summary of fuels, offline sample collection, and online thermodenuder experiments included in this work. A full list of the Fire Lab 2016 fuels and fire parameters is included in Selimovic et al.[3]

Fire Num	Date	Fuel	Offline filter samples[1]	Online thermodenuder experiment[2]	Online thermodenuder temperature (deg C)
81	27 Oct 2016	Subalpine fir	No	Yes	25, 250
84	31 Oct 2016	Chaparral (chamise)	Yes	No	
86	1 Nov 2016	Lodgepole Pine	Yes	No	
87	1 Nov 2016	Lodgepole Pine	Yes	No	
88	2 Nov 2016	Juniper	Yes	No	
89	2 Nov 2016	Ceanothus	Yes	No	
90	3 Nov 2016	Subalpine fir	Yes	No	
91	3 Nov 2016	Chaparral (manzanita)	Yes	No	
92	4 Nov 2016	Engelmann spruce	Yes	No	
93	4 Nov 2016	Peat	Yes	No	
94	5 Nov 2016	Chaparral (chamise)	Yes	No	
95	5 Nov 2016	Ponderosa pine	Yes	No	
96	6 Nov 2016	Longleaf pine	Yes	No	
97	6 Nov 2016	Longleaf pine	Yes	No	
98	8 Nov 2016	Ponderosa pine	Yes	No	
99	8 Nov 2016	Dung	Yes	No	
100	9 Nov 2016	Excelsior	Yes	No	
101	9 Nov 2016	Ponderosa pine	Yes	No	
102	10 Nov 2016	Engelmann spruce	No	Yes	25, 100, 150, 200, 250
103	10 Nov 2016	Dung	No	Yes	25, 75, 90, 125, 150, 250, 260
105	11 Nov 2016	Ponderosa pine	No	Yes	25, 60,100, 140
106	12 Nov 2016	Ponderosa pine	No	Yes	25, 60, 100, 140

[1]Indicates collection of a paired set of undenuded (25 °C) and denuded (250 °C) filters.
[2]Indicates measurements with varying thermodenuder temperatures sampled by the BrC-PILS, AMS, and CRD-PAS.

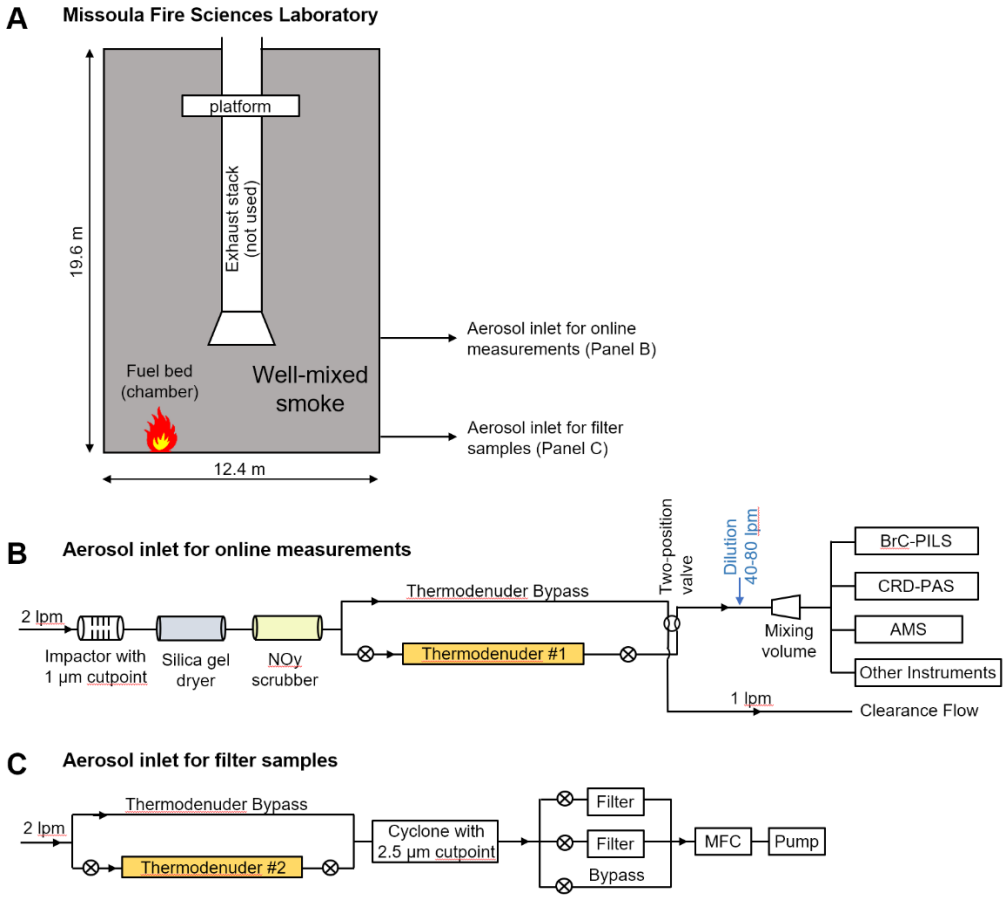

Figure B-1. (a) Diagram of the burn chamber at the Missoula Fire Sciences Laboratory; (b) Schematic of the inlet for online aerosol measurements; (c) Schematic of the inlet for offline filter samples.

Table B-2. Aerosol measurements from the Fire Sciences Laboratory 2016 study used in this analysis.

Online Measurement	**Technique**	**Wavelength (nm)**	**Reference**
Water-soluble aerosol absorption	PILS coupled to liquid waveguide capillary cell	300-600 nm	Zeng et al. (2021);[1] Washenfelder et al. (2022)[1]
Total aerosol absorption	Photoacoustic spectroscopy	401, 532, and 661 nm	Lack et al. (2012)[4]
Water-soluble organic aerosol concentration	PILS coupled to total organic carbon analyzer	N/A	Zeng et al. (2021);[4] Washenfelder et al. (2022)[4]
Total organic aerosol concentration	Compact time-of-flight aerosol mass spectrometer	N/A	Liao et al. (2017)[4]
Offline Measurement	**Technique**	**Wavelength (nm)**	**Reference**
Aerosol absorption of molecules separated by MW	Size exclusion chromatography coupled to diode array detector	190-800 nm	Di Lorenzo et al. (2017);[4] Lyu et al. (2021);[4] Azzarello et al. (2023)[4]
Aerosol absorption of molecules separated by polarity (*kow*)	High performance liquid chromatography coupled to diode array detector	190-800 nm	Fleming et al. (2020)[4]

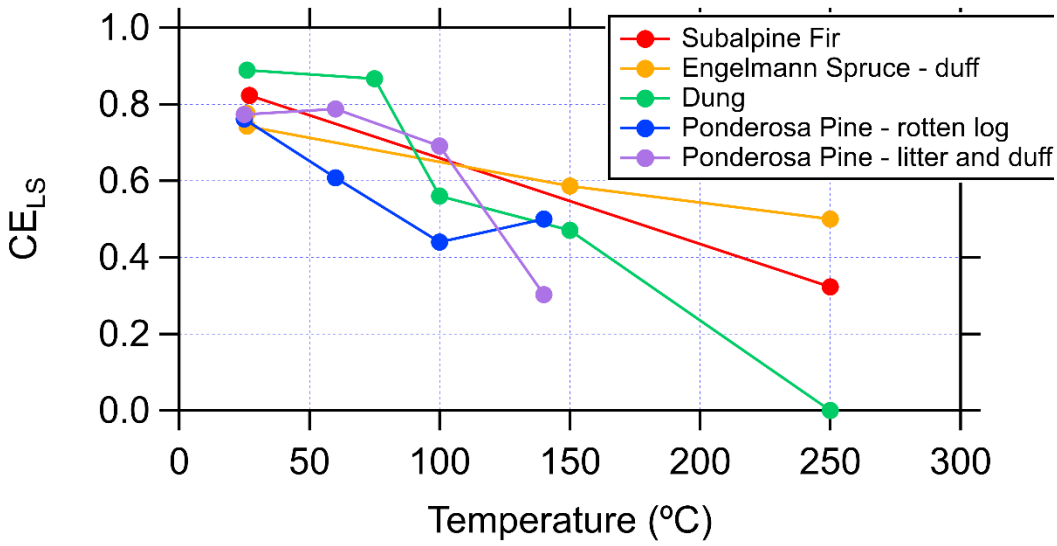

Figure B-2. AMS collection efficiency measured by light scattering as a function of temperature for the experiments shown in Figure 3-2.

B.2 Size exclusion chromatography elution profile

The offline filter samples were analyzed using SEC-UV to measure absorption as function of molecular size. Analysis by SEC-UV allows us to examine the molecular size of BrC chromophores as a function of retention time. As the mobile phase carries the sample through the porous stationary phase of a SEC column, high MW molecules that exceed the size of the pores will flow directly through the column, passing the pores. This will result in an early elution time within the void volume. If absorbing species are small enough to penetrate the pores, they will spend more time in the column and elute later. All molecules that are smaller than the limit to fully penetrate the pores of the stationary phase will elute in the exclusion volume.

B.3 Reverse-phase high performance liquid chromatography (HPLC-UV) to determine log(K_{ow})

The octanol-water partitioning coefficient describes a physical property of compounds. Specifically, it provides insight into the hydrophobicity and/or hydrophilicity or a molecule, with greater log(K_{ow}) values corresponding to molecules with greater partitioning into a medium of

appreciable organic composition. An estimate of log(K_{ow}) values can be achieved by using the linear regression analysis between K_{ow} values of standard compounds and the retention factor k'. The HPLC-UV analysis employed a gradient elution scheme. As a result, to estimate the K_{ow} that correspond to the peaks, multiple isocratic separations were performed. The capacity factor of compounds eluting from the reverse-phase column is determined by[10]:

$$k' = (t_r - t_0) / t_0$$

where t_r is the retention time of the compound and t_0 is the retention time of a compound that is not retained on the column's stationary phase; thiourea was the compound used. The relationship between k' and log(K_{ow}) is linear and defined by:

$$\log(K_{ow}) = \log k' \, m + b$$

Reverse-phase liquid chromatography takes advantage of the fact that compounds with high K_{ow} values elute later off the column than compounds with lower K_{ow} values.[11] To predict log(K_{ow}) from k', various isocratic separations need to be performed. This procedure includes isocratic separations with mobile phase compositions that reflect the composition of the gradient scheme where compounds were eluting off the column. The linear gradient scheme consisted of (A) 0.1% acetic acid in water and (B) acetonitrile. Peaks were observed at compositions between 12 to 22 minutes which corresponds to compositions that varied between 40 to 90% organic phase. Therefore, the following isocratic separations are appropriate to run:

A (DIW 0.1% Acetic Acid)	B (ACN)
65%	35%
50%	50%
35%	65%
20%	80%

Standards of known K_{ow} values were run for each isocratic separation and k' values were determined for each compound. A plot of k' versus percentage of organic solvent was used to determine the k' of the peaks from the gradient separation. The retention time for thiourea was similar for the isocratic runs; therefore, to convert elution retention time to $\log(K_{ow})$, we can determine k' for each time point between 10 to 22 mins. Using the linear regression from $\log(K_{ow})$ versus $\log(k')$, we substitute the $\log(k')$ values to determine $\log(K_{ow})$ at each retention time point. This calculation is performed for each isocratic run and an average of $\log(K_{ow})$ is determined.

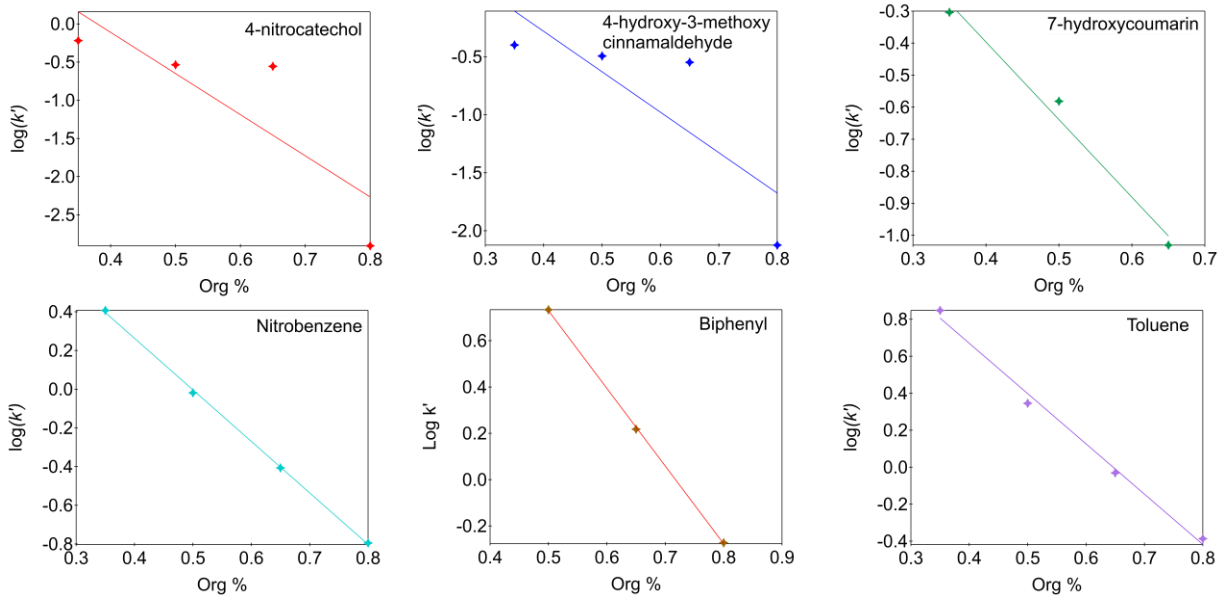

Figure B-3. Plots of logarithm capacity factors, k' as a function of organic modifier percentage for each reference standard.

Table B-3. $\log(K_{ow})$ of reference compounds

Standard	**$\log(K_{ow})$**	**$\log(K_{ow})$ Source**
4-Hydroxy-3-methoxycinnaldehyde	1.16	KOWWIN v1.67 estimate[12]
7-Hydroxycoumarin	1.58	WSKOW v1.41 estimate[13]
4-Nitrocatechol	1.66	Hansch et al. (1995)[14]
Nitrobenzene	1.85	Lei et al. (2008)[15]
Toluene	2.73	Hansch et al. (1995)[14]
Biphenyl	4.01	Hansch et al. (1995)[14]

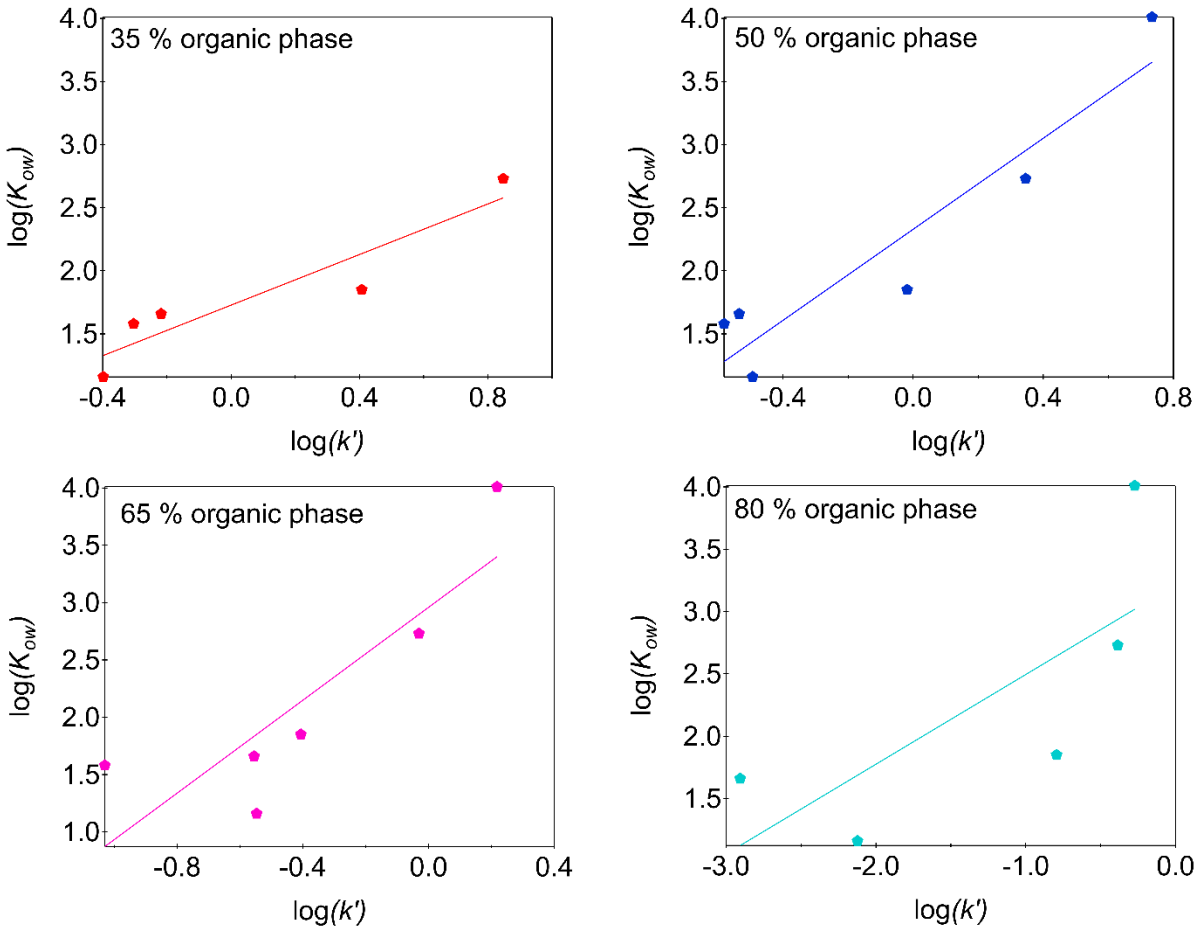

Figure B-4. Relationship between log*(K_{ow})* and log*(k′)* for each isocratic analysis.

Table B-4. Linear regression of log*(K_{ow}) versus* log(*k′*)

Linear Fit	Organic composition (%)	R^2
$\log(K_{ow}) = (1.02 \pm 0.23) \times \log(k') + (1.73 \pm 0.11)$	35	0.87
$\log(K_{ow}) = (1.80 \pm 0.33) \times \log(k') + (2.33 \pm 0.17)$	50	0.88
$\log(K_{ow}) = (2.02 \pm 0.62) \times \log(k') + (2.96 \pm 0.35)$	65	0.73
$\log(K_{ow}) = (0.72 \pm 0.37) \times \log(k') + (3.22 \pm 0.62)$	80	0.56

Table B-5. Compounds emitted from controlled burns during FIREX 2016 measured by Fleming et al. (2020).[9] Literature log*(K_{ow})* values are estimates retrieved from KOWWIN v1.67 and calculated log*(K_{ow})* values were determined with reference to Hansch and Leo (1979).[16]

Compound	MW (g/mol)	Literature log*(K_{ow})*	Calculated log*(K_{ow})*	Structure	O:C
Coniferaldehyde ($C_{10}H_{10}O_3$)	178.18	1.16	2.17	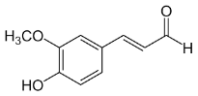	0.3
Nodakenetin ($C_{14}H_{14}O_4$)	246.26	1.85	2.31	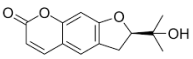	0.3
Sinapaldehyde ($C_{11}H_{12}O_4$)	208.21	0.99	2.38	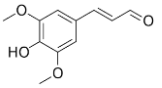	0.4
Veratraldehyde ($C_9H_8O_3$)	166.18	2.39	2.3	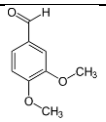	0.3
5-Nitropyrogallol ($C_6H_5NO_5$)	171.11	1.37	0.31	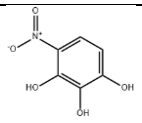	0.8
Kaempferol ($C_{15}H_{10}O_6$)	286.23	1.96	2.79	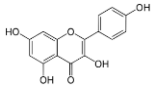	0.4
Umbelliferone ($C_9H_6O_3$)	162.14	1.58	1.99	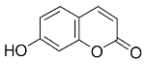	0.3
Hydroxynitroguaiacol ($C_7H_7NO_4$)	169.13	1.24	1.4	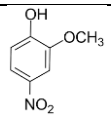	0.7
Nitrocatechol ($C_6H_5NO_4$)	155.11	1.43	0.98	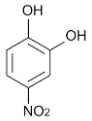	0.7
Salicylic acid ($C_7H_6O_3$)	138.12	2.24	1.19	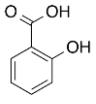	0.4
Diosmetin ($C_{16}H_{12}O_6$)	300.26	2.6 - 3.1	2.12	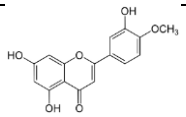	0.4

Vanillic acid($C_8H_8O_4$)	168.14	1.43	1.4	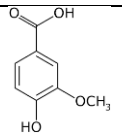	0.2

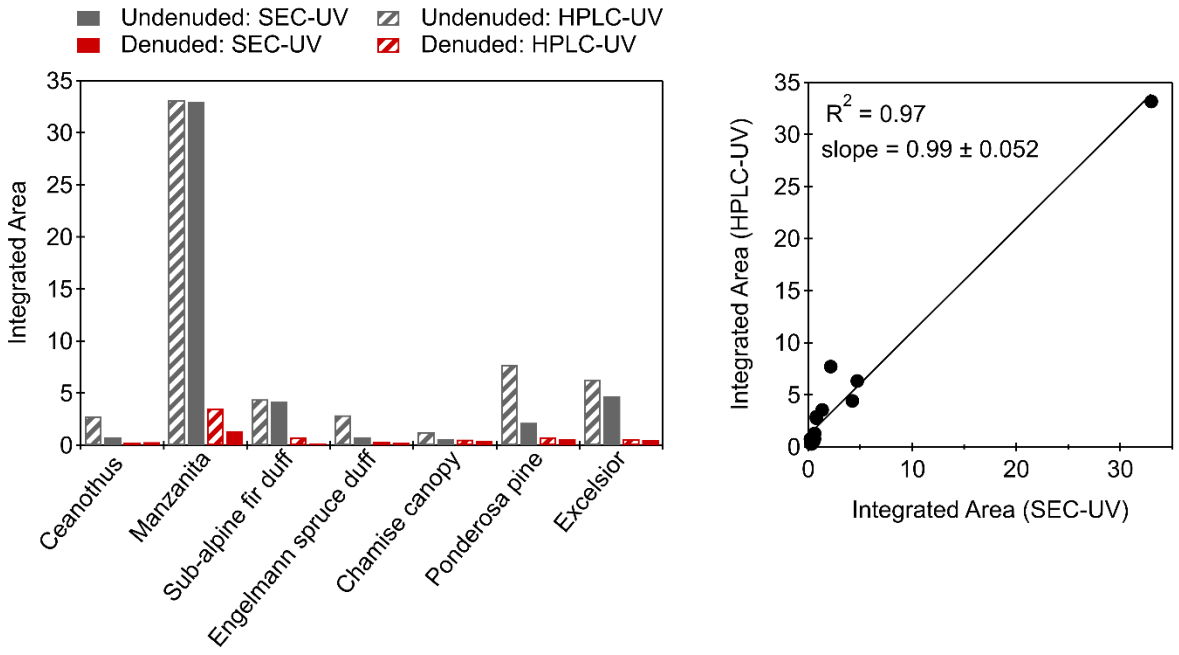

Figure B-5. The correlation between absorption signal measured by SEC-UV and HPLC-UV.

Table B-6. Previous studies that determined the log(C_{sat}) ranges for their biomass burning emissions from controlled burns, simulated organic aerosol, or field measurements.

Study that applied the VBS	**Source of measurements**	**log(C_{sat}) range**
This study	Controlled combustion	-5.1 to 0.4
Pagonis et al. 2023	Field measurements	-2 to 5
May et al. 2013	Controlled combustion	-2 to 4
Shingler et al. 2016	Field measurements	-6 to 3
Theodoritsi et al. 2021	Simulation of biomass burning organic aerosol	-2 to 6
Hatch et al. 2018	Controlled combustion	0 to 7
Liang et al. 2022	Field measurements	-2.5 to 4.5

B.4 Categorizing the fuels into woody, duff, and canopy to asses molecular weight classes contribution to total absorption.

Table B-7 categorizes the fuels into three groups: woody fuels (lodgepole pine, juniper, ceanothus, manzanita, longleaf pine, and excelsior), duff fuels (subalpine fir duff and Engelmann spruce) and canopy fuels (chamise canopy, ponderosa pine canopy, and lodgepole pine canopy). Across all fuel categories for undenuded sampling, high MW species accounted for approximately 6 % of total absorption while low MW species dominated absorption, contributing to between 63 to 91 % depending on the fuel type. For the thermally-denuded samples, low MW species also dominated absorption by contributing 80 to 84 % whereas high MW species showed a slight increase in contribution, ranging from 15 to 17% to total absorption.

Table B-7. Contribution of high, low, and unidentified MW species to total absorption for undenuded and denuded sampling across the three categories of fuel.

	Woody (lignin rich)	Duff (oxygenated organics)	Canopy (waxy compounds; long chain hydrocarbons)
Undenuded High MW	6% ± 5%	6% ± 2%	6% ± 1%
Undenuded Low MW	80% ± 15%	91% ± 7%	63% ± 8%
Undenuded Unidentified MW	14% ± 17%	3% ± 5%	31% ± 9%
Denuded High MW	17% ± 16%	15% ± 9%	16% ± 5%
Denuded Low MW	80% ± 23%	85% ± 9%	84% ± 5%
Denuded Unidentified MW	3% ± 7%	0% ± 0%	0% ± 0%

B. References

(1) Zeng, L.; Sullivan, A. P.; Washenfelder, R. A.; Dibb, J.; Scheuer, E.; Campos, T. L.; Katich, J. M.; Levin, E.; Robinson, M. A.; Weber, R. J. Assessment of Online Water-Soluble Brown Carbon Measuring Systems for Aircraft Sampling. Atmospheric Measurement Techniques 2021, 14 (10), 6357–6378. https://doi.org/10.5194/amt-14-6357-2021.

(2) Washenfelder, R. A.; Azzarello, L.; Ball, K.; Brown, S. S.; Decker, Z. C. J.; Franchin, A.; Fredrickson, C. D.; Hayden, K.; Holmes, C. D.; Middlebrook, A. M.; Palm, B. B.; Pierce, R. B.; Price, D. J.; Roberts, J. M.; Robinson, M. A.; Thornton, J. A.; Womack, C. C.; Young, C. J. Complexity in the Evolution, Composition, and Spectroscopy of Brown Carbon in Aircraft Measurements of Wildfire Plumes. Geophysical Research Letters 2022, 49 (9), e2022GL098951. https://doi.org/10.1029/2022GL098951.

(3) Selimovic, V.; Yokelson, R. J.; Warneke, C.; Roberts, J. M.; de Gouw, J.; Reardon, J.; Griffith, D. W. T. Aerosol Optical Properties and Trace Gas Emissions by PAX and OP-FTIR for Laboratory-Simulated Western US Wildfires during FIREX. Atmospheric Chemistry and Physics 2018, 18 (4), 2929–2948. https://doi.org/10.5194/acp-18-2929-2018.

(4) Lack, D. A.; Richardson, M. S.; Law, D.; Langridge, J. M.; Cappa, C. D.; McLaughlin, R. J.; Murphy, D. M. Aircraft Instrument for Comprehensive Characterization of Aerosol Optical Properties, Part 2: Black and Brown Carbon Absorption and Absorption Enhancement Measured with Photo Acoustic Spectroscopy. Aerosol Science and Technology 2012, 46 (5), 555–568. https://doi.org/10.1080/02786826.2011.645955.

(5) Liao, J.; Brock, C. A.; Murphy, D. M.; Sueper, D. T.; Welti, A.; Middlebrook, A. M. Single-Particle Measurements of Bouncing Particles and in Situ Collection Efficiency from an Airborne Aerosol Mass Spectrometer (AMS) with Light-Scattering Detection. Atmospheric Measurement Techniques 2017, 10 (10), 3801–3820. https://doi.org/10.5194/amt-10-3801-2017.

(6) Di Lorenzo, R. A.; Washenfelder, R. A.; Attwood, A. R.; Guo, H.; Xu, L.; Ng, N. L.; Weber, R. J.; Baumann, K.; Edgerton, E.; Young, C. J. Molecular-Size-Separated Brown Carbon Absorption for Biomass-Burning Aerosol at Multiple Field Sites. Environmental Science and Technology 2017, 51 (6), 3128–3137. https://doi.org/10.1021/acs.est.6b06160.

(7) Lyu, M.; Thompson, D. K.; Zhang, N.; Cuss, C. W.; Young, C. J.; Styler, S. A. Unraveling the Complexity of Atmospheric Brown Carbon Produced by Smoldering Boreal Peat Using Size-Exclusion Chromatography with Selective Mobile Phases. Environ. Sci.: Atmos. 2021, 1 (5), 241–252. https://doi.org/10.1039/D1EA00011J.

(8) Azzarello, L.; Washenfelder, R. A.; Robinson, M. A.; Franchin, A.; Womack, C. C.; Holmes, C. D.; Brown, S. S.; Middlebrook, A.; Newberger, T.; Sweeney, C.; Young, C. J. Characterization of Water-Soluble Brown Carbon Chromophores from Wildfire Plumes in the Western USA Using Size-Exclusion Chromatography. Atmospheric Chemistry and Physics 2023, 23 (24), 15643–15654. https://doi.org/10.5194/acp-23-15643-2023.

(9) Fleming, L. T.; Lin, P.; Roberts, J. M.; Selimovic, V.; Yokelson, R.; Laskin, J.; Laskin, A.; Nizkorodov, S. A. Molecular Composition and Photochemical Lifetimes of Brown Carbon Chromophores in Biomass Burning Organic Aerosol. Atmospheric Chemistry and Physics 2020, 20 (2), 1105–1129. https://doi.org/10.5194/acp-20-1105-2020.

(10) Hayward, S. J.; Lei, Y. D.; Wania, F. Comparative Evaluation of Three High-Performance Liquid Chromatography–Based Kow Estimation Methods for Highly Hydrophobic Organic Compounds: Polybrominated Diphenyl Ethers and Hexabromocyclododecane. Environmental Toxicology and Chemistry 2006, 25 (8), 2018–2027. https://doi.org/10.1897/05-675R.1.

(11) Kaune, A.; Knorrenschild, M.; Kettrup, A. Predicting 1-Octanol-Water Partition Coefficient by High-Performance Liquid Chromatography Gradient Elution. Fresenius' Journal of Analytical Chemistry 1995, 352 (3), 303–312. https://doi.org/10.1007/BF00322226.

(12) U.S. Environmental Protection Agency (EPA). KOWWIN v1.67: Log Octanol-Water Partition Coefficient (LogKow), 2011. https://www.epa.gov/tsca-screening-tools/epi-suitetm-estimation-program-interface.

(13) U.S. Environmental Protection Agency (EPA). WSKOW v1.41: Water Solubility Estimation Model, 2011. https://www.epa.gov/tsca-screening-tools/epi-suitetm-estimation-program-interface.

(14) Hansch, C.; Leo, A.; Hoekman, D. H.; Society, A. C. Exploring QSAR.: Hydrophobic, Electronic, and Steric Constants; ACS professional reference book; American Chemical Society, 1995.

(15) Lei, B.; Li, J.; Liu, H.; Yao, X. Accurate Prediction of Aquatic Toxicity of Aromatic Compounds Based on Genetic Algorithm and Least Squares Support Vector Machines. QSAR & Combinatorial Science 2008, 27 (7), 850–865.

(16) Hansch, C.; Leo, A. *Substituent Constants for Correlation Analysis in Chemistry and Biology*; Wiley: New York, 1979.

(17) Pagonis, D.; Selimovic, V.; Campuzano-Jost, P.; Guo, H.; Day, D. A.; Schueneman, M. K.; Nault, B. A.; Coggon, M. M.; DiGangi, J. P.; Diskin, G. S.; Fortner, E. C.; Gargulinski, E. M.; Gkatzelis, G. I.; Hair, J. W.; Herndon, S. C.; Holmes, C. D.; Katich, J. M.; Nowak, J. B.; Perring, A. E.; Saide, P.; Shingler, T. J.; Soja, A. J.; Thapa, L. H.; Warneke, C.; Wiggins, E. B.; Wisthaler, A.; Yacovitch, T. I.; Yokelson, R. J.; Jimenez, J. L. Impact of Biomass Burning Organic Aerosol Volatility on Smoke Concentrations Downwind of Fires. Environ. Sci. Technol. 2023, 57 (44), 17011–17021. https://doi.org/10.1021/acs.est.3c05017.

(18) May, A. A.; Levin, E. J. T.; Hennigan, C. J.; Riipinen, I.; Lee, T.; Collett Jr., J. L.; Jimenez, J. L.; Kreidenweis, S. M.; Robinson, A. L. Gas-Particle Partitioning of Primary Organic Aerosol

Emissions: 3. Biomass Burning. Journal of Geophysical Research: Atmospheres 2013, 118 (19), 11,327-11,338. https://doi.org/10.1002/jgrd.50828.

(19) Shingler, T.; Crosbie, E.; Ortega, A.; Shiraiwa, M.; Zuend, A.; Beyersdorf, A.; Ziemba, L.; Anderson, B.; Thornhill, L.; Perring, A. E.; Schwarz, J. P.; Campazano-Jost, P.; Day, D. A.; Jimenez, J. L.; Hair, J. W.; Mikoviny, T.; Wisthaler, A.; Sorooshian, A. Airborne Characterization of Subsaturated Aerosol Hygroscopicity and Dry Refractive Index from the Surface to 6.5 Km during the SEAC4RS Campaign. Journal of Geophysical Research: Atmospheres 2016, 121 (8), 4188–4210. https://doi.org/10.1002/2015JD024498.

(20) Theodoritsi, G. N.; Ciarelli, G.; Pandis, S. N. Simulation of the Evolution of Biomass Burning Organic Aerosol with Different Volatility Basis Set Schemes in PMCAMx-SRv1.0. Geoscientific Model Development 2021, 14 (4), 2041–2055. https://doi.org/10.5194/gmd-14-2041-2021.

(21) Hatch, L. E.; Rivas-Ubach, A.; Jen, C. N.; Lipton, M.; Goldstein, A. H.; Barsanti, K. C. Measurements of I/SVOCs in Biomass-Burning Smoke Using Solid-Phase Extraction Disks and Two-Dimensional Gas Chromatography. Atmospheric Chemistry and Physics 2018, 18 (24), 17801–17817. https://doi.org/10.5194/acp-18-17801-2018.

(22) Liang, Y.; Stamatis, C.; Fortner, E. C.; Wernis, R. A.; Van Rooy, P.; Majluf, F.; Yacovitch, T. I.; Daube, C.; Herndon, S. C.; Kreisberg, N. M.; Barsanti, K. C.; Goldstein, A. H. Emissions of Organic Compounds from Western US Wildfires and Their Near-Fire Transformations. Atmospheric Chemistry and Physics 2022, 22 (15), 9877–9893. https://doi.org/10.5194/acp-22-9877-2022.

Chapter 4

Investigating the role of aging on the organic and inorganic composition of size-resolved biomass burning aerosol

4.1 Abstract

Wildfire activity has intensified in Canada in recent decades. Carbonaceous aerosol emitted from wildfires includes brown carbon (BrC), which represents a complex mixture of compounds with varying ability to absorb light in the UV-visible region. The atmospheric evolution of BrC remains uncertain. During July 2021, we deployed a micro-orifice uniform deposit impactor (MOUDI) for 7 days to collect size-resolved aerosol during a smoke intrusion event in Toronto, Ontario. We applied a back trajectory analysis and the trajectory-fire interception method (TFIM), which estimated that the smoke sampled was aged 30-40 hrs and originated from forest fires in northern Ontario. Multiple chromatographic methods were applied to characterize the chemical and optical properties of the aerosol. Size-exclusion chromatography coupled to ultraviolet-visible absorption spectroscopy (SEC-UV) showed that BrC absorption was dominated by high molecular weight (>500 Da) species. Reverse phase chromatography coupled to UV-vis absorption spectroscopy (HPLC-UV) indicated the presence of moderately hydrophobic ($\log(K_{ow})$ >3) compounds, which may be consistent with oligomeric compounds that can persist during atmospheric transport. Ion chromatography with conductivity detection (IC-CD) showed that the molar ratio of alkylamines to ammonium (NR_3H^+/NH_4^+) ranged from 0.3 to 3.6, values comparable to those previously reported in a marine environment. These chromatographic analyses of the Toronto MOUDI samples are compared to fresh emissions from controlled combustions during FIREX 2016. Although the amines likely reflect a mixture of biomass burning and local sources, this work aligns with previous studies that have shown aqueous reactions involving ammonia, amines, and carbonyl compounds contribute to the formation of high molecular weight nitrogen-containing species.

4.2 Introduction

Canadian forests cover nearly 362 million ha, which comprise an estimated 8.5% of the global forested area.[1,2] Wildfires in Canadian forested land has always been present; however, in recent years the wildfires in Canada have been record setting. Fuel aridity, ignition sources, and weather contribute to the prevalence of wildfires, and climate change has intensified these drivers. Canada's climate is warming at twice the global rate where the mean annual temperature has increased 1.7°C since 1948[3] and the annual area burned in the country has steadily increased since the 1950s, where the length of wildfire season also increased in recent decades.[4] For example, in 2023 Canadian wildfires were so intense, a recording breaking 15 million ha of land was burned, which was more than seven times the average annual burned area compared to the previous four decades.[5]

Wildfires impact air quality by releasing a complex mixture of emissions. Multiple studies have assessed emission and aging processes during long-range transport of biomass fuel in diverse regions, such as North America, Siberia, Amazonia, and Africa.[6–12] Biomass contains biopolymers such as lignin and cellulose, and the pyrolysis of such compounds is known contribute to the emissions of oxygenated organics including phenolic compounds (e.g. catechol, guaiacol, and coniferaldehyde),[13] organic acids (e.g. formic acid, acetic acid, malonic, succinic),[14–16] furans, and coumarins in addition to major gases such as carbon dioxide, carbon monoxide, reduced nitrogen species, nitric oxide, methane, and volatile organic compounds. Carbonaceous aerosol emitted from wildfires include black carbon (BC), which is elemental carbon associated with condensed organics and broadly absorbs across the ultraviolet (UV) to infrared wavelengths[17] and brown carbon (BrC), which is partially water-soluble and absorbs most strongly in the ultraviolet-visible (UV-vis) region. Additional sources of BrC to the atmosphere include fossil fuel combustion,[18,19]

and the release of biogenic matter.[20] The two major sources of BrC are biomass burning[21] and secondary formation via aqueous phase reactions, including oligomerization.[22,23] Long range transport of biomass burning emissions have been measured in previous studies.[24–26] In the atmosphere, BrC is susceptible to aging processes which include dilution,[27] photolysis, and oxidation with OH, O_3, and NO_3.[28–30] To measure the absorption and chemical properties of biomass burning derived BrC close to the source and its evolution downwind, kinetic models,[31] controlled burns,[13] and field campaigns utilizing aircrafts have been used.[24,32] During atmospheric transport, BrC can undergo photoenhancement, photobleaching, or minimal change to absorption.[31,33,34] Uncertainty remains regarding how the composition and absorption properties of BrC chromophores evolve during atmospheric transport.

Understanding the chemical evolution of BrC species requires characterization of primary emissions. This is typically assessed by controlled combustion experiments. Previous studies have pyrolyzed fuels characteristic to certain regions to identify common molecular structures and functional groups of BrC.[13,35–37] Brown carbon typically consists of highly conjugated systems, and functionalized with aliphatic, aromatic, hydroxyl, and carbonyl groups.[13] The combination of chromophores with varying abilities to absorb in the UV-vis region contributes to the observable brown colour.[38] The formation of secondary BrC has been demonstrated in controlled laboratory experiments, including aqueous-phase reactions of simple carbonyl compounds with amines and ammonium,[39–41] and aqueous-phase reactions that produce light-absorbing oligomers.[22,23,42]

Wildfires are also an important source of aerosol to the atmosphere. Particle size distributions within smoke plumes can vary depending on fuel type and combustion conditions (flaming or smoldering) and evolves due to condensation and coagulation within plumes as the smoke ages.[43–45] The net impact of organic aerosol condensation and evaporation on particle size

distribution is complex because these two processes can occur simultaneously, with wildfire size, intensity, and dilution rate influencing the organic aerosol concentration in the center and perimeter of the smoke plume.[46] It is important to investigate the aerosol size composition of biomass burning derived BrC to better understand its atmospheric evolution.[47] For example, Di Lorenzo et al. measured size resolved aerosol of an aged smoke plume originating from boreal forest fires and observed that fine-mode aerosol (0.10 μm < Dp < 1.0 μm) contained the largest fraction of BrC, with smaller absorption measured in ultrafine (0.010 μm < Dp < 0.10 μm) and coarse (1.0 μm < Dp < 10 μm) modes. Their results showed that high MW chromophores dominated absorption across all aerosol size ranges, but as the aerosol size decreased, lower MW species accounted for an increasing fraction of total absorption.[47] This observation is supported by Lee et al. which observed lower MW fractions of biomass burning organic aerosol were more abundant in smaller diameter particles.[48] Additional studies have also highlighted the importance of investigating the evolution of size distribution and assessing PM size ranges for human health concerns. For example, Sparks et al. measured the size distribution of biomass burning aerosol during a smoke intrusion in the San Francisco Bay Area and observed size dependent infiltration of spherical carbon-rich submicron particles indoors (0.15 μm to 0.45 μm) which were formed during aging through condensation of gas-phase organics, dehydration reactions, and polymerization of organics.[49]

Alkylamines (R_3N) are rarely measured in aerosol studies due the lack of standardized analytical methods. In the presence of OH, their lifetime is on the order of a several hours to a day, compared to approximately one month for ammonia (NH_3).[50] Despite, their short lifetimes, R_3N are important to measure because they can contribute to secondary BrC formation. Alkylamines have been detected in biomass burning aerosol,[51,52] where concentrations have been observed to

be over a magnitude lower than that of ammonium.[53] However, Di Lorenzo et al. observed strong correlations between BrC and several R_3N (e.g. dimethylamine (DMA) and diethylamine (DEA)) during a smoke intrusion event in St John's Newfoundland and Labrador. Notably, they reported instances in which molar concentration of DEA exceeded that of ammonium, suggesting that alkylamines may have originated from additional sources or be introduced during atmospheric transport.[47]

Multiple analytical methods have been applied to investigate the molecular structures that comprise BrC. This includes various chromatographic applications such as high-performance reverse phase chromatography coupled to high resolution mass spectrometry,[13] and size-exclusion chromatography coupled to UV-vis absorption spectroscopy (SEC-UV).[25,54–57] From the SEC-UV analyses, aged BrC is typically comprised of high molecular weight (MW) species (>400 to 500 Da) with unknown structural identities,[25,56] as low MW are less persistent due to volatilization and oxidation processes.[25] To describe the polarity of BrC compounds, the octanol-water partition coefficient, $\log(K_{ow})$ can be assigned by applying HPLC-UV.[57] Further, ion chromatography with conductivity detection (IC-CD) methods have been developed and applied to quantify of alkylamines.[51,58,59] In these studies, various alkylamines were detected including DEA and DMA, indicating the presence of reduced nitrogen species that may contribute to BrC formation.[47]

In this work, we collected size-resolved aerosol during a smoke intrusion event in Toronto, Ontario, Canada in July 2021. During sampling, we captured a smoke plume aged approximately 30-40 hrs that originated from forest fires burning in northern Ontario. Multiple chromatographic methods were applied to characterize the chemical and optical properties of the aerosol; SEC-UV was used to determine the absorption contribution of high and low MW BrC species, HPLC-UV was applied to estimate $\log(K_{ow})$ values to assess hydrophobicity, and IC-CD to measure inorganic

anions and cations, and alkylamines. The objective of this work is to compare these results with previous analyses of fresh and aged biomass burning aerosol to evaluate if BrC evolution during atmospheric transport is consistent across different plumes. We also investigate the presence of alkylamines in urban regions with and without biomass burning influence and explore the potential role biomass burning has on alkylamine emissions, including the analysis of fresh emissions from controlled combustions at the Missoula Fire Sciences Laboratory during the Fire Influence on Regional to Global Environments (FIREX) FireLab 2016 campaign.

4.3 Methodology

4.3.1 Sample collection in Toronto

Sampling in Toronto, Ontario, Canada occurred between July 20th to July 27th, 2021, during a smoke intrusion originating from forest fires in northern Ontario. A cascade impactor referred to as the nano-microorifice uniform deposit impactor (nanoMOUDI; model 122-R, MSP Corporation, Shoreview, MN, USA) (Figure C-1) was deployed on the roof of the Petrie Science and Engineering Building (43.7739° N, 79.5068° W) on the York University campus and collected aerosol onto aluminum substrates at 30 L min^{-1} for a total of 164 hrs. The nanoMOUDI consists of an inlet with an 18 μm cutoff, followed by 13 stages which separate aerosol by aerodynamic diameter into 13 size fractions (10 – 0.010 μm). At each stage, there is uniform deposition of the aerosol due to the rotation of the impaction plate. Prior to deploying the nanoMOUDI, the aluminum substrates were rinsed with methanol and ultra-pure Milli-Q water (DIW, resistivity of 18.2 MΩ cm) to remove organic and water-soluble contaminants and then baked at 550 ℃ to remove any remaining volatile species.

4.3.2 Identifying periods of wildfire influence, locating the fires, and assessing transport time

Fire locations were determined from the Canadian Wildland Fire Information System (CWFIS)[60] and Fire Information for Resource Management System US/Cananda (FIRMS).[61] Airmass back trajectory analyses was determined by applying the hybrid single-particle LaGrangian integrated trajectory (HYSPLIT) model.[62] During the sampling period, elevated levels of $PM_{2.5}$ were observed in Toronto from July 19 11:00 am ET to July 20 at 4:00 pm ET, and again from July 25 at 2:00 pm ET to July 26 at 9:00 am ET (Figure C-2). During these timeframes, $PM_{2.5}$ reached ~60 $\mu g/m^3$ and ~70 $\mu g/m^3$, respectively, which impacted visibility and air quality. These periods were used as reference points to generate the 24 hr back trajectory analyses to investigate the influence of wildfires. While simultaneous $PM_{2.5}$ enhancement and active wildfires in northern Ontario may suggest a smoke intrusion, assessment of $PM_{2.5}$ alone may not be sufficient to confirm the impact from the wildfires. We applied the trajectory-fire interception method (TFIM),[63] which counts the number of spatial interceptions between the HYSPLIT back trajectories and fire hots spots confirmed by FIRMS and CWFIS. HYSPLIT trajectories were run using North American Mesoscale Forecast System (NAM) meteorological data with 12 km resolution.[64] In accordance with the TFIM framework, an interception was deemed to have occurred if the back trajectory and a reported fire hotspot was within 50 km of each other. Figures C-3 and C-4 shows the overlaid HYSPLIT back trajectories and fire hotspots, and Table C-1 summarizes the number of interceptions. This analysis provides evidence that the air mass sampled in Toronto was influenced by long-range transport of wildfire smoke from northwestern Ontario.

4.3.3 Black carbon, NO_x, and $PM_{2.5}$ data acquisition

Black carbon (BC) and nitrogen oxides (NO_x), and particulate matter ($PM_{2.5}$) data was retrieved from the Toronto North air quality monitoring station operated by the Ontario Ministry

of Environment Conservation and Parks (MECP). Black carbon was measured by a Teledyne API Model 633 Aethalometer Black Carbon Monitor and NO_x was measured by a Thermo TEI49i. One-minute resolution data was retrieved from the sampling period to provide supporting evidence of biomass burning influence during the smoke intrusion. Hourly $PM_{2.5}$ data was measured by the Thermo Scientific Model 5030i SHARP Monitor.

4.3.4 Sample extraction of Toronto MOUDI samples

The aluminum substrates were removed from the impaction plates and transferred into pre-cleaned falcon tubes to be extracted in 5 mL de-ionized water by sonication (Branson 5510 Sonicator) at room temperature for one hour. Following sonication, the extracts were filtered using Iso-Disc™ PTFE filters (13 mm x 0.2 μm) to ensure that filter debris and insoluble particles suspended in the solvent was not transferred into the sample vials used for the offline chromatographic separations.

4.3.5 Overview of the Fire Science Laboratory Study

The FIREX FireLab campaign was based at the U.S. Forest Service's Fire Sciences Laboratory in Missoula, Montana during October–November 2016. The Fire Sciences Laboratory has been described previously.[65,66] Briefly, approximately 0.2 to 0.44 kg of fuel was placed onto a fuel bed and ignited within a main combustion chamber (12.5 m × 12.5 m × 22 m with a total volume of ~3000 m^3). The fuels were characteristic of the western U.S. and were primarily collected from the Clearwater Wildlife Management Area which is managed by the state of Montana and the Lubrecht Experimental Forest which is managed by the University of Montana. The offline sampling of the fresh biomass burning smoke is described in Azzarello et al. Briefly, the aerosol inlet was ~ 30 m in length of 0.64 cm o.d. copper tubing; the sampling flow rate 2.0 slpm which was controlled by a mass flow controller (Alicat Scientific, Tucson, AZ, USA). A

cyclone (URG-2000-30ED; URG Corp, Chapel Hill, NC, USA) with nominal 2.5 μm cutpoint at 2.4 slpm removed large particles. Aerosol particles were collected on pre-muffled (500 °C, 4 h) 47 mm quartz fiber filters (Tissuquartz 2500QAT-UP; Pall Life Sciences, Washington, NY, USA). After collection, the filters were wrapped in pre-muffled (500 °C, 4 hours) aluminum foil and stored at -20 °C until analysis. The filters were subsampled with a 10 mm arch punch, transferred to a pre-cleaned polypropylene sample tube, and sonicated with 1 mL of ultra-pure Milli-Q water (DIW; resistivity of 18.2 MΩ cm) for 1 hr prior.

4.3.6 Chromatography analyses

4.3.6.1 Size-exclusion chromatography with UV-vis absorption detection

Separation by SEC-UV provides context about light absorption properties of BrC species by providing a MW distribution profile. The separation method and categorization of MW classes have been previously described by Di Lorenzo et al. and Azzarello et al.[51,56] Briefly, the samples were separated using an aqueous-gel-filtration column, with a MW range of 250 Da to 75 kDa (Polysep-GFC-P 3000, Phenomenex, Torrance, CA). Size-resolved species were detected by a diode-array detector from 190 to 800 nm (UltiMate 3000, Thermo Fisher Scientific, Sunnyvale, CA) coupled to an ion chromatograph (ICS 6000; Thermo Fisher Scientific) pump with a Dionex AS autosampler (Thermo Fisher Scientific). An isocratic separation method was applied using a mobile phase that contained a 1:1 mixture of acetonitrile and 25 mM ammonium acetate in solution at a flow rate of 1 mL min^{-1} and a sample injection volume of 100 μL. DIW was injected as a method blank, and no detectable signal was observed. The MW of the resolved species is grouped into three categories: high MW refers to greater than 500 Da, low MW refers to less than 500 Da, and unidentified MW describes peaks that eluted past the exclusion volume of the SEC column. To estimate the MW distribution, we applied a previously described calibration scheme.[25]

4.3.6.2 Ion chromatography with conductivity detection

Chromatographic separation of inorganic cations and anions, and alkylamines was performed using the Thermo Scientific ICS-6000 with suppressed conductivity detection measured in micro-siemens (μS). The suppressor model used for the separations was the Dionex DRS 600 4 mm. Anions were separated using a multi-step gradient scheme, AS23-4μm (4 x 250 mm) analytical column fitted with an AG23- 4μm (4 x 50 mm) guard column, and a TAC-ULP1 (5 x 23 mm) concentrator column. Using a premixed anion standard concentrate (Dionex seven-cation II, P/ N: 057590, Thermo Scientific, Sunnyvale, CA, USA), a primary stock solution was prepared to make five anion standard solutions and two check standards via serial dilutions. The anions that were quantified include chloride (Cl^-), nitrate (NO_3^-), and sulphate (SO_4^{-2}). A 100 mM sodium hydroxide (NaOH) (50-52% w/w, Sigma Aldrich) solution was prepared as eluent at a column flow rate of 1 mL min^{-1}, and a sample injection volume of 1 mL was used. The column temperature was 30 °C and the run time was 30 mins. The gradient elution scheme for the anion separation had an initial concentration of 10 mM of NaOH at 0-15 mins. The concentration was increased to 60 mM of NaOH from 20-25 mins, then the concentration was decreased back to 10 mM of NaOH for the remaining 25-30 mins run time. The chromatographic separation of inorganic cations and alkylamines is described in Salehpoor et al.[58] Briefly, a multi-step gradient scheme using a CS19-4μm (4 x 250 mm) analytical column fitted with a CG19-4μm (4 x 50 mm) guard column, and a TCC-ULP1 (5 x 23 mm) concentrator column were used to separate cations. Using a premixed cation standard concentrate (Dionex six-cation II, P/ N: 046070, Thermo Scientific, Sunnyvale, CA, USA) a primary stock solution was prepared to make five standard solutions and two check standards via serial dilutions. The inorganic cations that were quantified include sodium (Na^+), ammonium (NH_4^+), and potassium (K^+). Primary stock solutions of the following alkylamines:

dimethylamine (DMA, 40% w/w), trimethylamine (TMA, 45% w/w), monoethylamine (MEA, 70% w/w), diethylamine (DEA, >99.5% w/w), triethylamine (TEA, >99.5% w/w), monopropylamine (MPA, >99% w/w), isomonopropylamine (iMPA, >99.5% w/w), monobutylamine (MBA, 99.5% w/w), monoethanolamine (MEtA, >98% w/w) were purchased from Sigma Aldrich to prepare calibration standard solutions. A 0.1 M methanesulfonic acid (MSA) (Sigma Aldrich) solution was prepared as eluent at a column flow rate of 1.25 mL min^{-1} and a sample injection volume of 1 mL. The column temperature was 55 °C and the run time was 35 mins. A gradient scheme was used where the eluent started at an initial concentration of 1 mM MSA that ran from 0 to 20 mins, then 4 mM of MSA from 20 to 25 mins. This concentration was held constant from 25 to 30 mins, then the concentration MSA was increased to 8 mM and was held constant for 30 to 35 mins long. Finally, decreasing the concentration of MSA back to 1 mM remaining run time. The LOD and LOQ for each ion by IC-CD are summarized in Table C-2.

4.3.6.3 Extended Aerosol Inorganic Model simulation

To assess the aerosol pH based on the IC-CD measurements, the extended aerosol inorganic model (E-AIM) IV was applied. Aerosol pH was calculated using equation 4.1.[67,68]

$$\text{Eq 4.1: } \text{pH} = -\log(a_H^+) = -\log\left(f_H^+ \times \chi_H^+ \times 55.509\right)$$

Where $a_H^+$is the activity coefficient of the hydrogen ion in aerosol liquid water, f_H^+ is the hydrogen ion mole-fraction-based activity coefficient, χ_H^+ is the mole fraction of the hydrogen ion, and 55.509 is the conversion factor from mole-based activity coefficient to molality-based on.[67,68] Model IV was selected due the inclusion of non-volatile cations including Na^+, and K^+ (the input of Na^+ concentrations represented the sum of Na^+ and K^+.[68,69] The temperature and humidity inputs were an average during the sampling period.

4.3.6.4 High-performance liquid chromatography with UV-vis absorption detection

The HPLC offline analysis was completed using the same pump and detector as described in Section 4.3.6.1. Samples were separated using a C18 column (2.1 mm × 100 mm × 5 µm, Kinetex Phenomenex; Torrance, CA, USA). The mobile phase was comprised of (A) 0.1% acetic acid in DIW and (B) acetonitrile combined as follows: 95% A held for 5 mins and linearly decreased over the next 20 mins until a 5% A was reached. This was held for 15 mins, and the conditions returned to 95% A in the following 1 min to re-equilibrate. To contextualize the hydrophobicity of compounds separated by the HPLC-UV method, we considered the octanol-water partition coefficient, K_{ow}. This method has been previously described.[57] Briefly, log(K_{ow}) values were assigned to retention times of resolved peaks using multiple isocratic schemes. Briefly, log(K_{ow}) values were assigned to retention times of resolved peaks using multiple isocratic schemes.[70,71] Solutions of 4-nitrocatechol (>96%, Sigma Aldrich;), 4-hydroxy-3-methoxycinnamaldehyde (98%, Sigma Aldrich), 7-hydroxycoumarin (99%, Sigma Aldrich), biphenyl (99%, Sigma Aldrich), nitrobenzene (99%, Sigma Aldrich;), and toluene (99.5%, Sigma Aldrich;) with concentrations of 39, 34, 37, 3.9, 35, 35 nmol mL^{-1}, respectively. These were prepared and run under the following isocratic conditions: (i) 65% A and 35% B, (ii) 50% A and 50% B, (iii) 35% A and 65% B, and (iv) 20% A and 80% B. To determine k', a solution of thiourea (99%, Sigma Aldrich) was used to identify the void volume. The log(K_{ow}) of these standard compounds ranged from 1.66 to 4.01. Calibration plots and the determination of k' and log(K_{ow}) are included in Appendix C.

4.4 Results and Discussion

4.4.1 Biomass influence and aging

The smoke intrusion in Toronto, Ontario during July 2021 originated from forest fires in northern Ontario. Local air quality monitoring stations recorded elevated levels of BC and $PM_{2.5}$ during the smoke intrusion. During the sampling week, there were two periods of elevated levels of $PM_{2.5}$ observed in Toronto. The duration of the first event was approximately 29 hrs, where the average mass concentration was 37 $\mu g/m^3$. The second event lasted for approximately 19 hrs, with a 24-hour average $PM_{2.5}$ concentration of 29 $\mu g/m^3$, which exceeded Canada's air quality guideline of 27 $\mu g/m^3$. We confirmed that the elevated $PM_{2.5}$ was not fully explained by local emissions by comparing BC-NO_x relationships during our sampling period to a biomass burning-free period (July 2021) and another biomass burning-influenced period (July 2023, Figure C-5). During the smoke heavy intrusion in July 2021, there was a slope of 0.7 and a R^2 of 0.86 whereas during the smoke free period there was a slope of 0.05 and a R^2 of 0.98. In an urban region, a strong correlation and a low BC and NO_x ratio indicates emissions are from a common source. These trends support that elevated BC and $PM_{2.5}$ during July 2021 was driven by transported forest fire smoke rather than local combustion sources.

While simultaneous $PM_{2.5}$ enhancement and active forest fires in northern Ontario may suggest a smoke intrusion, assessment of $PM_{2.5}$ and the relationship between BC and NO_x may not be sufficient to confirm that the air mass sampled in Toronto was positively impacted by the forest fires. We also used a fire source apportionment method (TFIM) to confirm the role of biomass burning. Table C-1 (and Text C.1) lists the number of active fires for both smoke events, where there was a total of 13 active forest fires detected with a total of 47 interceptions. These findings satisfied the 20-intercept minimum for 24 hr back trajectory analysis outlined by the TFIM

model,[63] confirming that Toronto was in fact influenced by smoke from fires burning in northern Ontario.

4.4.2 Molecular weight distribution from SEC-UV analysis

Aerosol was collected in three size ranges: ultrafine (0.01 μm < Dp < 0.1 μm), fine (0.1 μm < Dp < 1.0 μm), and coarse mode (1 μm < Dp < 10 μm). In the ultrafine mode, low MW species comprised about half of total absorption (50.47%). In the fine mode, high MW species dominated absorption with 61% and the coarse mode only contained low MW species. Overall, 92% of total BrC absorption was in the fine mode, with high MW species contributing to 58% of total measured absorption. This is generally consistent with a similar analysis conducted previously on 48 hr-aged biomass burning aerosol, in which fine-mode aerosol contained the largest fraction of BrC absorption (93%), with high MW species dominating across all size ranges and the contribution of low MW to absorption increasing as aerosol size decreased.[47] The particle size distribution of an initial smoke plume is variable; typically, the ultrafine mode is dominant close to the fire which has been observed in laboratory and field studies.[72–74] As smoke undergoes aging during atmospheric transport ultrafine particles can shift to the fine mode[75] while additional aging processes such as dilution and evaporation of volatile species, photolysis, and oxidation further alter the chemical and absorption properties of BrC.[28–30] Urban areas impacted by biomass burning and those without biomass burning influence have shown enhanced BrC absorption in the fine mode. The dominance of BrC absorption in the fine mode in the aged Toronto samples is expected and is consistent with previous studies that measured size resolved aerosol in urban regions.[76,77]

Figure 4-1 displays absorption density plots for the Toronto samples and samples collected in St. John's, Newfoundland during a smoke intrusion from boreal forest fires in Quebec.[47] The

dominant presence of high MW species in the Toronto samples broadly aligns with previous analyses that applied SEC-UV to aged biomass burning-derived samples. Previous studies of fresh and near source emission sampling reported greater contribution from low MW species. Our previous analyses applying SEC-UV to controlled burns of western U.S. fuels showed that low MW species dominated fresh emissions[57] and a similar dominance of low MW species was observed in wildfire emissions aged 0 to 5 hours.[56] Di Lorenzo et al. sampled smoke plumes that corresponded to plume ages ranging from 10 to > 72 hrs in eastern Canada and observed that the contribution of high MW species to absorption increased with increasing plume age.[25] An exception to this trend was reported from wildfire aerosol in Greece with a transport time of 1 to 70 hrs and observed that high MW species dominated absorption of fresh and aged smoke.[55] The Toronto sample set, aged approximately 30-40 hrs, aligns with most previous work, where aging increases MW. Collectively these studies suggest that high MW species are generally lower in volatility and more photochemically stable than low MW precursors and/or secondary processing such as oligomerization formation shifts towards high MW species dominating absorption with aging.

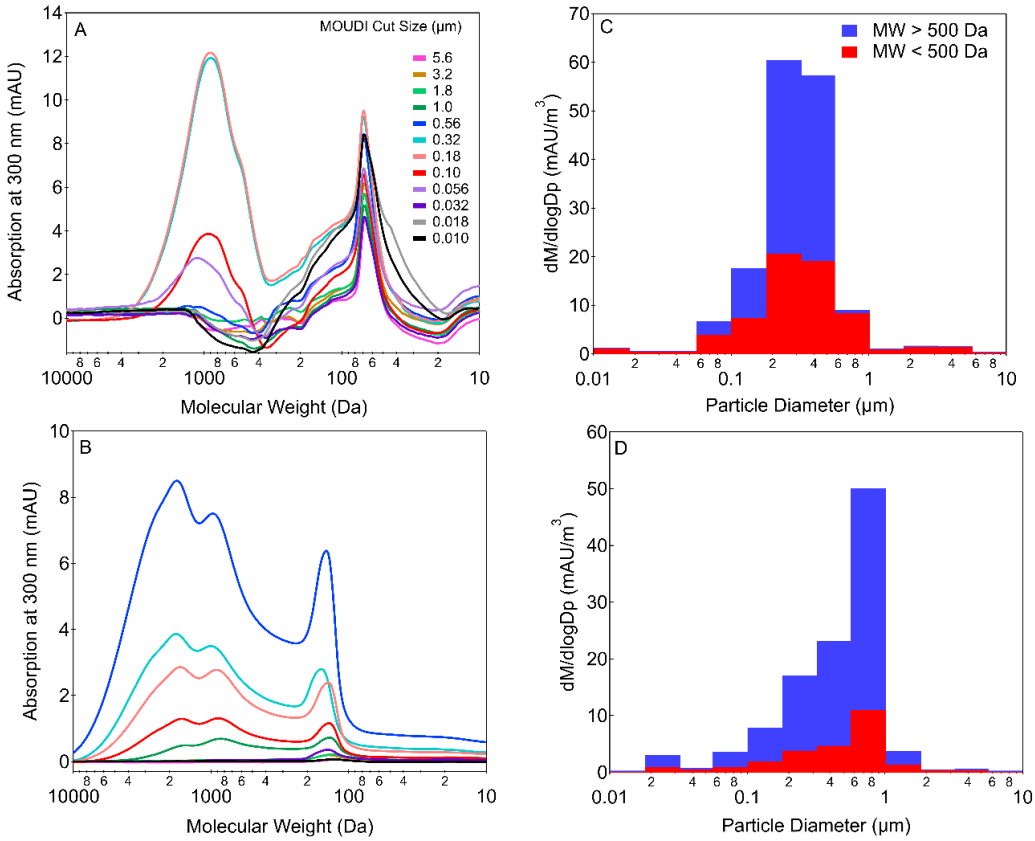

Figure 4-1. Absorption density plots by the SEC-UV analysis of each size bin for the (A) Toronto samples and (B) St. John's samples. Aerosol size distribution of high and low MW BrC chromophores for (C) Toronto and (D) St. John's (traces are stacked to reflect total absorption at each size bin).

4.4.3 Aerosol ionic composition and pH

4.4.3.1 Major ions

We applied IC-CD to quantify inorganic ions, alkylamines, and detect organic acids in the size-resolved samples collected during the smoke intrusion in Toronto (Figure 4-2). This analysis aimed to characterize the ionic composition, assess aerosol acidity, and investigate aging processes. Biomass burning releases large amounts of NO_x, SO_2, and NH_3 to the atmosphere,[78,79] which are precursors that oxidize to form the aerosol-phase products: NO_3^-, SO_4^{2-}, and NH_4^+.[80,81] This is consistent with our observations as the dominant anions were SO_4^{2-} followed by NO_3^- and

Cl^-, and the major cations were Na^+, NH_4^+ and K^+. Tables C-3 to C-6 summarizes the measured ions and the anion and cation charge sums. There is an excess in anions in the coarse mode which likely reflects the absence of Ca^{2+} and Mg^{2+} measurements due to suppressor limitations during the cation analysis[58] while in the fine mode there tends to be a excess in cations which indicates that apart from the measured inorganic anions (SO_4^{2-}, NO_3^-, and Cl^-), other negatively charged species (e.g. organic acids) may contribute to the charge balance ratio.[82] The inorganic measurements of our samples align with previous studies that sampled other aged biomass burning plumes; Pratt and Prather et al. reported that aged organic carbon particles contained > 50% by volume secondary species, which were primarily NH_4NO_3, $(NH_4)_2SO_4$, and alkylamines.[83]

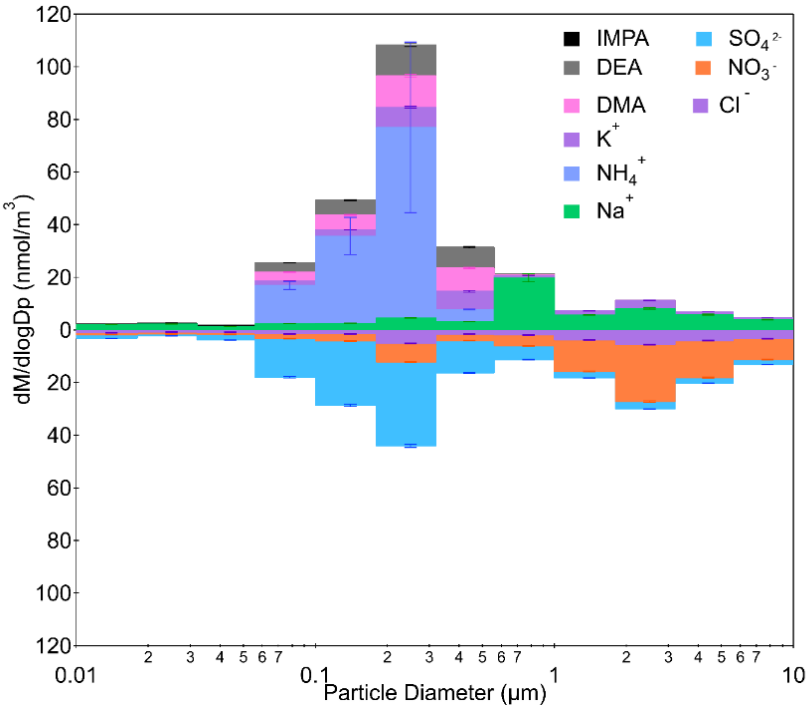

Figure 4-2. Molar distribution of the inorganic cations and alkylamines and inorganic anions from the Toronto MOUDI samples. The error bars represent the uncertainty based on the propagation of errors for each ion. The aerosol mass loading size distribution is displayed in Figure C-6.

Chemical aging of biomass-burning derived aerosol can be inferred from transformations of potassium salts. Fresh biomass burning plumes can be characterized by high KCl whereas aged

biomass burning aerosol has been associated with KNO_3 and K_2SO_4 due to acid displacement reactions with sulfuric acid and nitric acid.[84,85] Previous smoke intrusion studies also report characteristics consistent with aged biomass burning aerosol, providing additional insights into its composition. Owega et al. sampled in Toronto during a smoke intrusion from forest fires in Quebec and reported elevated levels of SO_2 and fine mode particles enriched with K^+ and SO_4^{2-}.[86] Similarly, Saarnio et al. also measured fine mode particles enriched with SO_4^{2-}, NH_4^+, and NO_3^- in Helsinki, Finland when sampling aged smoke from boreal and agricultural fires.[87] Controlled combustion experiments from Guo et al. also support the evolution of ionic species during aging; they observed fresh samples contained negligible NO_3, where NO_3^- increased after two days of aging and then declined after seven days as SO_4^{2-} increased. This demonstrated that SO_4^{2-} formation becomes increasingly dominant during atmospheric aging.[88]

4.4.3.2 Organic acids

The presence of organic acids was qualitatively investigated (Table C-7 and Text C.2) to address the cation excess in the fine mode, which indicate the presence of unmeasured anionic species. Organic acids are constituents of biomass burning aerosol and can contribute to aerosol acidity,[14,89] affect aqueous phase chemistry,[90] and gas-aerosol partitioning.[91] Based on elution ranges for organic acids,[82] in all size ranges of our Toronto samples there is evidence of monoacids, in the fine mode there is indication of dicarboxylic acids, and in both the fine and ultrafine modes there is potentially polycarboxylates. Organic acids can be emitted directly from biomass burning and or formed through secondary processes.[92] Although these compounds were not quantified, these observations are consistent with previous measurements of organic acids in wildfire smoke. Fine-mode particles may be enriched with low MW monoacids due to gas-phase oxidation of

volatile organic compounds, where aqueous-phase oxidation can lead to the formation of dicarboxylic acids.[92]

The Toronto samples were influenced by atmospheric processing and mixing with local emissions during transport as they correspond to a plume age range of 30-40 hrs. Therefore, the organic acids inferred are not uniquely attributed to primary biomass burning emissions. In fresh wildfire plumes, small organic acids such as formic and acetic acid have been observed to be directly emitted[92] and persist up to 8 hrs.[14] During atmospheric aging, these compounds can undergo aqueous-phase reactions and oligomerizations to form higher MW organic acids. For example, high MW multifunctional organics (e.g. humic-like substances) have been produced from reactions of small aldehydes with ammonium and amines and oligomerization of water-soluble organics during cloud processing of wildfire smoke.[93–95] Further, Cook et al. sampled in New York during smoke intrusions from Canadian wildfires and observed oligomeric species and organic acids (e.g. glycolic acid, pyruvic acid, malonic acid, succinic acid).[15] In more recent work, Tripathy et al. showed that in aged smoke plumes, heavier organic acids dominated dissolved organic carbon.[92] These findings suggest that the smaller organic acids observed in the Toronto samples likely come from sources closer to the sampling site and polycarboxylates observed in this work may reflect secondary formation during plume aging.

Investigating the chemical composition of aerosol can provide insight into aerosol pH, which can be used to help interpret the UV-visible spectra from the SEC-UV analysis. Previous studies have observed that as pH increases, absorption spectra tend to shift toward longer wavelengths; this trend is attributed to the proton dissociation of acidic functional groups.[96,97] Smoke plumes are highly enriched in organic matter and the associated particles can be acidic.[92,98,99] Direct pH measurement of the aqueous extracts yielded a pH of approximately 4;

however, this measurement represents the acidity of diluted bulk solution rather than the aerosol liquid phase. The ionic composition of measurements from the IC-CD analysis were applied to the E-AIM simulation (Model IV), which estimated a pH of approximately 1. These results are consistent with previous summertime studies in Toronto: Tao and Murphy estimated $PM_{2.5}$ pH values of ~ 1 to 2 using E-AIM, and Arangio et al. found summer pH between 1.7 to 3.6, identifying SO_4^{2-} as the main driver of the liquid water content.[68,100]

4.4.3.3 Alkylamines

Alkylamines are important to measure because, they can contribute to secondary BrC formation. Amines can undergo aqueous reactions with carbonyls (e.g. glyoxal and methylglyoxal), producing oligomers and nitrogen containing chromophores.[39,101] In urban regions, potential sources include vehicle emissions,[102] and wastewater treatment plants.[103] In our Toronto samples, DMA and DEA were the dominant alkylamines observed. Alkylamines have been reported during another North American smoke-intrusion event. Di Lorenzo et al. measured MMA, DMA, TMA, MEA, DEA, and TEA during a smoke intrusion in St. John's, Newfoundland; DMA and DEA where the highest in the 0.32 – 0.56 μm size bin and DEA even exceeding ammonium in two size bins,[47] which was unexpected because previous studies reported alkylamines in biomass derived aerosol, where the levels were lower than that of ammonium.[51,104,105] For the St. John's samples, BrC absorption correlated more strongly with amines than with other traditional biomass burning markers, implying that amines potentially participated in secondary BrC formation and the marine environment enriched the biomass burning plume in reduced nitrogen species. In contrast, the Toronto plume did not pass over a marine environment and fewer amine compounds were detected; however, the overall trend was similar, with increasing amine quantities correlating to greater BrC absorption (Figure C-7). However, the

measurement of DMA and DEA is consistent with previous measurements in Toronto reported by Yang et al. and VandenBoer et al. who also observed these compounds as major alkylamines in the absence of wildfire influence.[59,106] This potentially suggest that alkylamines emitted from local sources (e.g. vehicles) potentially contributed to BrC formation during transport, which is consistent with controlled laboratory experiments showing BrC formation from reactions between reduced nitrogen compounds and carbonyls.[23] Similar observations in other urban regions in China, Philippines, and Italy reported DEA and DMA as dominant amines,[107–109] supporting that smoke from northwestern Ontario mixed with additional sources during transport.

To assess the contribution of amines to the total reduced nitrogenous species measured, Figure 4-3 displays the molar ratio of total amines to ammonium (R_3NH^+/NH_4^+), which ranges from 0.3 to 3.6. These values are comparable to ratios reported during the St. John's smoke intrusion event which ranged from 0.2 to 2 in the fine mode.[51] In the absence of wildfire influence, VandenBoer et al. also sampled in Toronto and similarly observed a strong size dependence in the fine mode, where the molar R_3NH^+/NH_4^+ ratios were much lower, ranging between 0.005 to 0.2 (Figure 4-3).[59] To investigate whether we measured persistent alkylamines from the forest fires that contributed to the enhancement, we applied the method described in Section 4.3.5 to samples collected during the FIREX FireLab study where fuels found throughout the western U.S were pyrolyzed. In these samples, alkylamines were not detected, which potentially suggests that amine formation was limited under fresh combustion conditions. To evaluate the potential contribution of undetected amines, an upper-limit R_3NH^+/NH_4^+ ratio was estimated by summing the LODs for the dominant amines, DEA and DMA, and dividing by the lowest NH_4^+ measured. This yielded an upper limit of 12% for the FIREX FireLab samples.

Therefore, to further investigate the potential contribution of amines in our Toronto samples where R_3NH^+ was below detection and to assess the extent to which undetected amines might influence source attribution, a similar upper-limit analysis was determined for the fine mode. This yielded a plume-wide upper limit of 5.8%. This means that even if amines were present at levels just below detection they would only contribute at most ~6%. In considering, the presence of alkylamine in Toronto under non-smoky conditions (VandenBoer et al. measurements[59]), the elevated NR_3^+/NH_4^+ ratio, and the absence of amines from fresh controlled burns, the amines in the Toronto samples potentially reflect a combination of atmospheric aging processes and a mixture of urban and biomass-burning sources and cannot be uniquely attributed to the smoke intrusion.

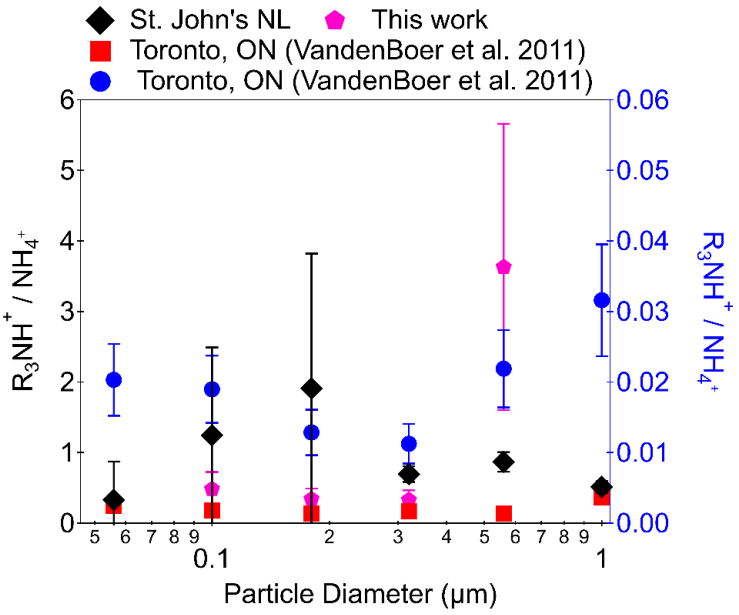

Figure 4-3. Ratio of the sum of particulate amines to ammonium (moles/moles) as a function of particle diameter during the Toronto smoke intrusion from this work (pink), aged biomass burning samples collected in St. John's Newfoundland where the smoke originated from Quebec and Labrador during the summer of 2013 reported by Place et al (black),[51] and in Toronto, Ontario with no reported biomass burning influence which is described in VandenBoer et al.[59] The error bars represent the uncertainty based on the propagation of errors for each ion.

4.4.3.4 Octanol-water partitioning coefficient from HPLC-UV analysis

Reverse phase HPLC can be used to separate BrC species based on polarity and characterize chemical properties, where more polar compounds elute prior to relatively less polar compounds. To describe the hydrophobicity of the compounds separated by the HPLC-UV analysis, we use the octanol-water partition coefficient. This assignment is based on the relationship between the capacity factor (k′) and the elution of compounds with a known log(K_{ow}).[110] Assessment of the log(K_{ow}) can infer the fate of organic compounds in the environment; the greater the value of K_{ow}, the greater tendency to partition into a medium with appreciable organic composition. Compounds with a higher K_{ow} value, have a greater affinity to the stationary phase of a reverse phase column and will elute later compared to compounds with lower K_{ow} values. Figure 4-4 shows the reverse-phase HPLC-UV separation of BrC species of the Toronto samples and FIREX 2016 samples which represent fresh smoke emissions from fuels characteristic of the western U.S. For our aged Toronto samples, the retention time of the eluted compounds correspond to a log(K_{ow}) range of 3.1 to 3.3 and the previously reported fresh emissions (from FIREX 2016) corresponded to 2.9 to 3.5.[57] We can infer that compounds with experimental log(K_{ow}) values have similar chemical properties; this includes, oxygenated species like alcohols, ketones, ethers such as phenetole, benzophenone, 4-propyl phenol, and 4-butyl phenol have log(K_{ow}) values of 2.51, 3.18, 3.2, and 3.65, respectively.[111] This suggests that peaks observed in Figure 4-4 correspond to compounds that are functionalized with aliphatic, aromatic, hydroxyl, and carbonyl groups.

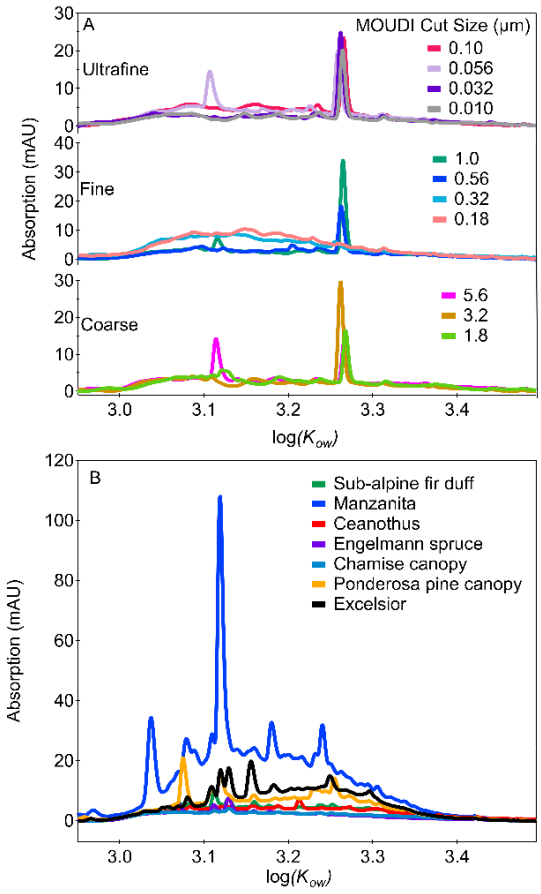

Figure 4-4. The log(K_{ow}) analysis by HPLC-UV for the (A) Toronto samples grouped into ultrafine, fine, and coarse mode and (B) the FIREX FireLab 2016 samples from controlled combustions of fuels characteristic to the western United States.

It is widely known that BrC species can be functionalized as such, however the similarities between the Toronto and FIREX 2016 HPLC-UV analyses is unexpected because the Toronto smoke was aged while the FIREX FireLab 2016 samples were freshly burned. Additionally, based on the SEC-UV analysis, absorption was dominated by high MW species whereas the FIREX 2016 samples represent fresh emissions from western U.S fuels and absorption is dominated by low MW species. Several factors can be considered to address this similarity between these sample sets. Atmospheric processing can form less-polar oligomeric species. Di Lorenzo et al. suggested that low MW fractions oligomerize within the particle during transport forming larger MW species

or high MW fractions can persist after 72 hrs of atmospheric transport.[25] In addition, secondary BrC can form by aqueous phase reactions with simple carbonyl compounds.[22,23,42] Laboratory studies have demonstrated oligomerization pathways yielding dimers through pentamers,[81,101,112] and light-absorbing nitrogen-heterocycles and non-volatile oligomers on sub-micrometer aerosols.[23] These mechanisms are consistent with enrichment of high MW BrC observed in our Toronto samples. The selective partitioning and atmospheric processing may also remove more polar compounds over long range transport as water-soluble, oxygenated compounds are more likely to undergo cloud processing or wet deposition, leaving behind more hydrophobic enriched aerosol. Differences in fuel type provide another consideration; boreal fuels in northern Ontario are rich in terpenoids, which may emit more hydrophobic precursors. Further, the measured log(K_{ow}) values of the Toronto samples could represent the fraction that was deposited and retained onto the nanoMOUDI filters, which could have biases towards retaining the low-volatility, condensed-phase fraction, which tends to be higher MW and less polar rather than the more oxidized, volatile species that are likely to repartition to the gas phase.

4.5 Conclusion

The combination of the TFIM analysis, the relationship between BC and NO_x, the elevated $PM_{2.5}$ levels, indicate the smoke intrusion in Toronto during July 2021 originated from forest fires in northern Ontario. The inorganic ionic composition reflects secondary processes such as acid displacement during plume aging. The amines reflect a mixture of urban and biomass-burning sources and cannot be uniquely attributed to the smoke intrusion. However, there is limited measurements of amines in urban regions, including Toronto; this work emphasized the importance of measuring alkylamines as the R_3NH^+/NH_4^+ ratios were comparable to a marine environment and increasing quantities of amines correlated to greater BrC absorption. Amine–

carbonyl reactions are known to produce nitrogen-containing oligomers with enhanced light absorption; the amine–BrC relationship is also consistent with the SEC-UV and log(K_{ow}) findings, which showed a dominance of high-MW species and moderately polar (log(K_{ow}) >3) oligomers. The dominance of fine mode BrC absorption is consistent with our understanding of fine mode aerosol typically containing higher concentrations of water-soluble organic carbon and the fine mode having the greatest surface-area to volume ratio. The dominant presence of high MW species supports the findings of previous analyses that applied SEC-UV to biomass burning derived samples and aligns with our understanding of secondary processes that can contribute to the formation of high MW species. During long range transport, aging can produce less-polar oligomeric species and atmospheric processing may also remove more polar compounds leaving behind more hydrophobic compounds. Thus, the presence of fine mode amines, their positive correlation with BrC absorption, and the SEC-UV and log(K_{ow}) results collectively indicate that secondary BrC formation through oligomerization was an important aging pathway in this ~30-40-hour aged smoke plume.

4.6 References

(1) Government of Canada. *The State of Canada's Forests Annual Report*; 2022. https://natural-resources.canada.ca/forest-forestry/state-canada-forests/state-canada-forests.

(2) Food and Agriculture Organization of the United Nations. *Global Forest Resources Assessment 2020*; 2020. https://doi.org/10.4060/ca9825en.

(3) Bush, E.; Lemmen, D. S. *Canada's Changing Climate Report; Government of Canada*; 2019. https://publications.gc.ca/collections/collection_2019/eccc/En4-368-2019-eng.pdf.

(4) Hanes, C. C.; Wang, X.; Jain, P.; Parisien, M.-A.; Little, J. M.; Flannigan, M. D. Fire-Regime Changes in Canada over the Last Half Century. *Can. J. For. Res.* **2019**, *49* (3), 256–269. https://doi.org/10.1139/cjfr-2018-0293.

(5) Jain, P.; Barber, Q. E.; Taylor, S. W.; Whitman, E.; Castellanos Acuna, D.; Boulanger, Y.; Chavardès, R. D.; Chen, J.; Englefield, P.; Flannigan, M.; Girardin, M. P.; Hanes, C. C.; Little, J.; Morrison, K.; Skakun, R. S.; Thompson, D. K.; Wang, X.; Parisien, M.-A. Drivers and Impacts of the Record-Breaking 2023 Wildfire Season in Canada. *Nature Communications* **2024**, *15* (1), 6764. https://doi.org/10.1038/s41467-024-51154-7.

(6) Capes, G.; Johnson, B.; McFiggans, G.; Williams, P. I.; Haywood, J.; Coe, H. Aging of Biomass Burning Aerosols over West Africa: Aircraft Measurements of Chemical Composition, Microphysical Properties, and Emission Ratios. *Journal of Geophysical Research: Atmospheres* **2008**, *113* (D23). https://doi.org/10.1029/2008JD009845.

(7) Bougiatioti, A.; Stavroulas, I.; Kostenidou, E.; Zarmpas, P.; Theodosi, C.; Kouvarakis, G.; Canonaco, F.; Prévôt, A. S. H.; Nenes, A.; Pandis, S. N.; Mihalopoulos, N. Processing of Biomass-Burning Aerosol in the Eastern Mediterranean during Summertime. *Atmospheric Chemistry and Physics* **2014**, *14* (9), 4793–4807. https://doi.org/10.5194/acp-14-4793-2014.

(8) Konovalov, I. B.; Beekmann, M.; Berezin, E. V.; Petetin, H.; Mielonen, T.; Kuznetsova, I. N.; Andreae, M. O. The Role of Semi-Volatile Organic Compounds in the Mesoscale Evolution of Biomass Burning Aerosol: A Modeling Case Study of the 2010 Mega-Fire Event in Russia. *Atmospheric Chemistry and Physics* **2015**, *15* (23), 13269–13297. https://doi.org/10.5194/acp-15-13269-2015.

(9) Laing, J. R.; Jaffe, D. A.; Hee, J. R. Physical and Optical Properties of Aged Biomass Burning Aerosol from Wildfires in Siberia and the Western USA at the Mt. Bachelor Observatory. *Atmospheric Chemistry and Physics* **2016**, *16* (23), 15185–15197. https://doi.org/10.5194/acp-16-15185-2016.

(10) Zhou, S.; Collier, S.; Jaffe, D. A.; Briggs, N. L.; Hee, J.; Sedlacek III, A. J.; Kleinman, L.; Onasch, T. B.; Zhang, Q. Regional Influence of Wildfires on Aerosol Chemistry in the Western US and Insights into Atmospheric Aging of Biomass Burning Organic Aerosol. *Atmospheric Chemistry and Physics* **2017**, *17* (3), 2477–2493. https://doi.org/10.5194/acp-17-2477-2017.

(11) Smith, D. M.; Fiddler, M. N.; Pokhrel, R. P.; Bililign, S. Laboratory Studies of Fresh and Aged Biomass Burning Aerosol Emitted from East African Biomass Fuels – Part 1: Optical Properties. *Atmospheric Chemistry and Physics* **2020**, *20* (17), 10149–10168. https://doi.org/10.5194/acp-20-10149-2020.

(12) Wang, X.; Firouzkouhi, H.; Chow, J. C.; Watson, J. G.; Ho, S. S. H.; Carter, W.; De Vos, A. S. M. Chemically Speciated Air Pollutant Emissions from Open Burning of Household Solid Waste from South Africa. *Atmospheric Chemistry and Physics* **2023**, *23* (24), 15375–15393. https://doi.org/10.5194/acp-23-15375-2023.

(13) Fleming, L. T.; Lin, P.; Roberts, J. M.; Selimovic, V.; Yokelson, R.; Laskin, J.; Laskin, A.; Nizkorodov, S. A. Molecular Composition and Photochemical Lifetimes of Brown Carbon Chromophores in Biomass Burning Organic Aerosol. *Atmospheric Chemistry and Physics* **2020**, *20* (2), 1105–1129. https://doi.org/10.5194/acp-20-1105-2020.

(14) Permar, W.; Wielgasz, C.; Jin, L.; Chen, X.; Coggon, M. M.; Garofalo, L. A.; Gkatzelis, G. I.; Ketcherside, D.; Millet, D. B.; Palm, B. B.; Peng, Q.; Robinson, M. A.; Thornton, J. A.; Veres, P.; Warneke, C.; Yokelson, R. J.; Fischer, E. V.; Hu, L. Assessing Formic and Acetic Acid Emissions and Chemistry in Western U.S. Wildfire Smoke: Implications for Atmospheric Modeling. *Environ. Sci.: Atmos.* **2023**, *3* (11), 1620–1641. https://doi.org/10.1039/D3EA00098B.

(15) Cook, R. D.; Lin, Y.-H.; Peng, Z.; Boone, E.; Chu, R. K.; Dukett, J. E.; Gunsch, M. J.; Zhang, W.; Tolic, N.; Laskin, A.; Pratt, K. A. Biogenic, Urban, and Wildfire Influences on the Molecular Composition of Dissolved Organic Compounds in Cloud Water. *Atmospheric Chemistry and Physics* **2017**, *17* (24), 15167–15180. https://doi.org/10.5194/acp-17-15167-2017.

(16) Kawamura, K.; Bikkina, S. A Review of Dicarboxylic Acids and Related Compounds in Atmospheric Aerosols: Molecular Distributions, Sources and Transformation. *Atmospheric Research* **2016**, *170*, 140–160. https://doi.org/10.1016/j.atmosres.2015.11.018.

(17) Laskin, A.; Laskin, J.; Nizkorodov, S. A. Chemistry of Atmospheric Brown Carbon. *Chemical Reviews* **2015**, *115* (10), 4335–4382. https://doi.org/10.1021/cr5006167.

(18) Bond, T. C. Spectral Dependence of Visible Light Absorption by Carbonaceous Particles Emitted from Coal Combustion. *Geophysical Research Letters* **2001**, *28* (21), 4075–4078. https://doi.org/10.1029/2001GL013652.

(19) Zhang, X.; Lin, Y.-H.; Surratt, J. D.; Zotter, P.; Prévôt, A. S. H.; Weber, R. J. Light-Absorbing Soluble Organic Aerosol in Los Angeles and Atlanta: A Contrast in Secondary Organic Aerosol. *Geophysical Research Letters* **2011**, *38* (21). https://doi.org/10.1029/2011GL049385.

(20) Andreae, M. O.; Crutzen, P. Atmospheric Aerosols: Biogeochemical Sources and Role in Atmospheric Chemistry. *Science* **1997**, No. 276, 1052–1058. https://doi.org/10.1126/science.276.5315.1052.

(21) Washenfelder, R.; Attwood, A.; Brock, C.; Guo, H.; Xu, L.; Weber, R.; Ng, N.; Allen, H.; Ayres, B.; Baumann, K.; Cohen, R.; Draper, D.; Duffey, K.; Edgerton, E.; Fry, J.; Hu, W.; Jimenez, J.; Palm, B.; Romer, P.; Brown, S. Biomass Burning Dominates Brown Carbon Absorption in the Rural Southeastern United States. *Geophysical Research Letters* **2015**, *42* (2), 653–664. https://doi.org/10.1002/2014GL062444.

(22) De Haan, D. O.; Tapavicza, E.; Riva, M.; Cui, T.; Surratt, J. D.; Smith, A. C.; Jordan, M.-C.; Nilakantan, S.; Almodovar, M.; Stewart, T. N.; de Loera, A.; De Haan, A. C.; Cazaunau, M.; Gratien, A.; Pangui, E.; Doussin, J.-F. Nitrogen-Containing, Light-Absorbing Oligomers Produced in Aerosol Particles Exposed to Methylglyoxal, Photolysis, and Cloud Cycling. *Environ. Sci. Technol.* **2018**, *52* (7), 4061–4071. https://doi.org/10.1021/acs.est.7b06105.

(23) Li, Y.; Ji, Y.; Zhao, J.; Wang, Y.; Shi, Q.; Peng, J.; Wang, Y.; Wang, C.; Zhang, F.; Wang, Y.; Seinfeld, J. H.; Zhang, R. Unexpected Oligomerization of Small α-Dicarbonyls for Secondary Organic Aerosol and Brown Carbon Formation. *Environ. Sci. Technol.* **2021**, *55* (8), 4430–4439. https://doi.org/10.1021/acs.est.0c08066.

(24) Forrister, H.; Liu, J.; Scheuer, E.; Dibb, J.; Ziemba, L.; Thornhill, K. L.; Anderson, B.; Diskin, G.; Perring, A. E.; Schwarz, J. P.; Campuzano-Jost, P.; Day, D. A.; Palm, B. B.; Jimenez, J. L.; Nenes, A.; Weber, R. J. Evolution of Brown Carbon in Wildfire Plumes. *Geophysical Research Letters* **2015**, *42* (11), 4623–4630. https://doi.org/10.1002/2015GL063897.

(25) Di Lorenzo, R. A.; Washenfelder, R. A.; Attwood, A. R.; Guo, H.; Xu, L.; Ng, N. L.; Weber, R. J.; Baumann, K.; Edgerton, E.; Young, C. J. Molecular-Size-Separated Brown Carbon Absorption for Biomass-Burning Aerosol at Multiple Field Sites. *Environmental Science and Technology* **2017**, *51* (6), 3128–3137. https://doi.org/10.1021/acs.est.6b06160.

(26) Johnson, M. S.; Strawbridge, K.; Knowland, K. E.; Keller, C.; Travis, M. Long-Range Transport of Siberian Biomass Burning Emissions to North America during FIREX-AQ. *Atmospheric Environment* **2021**, *252*, 118241. https://doi.org/10.1016/j.atmosenv.2021.118241.

(27) Hodshire, A. L.; Ramnarine, E.; Akherati, A.; Alvarado, M. L.; Farmer, D. K.; Jathar, S. H.; Kreidenweis, S. M.; Lonsdale, C. R.; Onasch, T. B.; Springston, S. R.; Wang, J.; Wang, Y.; Kleinman, L. I.; Sedlacek III, A. J.; Pierce, J. R. Dilution Impacts on Smoke Aging: Evidence in Biomass Burning Observation Project (BBOP) Data. *Atmospheric Chemistry and Physics* **2021**, *21* (9), 6839–6855. https://doi.org/10.5194/acp-21-6839-2021.

(28) Browne, E. C.; Zhang, X.; Franklin, J. P.; Ridley, K. J.; Kirchstetter, T. W.; Wilson, K. R.; Cappa, C. D.; Kroll, J. H. Effect of Heterogeneous Oxidative Aging on Light Absorption by Biomass Burning Organic Aerosol. *Aerosol Science and Technology* **2019**, *53* (6), 663–674. https://doi.org/10.1080/02786826.2019.1599321.

(29) Li, C.; He, Q.; Hettiyadura, A. P. S.; Käfer, U.; Shmul, G.; Meidan, D.; Zimmermann, R.; Brown, S. S.; George, C.; Laskin, A.; Rudich, Y. Formation of Secondary Brown Carbon in Biomass Burning Aerosol Proxies through NO(3) Radical Reactions. *Environ Sci Technol* **2020**, *54* (3), 1395–1405. https://doi.org/10.1021/acs.est.9b05641.

(30) Schnitzler, E. G.; Liu, T.; Hems, R. F.; Abbatt, J. P. D. Emerging Investigator Series: Heterogeneous OH Oxidation of Primary Brown Carbon Aerosol: Effects of Relative Humidity and Volatility. *Environ Sci Process Impacts* **2020**, *22* (11), 2162–2171. https://doi.org/10.1039/d0em00311e.

(31) Schnitzler, E. G.; Gerrebos, N. G. A.; Carter, T. S.; Huang, Y.; Heald, C. L.; Bertram, A. K.; Abbatt, J. P. D. Rate of Atmospheric Brown Carbon Whitening Governed by Environmental Conditions. *Proc Natl Acad Sci U S A* **2022**, *119* (38), e2205610119. https://doi.org/10.1073/pnas.2205610119.

(32) Warneke, C.; Schwarz, J. P.; Dibb, J.; Kalashnikova, O.; Frost, G.; Al-Saad, J.; Brown, S. S.; Brewer, Wm. A.; Soja, A.; Seidel, F. C.; Washenfelder, R. A.; Wiggins, E. B.; Moore, R. H.; Anderson, B. E.; Jordan, C.; Yacovitch, T. I.; Herndon, S. C.; Liu, S.; Kuwayama, T.; Jaffe, D.; Johnston, N.; Selimovic, V.; Yokelson, R.; Giles, D. M.; Holben, B. N.; Goloub, P.; Popovici, I.; Trainer, M.; Kumar, A.; Pierce, R. B.; Fahey, D.; Roberts, J.; Gargulinski, E. M.; Peterson, D. A.; Ye, X.; Thapa, L. H.; Saide, P. E.; Fite, C. H.; Holmes, C. D.; Wang, S.; Coggon, M. M.; Decker, Z. C. J.; Stockwell, C. E.; Xu, L.; Gkatzelis, G.; Aikin, K.; Lefer, B.; Kaspari, J.; Griffin, D.; Zeng, L.; Weber, R.; Hastings, M.; Chai, J.; Wolfe, G. M.; Hanisco, T. F.; Liao, J.; Campuzano Jost, P.; Guo, H.; Jimenez, J. L.; Crawford, J.; The FIREX-AQ Science Team. Fire Influence on Regional to Global Environments and Air Quality (FIREX-AQ). *Journal of Geophysical Research: Atmospheres* **2023**, *128* (2), e2022JD037758. https://doi.org/10.1029/2022JD037758.

(33) Washenfelder, R. A.; Azzarello, L.; Ball, K.; Brown, S. S.; Decker, Z. C. J.; Franchin, A.; Fredrickson, C. D.; Hayden, K.; Holmes, C. D.; Middlebrook, A. M.; Palm, B. B.; Pierce, R. B.; Price, D. J.; Roberts, J. M.; Robinson, M. A.; Thornton, J. A.; Womack, C. C.; Young, C. J. Complexity in the Evolution, Composition, and Spectroscopy of Brown Carbon in Aircraft Measurements of Wildfire Plumes. *Geophysical Research Letters* **2022**, *49* (9), e2022GL098951. https://doi.org/10.1029/2022GL098951.

(34) Zeng, L.; Sullivan, A. P.; Washenfelder, R. A.; Dibb, J.; Scheuer, E.; Campos, T. L.; Katich, J. M.; Levin, E.; Robinson, M. A.; Weber, R. J. Assessment of Online Water-Soluble Brown Carbon Measuring Systems for Aircraft Sampling. *Atmospheric Measurement Techniques* **2021**, *14* (10), 6357–6378. https://doi.org/10.5194/amt-14-6357-2021.

(35) Lin, P.; Aiona, P. K.; Li, Y.; Shiraiwa, M.; Laskin, J.; Nizkorodov, S. A.; Laskin, A. Molecular Characterization of Brown Carbon in Biomass Burning Aerosol Particles. *Environmental Science and Technology* **2016**, *50* (21), 11815–11824. https://doi.org/10.1021/acs.est.6b03024.

(36) Hems, R. F.; Schnitzler, E. G.; Bastawrous, M.; Soong, R.; Simpson, A. J.; Abbatt, J. P. D. Aqueous Photoreactions of Wood Smoke Brown Carbon. *ACS Earth Space Chem.* **2020**, *4* (7), 1149–1160. https://doi.org/10.1021/acsearthspacechem.0c00117.

(37) Li, X.; Xiao, M.; Xu, X.; Zhou, J.; Yang, K.; Wang, Z.; Zhang, W.; Hopke, P. K.; Zhao, W. Light Absorption Properties of Organic Aerosol from Wood Pyrolysis: Measurement Method

Comparison and Radiative Implications. *Environ Sci Technol* **2020**, *54* (12), 7156–7164. https://doi.org/10.1021/acs.est.0c01475.

(38) Hems, R. F.; Schnitzler, E. G.; Liu-Kang, C.; Cappa, C. D.; Abbatt, J. P. D. Aging of Atmospheric Brown Carbon Aerosol. *ACS Earth and Space Chemistry* **2021**, *5* (4), 722–748. https://doi.org/10.1021/acsearthspacechem.0c00346.

(39) Yang, L.; Huang, R.-J.; Shen, J.; Wang, T.; Gong, Y.; Yuan, W.; Liu, Y.; Huang, H.; You, Q.; Huang, D. D.; Huang, C. New Insights into the Brown Carbon Chromophores and Formation Pathways for Aqueous Reactions of α-Dicarbonyls with Amines and Ammonium. *Environ. Sci. Technol.* **2023**, *57* (33), 12351–12361. https://doi.org/10.1021/acs.est.3c04133.

(40) Zarzana, K. J.; De Haan, D. O.; Freedman, M. A.; Hasenkopf, C. A.; Tolbert, M. A. Optical Properties of the Products of α-Dicarbonyl and Amine Reactions in Simulated Cloud Droplets. *Environ Sci Technol* **2012**, *46* (9), 4845–4851. https://doi.org/10.1021/es2040152.

(41) Marrero-Ortiz, W.; Hu, M.; Du, Z.; Ji, Y.; Wang, Y.; Guo, S.; Lin, Y.; Gomez-Hermandez, M.; Peng, J.; Li, Y.; Secrest, J.; Zamora, M. L.; Wang, Y.; An, T.; Zhang, R. Formation and Optical Properties of Brown Carbon from Small α-Dicarbonyls and Amines. *Environ. Sci. Technol.* **2019**, *53* (1), 117–126. https://doi.org/10.1021/acs.est.8b03995.

(42) Ji, Y.; Shi, Q.; Ma, X.; Gao, L.; Wang, J.; Li, Y.; Gao, Y.; Li, G.; Zhang, R.; An, T. Elucidating the Critical Oligomeric Steps in Secondary Organic Aerosol and Brown Carbon Formation. *Atmospheric Chemistry and Physics* **2022**, *22* (11), 7259–7271. https://doi.org/10.5194/acp-22-7259-2022.

(43) Hodshire, A. L.; Bian, Q.; Ramnarine, E.; Lonsdale, C. R.; Alvarado, M. J.; Kreidenweis, S. M.; Jathar, S. H.; Pierce, J. R. More Than Emissions and Chemistry: Fire Size, Dilution, and Background Aerosol Also Greatly Influence Near-Field Biomass Burning Aerosol Aging. *Journal of Geophysical Research: Atmospheres* **2019**, *124* (10), 5589–5611. https://doi.org/10.1029/2018JD029674.

(44) Sakamoto, K. M.; Laing, J. R.; Stevens, R. G.; Jaffe, D. A.; Pierce, J. R. The Evolution of Biomass-Burning Aerosol Size Distributions Due to Coagulation: Dependence on Fire and Meteorological Details and Parameterization. *Atmospheric Chemistry and Physics* **2016**, *16* (12), 7709–7724. https://doi.org/10.5194/acp-16-7709-2016.

(45) Hosseini, S.; Li, Q.; Cocker, D.; Weise, D.; Miller, A.; Shrivastava, M.; Miller, J. W.; Mahalingam, S.; Princevac, M.; Jung, H. Particle Size Distributions from Laboratory-Scale Biomass Fires Using Fast Response Instruments" Published in Atmos. Chem. Phys., 10, 8065–8076, 2010. *Atmospheric Chemistry and Physics* **2010**, *10* (17), 8511–8511. https://doi.org/10.5194/acp-10-8511-2010.

(46) June, N. A.; Hodshire, A. L.; Wiggins, E. B.; Winstead, E. L.; Robinson, C. E.; Thornhill, K. L.; Sanchez, K. J.; Moore, R. H.; Pagonis, D.; Guo, H.; Campuzano-Jost, P.; Jimenez, J. L.; Coggon, M. M.; Dean-Day, J. M.; Bui, T. P.; Peischl, J.; Yokelson, R. J.; Alvarado, M. J.; Kreidenweis, S. M.; Jathar, S. H.; Pierce, J. R. Aerosol Size Distribution Changes in FIREX-

AQ Biomass Burning Plumes: The Impact of Plume Concentration on Coagulation and OA Condensation/Evaporation. *Atmospheric Chemistry and Physics* **2022**, *22* (19), 12803–12825. https://doi.org/10.5194/acp-22-12803-2022.

(47) Di Lorenzo, R. A.; Place, B. K.; VandenBoer, T. C.; Young, C. J. Composition of Size-Resolved Aged Boreal Fire Aerosols: Brown Carbon, Biomass Burning Tracers, and Reduced Nitrogen. *ACS Earth and Space Chemistry* **2018**, *2* (3), 278–285. https://doi.org/10.1021/acsearthspacechem.7b00137.

(48) Lee, A. K. Y.; Willis, M. D.; Healy, R. M.; Wang, J. M.; Jeong, C.-H.; Wenger, J. C.; Evans, G. J.; Abbatt, J. P. D. Single-Particle Characterization of Biomass Burning Organic Aerosol (BBOA): Evidence for Non-Uniform Mixing of High Molecular Weight Organics and Potassium. *Atmospheric Chemistry and Physics* **2016**, *16* (9), 5561–5572. https://doi.org/10.5194/acp-16-5561-2016.

(49) Sparks, T. L.; Wagner, J. Composition of Particulate Matter during a Wildfire Smoke Episode in an Urban Area. *Aerosol Science and Technology* **2021**, *55* (6), 734–747. https://doi.org/10.1080/02786826.2021.1895429.

(50) Atkinson, R.; Baulch, D. L.; Cox, R. A.; Hampson, R. F., Jr.; Kerr, J. A.; Rossi, M. J.; Troe, J. Evaluated Kinetic, Photochemical and Heterogeneous Data for Atmospheric Chemistry: Supplement V. IUPAC Subcommittee on Gas Kinetic Data Evaluation for Atmospheric Chemistry. *Journal of Physical and Chemical Reference Data* **1997**, *26* (3), 521–1011. https://doi.org/10.1063/1.556011.

(51) Place, B. K.; Quilty, A. T.; Di Lorenzo, R. A.; Ziegler, S. E.; VandenBoer, T. C. Quantitation of 11 Alkylamines in Atmospheric Samples: Separating Structural Isomers by Ion Chromatography. *Atmospheric Measurement Techniques* **2017**, *10* (3), 1061–1078. https://doi.org/10.5194/amt-10-1061-2017.

(52) Maudlin, L. C.; Wang, Z.; Jonsson, H. H.; Sorooshian, A. Impact of Wildfires on Size-Resolved Aerosol Composition at a Coastal California Site. *Atmospheric Environment* **2015**, *119*, 59–68. https://doi.org/10.1016/j.atmosenv.2015.08.039.

(53) Ge, X.; Wexler, A. S.; Clegg, S. L. Atmospheric Amines – Part I. A Review. *Atmospheric Environment* **2011**, *45* (3), 524–546. https://doi.org/10.1016/j.atmosenv.2010.10.012.

(54) Wong, J. P. S.; Nenes, A.; Weber, R. J. Changes in Light Absorptivity of Molecular Weight Separated Brown Carbon Due to Photolytic Aging. *Environmental Science & Technology* **2017**, *51* (15), 8414–8421. https://doi.org/10.1021/acs.est.7b01739.

(55) Wong, J. P. S.; Tsagkaraki, M.; Tsiodra, I.; Mihalopoulos, N.; Violaki, K.; Kanakidou, M.; Sciare, J.; Nenes, A.; Weber, R. J. Atmospheric Evolution of Molecular-Weight-Separated Brown Carbon from Biomass Burning. *Atmospheric Chemistry and Physics* **2019**, *19* (11), 7319–7334. https://doi.org/10.5194/acp-19-7319-2019.

(56) Azzarello, L.; Washenfelder, R. A.; Robinson, M. A.; Franchin, A.; Womack, C. C.; Holmes, C. D.; Brown, S. S.; Middlebrook, A.; Newberger, T.; Sweeney, C.; Young, C. J. Characterization of Water-Soluble Brown Carbon Chromophores from Wildfire Plumes in the Western USA Using Size-Exclusion Chromatography. *Atmospheric Chemistry and Physics* **2023**, *23* (24), 15643–15654. https://doi.org/10.5194/acp-23-15643-2023.

(57) Azzarello, L.; Washenfelder, R. A.; Womack, C. C.; Franchin, A.; Middlebrook, A. M.; Young, C. J. Molecular Properties of Brown Carbon Aerosol from Biomass Burning of Wildland Fuels at the Fire Sciences Laboratory. *ACS EST Air* **2025**, *2* (5), 759–772. https://doi.org/10.1021/acsestair.4c00264.

(58) Salehpoor, L.; VandenBoer, T. C. Suppressor and Calibration Standard Limitations in Cation Chromatography of Ammonium and 10 Alkylamines in Atmospheric Samples. *Anal. Methods* **2023**, *15* (31), 3822–3842. https://doi.org/10.1039/D3AY01158E.

(59) VandenBoer, T. C.; Petroff, A.; Markovic, M. Z.; Murphy, J. G. Size Distribution of Alkyl Amines in Continental Particulate Matter and Their Online Detection in the Gas and Particle Phase. *Atmospheric Chemistry and Physics* **2011**, *11* (9), 4319–4332. https://doi.org/10.5194/acp-11-4319-2011.

(60) Natural Resources Canada. Canadian National Fire Database. Interactive Map. https://cwfis.cfs.nrcan.gc.ca/interactive-map?zoom=0&center=845688.3413766827%2C1079185.9283718567&month=7&day=21&year=2021#iMap.

(61) NASA, U.S. Forest Service. Fire Information for Resource Management System (FIRMS) US/Canada., 2021. https://firms.modaps.eosdis.nasa.gov/usfs/map/#d:2021-07-20;l:fires_all,countries,graticule,earth;@-80.0,47.4,8.2z.

(62) Stein, A. F.; Draxler, R. R.; Rolph, G. D.; Stunder, B. J. . B.; Cohen, M. D.; Ngan, F. NOAA's HYSPLIT Atmospheric Transport and Dispersion Modeling System.

(63) Schneider, S. R.; Lee, K.; Santos, G.; Abbatt, J. P. D. Air Quality Data Approach for Defining Wildfire Influence: Impacts on PM2.5, NO2, CO, and O3 in Western Canadian Cities. *Environ. Sci. Technol.* **2021**, *55* (20), 13709–13717. https://doi.org/10.1021/acs.est.1c04042.

(64) Chan, I.; Schneider, S. R.; Cheng, A.; Styler, S. A. Wildfire Smoke Contributions to Polycyclic Aromatic Hydrocarbon Loadings in Western Canadian Urban Surface Grime. *Environ. Sci. Technol.* **2025**, *59* (5), 2745–2753. https://doi.org/10.1021/acs.est.4c09630.

(65) McMeeking, G. R.; Kreidenweis, S. M.; Baker, S.; Carrico, C. M.; Chow, J. C.; Collett Jr., J. L.; Hao, W. M.; Holden, A. S.; Kirchstetter, T. W.; Malm, W. C.; Moosmüller, H.; Sullivan, A. P.; Wold, C. E. Emissions of Trace Gases and Aerosols during the Open Combustion of Biomass in the Laboratory. *Journal of Geophysical Research: Atmospheres* **2009**, *114* (D19). https://doi.org/10.1029/2009JD011836.

(66) Selimovic, V.; Yokelson, R. J.; Warneke, C.; Roberts, J. M.; de Gouw, J.; Reardon, J.; Griffith, D. W. T. Aerosol Optical Properties and Trace Gas Emissions by PAX and OP-FTIR for Laboratory-Simulated Western US Wildfires during FIREX. *Atmospheric Chemistry and Physics* **2018**, *18* (4), 2929–2948. https://doi.org/10.5194/acp-18-2929-2018.

(67) Robinson, R. A.; Stokes, R. H. *Electrolyte Solutions*; Courier Corporation, Dover Publications; New York, USA, 2002.

(68) Tao, Y.; Murphy, J. G. The Sensitivity of $PM_{2.5}$ Acidity to Meteorological Parameters and Chemical Composition Changes: 10-Year Records from Six Canadian Monitoring Sites. *Atmospheric Chemistry and Physics* **2019**, *19* (14), 9309–9320. https://doi.org/10.5194/acp-19-9309-2019.

(69) Friese, E.; Ebel, A. Temperature Dependent Thermodynamic Model of the System H+−NH4+−Na+−SO42−−NO3−−Cl−−H2O. *J. Phys. Chem. A* **2010**, *114* (43), 11595–11631. https://doi.org/10.1021/jp101041j.

(70) Hayward, S. J.; Lei, Y. D.; Wania, F. Comparative Evaluation of Three High-Performance Liquid Chromatography–Based Kow Estimation Methods for Highly Hydrophobic Organic Compounds: Polybrominated Diphenyl Ethers and Hexabromocyclododecane. *Environmental Toxicology and Chemistry* **2006**, *25* (8), 2018–2027. https://doi.org/10.1897/05-675R.1.

(71) Han, S.; Liang, C.; Qiao, J.; Lian, H.; Ge, X.; Chen, H. A Novel Evaluation Method for Extrapolated Retention Factor in Determination of N-Octanol/Water Partition Coefficient of Halogenated Organic Pollutants by Reversed-Phase High Performance Liquid Chromatography. *Analytica Chimica Acta* **2012**, *713*, 130–135. https://doi.org/10.1016/j.aca.2011.11.020.

(72) Wardoyo, A. Y. P.; Morawska, L.; Ristovski, Z. D.; Jamriska, M.; Carr, S.; Johnson, G. Size Distribution of Particles Emitted from Grass Fires in the Northern Territory, Australia. *Atmospheric Environment* **2007**, *41* (38), 8609–8619. https://doi.org/10.1016/j.atmosenv.2007.07.020.

(73) Keshtkar, H.; Ashbaugh, L. L. Size Distribution of Polycyclic Aromatic Hydrocarbon Particulate Emission Factors from Agricultural Burning. *Atmospheric Environment* **2007**, *41* (13), 2729–2739. https://doi.org/10.1016/j.atmosenv.2006.11.043.

(74) Formenti, P.; Elbert, W.; Maenhaut, W.; Haywood, J.; Andreae, M. O. Chemical Composition of Mineral Dust Aerosol during the Saharan Dust Experiment (SHADE) Airborne Campaign in the Cape Verde Region, September 2000. *Journal of Geophysical Research: Atmospheres* **2003**, *108* (D18). https://doi.org/10.1029/2002JD002648.

(75) Janhäll, S.; Andreae, M. O.; Pöschl, U. Biomass Burning Aerosol Emissions from Vegetation Fires: Particle Number and Mass Emission Factors and Size Distributions. *Atmospheric Chemistry and Physics* **2010**, *10* (3), 1427–1439. https://doi.org/10.5194/acp-10-1427-2010.

(76) Liu, J.; Bergin, M.; Guo, H.; King, L.; Kotra, N.; Edgerton, E.; Weber, R. J. Size-Resolved Measurements of Brown Carbon in Water and Methanol Extracts and Estimates of Their Contribution to Ambient Fine-Particle Light Absorption. *Atmospheric Chemistry and Physics* **2013**, *13* (24), 12389–12404. https://doi.org/10.5194/acp-13-12389-2013.

(77) Zhang, X.; Lin, Y.-H.; Surratt, J. D.; Weber, R. J. Sources, Composition and Absorption Ångström Exponent of Light-Absorbing Organic Components in Aerosol Extracts from the Los Angeles Basin. *Environ. Sci. Technol.* **2013**, *47* (8), 3685–3693. https://doi.org/10.1021/es305047b.

(78) Akagi, S. K.; Yokelson, R. J.; Wiedinmyer, C.; Alvarado, M. J.; Reid, J. S.; Karl, T.; Crounse, J. D.; Wennberg, P. O. Emission Factors for Open and Domestic Biomass Burning for Use in Atmospheric Models. *Atmospheric Chemistry and Physics* **2011**, *11* (9), 4039–4072. https://doi.org/10.5194/acp-11-4039-2011.

(79) Andreae, M. O.; Merlet, P. Emission of Trace Gases and Aerosols from Biomass Burning. *Global Biogeochemical Cycles* **2001**, *15* (4), 955–966. https://doi.org/10.1029/2000GB001382.

(80) Han, B.; Zhang, R.; Yang, W.; Bai, Z.; Ma, Z.; Zhang, W. Heavy Haze Episodes in Beijing during January 2013: Inorganic Ion Chemistry and Source Analysis Using Highly Time-Resolved Measurements from an Urban Site. *Science of The Total Environment* **2016**, *544*, 319–329. https://doi.org/10.1016/j.scitotenv.2015.10.053.

(81) Li, J.; Wang, G.; Aggarwal, S. G.; Huang, Y.; Ren, Y.; Zhou, B.; Singh, K.; Gupta, P. K.; Cao, J.; Zhang, R. Comparison of Abundances, Compositions and Sources of Elements, Inorganic Ions and Organic Compounds in Atmospheric Aerosols from Xi'an and New Delhi, Two Megacities in China and India. *Science of The Total Environment* **2014**, *476–477*, 485–495. https://doi.org/10.1016/j.scitotenv.2014.01.011.

(82) Tao, Y.; Moravek, A.; Furlani, T. C.; Power, C. E.; VandenBoer, T. C.; Chang, R. Y.-W.; Wiacek, A.; Young, C. J. Acidity of Size-Resolved Sea-Salt Aerosol in a Coastal Urban Area: Comparison of Existing and New Approaches. *ACS Earth Space Chem.* **2022**, *6* (5), 1239–1249. https://doi.org/10.1021/acsearthspacechem.1c00367.

(83) Pratt, K. A.; Prather, K. A. Real-Time, Single-Particle Volatility, Size, and Chemical Composition Measurements of Aged Urban Aerosols. *Environ. Sci. Technol.* **2009**, *43* (21), 8276–8282. https://doi.org/10.1021/es902002t.

(84) Cao, F.; Zhang, S.-C.; Kawamura, K.; Zhang, Y.-L. Inorganic Markers, Carbonaceous Components and Stable Carbon Isotope from Biomass Burning Aerosols in Northeast China. *Science of The Total Environment* **2016**, *572*, 1244–1251. https://doi.org/10.1016/j.scitotenv.2015.09.099.

(85) Li, J.; Pósfai, M.; Hobbs, P. V.; Buseck, P. R. Individual Aerosol Particles from Biomass Burning in Southern Africa: 2, Compositions and Aging of Inorganic Particles. *Journal of*

Geophysical Research: Atmospheres **2003**, *108* (D13). https://doi.org/10.1029/2002JD002310.

(86) Owega, S.; Evans, G. J.; Jervis, R. E.; Fila, M.; D'Souza, R.; Khan, B.-U.-Z. Long-Range Sources of Toronto Particulate Matter (PM2.5) Identified by Aerosol Laser Ablation Mass Spectrometry (LAMS). *Atmospheric Environment* **2004**, *38* (33), 5545–5553. https://doi.org/10.1016/j.atmosenv.2004.06.034.

(87) Saarnio, K.; Aurela, M.; Timonen, H.; Saarikoski, S.; Teinilä, K.; Mäkelä, T.; Sofiev, M.; Koskinen, J.; Aalto, P. P.; Kulmala, M.; Kukkonen, J.; Hillamo, R. Chemical Composition of Fine Particles in Fresh Smoke Plumes from Boreal Wild-Land Fires in Europe. *Sci Total Environ* **2010**, *408* (12), 2527–2542. https://doi.org/10.1016/j.scitotenv.2010.03.010.

(88) Guo, X.; Wang, X.; Dai, W.; Ho, K. F.; Liu, S.; Wang, Q.; Shen, M.; Liu, Y.; Zhang, Y.; Cao, Y.; Qi, W.; Li, L.; Li, L.; Li, J. Effects of Atmospheric Aging Processes on Carbonaceous Species and Water-Soluble Inorganic Ions in Biomass Burning Aerosols. *Atmospheric Environment* **2022**, *288*, 119322. https://doi.org/10.1016/j.atmosenv.2022.119322.

(89) Andreae, M. O.; Talbot, R. W.; Andreae, T. W.; Harriss, R. C. Formic and Acetic Acid over the Central Amazon Region, Brazil: 1. Dry Season. *Journal of Geophysical Research: Atmospheres* **1988**, *93* (D2), 1616–1624. https://doi.org/10.1029/JD093iD02p01616.

(90) Jacob, D. J. Chemistry of OH in Remote Clouds and Its Role in the Production of Formic Acid and Peroxymonosulfate. *Journal of Geophysical Research: Atmospheres* **1986**, *91* (D9), 9807–9826. https://doi.org/10.1029/JD091iD09p09807.

(91) Metzger, S.; Mihalopoulos, N.; Lelieveld, J. Importance of Mineral Cations and Organics in Gas-Aerosol Partitioning of Reactive Nitrogen Compounds: Case Study Based on MINOS Results. *Atmospheric Chemistry and Physics* **2006**, *6* (9), 2549–2567. https://doi.org/10.5194/acp-6-2549-2006.

(92) Tripathy, A.; Khwaja, H. A.; Hussain, M. M.; Yerger, E.; Kelting, D.; Lawrence, C. E.; Casson, P.; Snyder, P.; Lombardo, S.; Pittman, N.; DeMarle, K.; Patel, R.; Hammond, L.; Apel, E. C.; Hornbrook, R. S.; Hills, A. J.; Brandt, R.; McKim, S.; Schlemmer, J.; Lance, S. Organic Acids and Cloud Droplet Acidity in Recent Years at Whiteface Mountain, NY, with a Focus on Wildfire Smoke Influence. *Atmospheric Chemistry and Physics* **2026**, *26* (6), 3951–3972. https://doi.org/10.5194/acp-26-3951-2026.

(93) Salma, I.; Ocskay, R.; Láng, G. G. Properties of Atmospheric Humic-like Substances – Water System. *Atmospheric Chemistry and Physics* **2008**, *8* (8), 2243–2254. https://doi.org/10.5194/acp-8-2243-2008.

(94) Hawkins, L. N.; Lemire, A. N.; Galloway, M. M.; Corrigan, A. L.; Turley, J. J.; Espelien, B. M.; De Haan, D. O. Maillard Chemistry in Clouds and Aqueous Aerosol As a Source of Atmospheric Humic-Like Substances. *Environ. Sci. Technol.* **2016**, *50* (14), 7443–7452. https://doi.org/10.1021/acs.est.6b00909.

(95) Laskin, A.; West, C. P.; Hettiyadura, A. P. S. Molecular Insights into the Composition, Sources, and Aging of Atmospheric Brown Carbon. *Chem. Soc. Rev.* **2025**, *54* (3), 1583–1612. https://doi.org/10.1039/D3CS00609C.

(96) Hinrichs, R. Z.; Buczek, P.; Trivedi, J. J. Solar Absorption by Aerosol-Bound Nitrophenols Compared to Aqueous and Gaseous Nitrophenols. *Environ Sci Technol* **2016**, *50* (11), 5661–5667. https://doi.org/10.1021/acs.est.6b00302.

(97) Mo, Y.; Li, J.; Liu, J.; Zhong, G.; Cheng, Z.; Tian, C.; Chen, Y.; Zhang, G. The Influence of Solvent and pH on Determination of the Light Absorption Properties of Water-Soluble Brown Carbon. *Atmospheric Environment* **2017**, *161*, 90–98. https://doi.org/10.1016/j.atmosenv.2017.04.037.

(98) Smolyakov, B. S.; Makarov, V. I.; Shinkorenko, M. P.; Popova, S. A.; Bizin, M. A. Effects of Siberian Wildfires on the Chemical Composition and Acidity of Atmospheric Aerosols of Remote Urban, Rural and Background Territories. *Environmental Pollution* **2014**, *188*, 8–16. https://doi.org/10.1016/j.envpol.2014.01.017.

(99) Behera, S. N.; Cheng, J.; Balasubramanian, R. In Situ Acidity and pH of Size-Fractionated Aerosols during a Recent Smoke-Haze Episode in Southeast Asia. *Environmental Geochemistry and Health* **2015**, *37* (5), 843–859. https://doi.org/10.1007/s10653-014-9660-1.

(100) Arangio, A. M.; Shahpoury, P.; Dabek-Zlotorzynska, E.; Nenes, A. Seasonal Aerosol Acidity, Liquid Water Content and Their Impact on Fine Urban Aerosol in SE Canada. *Atmosphere* **2022**, *13* (7). https://doi.org/10.3390/atmos13071012.

(101) Hastings, W. P.; Koehler, C. A.; Bailey, E. L.; De Haan, D. O. Secondary Organic Aerosol Formation by Glyoxal Hydration and Oligomer Formation: Humidity Effects and Equilibrium Shifts during Analysis. *Environ. Sci. Technol.* **2005**, *39* (22), 8728–8735. https://doi.org/10.1021/es0504461.

(102) Pierson, W. R.; Brachaczek, W. W. Emissions of Ammonia and Amines from Vehicles on the Road. *Environ. Sci. Technol.* **1983**, *17* (12), 757–760. https://doi.org/10.1021/es00118a013.

(103) Calderón, S. M.; Poor, N. D.; Campbell, S. W. Estimation of the Particle and Gas Scavenging Contributions to Wet Deposition of Organic Nitrogen. *Atmospheric Environment* **2007**, *41* (20), 4281–4290. https://doi.org/10.1016/j.atmosenv.2006.06.067.

(104) De Haan, D. O.; Tolbert, M. A.; Jimenez, J. L. Atmospheric Condensed-Phase Reactions of Glyoxal with Methylamine. *Geophysical Research Letters* **2009**, *36* (11). https://doi.org/10.1029/2009GL037441.

(105) De Haan, D. O.; Hawkins, L. N.; Kononenko, J. A.; Turley, J. J.; Corrigan, A. L.; Tolbert, M. A.; Jimenez, J. L. Formation of Nitrogen-Containing Oligomers by Methylglyoxal and Amines in Simulated Evaporating Cloud Droplets. *Environ. Sci. Technol.* **2011**, *45* (3), 984–991. https://doi.org/10.1021/es102933x.

(106) Yang, X.; Murphy, J. G.; Tao, Y. Particle Size Dependence and Phase Partitioning of Dimethylamine and Diethylamine in an Urban Atmosphere across Seasons. *ACS Earth Space Chem.* **2025**, *9* (4), 888–897. https://doi.org/10.1021/acsearthspacechem.4c00403.

(107) Cruz, M. T.; Bañaga, P. A.; Betito, G.; Braun, R. A.; Stahl, C.; Aghdam, M. A.; Cambaliza, M. O.; Dadashazar, H.; Hilario, M. R.; Lorenzo, G. R.; Ma, L.; MacDonald, A. B.; Pabroa, P. C.; Yee, J. R.; Simpas, J. B.; Sorooshian, A. Size-Resolved Composition and Morphology of Particulate Matter during the Southwest Monsoon in Metro Manila, Philippines. *Atmospheric Chemistry and Physics* **2019**, *19* (16), 10675–10696. https://doi.org/10.5194/acp-19-10675-2019.

(108) Huang, S.; Song, Q.; Hu, W.; Yuan, B.; Liu, J.; Jiang, B.; Li, W.; Wu, C.; Jiang, F.; Chen, W.; Wang, X.; Shao, M. Chemical Composition and Sources of Amines in PM2.5 in an Urban Site of PRD, China. *Environmental Research* **2022**, *212*, 113261. https://doi.org/10.1016/j.envres.2022.113261.

(109) Perrone, M. G.; Zhou, J.; Malandrino, M.; Sangiorgi, G.; Rizzi, C.; Ferrero, L.; Dommen, J.; Bolzacchini, E. PM Chemical Composition and Oxidative Potential of the Soluble Fraction of Particles at Two Sites in the Urban Area of Milan, Northern Italy. *Atmospheric Environment* **2016**, *128*, 104–113. https://doi.org/10.1016/j.atmosenv.2015.12.040.

(110) Kaune, A.; Knorrenschild, M.; Kettrup, A. Predicting 1-Octanol-Water Partition Coefficient by High-Performance Liquid Chromatography Gradient Elution. *Fresenius' Journal of Analytical Chemistry* **1995**, *352* (3), 303–312. https://doi.org/10.1007/BF00322226.

(111) Mackay, D.; Shiu, W.-Y.; Lee, S. C. *Handbook of Physical-Chemical Properties and Environmental Fate for Organic Chemicals*; CRC Press, 2006; Vol. 2.

(112) Gomez, M. E.; Lin, Y.; Guo, S.; Zhang, R. Heterogeneous Chemistry of Glyoxal on Acidic Solutions. An Oligomerization Pathway for Secondary Organic Aerosol Formation. *J. Phys. Chem. A* **2015**, *119* (19), 4457–4463. https://doi.org/10.1021/jp509916r.

Appendix C: Supporting Information for Chapter 4

Figure C-1. Photographs of MOUDI filters following sampling.

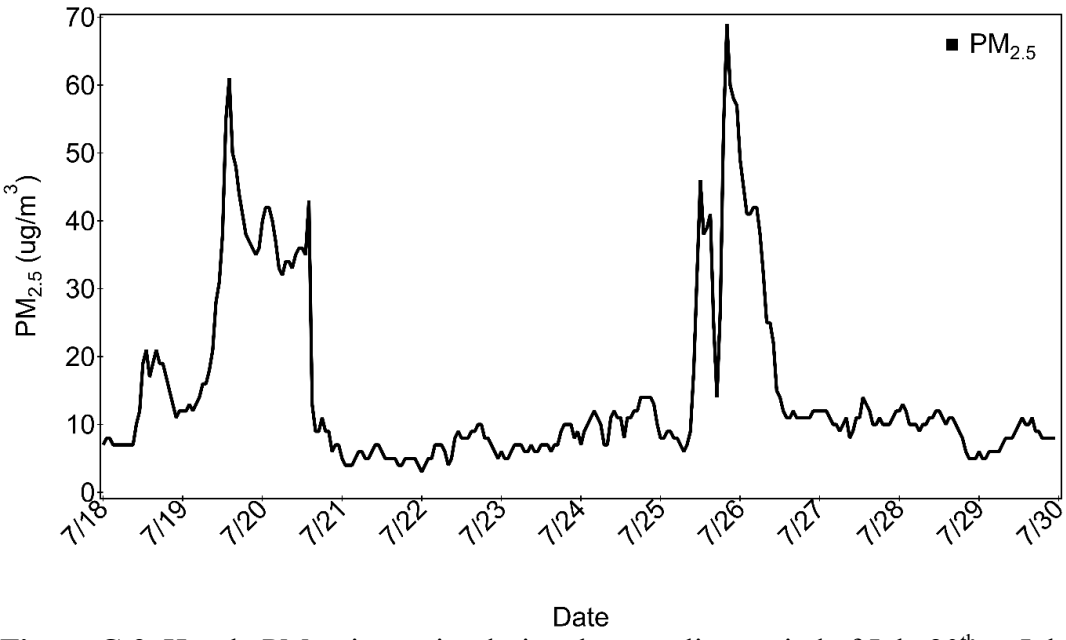

Figure C-2. Hourly $PM_{2.5}$ timeseries during the sampling period of July 20th to July 27th. Data retrieved from the Ministry of Environment Conservation and Parks (MECP) (Toronto North Station).

Table C-1. Coordinates of fire hotspots detected from (CWFIS) and FIRMS and the number of interceptions from 24 hr back trajectory determined based on the TFIM model.

Hotspots identified for first smoke intrusion during sampling period			
Hot Spot Number	Hot Spot Coordinates	Recorded Start date of Fire	Interceptions
1	48, -82.02	2021-07-09	7
2	49.46, -84.33	2021-07-21	0
3	48.92, -85.91	2021-07-16	0
4	49.0219, -80.3323	2021-07-20 12:22:00	0
5	48.2541, -79.02028	2021-07-19 03:33:00	0
6	48.25072, -79.02169	2021-07-19 03:33:00	0
7	46.29191, -80.22802	2021-07-21 14:22:00	21
Hotspots identified for second smoke intrusion during sampling period			
1	46.57881, -80.79082	2021-07-25 03:21:00	0
2	46.57552, -80.79187	2021-07-25 03:21:00	0
3	46.5238, -84.37471	2021-07-25 03:21:00	6
4	46.51873, -84.39446	2021-07-25 03:21:00	6
5	46.51513, -84.39534	2021-07-25 03:21:00	7
6	46.19765, -82.69908	2021-07-25 03:21:00	0

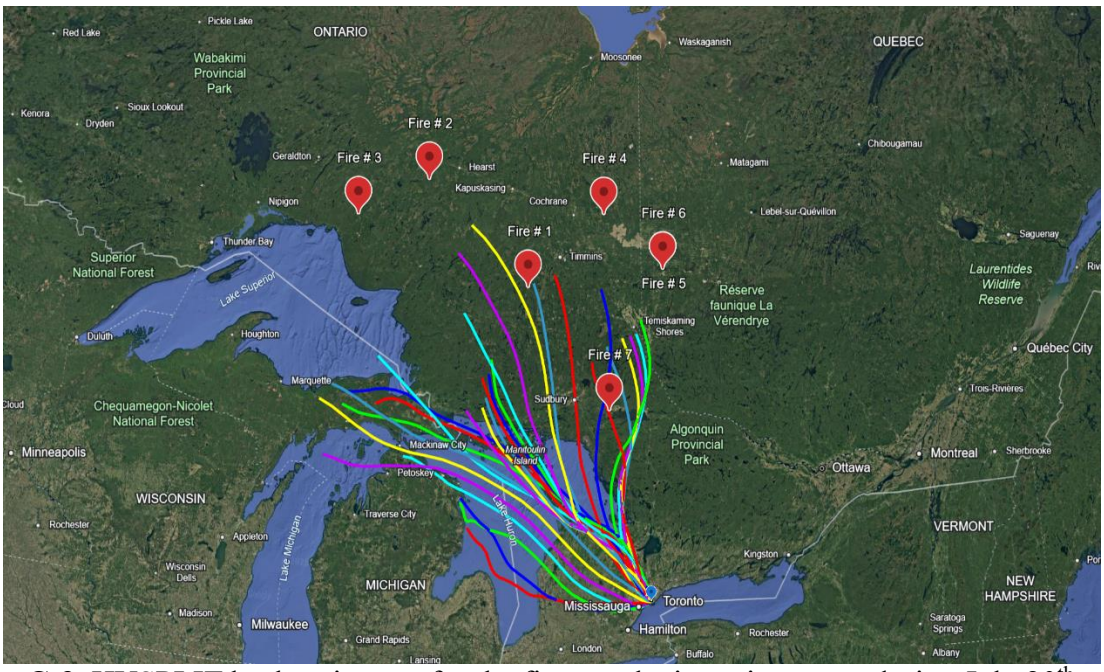

Figure C-3. HYSPLIT back trajectory for the first smoke intrusion event during July 20th to July 27th, 2021. Hotspot locations are noted by the red pins for a total of 28 interceptions.

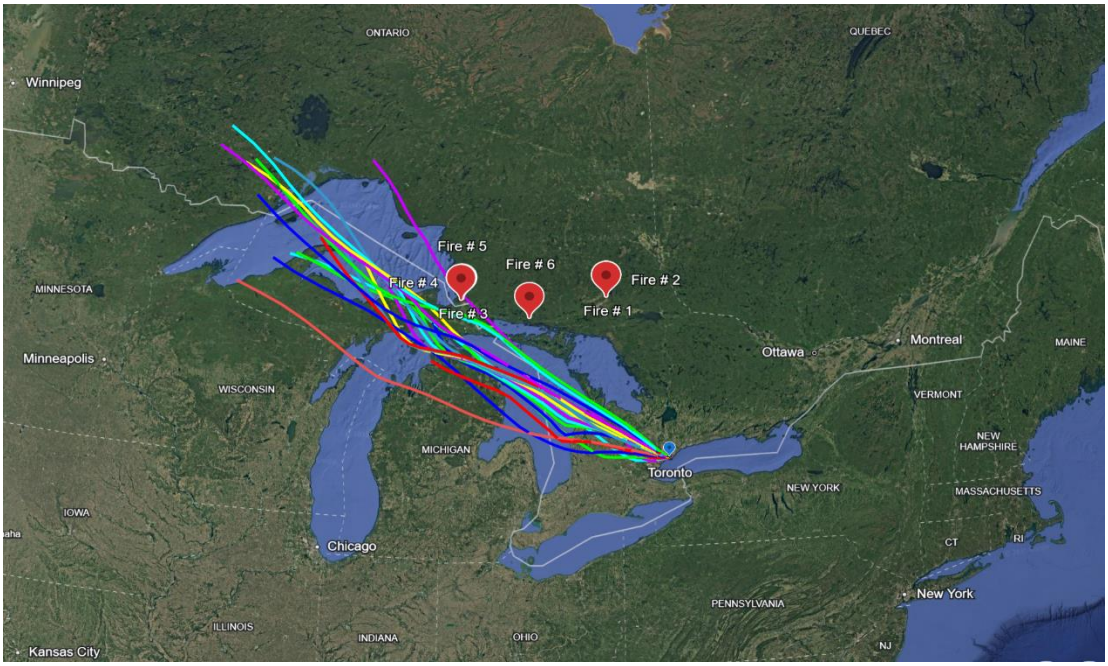

Figure C-4. HYSPLIT back trajectory for the second smoke intrusion event during July 20th to July 27th, 2021. Hotspot locations are noted by the red pins for a total of 19 interceptions.

C.1 Smoke intrusion assessment from northern Ontario forest fires

In addition to the HYSPLIT analysis, to further decipher between the transported air mass from local sources, BC-NO_x relationships were assessed and compared across three periods: (i) the July 2021 smoke intrusion, (ii) a non-smoke period in July 2022, and (iii) a moderate smoke influence period in July 2023 (Figure C-5). During the heavy smoke intrusion in July 2021, there is a slope of 0.7 and a R^2 of 0.86 whereas the July 2022 non-smoke period has a lower slope of 0.05 and the greatest correlation (R^2 = 0.98), and during the moderately smoke impacted time in July 2023, we have a slope of 0.83 and a R^2 of 0.77. In an urban region, when there are a strong correlation and a lower slope between BC and NO_x, this indicates that emissions are from a common source as there is higher NO_x than BC. A decreased correlation accompanied by a higher slope signifies that another source is involved, such as biomass burning. These trends confirm that elevated BC and $PM_{2.5}$ during July 2021 was driven by transported forest fire smoke rather than local combustion sources. To further, emphasize our certainty that the July 2021 sampling period

was indeed impacted by forest fires in northwestern Ontario, we applied the TFIM framework. During the first intrusion episode, seven active fires were identified, where two of these fires were determined to have intersected the air masses that reached the Toronto as a total of 28 interceptions were determined based on the 24 hr back trajectory analysis. During the second episode, six fire hotspots were identified, with three identified to have impacted the sampled air mass, the TFIM identified 19 intercepts. These two smoke intrusion episodes satisfied the 20-intercept minimum outlined by TFIM model.

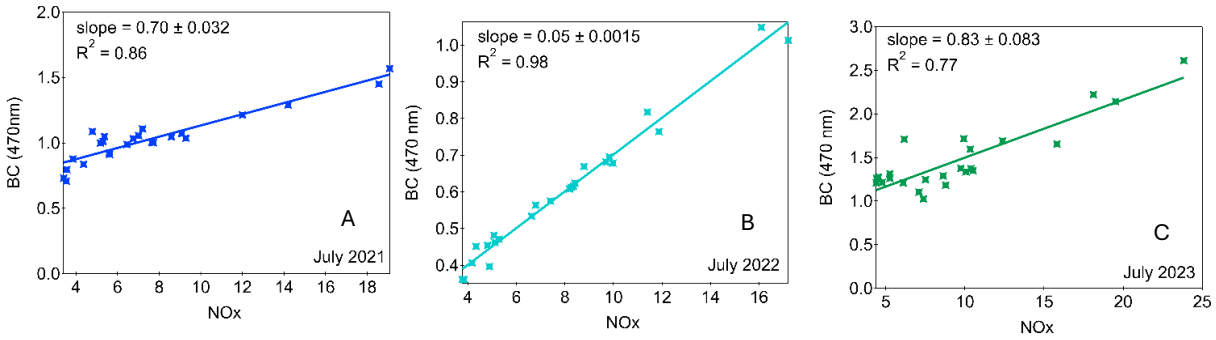

Figure C-5. BC-NO_x relationship for (A) July 2021 during the sampling period and (B) during the same week in July 2022 where no smoke intrusion was observed, and (C) during the same week in July 2023 when there was a moderate impact from smoke plumes.

Table C-2. LOD and LOQ of each ion.

Ion	LOD (µg)	LOQ (µg)
Na^+	$3.12\times 10^{-4} \pm 1.30\times 10^{-3}$	$1.01\times 10^{-2} \pm 4.33\times 10^{-3}$
NH_4^+	$1.59\times 10^{-5} \pm 7.79\times 10^{-7}$	$5.32\times 10^{-6} \pm 2.59\times 10^{-6}$
K+	$6.31\times 10^{-6} \pm 4.14\times 10^{-7}$	$1.51\times 10^{-4} \pm 1.38\times 10^{-4}$
DMA	$5.24\times 10^{-5} \pm 4.77\times 10^{-6}$	$1.74\times 10^{-4} \pm 1.59\times 10^{-5}$
DEA	$1.47\times 10^{-3} \pm 1.54\times 10^{-4}$	$4.92\times 10^{-3} \pm 5.16\times 10^{-4}$
IMPA	$1.32\times 10^{-4} \pm 6.77\times 10^{-5}$	$4.40\times 10^{-4} \pm 2.25\times 10^{-4}$
Cl^-	$6.85\times 10^{-4} \pm 2.90\times 10^{-4}$	$2.28\times 10^{-4} \pm 9.66\times 10^{-5}$
NO_3^-	$1.21\times 10^{-4} \pm 7.44\times 10^{-4}$	$4.03\times 10^{-4} \pm 2.48\times 10^{-5}$
SO_4^{2-}	$5.65\times 10^{-4} \pm 2.96\times 10^{-4}$	$1.88\times 10^{-4} \pm 9.86\times 10^{-5}$

Table C-3. Anion and cation charge sums, residual charge, and ionic ratios for each MOUDI stage.

MOUDI Stage # (D_{50} µm)	Charge Ratio [ΣCations (meq/L)−Σ Anions (meq/L)]	Charge Residual (%) [ΣCations (meq/L)−ΣAnions (meq/L)]/ ΣAnions (meq/L)	K^+/Cl^-	R_3NH^+/NH_4^+	$NH4+/SO_4^2$
2 (5.6)	0.32	-68.30	0.28		
3 (3.2)	0.31	-69.18	0.26		
4 (1.8)	0.34	-65.93	0.55		
5 (1)	0.35	-65.17	0.40		
6 (0.56)	1.29	28.68	0.46		
7 (0.32)	1.10	9.76	4.35	3.63	0.19
8 (0.18)	1.43	42.60	1.49	0.33	1.13
9 (0.1)	0.93	-7.10	1.63	0.34	0.68
10 (0.056)	0.78	-22.05	1.12	0.48	0.49
11 (0.032)	0.48	-52.19	0.00		
12 (0.018)	0.91	-8.62	0.00		
13 (0.01)	0.49	-50.90	0.00		

Table C-4. Summary of measured inorganic cation quantities per m^3 of air sampled.

MOUDI Stage # (D_{50} µm)	**K^+ (ug/m^3)**	**K^+ ($nmol/m^3$)**	**Na^+ (ug/m^3)**	**Na^+ ($nmol/m^3$)**	**NH_4^+ (ug/m^3)**	**NH_4^+ ($nmol/m^3$)**
2 (5.6)	0.011	0.285	0.028	1.211		
3 (3.2)	0.013	0.339	0.042	1.840		
4 (1.8)	0.037	0.958	0.059	2.553		
5 (1)	0.018	0.470	0.041	1.768		
6 (0.56)	0.011	0.273	0.142	6.161		
7 (0.32)	0.085	2.184	0.023	0.987	0.026	1.457
8 (0.18)	0.094	2.392	0.033	1.436	0.408	22.612
9 (0.1)	0.029	0.744	0.018	0.796	0.185	10.264
10 (0.056)	0.020	0.519	0.017	0.749	0.082	4.520
11 (0.032)			0.010	0.421		
12 (0.018)			0.016	0.705		
13 (0.01)			0.015	0.646		

Table C-5. Summary of measured alkylamines quantities per m^3 of air sampled.

MOUDI Stage # (D_{50} µm)	DMA (ug/m^3)	DMA ($nmol/m^3$)	DEA (ug/m^3)	DEA ($nmol/m^3$)	IMPA (ug/m^3)	IMPA($nmol/m^3$)
2 (5.6)						
3 (3.2)						
4 (1.8)						
5 (1)						
6 (0.56)	0.004	0.099	0.008	0.105		
7 (0.32)	0.126	2.805	0.182	2.482		
8 (0.18)	0.170	3.769	0.268	3.669		
9 (0.1)	0.079	1.754	0.127	1.736		
10 (0.056)	0.048	1.074	0.080	1.100		
11 (0.032)					0.009	0.151
12 (0.018)					0.006	0.109
13 (0.01)					0.003	0.054

Table C-6. Summary of measured anion quantities per m^3 of air sampled.

MOUDI Stage # (D_{50} µm)	Cl^- (ug/m^3)	Cl^- ($nmol/m^3$)	NO_3^- (ug/m^3)	NO_3^- ($nmole/m^3$)	SO_4^{2-} (ug/m^3)	SO_4^{2-} ($nmol/m^3$)
2 (5.6)	0.036	1.014	0.155	2.497	0.058	0.605
3 (3.2)	0.046	1.289	0.275	4.441	0.064	0.670
4 (1.8)	0.062	1.736	0.419	6.754	0.087	0.908
5 (1)	0.042	1.183	0.230	3.714	0.073	0.764
6 (0.56)	0.021	0.593	0.081	1.303	0.157	1.631
7 (0.32)	0.018	0.502	0.049	0.791	0.372	3.871
8 (0.18)	0.057	1.610	0.137	2.208	0.958	9.970
9 (0.1)	0.016	0.456	0.053	0.854	0.728	7.576
10 (0.056)	0.016	0.465	0.034	0.552	0.442	4.598
11 (0.032)	0.010	0.286	0.016	0.252	0.063	0.657
12 (0.018)	0.010	0.275	0.013	0.209	0.020	0.204
13 (0.01)	0.012	0.325	0.015	0.237	0.041	0.432

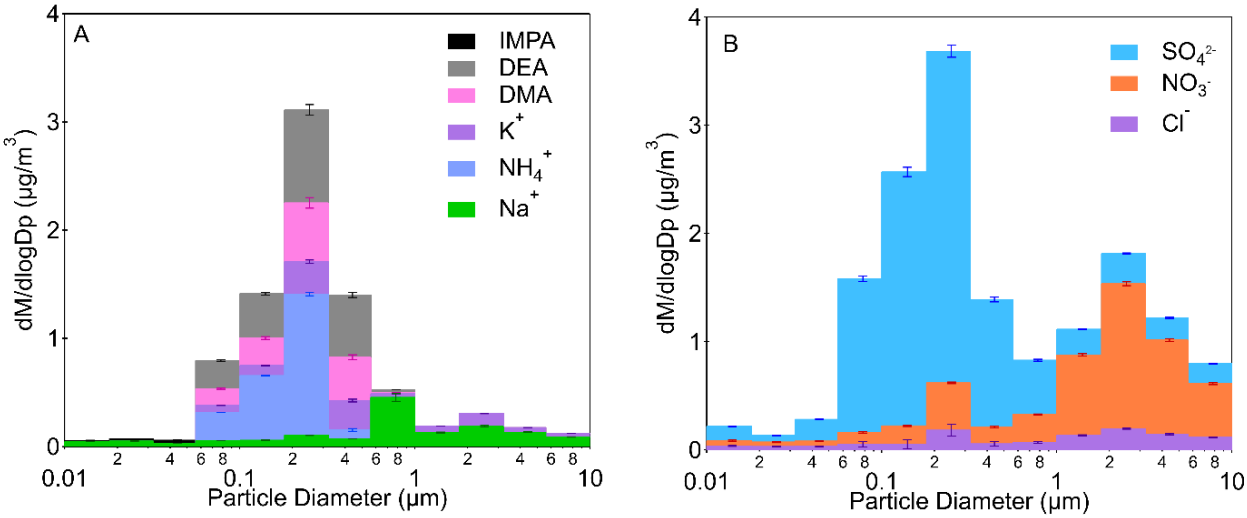

Figure C-6. Sum of aerosol mass loading size distribution of (a) inorganic cations and alkylamines and (b) inorganic anions from the Toronto MOUDI samples. The error bars represent the uncertainty based on the propagation of errors for each ion.

C.2 Qualitative assessment of organic acids

To complement inorganic ion and amine data, the presence of organic acids was qualitatively because these compounds contribute to aerosol acidity (Table C-7). By comparing unidentified anion peaks with the ThermoScientific application notes for the IonPac AS-23 column operated with a hydroxide gradient (5 mM to 40 mM).[1] Under these separation conditions, monoacids acids such as formate, acetate, and butyrate elute early (< 10 mM), dicarboxylic acids such as malonate, succinate, and oxalate elute later (≈ 20 mM), and polycarboxylates elute at greater strength (> 30 mM). Peaks observed across all size ranges for < 10 mM OH^- suggest the presence of monoacids, while the fine mode had additional peaks consistent with the presence of dicarboxylic acids. In both the fine and ultrafine modes, late eluting peaks (> 30 mM) were also observed, potentially corresponding to polycarboxylates. The detection of peaks across the size ranges supports the presence of organic acids in the Toronto smoke intrusion aerosol, consistent with prior reports of aged biomass-burning influence air masses.

Table C-7. Organic acids qualitatively detected for each MOUDI stage

Stage (D_{50} µm)	Unidentified Peak, RT min		Organic acid
2 (5.6)	4.71- 5.6767	10 mM	acetate, butyrate, formate
3 (3.2)	4.71- 5.6767	10 mM	acetate, butyrate, formate
4 (1.8)	4.74 – 5.19	10 mM	acetate, butyrate, formate
5 (1)	4.7267-5.6833	10 mM	acetate, butyrate, formate
6 (0.56)	4.7433- 8.47 23.277-26.13	10 mM 60 mM	acetate, butyrate, formate malonate, succinate, oxalate
7 (0.32)	5.1-15.053 21.43-24.153	10 Mm 60 mM	acetate, butyrate, formate malonate, succinate, oxalate
8 (0.18)	5.1-15.15 21.423-24.06	10 Mm 60 mM	acetate, butyrate, formate malonate, succinate, oxalate
9 (0.1)	5.1-15.23 21.45-24.177	10 Mm 60 mM	acetate, butyrate, formate malonate, succinate, oxalate
10 (0.056)	5.1-15.263 21.407-23.17	10 Mm 60 mM	acetate, butyrate, formate malonate, succinate, oxalate
11 (0.032)	5.1-15.007 24.037	10 Mm 60 mM	acetate, butyrate, formate malonate, succinate, oxalate
12 (0.018)	5.1-15.097 24.083	10 Mm 60 mM	acetate, butyrate, formate malonate, succinate, oxalate
13 (0.01)	5.1-15.007 24.14	10 Mm 60 mM	acetate, butyrate, formate malonate, succinate, oxalate

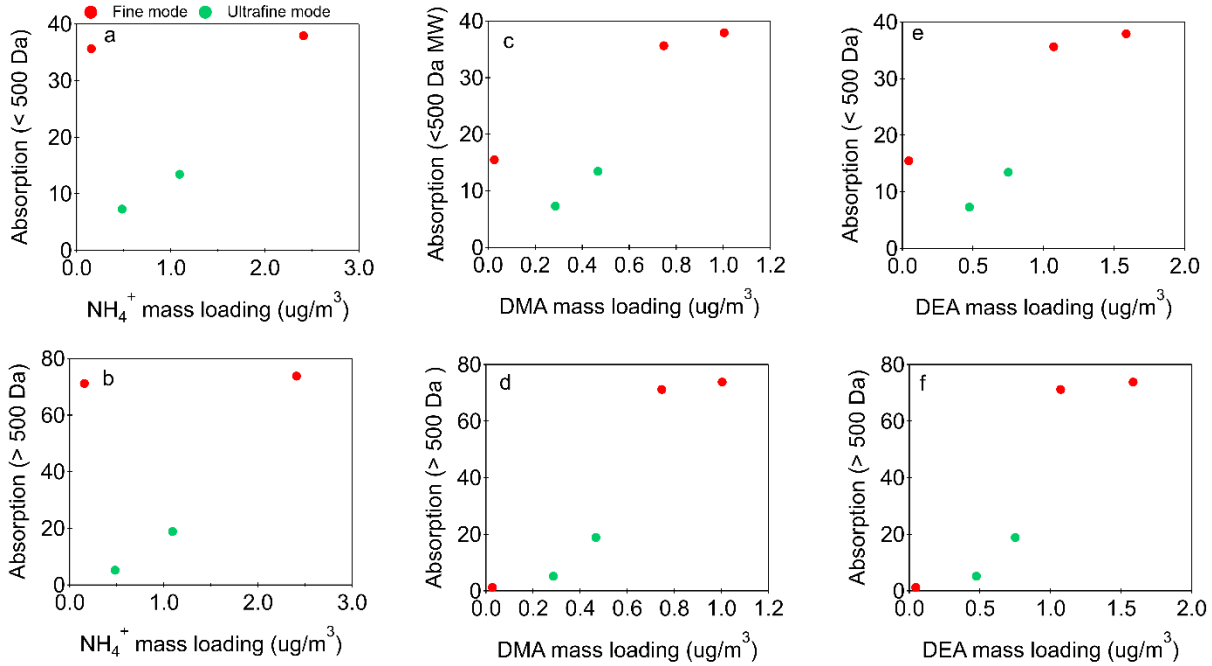

Figure C-7. Toronto smoke intrusion relationships between (a) ammonium and chromophores < 500 Da, (b) ammonium and chromophores > 500 Da, (c) DMA and chromophores < 500 Da, (d) DMA and chromophores > 500 Da, (e) DEA and chromophores < 500 Da, and (f) DEA and chromophores > 500. Red represents the fine mode and green represents the ultrafine mode.

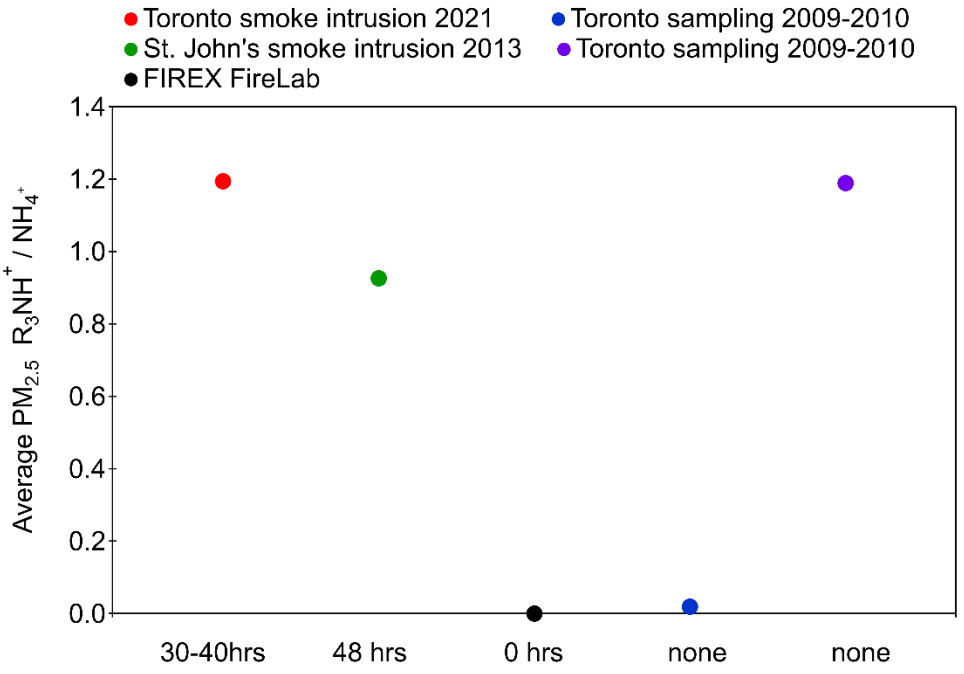

Figure C-8. Average $PM_{2.5}$ Amine-to-ammonium ratio for aged biomass burning samples (30-40hrs and 48hrs), fresh emissions from FIREX FireLab 2016, and for Toronto sampling with no reported biomass burning influence.[2,3]

Appendix C References

(1) Thermo Fisher. Dionex IonPac AS23 Column Product Manual, 2013.

(2) Place, B. K.; Quilty, A. T.; Di Lorenzo, R. A.; Ziegler, S. E.; VandenBoer, T. C. Quantitation of 11 Alkylamines in Atmospheric Samples: Separating Structural Isomers by Ion Chromatography. Atmospheric Measurement Techniques 2017, 10 (3), 1061–1078. https://doi.org/10.5194/amt-10-1061-2017.

(3) VandenBoer, T. C.; Petroff, A.; Markovic, M. Z.; Murphy, J. G. Size Distribution of Alkyl Amines in Continental Particulate Matter and Their Online Detection in the Gas and Particle Phase. Atmospheric Chemistry and Physics 2011, 11 (9), 4319–4332. https://doi.org/10.5194/acp-11-4319-2011.

Chapter 5

Conclusions and Future Directions

5.1 Conclusions

This work presents an integrated analytical approach to characterizing the chemical composition, absorption properties, and atmospheric evolution of water-soluble BrC emitted from biomass burning. This study combines three complementary datasets: (i) fresh wildfire emissions from controlled combustion experiments, (ii) airborne measurements of wildfire smoke plumes aged 0-5 hrs, and (iii) ground-based measurements of long-range transported smoke aged approximately 30-40 hours.

A suite of chromatographic analyses was applied across all data sets. Size-exclusion chromatography with UV-vis absorption (SEC-UV) was applied to investigate the relative contributions of high and low MW chromophores to BrC absorption. Reverse-phase chromatography (HPLC-UV) was applied to estimate log(K_{ow}) values and assess hydrophobicity of fresh and aged BrC species, and ion chromatography (IC-CD) was used to quantify inorganic ions and alkylamines in aged smoke mixed with urban air. This work showed that BrC absorption and its evolution is influenced by chromophore MW, volatility, hydrophobicity, and susceptibility to secondary processes during atmospheric aging.

Airborne measurements during FIREX-AQ, showed that freshly emitted BrC absorption was dominated by low MW chromophores (< 500 Da), where this observation was consistent with previous analyses that applied SEC-UV to investigate BrC absorption density. Brown carbon absorption trends as a function of plume age (over 0 to 5 hours) were varied, as some flights absorption increased, decreased, or stayed relatively constant. This variability emphasized the complexity of BrC formation and degradation processes. Comparisons between the online absorption measurements and the offline SEC-UV analysis showed discrepancies in absorption magnitude which suggested BrC sensitivity to sampling and measurement conditions. These

results emphasized the importance of intercomparison between measurement techniques when investigating BrC absorption.

Controlled combustion experiments of ambient and thermal denuded smoke further contextualized the chemical and absorption properties of primary BrC by integrating SEC-UV with the volatility basis-set framework and a log(K_{ow}) analysis. While the SEC-UV analysis showed that BrC absorption was dominated by low MW species, the volatility analysis showed that much of BrC species was classified within the low volatility organic compounds (LVOC) regime. Although these results appear counterintuitive, these observations capture different aspects of BrC composition. The inclusion the log(K_{ow}) analysis addressed these findings by indicating a log(K_{ow}) range of 2.9 to 3.5 which suggests that BrC species are moderately hydrophobic and therefore can partition into the organic phase of aerosol. Compounds within this log(K_{ow}) range have the potential to persist in the atmosphere, where they can undergo oxidation processes making them more water-soluble over time. Overall, these results demonstrate that log(K_{ow}) is a valuable complementary parameter for interpreting volatility, partitioning behaviour, and atmospheric persistence of BrC.

The ground-based measurements during a smoke intrusion event in Toronto, Ontario provided insight into the evolution of BrC during long range transport. Back trajectory analysis, elevated $PM_{2.5}$, and the relationship between BC and NO_x confirmed the air quality was impacted from forest fires in northwestern Ontario. The inorganic ionic composition reflected secondary processes during transport while the amines detected could not be uniquely attributed to the wildfire plume and likely reflect a mixture of urban and biomass burning sources. There are limited measurements of amines in urban regions and this work emphasized the importance of measuring alkylamines as the R_3NH^+/NH_4^+ ratios were comparable to a marine environment and increasing

quantities of amines correlated to greater BrC absorption. The dominance of high MW BrC species in the Toronto samples combined with moderate hydrophobicity inferred from the log(K_{ow}) analysis, supports our understanding that secondary processes during long range transport can produce less-polar, high MW, oligomeric species that can persist during transport.

Overall, this work demonstrates that absorption and chemical properties of BrC evolve after emission. Primary emissions determine the initial composition, while aging processes increasingly enhance the contribution of high MW species to absorption with plume age. This trend is consistent across the three datasets. The results highlight the need to integrate laboratory studies, field measurements, and multi-chemical analyses to characterize BrC absorption and evolution. Improved representation of BrC evolution, including hydrophobicity and oligomerization pathways is important for reducing uncertainty in estimates atmospheric persistence and ultimately, its radiative effects.

5.2 Future Directions

Wildfire activity is increasing in frequency and intensity, and future projections indicate that wildfire seasons will continue to expand under warming climate. Exposure to wildfire smoke is expected to impact air quality seasonally and through episodic events depending on the geographical location. This highlights the need for continuous measurements that can capture short-term smoke intrusions and longer-term impacts of biomass burning. Future work should prioritize long term monitoring strategies capable of investigating the evolution of chemical and optical properties of BrC across multiple fire seasons, plume ages, and geographic regions. A growing challenge in wildfire research is the increasing prevalence of wildland-urban interface fires, where combustion involves biomass fuel and infrastructure materials. These materials may introduce unique chemical signatures and potentially more persistent or toxic light absorbing

compounds into the atmosphere. Future studies should aim to characterize BrC emissions from these fires and assess how the chemical composition, molecular weight distributions, and hydrophobicity differ from those emitted from biomass burning. Integrating chemical markers of infrastructure fires with BrC measurements could help constrain source apportionment and improve our understanding about its implications on radiative effects and health impacts of wildfire smoke.

This work demonstrated that $\log(K_{ow})$ is a useful parameter to contextualize the atmospheric fate of BrC. To date, $\log(K_{ow})$ has been applied to biomass burning derived aerosol in a limited capacity, despite its relevance to assessing hydrophobicity, phase partitioning, and persistence during atmospheric transport. Future analyses that incorporate chromatographic methodologies can aim to expand the application of $\log(K_{ow})$ measured across of wider range wildfire conditions, including fuel type, combustion regimes, and plume ages to assess reproducibility of the trends observed in this work. By combining $\log(K_{ow})$ with the volatility basis set framework and with SEC-UV could further improve interpretation of BrC aging pathways and atmospheric persistence. The consistent observations across the data sets in this work and previous SEC-UV studies suggest that more aged smoke exhibits a greater contribution from higher MW species to total absorption which highlights the utility of SEC-UV for investigating BrC evolution. However, the limited number of studies applying SEC-UV suggests the need for broader implementation and comparison of this method. Future work can explore intercomparison studies across laboratories and field campaigns to establish robustness and explore sensitivities to chromatographic conditions. This work demonstrated that absorption measurements can differ between online and offline techniques, which highlighted the need to better understand how sample storage and separation conditions influence observed optical properties. Future chromatographic

studies should investigate or at the very least, acknowledge, the effects of storage conditions, aqueous versus filter-based collection, separation conditions, such as solvent composition, and pH, has on BrC absorption measurements. Addressing these aspects could be important to interpret difference between online and offline measurements and understanding how sample handling can impact our findings.

The role of alkylamines in secondary BrC formation and its detection in levels comparable to a marine environment warrants further investigation. This work also showed positive correlations between alkylamines and BrC absorption in aged smoke which suggests that amine-carbonyl and oligomerization chemistry contribute to BrC. There is a scarcity of amine measurements in urban and wildfire-influenced regions, therefore, future work should incorporate size-resolved aerosol sampling with offline or online (e.g. PILS coupled to IC-CD) amine quantification measurements to better constrain their sources and lifetimes.

To continue improving the representation of BrC evolution in modelling studies, the integration of laboratory studies, field measurements, and multi-parameter chemical analyses should continue. Model parameterizations often assume simple decay schemes (which may be true or long-term aging such as >50 hours), but do not necessarily capture the complex balance between chromophore formation and degradation observed with a few hours after emission. Vast data sets that address molecular weight, volatility, hydrophobicity, and chemical composition are needed to constrain processes that contribute to BrC absorption properties. Therefore, continued measurements and intercomparisons is critical to reduce uncertainty in estimates of BrC radiative forcing and to improve prediction on the impact wildfires have on air quality and climate.